# BULETINUL INSTITUTULUI POLITEHNIC DIN IASI

# BULETINUL INSTITUTULUI POLITEHNIC DIN IAŞI
# BULLETIN OF THE POLYTECHNIC INSTITUTE OF IAŞI
## Tomul LIV (LVIII)                                                          2008

## MATERIALS SCIENCE AND ENGINEERING

# BULETINUL INSTITUTULUI POLITEHNIC DIN IAŞI
# BULLETIN OF THE POLYTECHNIC INSTITUTE OF IAŞI
Tomul LIV (LVIII)                                                    2008

## ŞTIINŢA ŞI INGINERIA MATERIALELOR

# DETERMINATION OF THE MEAN SUBSTITUTIVE COEFFICIENT OF THERMAL CONDUCTIVITY FOR COLD DRIED CASTING MOULDS WITH FURANIC RESIN BINDERS

**BY**

**I. CIOBANU\*, I. CHIŞAMERA\*\*, S.I. MUNTEANU\*, A. CRIŞAN\*, V. MONESCU\*,
I. MĂRGINEANU\*\*, L. FIRESCU\*\*\***

**Abstract:** The paper presents the results of experimental research regarding determination of the substitutive thermal conductivity coefficient of cold dried moulds made from sands with furanic resin binders. The time related variation curves of temperature were determined for certain points of a cast part and of the casting mould. The experimental curves were compared to the cooling curves determined by computer simulation of the solidification of the same parts. Solidification was simulated for castings including cast iron plates with a = 20 mm wall thickness. Several successive simulations were carried out for different values of the substitutive thermal conductivity coefficient, until the real solidification time of the casting, experimentally determined by advanced thermal analysis, corresponded with the solidification time obtained by simulation.

**Key words:** solidification, simulation, casting, mould.

Knowing the value of the thermal conductivity coefficient of casting moulds is important for a realistic simulation of the solidification of castings. Typically solidification simulation software uses mean substitutive values of this coefficient. Utilization of the mean substitutive value of the thermal conductivity coefficient of the mould allows a simpler structure of the mathematical models and of the software. Consequently computers of lesser performance can be used for simulation, with a shorter duration of simulations. The value of the substitutive thermal conductivity coefficient of moulds is influenced by several factors:  type of the moulding sand, nature and content of the materials of the sand recipe, degree of stamping, sand graining, nature of the cast alloy, casting temperature of the alloy. Hence the requirement that, in order to implement specific solidification simulation software in the design of casting processes in foundries, the simulated results are compared to experimental ones, in order to ensure the veracity of simulation in the conditions of the respective foundry.

The matching of experimental results to simulated ones can be achieved in several ways:
- by comparison of the position of the experimentally obtained shrinkholes to the position of the hotspots obtained by simulation;
- by comparison of the time related variation curves of temperature in various points of the cast part as well as of the mould;
- by comparison of the solidification time measured experimentally in various points of the part with the solidification time obtained by simulation;

-   by comparison of the temperature distribution measured experimentally in a cross-section of the cast part with the simulated field in the same section and at the same time;
-   by comparison of the solidification time measured experimentally in the hot spots with the simulated values;
-   by verification of the experimentally determined shrinkhole volumes with the simulated ones, etc.

At the Faculty of Materials Science and Engineering of the Transilvania University of Braşov 2D software was developed based on a finite differences mathematical model, destined for the simulation of solidification of parts cast from eutectic grey cast iron. The paper presents the results obtained by the authors with regard to the determination of the value of the substitutive thermal conductivity coefficient for moulds made from chemically cold dry sand with furanic resin binder. The method of advanced thermal analysis was applied. The variation curves of temperature in several points of the cast part and of the mould were compared to the curves experimentally determined by advanced thermal analysis. The experimental determinations were carried out in the metal casting laboratory of the Faculty of Materials Science and Engineering of the Politehnica University of Bucharest, and simulations in the Laboratory for Modelling and optimisation of Metallurgical Processes of the Faculty of Materials Science and Engineering of the Transilvania University of Braşov.
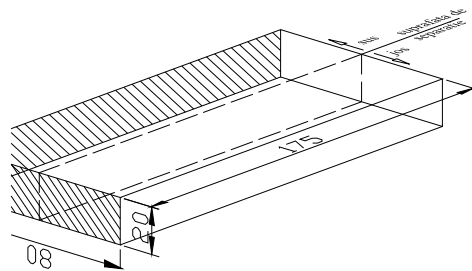


*Fig. 1. Experimentally cast part for the determination of temperature variation curves during alloy solidification.*

The part cast for this purpose was a grey cast iron plate of 20 mm thickness, as shown in figure 1. Figure 2 shows the assembly of the form used for casting. Points A, B, C and D are highlighted, where the time related experimental variation curves of temperature were determined. Table 1 includes the chemical composition of the grey cast iron used for the experiment, and table 2 the composition of the utilized moulding sand.

Figure 3 shows the execution of the casting form and the mounting of the thermocouples for temperature measurement. Figure 4 shows the casting of the alloy within the experiment.
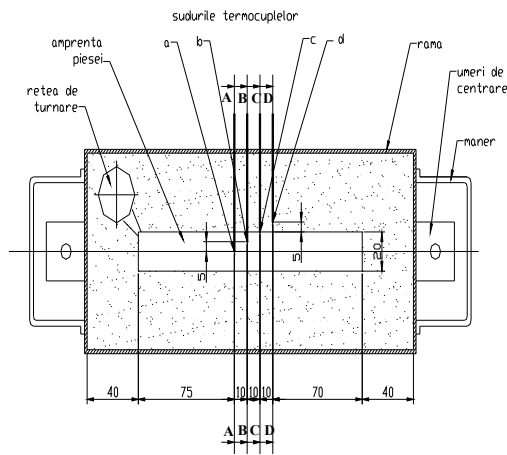
*Fig.2. Assembly of the casting mould and location of the points time related temperature measurement - A, B, C, D.*

*Table 1. Chemical composition of the cast iron used for the casting of the test pieces within the experiment.*

| No. | No. of test piece | Fe | C | Si | Mn | Ni | Cr | P | S |
|-----|-------------------|------|------|------|------|-------|-------|-------|-----|
| Unit of measure | | % | % | % | % | % | % | % | % |
| 1 | Test piece 1 | Base | 3.64 | 2.03 | 0.41 | 0.036 | 0.089 | 0.077 | 0.1 |

*Table 2. Composition of the sand used for the moulds.*

| No. | Type of moulding sand | Composition of the moulding sand, in % | | | | | |
|-----|-----------------------|-------------|------|-----------|-------|---------------|--------------------------------|
| | | Quartz sand | Clay | Bentonite | Water | Furanic resin | Hardener (Orthophosphoric acid) |
| 1 | Furanic resin | 100 | 0 | 0 | - | 4 (over 100%) | 30% from furanic resin |



*Fig. 3. Location of thermocouples on the mould during casting.*

*Fig.4. Mould casting of the liquid cast iron*

The time related variation curves of temperature based on advanced thermal analysis of cast iron allow determining the time related variation of the cooling rate. Based on analysis and interpretation of the data provided by these curves the temperature and time can be established at that phase transformations occur in the studied alloys. Figure 5 shows two such curves for a grey cast iron: the time related variation of temperature and the curve of the 1$^{st}$ order derivative (time related variation of the cooling rate). The start and end points of the transformations are highlighted by the points of inflexion on the cooling curves, and the extreme points on the variation curve of the cooling rate. Table 3 shows the symbols and significance of the real critical points highlighted by these curves. The computer programme developed for data processing within advance thermal analysis allows the calculation of higher order derivatives of the time related variation curves of temperature. These derivatives signify the variations of the phase transformation rate (acceleration), solidification included. The computer programme also allows the plotting of the curves representing these accelerations versus time, thus permitting interpretations related to the kinetics of the transformation. These data carry, however, no importance for the analysis of macro-solidification, hence these curves being not plotted anymore within this experiment.
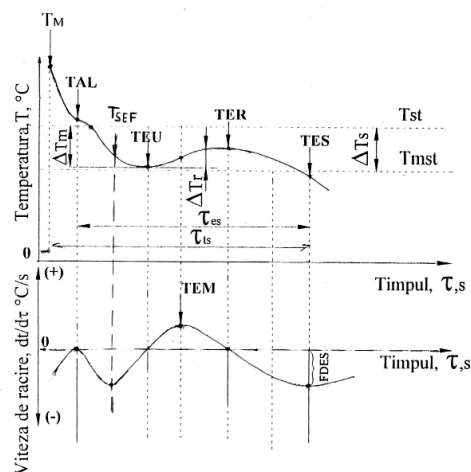


*Fig. 5. Diagram of the advanced thermal analysis curves for a grey cast iron.*

*Table 3. Notations and significance of the coordinates of the transformation points (temperature, time) highlighted by advanced thermal analysis.*

| No. | Symbol | Unit of measure | Physical significance |
|-----|--------|------------------|------------------------|
| 1 | $T_0$ | $^0C$ | Start (initial) temperature |
| 2 | $\tau_0$ | s | Start (initial) time |
| 3 | $T_M$ | $^0C$ | Maximum temperature of the liquid cast iron in the mould |
| 4 | $\tau_M$ | s | Moment when $T_M$ is reached |
| 5 | $T_{AL}$ | $^0C$ | Liquidus temperature of austenite |
| 6 | $\tau_{TAL}$ | s | Moment when $T_{AL}$ is reached |
| 7 | $T_{SEF}$ | $^0C$ | Starting moment of eutectic germination |
| 8 | $\tau_{TEF}$ | s | Moment when $T_{SEF}$ is reached |
| 9 | $T_{EU}$ | $^0C$ | Temperature of eutectic subcooling (minimum temperature of the eutectic transformation) |
| 10 | $\tau_{TEU}$ | s | Moment when $T_{EU}$ is reached |
| 11 | $T_{TEM}$ | $^0C$ | Temperature corresponding to the maximum recalescence (reheating) rate determined by the release of latent solidification heat |
| 12 | $\tau_{TEM}$ | s | Moment when $T_{TEM}$ is reached |
| 13 | $T_{ER}$ | $^0C$ | Maximum temperature reached consequently to recalescence generated by the eutectic transformation |
| 14 | $\tau_{TER}$ | s | Moment when $T_{TER}$ is reached |
| 15 | $T_{ES}$ | $^0C$ | Solidus temperature (temperature at end of solidification) |
| 16 | $\tau_{TES}$ | s | Moment when TES is reached |
| 17 | $F_{DES}$ | $^0C/s$ | Minimum value of the first derivative at the end of solidification |
| 18 | $T_{st}$ | $^0C$ | Theoretical eutectic temperature according to the stable diagram |
| 19 | $T_{mst}$ | $^0C$ | Theoretical eutectic temperature according to the meta-stable diagram |
| 20 | $\Delta Tm$ | $^0C$ | Maximum degree of subcooling ($\Delta Tm = TST - TEU$) |
| 21 | $\Delta Tr$ | $^0C$ | Reheating ($\Delta Tr = TER - TEU$) |
| 22 | $\Delta Ts$ | $^0C$ | Domain of equilibrium of eutectic temperatures ($\Delta Ts = Tst - Tmet$) |

The paper presents the results related to the comparison of the temperature variation curves in point A at the centre of the part. Figure 6 shows the experimentally determined curves for the variation of temperature and cooling rate in point A (at the centre of the cast part) for a casting mould made from chemically hardened sand with furanic resin binder.
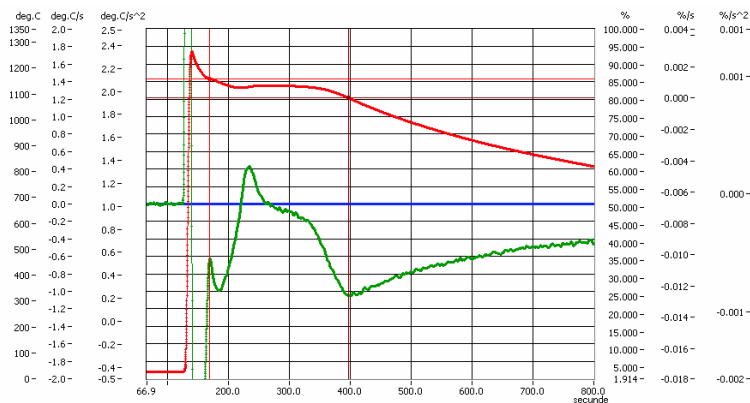


*Fig. 6. Variation of temperature and cooling rate in point A (centre of the part) for a part cast in the mould made from chemically hardened sand with furanic resin binder.*

*Table 4. Experimental results obtained by processing of the recorded advanced thermal analysis curves.*

| No. | Type of mould | Position of thermo-couple | Measured quantity | | | | | | | | | | | |
|---|---|---|---|---|---|---|---|---|---|---|---|---|---|---|
| | | | $\dfrac{T_0}{\tau_0}$ | $\dfrac{T_M}{\tau_M}$ | $\dfrac{T_{AL}}{\tau_{TAL}}$ | $\dfrac{T_{SEF}}{\tau_{SEF}}$ | $\dfrac{T_{EU}}{\tau_{TEU}}$ | $\dfrac{T_{TEM}}{\tau_{TEM}}$ | $\dfrac{T_{ER}}{\tau_{TER}}$ | $\dfrac{T_{ES}}{\tau_{TES}}$ | $F_{DES}$ | $T_{ST}$ | $T_{met}$ |
| Unit of measure | | | $\dfrac{^0C}{s}$ | $\dfrac{^0C}{s}$ | $\dfrac{^0C}{s}$ | $\dfrac{^0C}{s}$ | $\dfrac{^0C}{s}$ | $\dfrac{^0C}{s}$ | $\dfrac{^0C}{s}$ | $\dfrac{^0C}{s}$ | $\dfrac{^0C}{s}$ | $^0C$ | $^0C$ |
| 1 | Furanic resin | A | 27.3 127.3 | 1262.6 140.3 | 1158.7 170.0 | 1145.0 185.5 | 1123.5 221.5 | 1127.2 234.1 | 1132.9 267.9 | 1084.1 397.8 | - 1.054 | 1139.4 | 1122.6 |
| 2 | Furanic resin | B | 27.5 127.3 | 1232.8 141.7 | No | No | 1104.2 220.1 | 1105.7 231.3 | 1108.6 256.9 | 1060.3 399.5 | - 0.984 | | |
| 3 | Furanic resin | C | 27.1 127.3 | 1174.2 142.4 | No | No | 1065.6 223.7 | 1067 236.9 | 1069 270.3 | 1028.8 400.7 | - 0.911 | | |

The measured experimental values featured in table 4 allow the determination of the real solidification time in point A, the centre of the cast part, by equation (1):

$$\tau_S = \tau_{TES} - \tau_M = 397.8\text{-}140.3 = 257.5s \qquad\qquad (1)$$

In order to determine the mean substitutive value of the thermal conductivity coefficient that ensures a realistic simulation of the solidification of cast parts in such moulds, several successive simulations were carried out, for various values of this coefficient. The utilized values of the thermal conductivity coefficient were between $0.55 \div 1.05$ W/m/K. A total of 6 simulations were carried out.

The conditions for the simulations were:
- Side of lattice $\Delta$=0.001m,
- Time increment $\tau$= 0.02s;
- Temperature of the exterior environment $T_{ex}$=27.3 $^0$C;
- Coefficient of heat exchange with the exterior environment: $\alpha_{ex}$=10.0W/m$^2$/K;
- Solidus temperature of the alloy $T_{sme}$ = 1123.5 $^0$C;
- Thermal conductivity coefficient of the mould $\lambda_{fo}$ = 0.55; 1.05; 0.90; 0.82; 0.84 W/m/K;
- Thermal conductivity coefficient in the solid state of the cast alloy $\lambda_{sme}$ = 40W/m/K;
- Thermal conductivity coefficient in the liquid state of the cast alloy $\lambda_{lme}$ = 30 W/m/K;
- Specific heat of the mould $C_{fo}$ = 1170J/kg/K;
- Specific heat in the liquid state of the alloy $C_{lme}$ = 850W/Kg/K;
- Specific heat in the solid state of the alloy $C_{sme}$ = 750W/Kg/K;
- Density of the mould $\rho_{fo}$ = 1550Kg/m$^3$;
- Density of the alloy $\rho_{me}$ = 6700Kg/m$^3$;
- Initial temperature of the mould $T_{0fo}$=27.3 $^0$C;

The first two simulations considered a uniform initial temperature of the liquid alloy across the part section. The temperature in all points was assumed equal to the temperature in the part axis. Experimental measurements however, have shown that the initial temperature of the liquid alloy (temperature at time zero of experimental recordings) is not uniform through the part wall. The real temperature of the alloy is

greater along the axis of the part wall and falls towards the part – mould contact surface. This is due to the cooling of the alloy during the filling of the form. Hence the subsequent simulations (simulations 3 ÷ 6) considered a variable initial temperature of the liquid alloy through the part wall.

Table 5 shows the values of the initial temperatures of the liquid alloy considered for simulations 3÷ 6. Figures 7 ÷ 12 show the variation curves of temperature in point A at the centre of the cast part, obtained for the 6 simulations.

*Table 5. Values of the thermo-physical quantities used for the simulations (simulations 3 ÷ 6) for establishing the mean substitutive value of the conductivity coefficient of sand forms with furanic resin binder.*

| No. | Thermo-physical quantity | Physical symbol | Value $^0$C |
|-----|---|---|---|
| 1 | Initial temperature of the cast alloy in the part axis | $T_{ome}$ i=50 or 51 | 1262.6 |
| 2 | Initial temperature of the cast alloy at 1 mm distance from the part axis | $T_{ome}$ i=49 or 52 | 1256.6 |
| 3 | Initial temperature of the cast alloy at 2 mm distance from the part axis | $T_{ome}$ i=48 or 53 | 1250.6 |
| 4 | Initial temperature of the cast alloy at 3 mm distance from the part axis | $T_{ome}$ i=47 or 54 | 1244.6 |
| 5 | Initial temperature of the cast alloy at 4 mm distance from the part axis | $T_{ome}$ i=46 or 55 | 1238.6 |
| 6 | Initial temperature of the cast alloy at 5 mm distance from the part axis | $T_{ome}$ i=45 or 56 | 1232.6 |
| 7 | Initial temperature of the cast alloy at 6 mm distance from the part axis | $T_{ome}$ i=44 or 57 | 1218.6 |
| 8 | Initial temperature of the cast alloy at 7 mm distance from the part axis | $T_{ome}$ i=43 or 58 | 1204.6 |
| 9 | Initial temperature of the cast alloy at 8 mm distance from the part axis | $T_{ome}$ i=42 or 59 | 1190.6 |
| 10 | Initial temperature of the cast alloy at 9 mm distance from the part axis | $T_{ome}$ i=41 or 60 | 1174.6 |
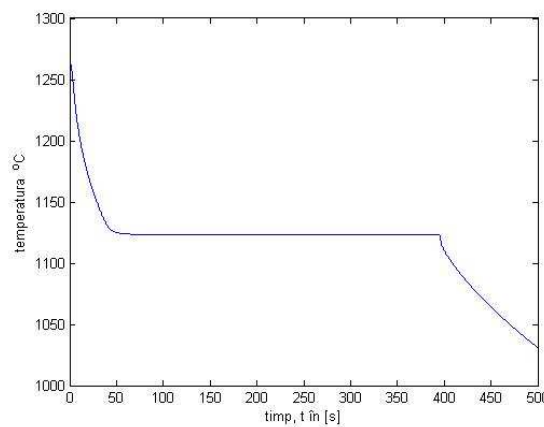


*Figure 7. Variation of temperature in point A versus time for simulation 1, $\lambda_{fo}$ = 0.55 W/m/K and uniform initial temperature of the metal in the part print*
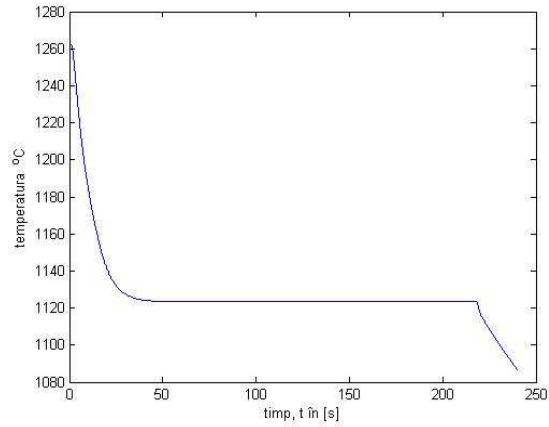
*Figure 8. Variation of temperature in point A versus time for simulation 2, $\lambda_{fo}$ = 1.05 W/m/K and uniform initial temperature of the metal in the part print.*
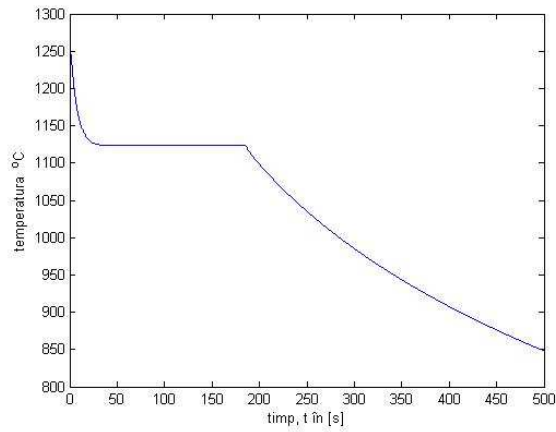


*Figure 9. Variation of temperature in point A versus time for simulation 3, $\lambda_{fo}$=1.05 W/m/K and variable initial temperature of metal in the part print*
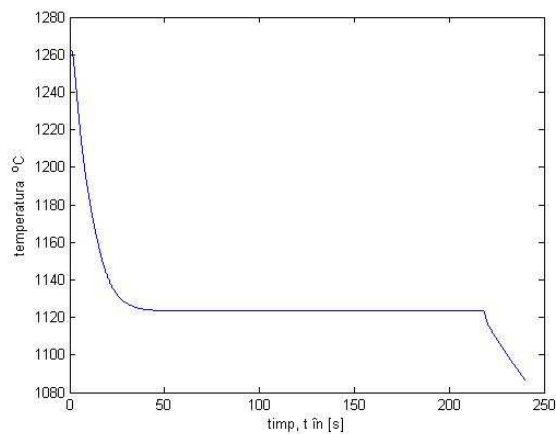


*Figure 10. Variation of temperature in point A versus time for simulation 4, $\lambda_{fo}$=0.90 W/m/K and variable initial temperature of metal in the part print*
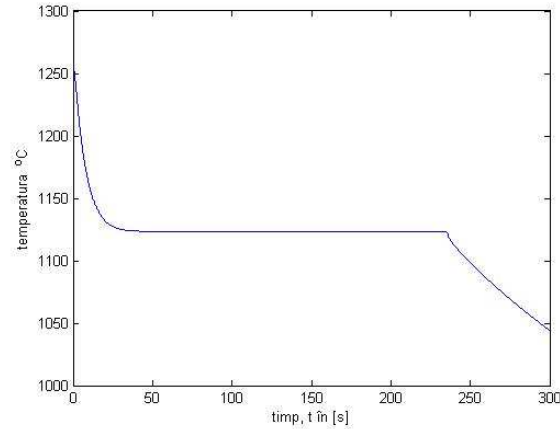
*Figure 11. Variation of temperature in point A versus time for simulation 5, $\lambda_{fo}$=0.82 W/m/K and variable initial temperature of metal in the part print*
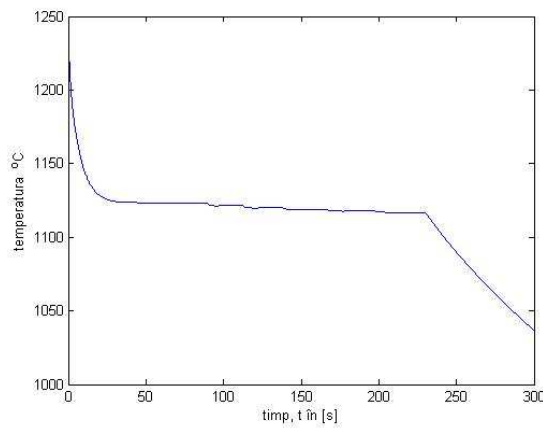


*Figure 12. Variation of temperature in point A versus time for simulation 6, $\lambda_{fo}$=0.84 W/m/K and variable initial temperature of metal in the part print*

*Table 6. Comparison of the experimentally measured results by advanced thermal analysis with the simulated ones, for the solidification of the plate of 20 mm thickness. Casting in sand moulds with furanic resin binder.*

| Point on the part | Experiment | | | Simulation | | | |
|---|---|---|---|---|---|---|---|
| | Initial temp. | Temp. at the end of solidification | Solidif. time | Coef. of thermal conductivity | Initial temp. of alloy | Temp. at the end of solidification | Solidif. time |
| Unit of measure. | $^0$C | $^0$C | s | W/m/K | $^0$C | $^0$C | s |
| A | 1262.6 | 1084.1 | 257.5 | 0.55 | 1262.6 | 1084.1 | 425.6 |
| | | | | 1.05 | 1262.6 | 1084.1 | 242.0 |
| | | | | 1.05 | 1262.6 | 1084.1 | 210.6 |
| | | | | 0.90 | 1262.6 | 1084.1 | 241.5 |
| | | | | 0.82 | 1262.6 | 1084.1 | 262.1 |
| | | | | 0.84 | 1262.6 | 1084.1 | 256.3 |

**Remark**: In simulations 1 and 2 the temperature of the liquid alloy in the part print was considered uniform through the part section.

Table 6 gives the values of the solidification time determined in the six simulations. The temperature at the end of solidification was assumed as $T_{ES}=1084.1$, this being the real temperature at the end of solidification revealed by advanced thermal analysis on the curve of the first derivative of temperature. This moment practically corresponds to the moment of solidification of the phosphorous eutectic and is smaller than the Fe-C eutectic temperature. Comparing the values of the solidification time determined by simulation and given in table 6 with the solidification time determined experimentally (equation 1) it can be noticed that these values correspond, in the case of a mean substitutive thermal conductivity coefficient of the mould of $\lambda_{fo} = 0.84$ W/m/K.

## REFERENCES

1. Sillen R. – **Stabilirea punctului eutectic real  - o condiţie esenţială pentru un control efficient al fontelor cu grafit nodula**r [Finding the true eutectic point – an essential task for efficient control of ductile iron]. In: *Revista de turnătorie*, no. 7/8, 2007, pp.10-11, Romania.
2. Sillen R. – **Producerea pieselor din grafit nodular fără maselote** [Production of ductile iron castings without feeders]. In: *Revista de turnătorie*, no. 5/6, 2007, pp. 3- 8, Romania.
3. Labreque C., Gagne M., – **Interpretarea curbelor de răcire a fontelor. Sinteză din literatura de specialitate** [Interpretation of cooling curves of cast irons. A literature review]. In: *Revista de turnătorie*, no. 11/12, 2007, pp. 22- 31, Romania.
4. Soporan V., Vamoş C., Pavai C. – **The numerical modelling of the solidification process**, Ed. Dacia, Cluj – Napoca, 2003.
5. Maşniţă, M., Ciobanu, I., Monescu, V., - **Research on the development of a program to simulate the solidification of castings using MATLAB**. In: *Metalurgia*, no. 7, 2006.
6. Maşniţă, M., Ciobanu, I., Monescu V., - **Computer programme to simulate the macro-solidification of a casting using MATLAB**. In: *RECENT,* no. 17, June 2006, pp. 61-67.

### DETERMINAREA COEFICIENTULUI MEDIU SUBSTITUTIV DE CONDUCTIVITATE TERMICĂ A FORMELOR ÎNTĂRITE LA RECE CU LIANT RĂŞINĂ FURANICĂ

**Rezumat:** Se prezintă rezultatele unei cercetări experimentale privind determinarea valorii coeficientului de conductivitate termică substitutiv al formelor întărite chimic la rece din amestec de formare cu liant din răşină furanică. S-au determinat experimental curbele de variaţie a temperaturii în funcţie de timp în puncte ale unei piese turnate şi al formei de turnare. Curbele experimentale s-au comparat cu curbele de răcire determinate prin simulare pe calculator la solidificarea aceloraşi piese. Piesele turnate a căror solidificare a fost simulată au fost plăci din fontă cu grosimea de perete a=20mm. S-au efectuat mai multe simulări succesive pentru valori diferite ale coeficientului de conductibilitate termică substitutiv, până când timpul real de solidificare al piesei turnate determinat experimental prin analiză termică avansată a corespuns cu timpul de solidificare determinat prin simulare

# ERRORS AT CASTINGS SOLIDIFICATION ANALYSIS BASED ON SOLIDIFICATION MODULE

BY

## IOAN CIOBANU; SORIN IOAN MUNTEANU; AUREL CRIŞAN; TIBOR BEDO

**Abstract**: It is shown that the solidification module, so that is calculated till now (the rapport between the casting volume and its contact aria with mould and cores) and called by the authors the geometric (or ideal) solidification module, isn't always correlated with the solidification time of castings. For this reason there is proposed a new equation to calculate the real solidification module. This attends to the real solidification conditions of castings inside the mould.

**Key words:** solidification, mathematical modelling , casting, solidification module

## 1. Introduction

One of the most important problems to be solved in relation to the design of casting technologies concerns the dimensioning of shrinkheads. A well-known method for shrinkhead design is based on the analysis of castings by means of the solidification module. This method has the following advantages:
- entails simple calculations;
- it is accessible to personnel of secondary education training level;
- allows swift decision making;
- it has general applicability;
- yields good or satisfying results, if correctly applied.
The paper shows that the computational relation of the solidification module, as known in literature at present may yield errors. By knowing these errors measures can be taken to avoid them. Starting from these errors an improved relation is proposed for the computation of the solidification module, taking into account the real conditions of solidification of parts and shrinkheads in the casting mould.

## 2. Geometrical solidification module

The concept of casting solidification module was initiated by Chvorinov in 1939 [1;2]. He calculated the solidification time for a plate of finite thickness "a" starting from analytical equations of the temperature field in casting and mould wall (equations established by Stephan in 1830 and Schwartz in 1931). These equations were established based on the following hypotheses:
- the contact surface between casting and mould is planar and infinite;
- the casting has infinite thickness;
- the mould wall has infinite thickness;

- the alloy solidifies at constant temperature($T_{Sme}$ – pure metal or eutectic alloy);
- the initial temperature inside the liquid alloy is uniform inside all part volume ($T_{0me}$);
- the initial temperature in the mould wall is uniform ($T_{0f}$);
- the mould instantaneous fill with liquid alloy;
- at metal–mould interface there is establishes in the first moment an initial contact temperature ($T_c$) which rest constant until the complete solidification of the part;
- the thermal characteristics of the liquid alloy ($\lambda_L$, $c_L$, $\rho_L$), of the solidified alloy ($\lambda_S$, $c_S$, $\rho_S$) and of the mould ($\lambda_f$, $c_f$, $\rho_f$) do not vary with temperature;
- the heat transmission in the system alloy-mould is made only by conductivity conforming with the Fourier equation;
- the heat transmission in the system alloy-mould is made unidirectional perpendicular on the metal-mould interface;

To calculate the solidification time for a plate type part, with finite thickness „a", the followings hypotheses are assumed by Chvorinov:

-  the analytic expression validity, for the temperature field established by Stephan and Schwartz is extended for the case of finite thickness parts;

-  it is assumed that the part solidification ends in the moment when the casting axis solidifies;

- the temperature gradient inside the part wall in the moment of its axis solidification ( part solidification end) is very small because of the alloy high thermal conductivity in solid state and can be neglected;

- the heat released by casting until solidification is entirely absorbed by the mould.

Based on these hypotheses, the solidification time analytic expression for a part with finite thickness can be determined writing the thermal balance between the heat released by the part to solidify ($Q_{rel}$) and the heat absorbed by the mould wall throw thermal conductibility at the part-mould interface ($Q_{abs}$) :

Equalizing, the heat released by part till solidification and the heat absorbed by mould, it obtains the equation:

$$\frac{2}{\sqrt{\pi}} \cdot \sqrt{\lambda_f \cdot c_f \cdot \rho_f} \cdot (T_c - T_{0f}) \cdot S \cdot \sqrt{t_s} = m[c_L(T_{0me} - T_{Sme}) + L] \tag{1}$$

where $t_S$ – represent the part solidification time; $\rho$ – density, c – specific heat, $\lambda$ – thermal conductivity, L – specific latent heat. The heat released by the part are write for the very small temperature gradient inside the part wall in the moment of solidification end.

In the case of a plate with finite thickness „a", cooled on the both sides, the solidification ends when the solidification front traverse the distance „a/2" (half of plate thickness). Replacing the mass for „a/2" part thickness in equation (1), by the equation m = V·$\rho_L$, it can be obtained the equation to calculate the solidification time „$t_S$" for the plate with thickness „a" and bilateral cooling. This is the same as the solidification time for a plate with thickness „a/2" and one side cooling:

$$t_S = \frac{\pi \cdot \rho_L^2 \cdot [c_L \cdot (T_{0me} - T_{Sme}) + L]^2}{4 \cdot \lambda_f \cdot c_f \cdot \rho_f \cdot (T_c - T_{0f})^2} \cdot \left(\frac{V}{S}\right)^2 \tag{2}$$

The first fraction represent a constant that depends of cast alloy and mould characteristics. The V/S fraction depend of casting geometry and was named by Chvorinov as „M' - **solidification module** of casting. So the equation (2) can be write as:

$$t_S = \frac{1}{k_S^2} \cdot \left(\frac{V}{S}\right)^2 = \frac{1}{k_S^2} \cdot M^2 \tag{3}$$

In this equation $k_S$ is named solidification constant given by the equation:

$$k_S = \frac{2\sqrt{\lambda_f \cdot c_f \cdot \rho_f} \cdot (T_c - T_{0f})}{\sqrt{\pi} \cdot \rho_L \cdot [c_L \cdot (T_{0me} - T_{Sme}) + L]} \tag{4}$$

From the equation (3) it can be observed that the solidification time for a plate with finite thickness „a" is direct proportional with square of the ratio between plate volume and contact surface with mould (the entire cooling surface of the plate) ratio named by Chvorinov as **solidification module** of casting that represent a geometric characteristics. Based on this observations Chvorinov extended the solidification time equation (3) established for a plate with finite thickness, at solidification time calculation for all castings (or zones of castings ) with any geometry. Because the solidification module calculated by Chvorinov equation depends only of casting geometry, we shall name the solidification module calculated with this equation as **geometrical solidification module ($M_g$)**. So:

$$M_g = \frac{V_{piesa}}{S_{racire}} \tag{5}$$

In some technical papers the geometrical solidification module is named equivalent thickness, equivalent radius or even **ideal solidification module**. The solidification module can by calculated for casting or for any casting zone. The castings feeders design based on solidification module considers the directional solidification principle from casing towards feeder. The feeders must be situated in the part zone that has the greatest solidification module, and the solidification module of divers zones of part must decrease towards feeder. The feeder must have a solidification module 1.2 ÷ 1.4 times higher than the part zone module where it is placed.

## 3. Errors at castings solidification analysis based on geometrical solidification module

The solidification module calculated with the equation (5), equation recommended now in technical literature, represents an **ideal solidification module** of castings because this equation suppose that the heat transfer during solidification, from casting to mould, develop with the same intensity throw entire contact surface between liquid metal and mould. In other words this equation started from the supposition that all casting surfaces contribute at part solidification in rapport with surfaces area. This hypothesis is true only in the case of parts with simple geometry (plate, long cylinder, sphere, massive parts without cut-off, protrusions or holes, generally parts bordered by convex surfaces)

The equation (3) shows that castings with higher solidification module have a longer solidification time. Continuing we shall analyze the case of some parts with simple geometry comparing their geometrical solidification module and their solidification time.

In the table 1 is given the geometrical solidification module value for parts with very simple geometry calculated with equation (5).

*Table 1. Geometrical solidification module values for parts with simple geometry.*
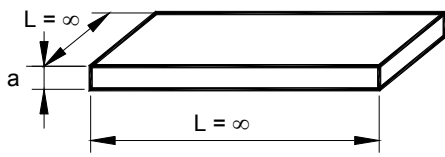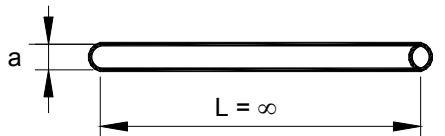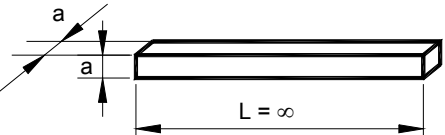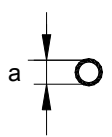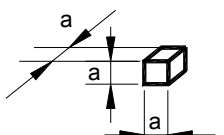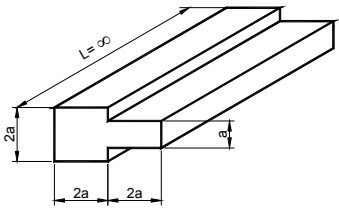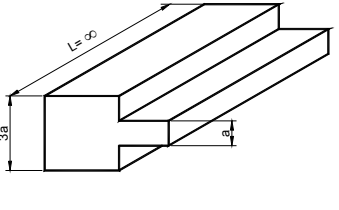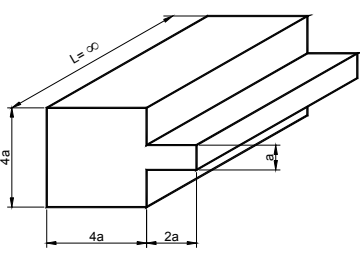
| No. | Casting sketch | Casting type | Geometric solidification module $M_g$ |
|---|---|---|---|
| 1 |  | Plate | $M_g = a/2$ |
| 2 |  | Cylindrical bar | $M_g = a/4$ |
| 3 |  | Square bar | $M_g = a/4$ |
| 4 |  | Sphere | $M_g = a/6$ |
| 5 |  | Cube | $M_g = a/6$ |

*Table 2. Geometrical solidification module values for parts without cavities.*

| No. | Casting sketch | Geometric solidification module Mg |
|-----|----------------|-----------------------------------|
| 1 |  | $M_g = 0.500a$ |
| 2 |  | $M = 0.687a$ |
| 3 |  | $M_g = 0.900a$ |

The solidification module values calculated with equation (5) for some massive parts without cavities are given in the table 2.

Comparing the geometric solidification module values from tables 1 and 2 with real data about castings solidification time, it can be observed that these are in accord with equation (3), so the parts with greater geometric solidification module have longer solidification time.

In the following, we show that the equation (3) about proportionality between the solidification time and the square of geometric solidification module isn't true for all castings. In the case of castings with complex geometry especially with cut off (concave surfaces) or small holes in rapport with wall thickness of the part, the solidification time estimation based on geometric solidification module, lead to wrong results.

In the case of cast parts of complex geometry, particularly with cavities (concave surfaces) or small openings in relation to the wall thickness of the part, the estimation of the solidification time based on the geometric solidification module leads to erroneous results.

This assertion is proved by the presentation of the case of solidification of cylindrical tube type parts, as shown in figure 1. The geometric solidification module computed by relation (5) for cylindrical tubular parts of wall thickness „a", of various internal radii ($r = 0$; $r = a$, $r = 2a$, $r = 6a$) and infinite length is in all cases the same, that is $Mg = a/2$. In this case relation (3) yields the conclusion that all cylindrical tubular parts of the same wall thickness have the same solidification time. Computer

simulation of the solidification of these parts, as well as experimental  measurements of the solidification time have shown that in reality the solidification time of tubular cylindrical parts depends on the d/a ratio. In the case of parts of small interior diameter (d/a < 2) the solidification time of the tubular cylindrical parts does not respect the proportionality with the square of the geometric solidification module (relation 3). This deviation is explained by the fact that in the case of parts with small interior diameter, the moulding batch inside (core) highly heats reducing the cooling capacity throw part interior surface.  It results that the real solidification module of tubular parts with small interior diameter (r < 2a) is different than geometric solidification module.
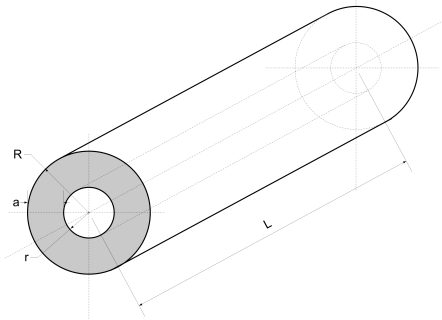


*Figure 1. Cylindrical tubular parts. Mg =a/2.*

*Table 3. Geometrical solidification module for U shape cast bars*

| No. | Casting sketch | Geometric solidification module Mg |
|-----|----------------|-------------------------------------|
| 1 |  | $M_g = \dfrac{61}{133}a = 0,458a$ |
| 2 |  | $M_g = \dfrac{13}{28}a = 0,464a$ |
| 3 |  | $M_g = \dfrac{17}{36}a = 0,472a$ |

In the table 3 there is presented another type of parts where the proportionality between the solidification time and the square of geometric solidification module isn't valid. This is the case of bars with U section, with wall thickness „a" and divers values for the opening „b", between parallel arms of the profile. In the table 3 is given the geometric solidification module for the distances b = a/5; b = a; b = 5a.

From this table we can see that by increasing the „b" distance between parallel arms of the profile, the casting solidification module Mg increase too from 0.458a to 0.464a and than to 0.472a. The increase of the solidification module induce the conclusion that the solidification time must be longer by increasing the „b" distance between parallel arms of the profile. This theoretical conclusion is opposed to experimental result. To better evidence this thing a systematic study was made by computer solidification simulation for bars with „U" section with the dimensions given in figure 2 and wall thickness a=20mm and c= 60mm. The „b" distance was varied in steps.
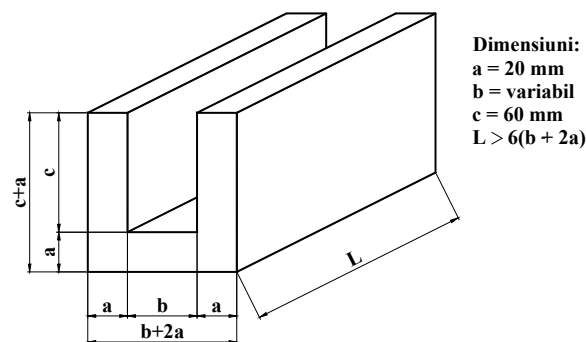


*Figure 2. The shape and dimensions for U bars U(axb)*

In the table 4 there are given the geometric solidification module values calculated with the following equation:

$$M_g = \frac{a(2a+b+2c)}{6a+2b+4c} \tag{6}$$

where a, b, c – are the part dimensions from figure 2. The equation (6) is obtained from equation (5) in the conditions of infinite length part.

*Table 4. Geometrical solidification module for U shape cast bars (a=20mm) in function of b dimension and geometrical characteristic b/a.*

| No. | Part symbol Ua×b | Dimension b [mm] | Geometrical characteristic of the section b/a | Geometrical solidification module Mg [mm] |
|---|---|---|---|---|
| 1 | U20×0 | 0 | 0 | 8.89 |
| 2 | U20×4 | 4 | 0.2 | 8.91 |
| 3 | U20×12 | 12 | 0.6 | 8.96 |
| 4 | U20×20 | 20 | 1.0 | 9.00 |
| 5 | U20×40 | 40 | 2.0 | 9.09 |
| 6 | U20×80 | 80 | 4.0 | 9.23 |
| 7 | U20×120 | 120 | 6.0 | 9.33 |
| 8 | U20×300 | 300 | 15.0 | 9.58 |

In the table 5 there are given the solidification time values (determined by simulation) for these bars. The solidification simulation was realized for the case of castings of eutectic grey cast iron in the following conditions: $T_{0me}=$ 1350$^o$C, $T_{SMe}$=1150$^o$C, $c_S$=750J/kg·K, $\rho_L = \rho_S$=6700kg/m$^3$, $\lambda_S$=40W/mK, $c_L$ =850J/kg·K, $\lambda_L$=30W/mK, $T_{0f}$=20$^o$C, $c_f$=1170J/kg·K, $\rho_f$=1550kg/m$^3$, $\lambda_f$=0,55W/mK. Figure 3 presents the geometrical solidification module dependence of the equivalent inner opening of the profile (b/a), while figure 4 represent the solidification time (obtained by simulation) dependence of the rapport b/a. It can be observed that nor in the case of these parts the proportionality with the square of geometric solidification module (eq. 3) is respected. These results conclude that in the case of bars with „U" section, the real solidification module that verifies the equation (3) is different from the geometric solidification module.

*Table 5. Solidification time for U shape cast bars (a=20mm) determined by simulation in function of b dimension and geometrical characteristic b/a.*

| No. | Part symbol Ua×b | Dimension b [mm] | Geometrical characteristic of the section b/a | Solidification time ts [s] |
|-----|------------------|------------------|-----------------------------------------------|----------------------------|
| 1 | U20×0 | 0 | 0 | 747.35 |
| 2 | U20×4 | 4 | 0.2 | 692.80 |
| 3 | U20×12 | 12 | 0.6 | 596.10 |
| 4 | U20×20 | 20 | 1.0 | 554.46 |
| 5 | U20×40 | 40 | 2.0 | 522.04 |
| 6 | U20×80 | 80 | 4.0 | 492.48 |
| 7 | U20×120 | 120 | 6.0 | 489.66 |
| 8 | U20×300 | 300 | 15.0 | 489.66 |



*Figure 3. Geometrical solidification module for U section bars, in function of the b/a rapport (wall thickness a=20mm)*
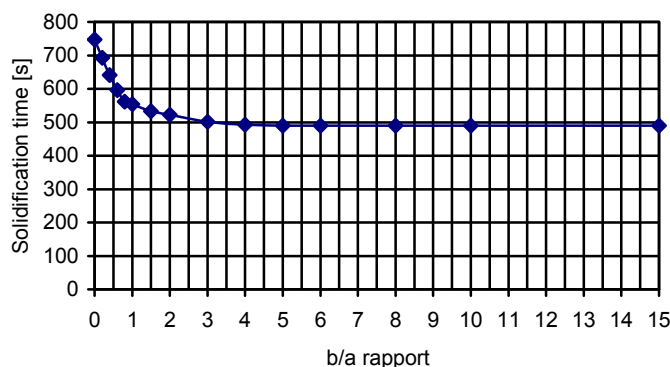
*Figure 4. Solidification time determined by solidification simulation in function of geometrical characteristic b/a, for U bars (wall thickness a=20mm)*

The results presented in figures 3 and 4 evidence that in the case of „U" bars with a small distance between parallel arms (b ≤ 5a), the solidification time is longer when „b" distance is smaller. These results are explained too by the fact that during casting the moulding batch surrounded by part (core) quickly heat at temperatures close to liquid alloy temperature. As result the heat transfer through inner surfaces reduces strongly or even stop. The moulding batch from the inner zone of the part heats quickly and stronger if the opening between arms is the smaller [5,6].

From these examples results that the geometric solidification module calculated with equation (5), that assume that all part surfaces contribute with the same intensity at its cooling and solidification, don't represents a correct base for castings solidification analysis.

## 4. The real solidification module

The authors of this paper propose a new equation to calculate the solidification module of castings, adapted to the real solidification and cooling condition of parts inside the mould. This equation allows to calculate the value of the real solidification module of castings:

$$M_r = \frac{V}{\sum_{i=1}^{n} k_i S_i} \qquad (7)$$

where: V represents the casting volume or of a portion of casting whose solidification module is calculated; n – the surfaces number that bound the casting (or casting zone) and are in contact with mould and cores (or with other casting zone) ; $S_i$ – the area of the surface indexed "i"; $k_i$ – the cooling coefficient corresponding to surface $S_i$.

The solidification module calculated with equation (7) named by us the real solidification module $(M_r)$ has the advantage that verifies the equation (3) in any cases. The cooling coefficient values $k_i$ will be calculated or adopted in function of the real contribution of the $S_i$ surface at heat transfer part-mould, during casting solidification. Its value depends on the followings factors:

- casting geometry and respective surface geometry;

- the position casting, gating system and feeders inside the mould;
- the presence of coolers or heat insulated materials in contact with some casing surfaces;
- different temperature of some mould walls (in the case of forced cooling or heating of some mould walls at casting in metal moulds).

The obtaining of correct values for the real solidification module of casting depends of the correct choosing of the cooling coefficients $k_i$. The cooling coefficients values must be fix by the equation (7) user based on theoretical computation regarding the heat transfer liquid alloy-mould in the respective zone, based on fundamental researches by computer solidification simulation or by similitude with parts with similar geometry.

In the case of external surfaces of the part where the heat transfer part-mould isn't affected by the local overheating of the mould (or core) or by others factors, the cooling coefficient has the value $k_i = 1$. In the case of internal or external cores with small volume (small thickness or diameter) comparing with the part walls thickness that surround them and quickly heat them at high temperatures, the $k_i$ coefficient has values less than one ($0 \leq k_i < 1$). In this cases the cooling coefficient usually depends of the rapport between core thickness (or the thickness of the batch moulding layer between part walls) and neighbourhood walls thickness.

In the case when on some surfaces are placed external coolers, the cooling coefficient corresponding to these surfaces has values greater that one ($k_i > 1$). The cooling coefficient value can be established in function of the rapport between cooler thickness and casting wall thickness and the thermal characteristics (specific heat, density, thermal conductivity) of the cooler and mould. In the case on some surfaces are applied refractory insulated paint or insulated core the cooling coefficient has values less then one ($k_i < 1$). In the case when some parts of the mould are forced heated or cooled (ex. at casting in metal moulds) the cooling coefficient can be established in function of the temperature of the mould wall in contact with the studied surface and the temperature in the rest of the mould.

The part position inside the mould, the gate system and feeders layout can influence **the real solidification module** of castings. So in the case of simultaneously casting of many parts in the same mould it is possible that the heat transfer intensity through some part surfaces to be influenced by other parts neighbourhoods or the proximity of gating system or feeders. More the attack section of the feeders and the area of the connecting section between pare and feeders must be subtract from the area of the surfaces that realise the part cooling (the area of the part surfaces in contact with the mould). In these conditions it is possible to obtain different values of the solidification module for the same part in different situations.

## 5. Conclusions

-**The geometric solidification module** calculated with the equation given in technical (Chvorinov equation) isn't correct correlated (conforming to equation 3) with the casting solidification time. The solidification module verify the equation (3) only in the case of parts without holes or cavities or in the case when these have very great dimensions comparing with casting wall thickness;

 - **The real solidification module** of castings characterises better the parts from point of view of solidification being all-time correlated with the solidification time conform with equation (3), that permit a correct analysis of casting solidification and a correct dimensioning of the feeders;

- **The real solidification module** of castings considers the real contribution of each surface at the heat transfer liquid alloy- mould during solidification;

- **The real solidification module** of castings is influenced by part geometry the presence of holes and cut-outs with small dimensions and by hot corner presence;

- **The real solidification module** of castings is influenced by the solidification conditions namely the presence at small distance of other parts, gating system, feeders as well as of the presence of coolers, core and insulated paints on some surfaces or by the temperature of some surfaces cooled or heated ;

- The cooling coefficients associated to castings surfaces used in **the real solidification module** calculation can be established based on thermodynamic calculation, based on fundamental researches by solidification simulation or by similitude,  in function of the distance between parts, surface geometry, walls temperatures, etc ;

- At the calculation of the **real solidification module** of castings the surface considered in the heat transfer part – mould must be reduced with the area of the gate runner and with the area of the channels that connect feeders to part;

## REFERENCES

1. Chvorinov N.: **Teoria solidificării pieselor turnate**, Giesserei 17 mai 1940, pag.177-186, Giesserei 31 mai 1940, pag.201-208, Giesserei 17 iunie 1940, pag.222-225.
2. Defretin G.: **Calcul des modules de solidification apparents des pieces de fonderie**,  Fonderie 384, decembrie 1978, pag. 355-361.
3. Bratu C., Sofroni L., Brabie V.: **Termofizica proceselor de turnare**, Institutul Politehnic Bucureşti, 1984
4. Sofroni L., Brabie V., Bratu C.: **Bazele teoretice ale turnării**, Editura Didactică şi Pedagogică, Bucureşti, 1980.
5. Munteanu S.I., Ciobanu I.,Crişan A.: **Simularea solidificării pieselor turnate de tipul barelor cu secţiune U** - Revista de turnătorie, nr. 9-10, 2004, ISSN 1224-21-44, pag. 25 – 29.
6. Ciobanu I., Munteanu S.I., Crişan A.: **Cercetări privind influenţa geometriei asupra solidificării barelor cu secţiune U,** Revista de turnătorie, nr. 11-12, 2004, ISSN 1224-21-44, pag. 20 – 24
7. Ciobanu I., Munteanu S., Crişan A**.:** *Influenţa  distanţei dintre piese în formă  asupra solidificării pieselor turnate,* Metalurgia, nr. 8, 1998, ISSN 0461/9579, pag. 18 – 27.
8 Soporan V., Vamoş C., Pavai C. – **The Numerical Modelling of the Solidification** Process, Ed. Dacia, Cluj – Napoca, 2003.
9. Soporan V., Constantinescu V. – **Modelling on a Macrostructural Level of the Alloy Solidification Process**, Ed. Dacia, Cluj – Napoca, 1995.
10. Soporan V., Constantinescu V., Crişan M. – **Solidification of Alloys – Theoretical Preliminaries**, Ed. Transilvania Press, Cluj – Napoca, 1995.

**ERORI LA ANALIZA SOLIDIFICĂRII PIESELOR TURNATE PE BAZA MODULULUI DE SOLIDIFICARE**

**Rezumat:** *Se arată că modulul de solidificare aşa cum se calculează în prezent (raportul dintre volumul piesei turnate şi aria suprafeţei de contact cu forma şi cu miezurile) numit de autori **modul de solidificare geometric (sau ideal)**, nu este totdeauna corelat cu timpul de solidificare al pieselor turnate. Se propune o nouă relaţie pentru calculul modulului de solidificare real al pieselor turnate. Aceasta ţine cont de condiţiile reale de solidificare a pieselor în forma de turnare.*

# EXPERIMENTAL TESTING OF SIMULATION SOFTWARE FOR THE SOLIDIFICATION PROCESSES OF CASTINGS

BY

**I. CIOBANU, S.I. MUNTEANU, A. CRISAN, M. MAŞNIŢĂ**

**Abstract**: The paper presents the results of experimental research regarding the solidification of castings from grey cast iron. The study focused on the solidification of bars of „U" shaped cross section (U section bars) of 20 mm wall thickness and various spans between the parallel arms. In the experimental castings the hot spots were identified by the position of the shrinkholes in their cross sections. In the computer simulations the hot spots were identified by analysis of the temperature field in the cast parts at the end of the solidification process. The experimental results were matched against those obtained by computer simulation.

**Key words:** solidification, simulation, cast parts, shrinkhole.

The mathematical models underlying the development of software for the simulation of cast parts solidification require the adopting of simplifying hypotheses of the physical phenomena accompanying the solidification process. Further more, the thermo-physical characteristics of the materials are not precisely known in all cases. In particular, the thermo-physical characteristics of moulds made from moulding sands have various values depending on the kind of materials included by the sand recipe, by their proportions, degree of stamping, sand graining, etc. Hence the requirement that, in order to implement specific solidification simulation software in the design of casting processes in foundries, the simulated results are compared, at least in the beginning to experimental ones.

The matching of experimental results to simulated ones can be achieved in several ways:

- by comparison of the position of the experimentally obtained shrinkholes to the position of the hotspots obtained by simulation;
- by comparison of the time related variation curves of temperature in various points of the cast part as well as of the mould;
- by comparison of the solidification time measured experimentally in various points of the part with the solidification time obtained by simulation;
- by comparison of the temperature distribution measured experimentally in a cross-section of the cast part with the simulated field in the same section and at the same time;
- by comparison of the solidification time measured experimentally in the hot spots with the simulated values;
- by verification of the experimentally determined shrinkhole volume with the simulated one, etc.

At the Faculty of Materials Science and Engineering of the Transilvania University of Braşov a 2D software was developed based on a finite differences mathematical model, destined for the simulation of solidification of parts cast from eutectic grey cast iron. The paper presents the results obtained by the authors with regard to the verification of this software by the method of comparison of the shrinkholes in the experimentally cast part with the position of the hot spots determined by simulation. This verification method is the most undemanding one as it does not require special measurement equipment, thus being usable in any foundry.

Verification has been achieved for the casting and solidification of U section bars with different spans between the parallel arms. This type of parts has been selected for the experimental research, as the symmetry of the cross section allows the utilisation of a 2D software for the subsequent simulation of the solidification. On the other hand, previous theoretical research has shown that in these parts the position of the shrinkholes is significantly influenced by the span between the parallel arms. Figure 1 presents the geometry of the U section bars used for the verification of the solidification simulation software. The cross section of the studied bar has been denoted by the symbol Uaxb, where "a" represents the thickness of the wall (a=20mm), and „b"- the span between the parallel arms.

Solidification was simulated for the casting of bars from eutectic cast iron at a casting temperature of $T_t=1350^0C$ using the values given in table 1 for the thermo-physical quantities. These values were adopted based on data from literature, used by other authors.

Table 2 features the data obtained by computer simulation of solidification, that is solidification time and the position of the hot spots. The coordinates of the hot spots are given in relation to a reference frame the origin of which lies in the intersection of the section axis with the exterior surfaces of the cross piece, as shown in figure 2.

The analysis of the distribution of hot spots in the cross section of the parts the solidification of which was studied by simulation has yielded three situations:

For bars with very small spans between the arms of the profile (b < 20 mm, and b< a, respectively) solidification ends in two symmetrical points in relation to the axis of the section. The hot spots are located on the interior part of the parallel arms (figure 3). The position of the hot spots in these parts is due to the small thickness of the moulding sand layer between the arms of the profile, thus allowing the strong heating of the moulding sand at the interior of the profile. The cooling capacity on the interior surface of the profile arms is very small, nearly zero.

For medium spans between the arms of the profile (b = 20÷40 mm, that is a ≤ b ≤ 2a) a single hot spot is generated in the part located in the cross piece connecting the two parallel arms. The hot spot is located on the symmetry axis of the section, close to the interior surface of the cross piece (figure 4). This position of the hot spots is due to the lesser heating of the moulding sand between the arms, for the considered spans of the profile. In this case the cooling capacity of the mould is affected only at the interior surface of the cross piece.

For larger spans between the parallel arms of the profile (b ≥ 60 mm, and b≥3a, respectively) also two hot spots are generated symmetrical to the section axis, located in the cross piece towards the warm corners of the section. The distance between the hot spots grows with the span between the parallel arms, their position in relation to

the warm corners of the part remaining fixed. This is due to the fact that for large spans between the arms of the profile, the cooling capacity at the interior of the part is affected only in the area of the warm corners.

In the second part, the paper presents the experimental research carried out in order to verify whether the results presented above, obtained by the simulation of solidification of U section bars using the presented thermo-physical values are confirmed by the practice of casting. Experimental research has monitored the location of the hot spots by the position of the shrinkholes, followed by the comparison of the experimental with the simulated results. For this purpose four representative bars of the simulated ones (table 2) were cast, that is U20x4, U20x20, U20x40 and U20x120. The bars were cast from Fc 250 cast iron, the various elements of their chemical composition located within the following intervals: 3.0-3.4%C, 1.8-2.5%Si, 0.6-0.8%Mn, max. 0.3% P, max. 0.12S%, the saturation degree of carbon being Sc = 0.89. Casting was carried out in moulds made from green sand, achieved by models from expanded polystyrene.

Figure 6 shows the gasification polystyrene models used for the moulds. Figure 7 shows the cast parts subsequent to solidification and knockout of the mould. In order to identify the position of the shrinkhole, the parts were cut across in the central point of their length.

Figures 8 to 11 show the photographs of the sectioned cast parts, highlighting the position of the shrinkholes. Next to each sectioned part the isothermal curves corresponding to the end of solidification are mapped, as well as the position of the hot spots obtained by simulation.

Firstly, the analysis of the experimentally cast parts shows that the shrinkholes are slightly dispersed. This is due on one hand by the smaller solidification contraction of grey cast iron, and on the other to the reduction of the feeding (alloy flowing) capacity in the solidification area towards the end of solidification. It can be however considered that the position of the hot spot corresponds to the centre of the area of porosity.

The comparison of the position of the shrinkholes of the experimentally cast parts with the position of the hot spots highlighted by computer simulation shows that for U20x4, U20x20 and U20x120 parts the position of the shrinkholes of the experimentally cast parts corresponds to the positions determined by computer simulation. In the case of the U20x40 bar a difference can be observed between the experimental and the simulated result. This is due to the fact that the values of the thermo-physical quantities used for simulation are average substitute values that have not been determined experimentally by more accurate measurement methods. The practical casting of parts was achieved in green moulds, the thermo-physical characteristics and in particular the thermal conductivity coefficient of the moulding sand being significantly influenced by humidity and the degree of stamping. The difference between the simulated position of the hot spot and the position of the shrinkhole in the experimentally cast U20x40 bar shows that the real value of the conductivity coefficient of the mould is greater than the value used for simulation. The cooling capacity of the sand at the interior of the part is high, and the effect of this difference is visible in the U20x40 bar. Consequently in this part the hot spot and hence the shrinkhole moved towards the warm corners of the part. The determination

of a realistic value of the coefficient of conductivity requires a large number of simulations with different, greater values of the mould thermal conductivity coefficient, until achievement of a correspondence of simulation and experiment.

*Table 1. The values of the thermo-physical parameters of the cast alloy (eutectic grey cast iron) and of the mould considered in the simulation of solidification.*

| No. | Physical quantity | Symbol | Unit of measure | Value |
|-----|-------------------|--------|-----------------|-------|
| 1 | Density of the liquid alloy | $\rho_L$ | kg/m$^3$ | 7070 |
| 2 | Density of the solid alloy | $\rho_S$ | kg/m$^3$ | 7286 |
| 3 | Thermal conductivity coefficient in the liquid state of the alloy | $\lambda_L$ | W/mK | 30 |
| 4 | Thermal conductivity coefficient in the solid state of the alloy | $\lambda_S$ | W/mK | 40 |
| 5 | Specific heat in the liquid state of the alloy | $c_L$ | J/kgK | 850 |
| 6 | Specific heat in the solid state of the alloy | $c_S$ | J/kgK | 1080 |
| 7 | Specific latent heat of the solidification of the alloy | $L$ | J/kg | 292800 |
| 8 | Density of mould material | $\rho_f$ | kg/m$^3$ | 1550 |
| 9 | Thermal conductivity coefficient of the mould | $\lambda_f$ | W/mK | 0,7 |
| 10 | Specific heat of the mould material | $c_f$ | J/kgK | 1200 |
| 11 | Heat transfer coefficient between mould and environment | $\alpha_{aer}$ | W/m$^2$K | 30 |
| 12 | Initial temperature of the liquid alloy. | $T_T$ | °C | 1350 |
| 13 | Solidification temperature of the alloy | $T_S$ | °C | 1153 |
| 14 | Environment temperature | $T_a$ | °C | 30 |

**Table 2.** *Solidification time and hot spots coordinates in an xOy frame of reference, with the origin in the intersection point of the part cross section symmetry axis with the external surface of the cross piece (walls thickness a = 20 mm).*

| No. | Part symbol | Dimension of span | Hot spot coordinates | | Solidification time |
|-----|-------------|-------------------|---------------------|--|---------------------|
| | | $b$ [mm] | $x$ [mm] | $y$ [mm] | $\tau$ [s] |
| 1 | U20x4 | 4 | -2 and 2 | 38 | 838.9 |
| 2 | U20x8 | 8 | -4 and 4 | 34 | 777.3 |
| 3 | U20x16 | 16 | -8 and 8 | 28 | 679.7 |
| 4 | U20x20 | 20 | 0 | 20 | 671.3 |
| 5 | U20x30 | 30 | 0 | 16 | 645.1 |
| 6 | U20x40 | 40 | 0 | 14 | 632.0 |
| 7 | U20x60 | 60 | -10 and 10 | 12 | 607.3 |
| 8 | U20x80 | 80 | -24 and 24 | 12 | 596.6 |
| 9 | U20x120 | 120 | -48 and 48 | 14 | 593.5 |
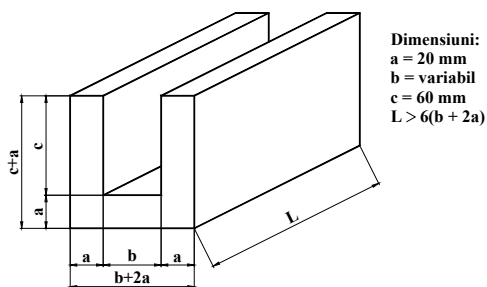
*Fig. 1. The geometry of bars with "U" section.*
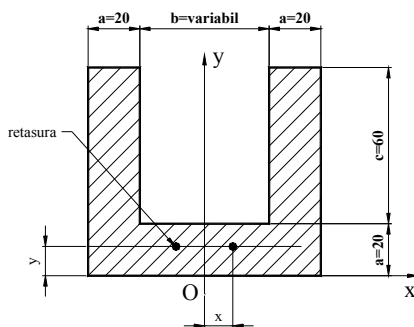


*Fig 2. Frame of reference used for the positioning of shrinkholes*
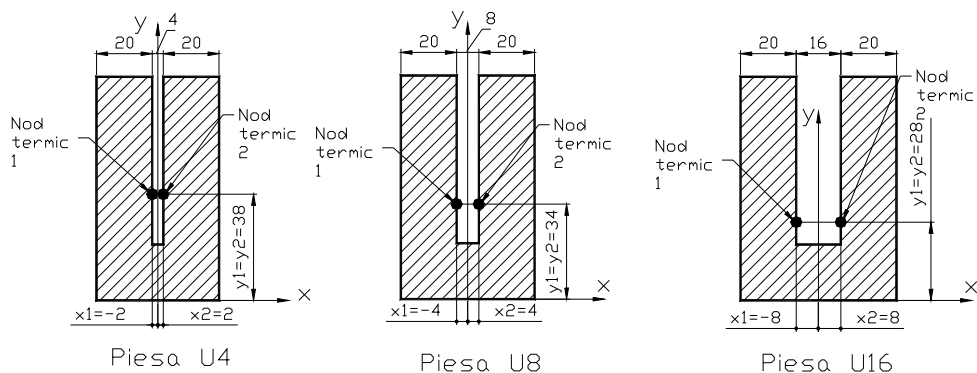


*Fig. 3 The hot spots position obtained by computer simulation in the case of parts U20x4, U20x8, U20x16.*
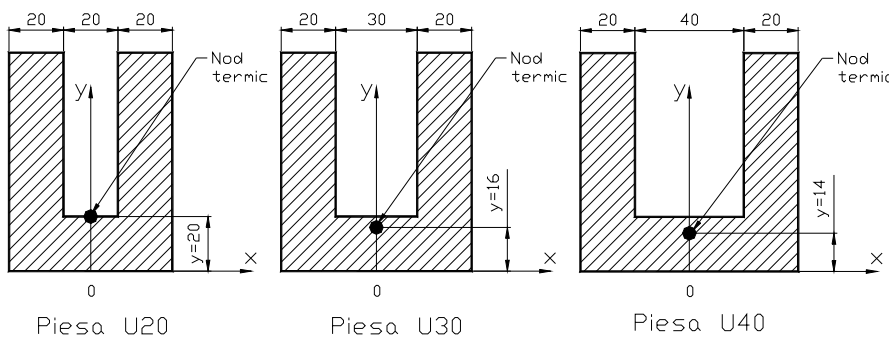


*Fig. 4 The hot spots position obtained by computer simulation in the case of parts U20x20, U20x30, U20x40.*
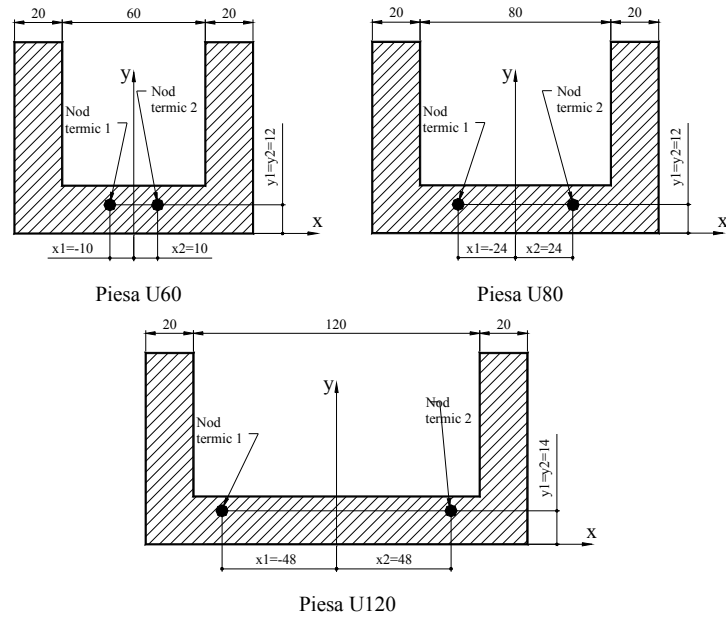
Fig. 5. The hot spots position obtained by computer simulation in the case of parts U20x60, U20x80, U20x120.
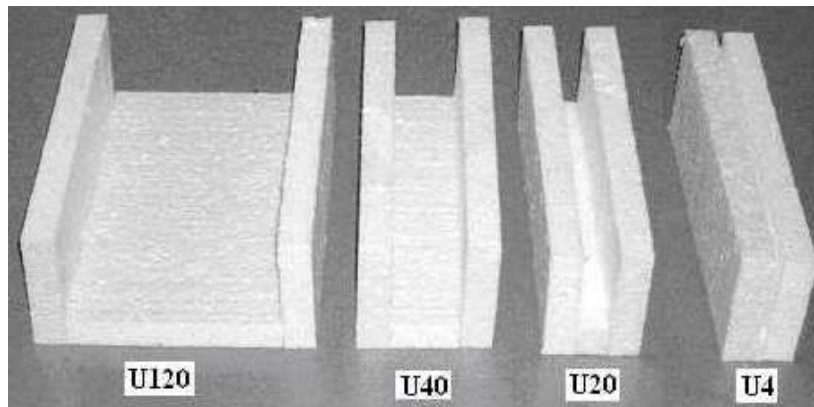


Fig. 6. Patterns used to cast U section parts (span between profile arms - 120, 40, 20 and 4 mm).
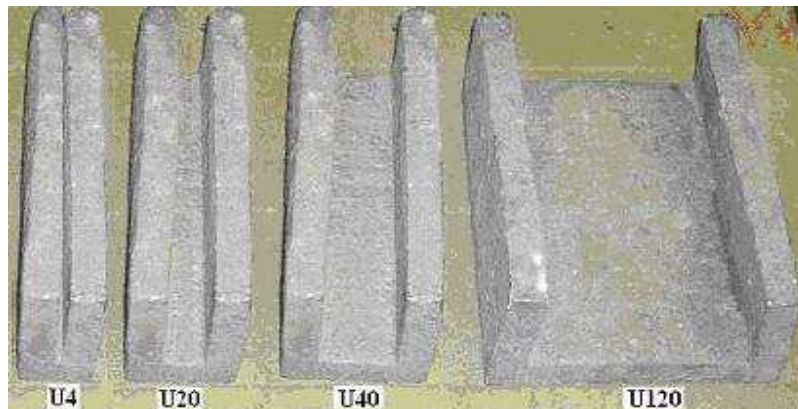


Fig. 7. Experimental parts cast in grey cast iron.
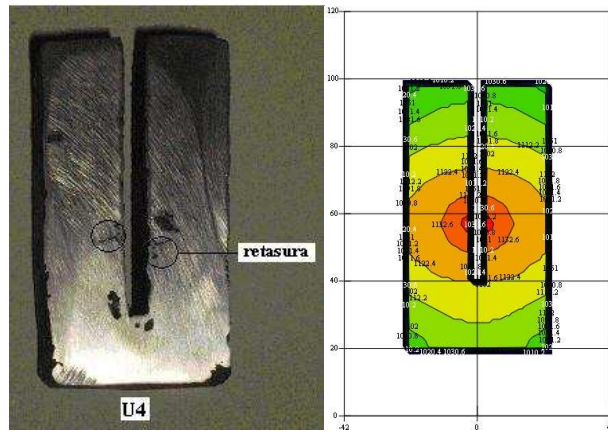
*Fig. 8. Cross section of part U20x4 and temperature field obtained by simulation.*
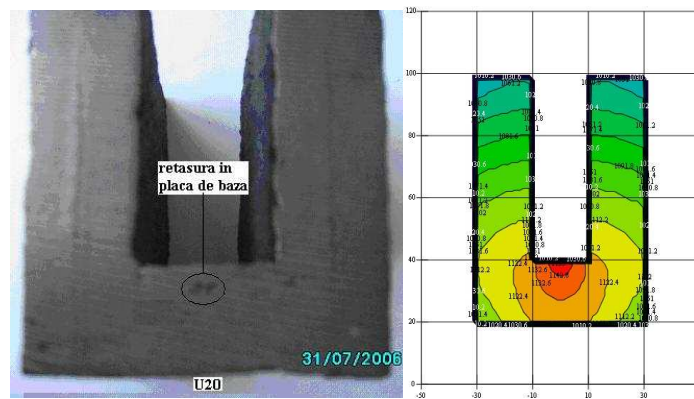


*Fig. 9.  Cross section of part U20x20 and temperature field obtained by simulation.*
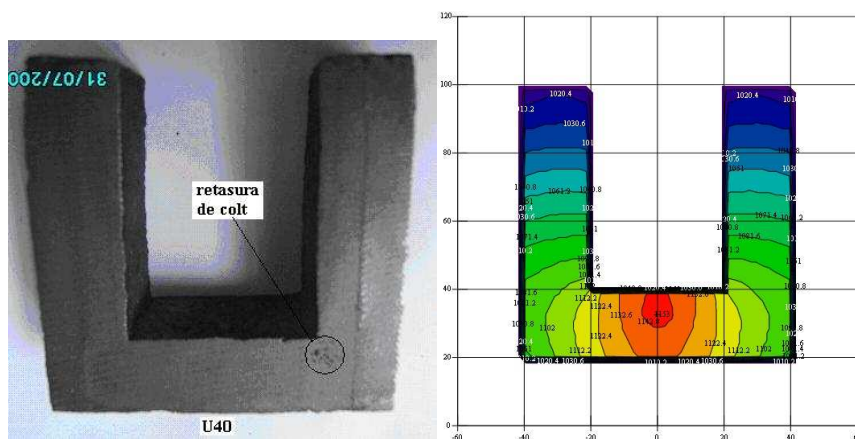


*Fig. 10. Cross section of part U20x40 and temperature field obtained by simulation.*
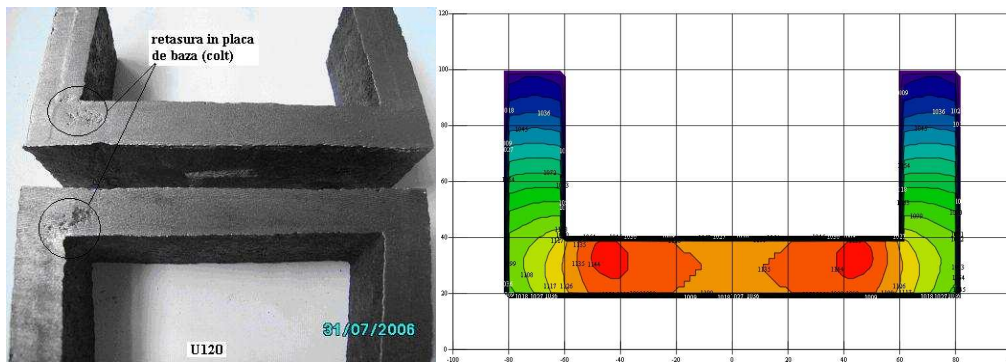
*Fig. 11. Cross section of part U20x120 and temperature field obtained by simulation*

**REFERENCES**

1. Munteanu S., Ciobanu I., Crişan A**. – Simulation of the Macro-Solidification of a U Section Bar Cast from Eutectic Cast Iron.** In: *Metalurgia International*, no. 6, 2005, pp. 38-50, ISSN 1582/2214.
2. Munteanu S., Ciobanu I., Crişan A**. - Research Concerning the Influence of Some Geometric Factors on the Solidification of U Section Bars**. In: *Metalurgia International*, no. 7, 2005, pp. 25-36, ISSN 1582-2214
3. Maşniţă M. **– Cercetări privind influenţa unor factori tehnologici şi constructivi asupra solidificării pieselor turnate, Teză de doctorat**, Universitatea Transilvania din Braşov, Braşov, 2007 / [Research on the Influence of Some Technological and Constructive Factors on the Solidification of Castings, Ph.D. Thesis, Transilvania University of Brasov, Brasov, 2007].
4. Soporan V., Vamoş C., Pavai C. **– The Numerical Modelling of the Solidification Process**, Ed. Dacia, Cluj – Napoca, 2003.
5. Sofroni L., Brabie V., Bratu C. **- Bazele teoretice ale turnării**, [Theoretical Bases of Casting], Editura Didactică şi Pedagogică, Bucureşti, 1980.
6. Soporan V., Constantinescu V. **– Modelling on a Macrostructural Level of the Alloy Solidification Process**, Ed. Dacia, Cluj – Napoca, 1995.
7. Soporan V., Constantinescu V., Crişan M. **– Solidification of Alloys – Theoretical Preliminaries**, Ed. Transilvania Press, Cluj – Napoca, 1995.

**TESTAREA EXPERIMENTALĂ A PROGRAMELOR DE SIMULARE PENTRU PROCESELE DE SOLIDIFICARE A PIESELOR TURNATE**

**Rezumat:** Se prezintă rezultatele unei cercetări experimentale privind solidificarea pieselor turnate din fontă cenuşie. S-a studiat solidificarea unor bare cu secţiune „U", având grosimea peretelui egală cu 20mm şi deschideri diferite între braţele paralele. În cazul pieselor turnate experimental nodurile termice au fost puse în evidenţă prin poziţia retasurilor în piesele turnate secţionate. În cazul simulării solidificării pe calculator, nodurile termice s-au pus în evidenţă prin analiza câmpului de temperatură din piese la momentul sfârşitului solidificării. Rezultatele experimentale au fost comparate cu rezultatele obţinute prin simularea solidificării pe calculator.

# MATHEMATICAL MODEL FOR SOLID FRACTION VARIATION WITH TEMPERATURE AT SOLIDIFICATION OF IRON – CARBON ALLOYS

BY

## Sorin Munteanu, Ioan Ciobanu, Aurel Crisan

**Abstract:** In realizing simulation software for alloy solidification it is necessary a mathematical modelling for solid fraction dependence on temperature. The equation describing the solid fraction variation are dependent on phase transformation types that alloys suffer during solidification: eutectic transformation, peritectic transformation, solubility variation depending on temperature, etc. The paper presents the equations describing the solid fraction variation in the case of iron – carbon alloys used by authors to create software for steel and cast iron macrosolidification simulation.

**Keywords:** solidification, Fe-C alloys, cast iron, steel, modelling

## 1. INTRODUCTION

Castings macrosolidification simulation is based on mathematical modelling of heat transfer processes and liquid-solid phase transformations followed by model description in computer language to realise software for engineering applications. Mathematical modelling of casting macrosolidification impose to express as analytical equations the alloys phase transformation temperatures (liquidus and solidus) depending on chemical composition and solid fraction evolution depending on temperature and chemical composition. These equations are specific for each alloy type and have particularities in function of equilibrium diagram shape (with eutectic transition, with peritectic transition, with solubility variation with temperature, etc.) For this reason in casting simulation must be realised different mathematical models and software for each composition range characterized by the same transformation at solidification. In the iron-carbon alloys all these transformation types are present, depending on chemical composition. So to simulate steel and cast iron solidification many models and software must be realised to cover the all range of chemical composition. In this paper there are presented the equations used by authors to compute the liquidus and solidus temperatures for iron-carbon alloys and also the equations to compute the solid fraction in function of temperature. This models lay on the basis for some application of solidification simulation for cast iron and steel castings.

## 2. SOLIDIFICATION TEMPERATURE FOR THE FE – C ALLOYS

In the slow cooling conditions, all alloys solidification ( including Fe-C alloys ) develop in conformity with equilibrium diagram. The equilibrium diagram gives information about critical temperatures (liquidus and solidus), constitutes and phases

formed in solidification equilibrium conditions and solid fraction in equilibrium at divers temperatures. For this reason the studies for modelling and simulation the alloys solidification are based on equilibrium diagrams.

The main feature of this equilibrium diagram is that it present two aspects, one stable (Fe-C) and another metastable (Fe-Fe$_3$C). The unalloyed steel, including those in castings, all time solidify in concordance with metastable diagram.

Cast iron purred in castings may solidify in different way depending on cooling conditions in respect with metastable diagram, or combined, partly conform with stable diagram and partly conform metastable diagram. Generally parts for machine building industry are cast in grey cast iron and present a primary crystallization conform with the stable diagram. So the grey cast iron solidification, in castings, occur in conformity with stable diagram.  As opposed to castings from unalloyed steels, used in machine building, the grey cast irons have a greater content of  accompanying elements (Si, Mn, P, S), which modify the critical point position (including solidus and liquidus temperature) in rapport with Fe-C diagram. For this reason in using the data from Fe-C diagram it is defined the equivalent carbon content (CE). The equation to calculate the equivalent carbon content is given by [1];

$$CE = C + 0,3(Si + P) + 0,4S + 0,22Al + 0,115Sb + 0,11Sn + 0,074Cu + 0,053Ni - 0,027Mn - 0,015Mo - 0,063Cr - 0,135V. \ [\%] \qquad (1)$$

Symbols represent the percentage of elements in cast iron composition. In the table are given the critical points coordinates from iron–carbon equilibrium diagram (C', E', F', S' are notation for stable diagram).

*Table 1. Critical points coordinates from iron–carbon equilibrium diagram*
*(C', E', F', S' are notation for stable diagram) [1].*

| Critical point | Temperature [$^0$C] | | | | Carbon content [%] | | | |
|---|---|---|---|---|---|---|---|---|
| | Hansen (1958) | STAS 2500-66 | Metals Handbook (1973) | Giesserei Kalender (1986) | Hansen (1958) | STAS 2500-66 | Metals Handbook (1973) | Giesserei Kalender (1986) |
| A | 1534 | 1536 | 1538 | 1536 | 0 | 0 | 0 | 0 |
| B | 1493 | 1493 | 1495 | 1493 | 0,51 | 0,5 | 0,5 | 0,533 |
| C | 1147 | 1147 | 1148 | 1147 | 4,3 | 4,3 | 4,3 | 4,302 |
| C' | 1153 | 1153 | 1154 | 1153 | 4,25 | - | 4,26 | 4,256 |
| D | - | - | - | 1252 | 6,67 | 6,67 | 6,67 | 6,689 |
| E | 1147 | 1147 | 1148 | 1147 | 2,06 | 2,04 | 2,11 | 2,14 |
| E' | 1153 | 1153 | 1154 | 1153 | 2,03 | - | 2,08 | 2,089 |
| F | 1147 | 1147 | 1148 | 1147 | 6,67 | 6,67 | 6,67 | 6,689 |
| G | 910 | 911 | 912 | 911 | 0 | 0 | 0 | 0 |
| H | 1493 | 1493 | 1495 | 1493 | 0,1 | 0,1 | 0,10 | 0,086 |
| J | 1493 | 1493 | 1495 | 1493 | 0,16 | - | 0,16 | 0,16 |
| K | 723 | 723 | 727 | 727 | 6,67 | 6,67 | 6,67 | 6,689 |
| L | 500 | 400 | 400 | - | 6,67 | 6,67 | 6,67 | - |
| M | 768 | 769 | 770 | - | - | - | - | - |
| N | 1390 | 1392 | 1394 | 1392 | 0 | 0 | 0 | 0 |
| O | 768 | 769 | 770 | - | - | - | - | - |
| P | 723 | 723 | 727 | 727 | 0,02 | - | 0,0218 | 0,034 |
| Q | 500 | 400 | 400 | - | 0,006 | - | 0,002 | - |
| S | 723 | 723 | 727 | 727 | 0,8 | 0,8 | 0,77 | 0,758 |
| S' | 738 | 738 | 738 | 736 | 0,69 | - | 0,68 | 0,688 |

To realise the mathematical models in this research it will be used the values given by Giesserei Kalender (1986) considering that are more recent and more realistic (determined using more precise techniques).

It is possible too for some mathematical modelling, to calculate the coordinates for main critical points in equilibrium diagram in function of cast iron chemical composition. So the maximum solubility of carbon in austenite at eutectic temperature ($C_E$ – carbon concentration in E point from equilibrium diagram) is given by [1]:

$$C_E = 2,03 – 2,08Ti – 0,35P – 0,3Mo - 0,12W - 0,11Si -0,09Ni - 0,08S – 0,07Cr – - 0,017\ Co +0,006Mn +0,014Cu + 0,08Al +0,18\ V.\ \ [\%] \qquad (2)$$

The eutectic and eutectoid transition temperatures in the stable system ($T_{C'}$ and $T_{S'}$) and in the metastable system ($T_C$ and $T_S$) can be calculated in rapport of alloying elements content using the equations [1]:

$$T'_C = T_{C\ stab} = 1153 + 7,5Si -30P – 2Cr, \quad [^0C] \qquad (3)$$

$$T_C = T_{C\ met} = 1145 - 10Si - 30P + 30Cr, \quad [^0C] \qquad (4)$$

$$T'_S = T_{S\ stab} = 738 + 35Si + 200P + 8Cr – 20Ni – 35(Mn - 1,7S)- 10Cu, \quad [^0C] \qquad (5)$$

$$T_S = T_{S\ met} = 723 + 25Si + 200P + 8Cr – 30Ni – 35(Mn - 1,7S) – 10Cu, \quad [^0C] \qquad (6)$$

The solidification starting temperature for iron – carbon alloys used in casters (OT steels and Fc and Fgn cast iron) are given by ABC'D' line (liquidus line from equilibrium diagram), and solidification ending temperature are given by AHJE'C'F" line (solidus line from the stable diagram). To make possible the solidification mathematical modelling for the all range of alloys from the system iron – carbon, it is necessary to express the temperature corresponding to these curves in function of carbon percent. The easiest approximation of this dependence is by first grade curves. This approximation is very close to reality. In the same time, the approximation by first grade equations assure a simplest mathematical model for the solidification process, conducting to simplest computer programs, because generate linear variation with temperature for the solidification fraction inside solidification range. In these conditions the equations for liquidus and solidus curves from iron – carbon equilibrium diagram are the followings:

The equation for AB curve, liquidus curve for Fe –C alloys (unalloyed cast steels), with carbon content between $0 \div 0,533$ %C:

$$T_{lichidus} = T_{AB} = \frac{T_B - T_A}{C_B - C_A} \cdot (C - C_A) + T_A , \quad [^0C] \qquad (7)$$

For Fe – C alloys with carbon content between $0,533 \div 4,256$ % (hypoeutectic steels and grey cast irons) the liquidus curve equation (BC' curve) is:

$$T_{lichidus} = T_{BC'} = \frac{T_{C'} - T_B}{C_{C'} - C_B} \cdot (C - C_B) + T_B, \quad [^0C] \tag{8}$$

The solidus curves have similar equations. So the AH curve for carbon content of $0 \div 0,086$ % is given by:

$$T_{solidus} = T_{AH} = \frac{T_H - T_A}{C_H - C_A} \cdot (C - C_A) + T_A, \quad [^0C] \tag{9}$$

The JE' curve corresponding to carbon contents $0,16 \div 2,089$ % has the equation:

$$T_{solidus} = T_{JE'} = \frac{T_{E'} - T_J}{C_{E'} - C_J} \cdot (C - C_J) + T_J, \quad [^0C] \tag{10}$$

For Fe – C alloys with carbon content between $2,089 \div 6,689$ (hypo and hypereutectic cast irons) the solidus curve E'C'F' (eutectic transition line) has the equation:

$$T_{solidus} = T_{E'C'F'} = T_{E'} = 1153, \quad [^0C] \tag{11}$$

In the equations $7 \div 11$, C represent carbon percent in the analyzed alloy, $T_A$, $T_B$, $T_{C'}$, $T_H$, $T_J$, $T_{E'}$ represent the critical point temperatures from iron– carbon diagram, $C_A$, $C_B$, $C_{C'}$, $C_H$, $C_J$, $C_{E'}$ – the carbon percent corresponding to critical points.

In the table 2 are given the equations with numerical coefficients for this curves obtained based on temperature values and carbon content from table 1(values from Giesserei Kallender).

**Table 2.** Liquidus and solidus temperature equations for iron-carbon alloys

| No. | Line type | Symbol | Validity range | Equation |
|---|---|---|---|---|
| unit | - | - | [%C] | T [$^0$C] and C [%] |
| 1 | Liquidus | AB | $0 \div 0,533$ | $T_{AB} = - 80,6754C + 1536$ |
| 2 | Liquidus | BC' | $0,533 \div 4,256$ | $T_{BC'} = - 91,3242(C- 0,533)+1493$ |
| 3 | Solidus | AH | $0 \div 0,086$ | $T_{AH} = - 500C + 1536$ |
| 4 | Solidus | HJ | $0,086 \div 0,16$ | $T_{HJ} = 1493$ |
| 5 | Solidus | JE' | $0,16 \div 2,089$ | $T_{JE'} = - 176,2571(C-0,16)+ +1493$ |
| 6 | Solidus | E'C'F' | $2,089 \div 6,689$ | $T_{E'C'F'} = 1153$ |

## 3. THE SOLIDIFIED FRACTION VARIATION IN FUNCTION OF TEMPERATURE IN THE CASE OF FE-C ALLOYS

Knowing the solid fraction evolution with temperature represent a first order problem in modelling and simulation the alloys solidification. In the case of macrosolidification modelling and simulation, the solid fraction variation can be determined applying the lever law.

The equations to model the solid fraction dependence by temperature must be singularized for each range and alloy type, in concordance with each equilibrium diagram specificity. In this research for modelling the iron − carbon alloys macrosolidification the solid fraction variation was approximate using the lever law applied to Fe-C equilibrium diagram.

For iron carbon alloys with carbon content in the range 0÷0,086 %C ( $0 \leq C \leq C_H$ ) the solid fraction variation in the solidification interval $T_L \div T_S$ was modelled using the sketch from fig. 1 and is given by the equation:

$$f_s = \frac{T_L - T}{T_L - T_S}$$

(12)

where: $T_L$ - the alloy liquidus temperature situated on AB line, and $T_S$ − solidus temperature situated on AH line.
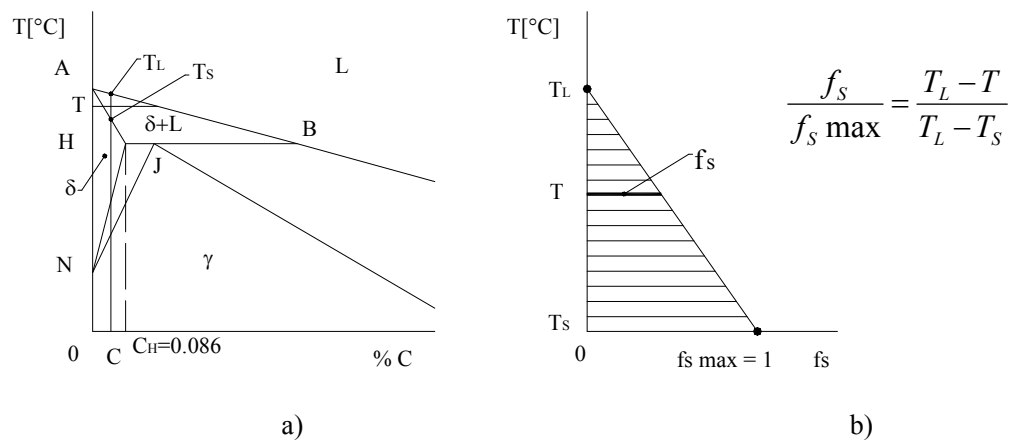


Fig. 1. Diagram to compute the solidification fraction for Fe – C alloys with carbon content $0 \leq C \leq C_H$ ($0 \leq C \leq 0,086$ %C)
a) Fe – C diagram, b) the solidification fraction depending on temperature between $T_L$ and $T_S$

For iron - carbon alloys (steels) with carbon content in the range 0,086 ÷ 0,16 %C (alloys situated in line with peritectic horizontal between $C_H$ and $C_J$), the solid fraction at a temperature T, in the temperature interval $T_L$ (liquidus temperature given by AB line) and $T_{HJB}$ (peritectic temperature ) can be established based on the sketch from fig. 3 and is given by:

$$f_S = \frac{T_L - T}{T_L - T_H} \cdot f_S^* = \frac{T_L - T}{T_L - T_H} \cdot \frac{C_B - C}{C_B - C_H}$$

(13)

In this equation $f_S^*$ represent the solid fraction in the vicinity of peritectic horizontal (at temperature $T_H$). Its value ($f_S^*$ ) can be obtained using the lever law at the peritectic horizontal level and has the value:

$$f_S^* = \frac{C_B - C}{C_B - C_H}$$

(14)

where: C represent the alloy carbon content (percentage).

The solid fraction calculated with eq. 13 has values between 0 and $f_S^*$. At this range of alloys the liquid fraction rest at peritectic temperature $f_L^* = (1 - f_S^*)$ solidify at constant temperature by peritectic transformation, releasing the latent solidification heat.



*Fig. 2 Diagram to compute the solidification fraction for Fe – C alloys with carbon content $C_H \leq C \leq C_J$ ( $0,086 \leq C \leq 0,16$ %C )*
*a) Fe – C diagram, b) the solidification fraction depending on temperature between $T_L$ and $T_S$*

For iron –carbon alloys with a carbon content in the range $0,16 \div 0,533$ %C (alloys with peritectic transformation and composition between $C_J$ and $C_B$) the solidification interval is comprised between liquidus temperature situated on AB curve and solidus temperature situated on JE' curve. The solid fraction is expressed based on sketch from fig. 3.
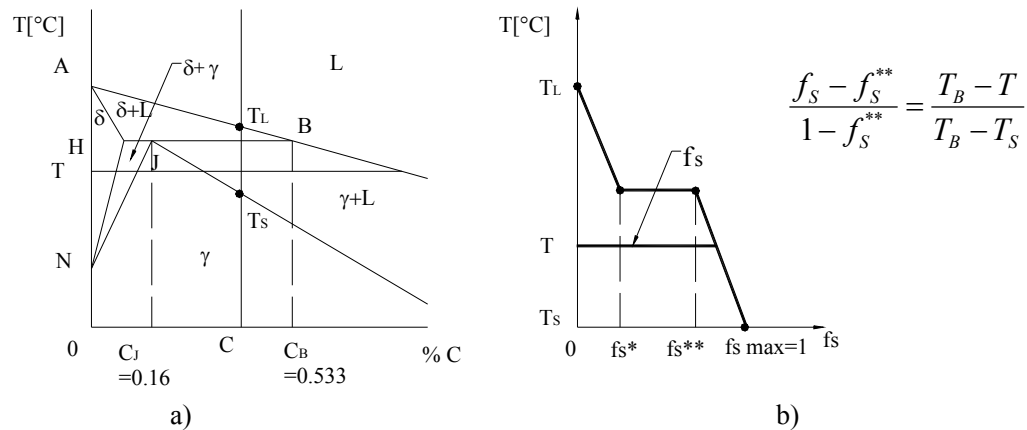


*Fig. 3. Diagram to compute the solidification fraction for Fe – C alloys with carbon content $C_J \leq C \leq C_B$ ( $0,16 \leq C \leq 0,533$ %C )*
*a) Fe – C diagram, b) the solidification fraction depending on temperature between $T_L$ and $T_S$*

In the temperature range $T_L$ and $T_{HJB}$ the solid fraction is given by eq. (13). At this alloy type a part of the liquid fraction rested at peritectic temperature ($T_{HJB}$ = $1493^0$C) solidify at constant temperature in conformity with peritectic transformation. The solid fraction that solidify at constant temperature (peritectic temperature) is given by the equation:

$$\Delta f_{peritectic} = f_S^{**} - f_S^* \tag{15}$$

where: $f_S^{**}$ represent the solid fraction calculated with the lever law quite under the peritectic horizontal. Its value ( $f_S^{**}$ ) is given by equation:

$$f_S^{**} = \frac{C_B - C}{C_B - C_J} \qquad (16)$$

At this range of alloys, under the peritectic horizontal, the solid fraction is computed using the sketch from fig. 3b with the equation:

$$f_S = f_s^{**} + \frac{T_B - T}{T_B - T_S} \cdot \left(1 - f_s^{**}\right) \qquad (17)$$

where $T_S$ represent the alloy solidus temperature given by JE' curve.

For iron – carbon alloys (steels) with carbon content in the range $0,533 \div 2,089$ %C (between $C_B$ and $C_{E'}$) the solid fraction can be computed based on the sketch from fig. 4. In this case the solid fraction at T temperature, inside the solidification range $(T_L - T_S)$ is given by the equation:

$$f_S = \frac{T_L - T}{T_L - T_S} \qquad (18)$$

where: $T_L$ is alloy liquidus temperature situated on BC' line, and $T_S$ is the solidus temperature situated on JE' line.    The solid fraction calculated with this equation has values in the range $f_S = 0 \div 1$.
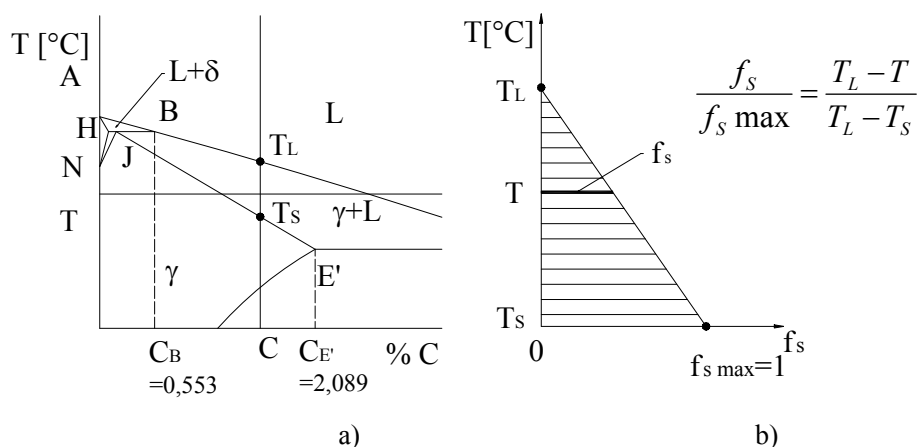


*Fig. 4. Diagram to compute the solidification fraction for Fe – C alloys with carbon content $C_B \leq C \leq C_{E'}$ ( 0,533≤C ≤2,089 %C )*
*a) Fe – C diagram, b) the solidification fraction depending on temperature between $T_L$ and $T_S$*

For alloys with carbon content between $2,089 \div 4,256$ %C (hypoeutectic cast irons ) the solid fraction at T temperatures inside the solidification interval $T_L$ (liquidus temperature situated on BC' line) and $T_S$ (solidus temperature situated on eutectic horizontal E'C') can be computed based on the sketch from fig. 5, by equation:

$$f_S = \frac{T_L - T}{T_L - T_{C'}} \cdot f_S^{***} = \frac{T_L - T}{T_L - T_{C'}} \cdot \frac{C_{C'} - C}{C_{C'} - C_{E'}} \tag{19}$$



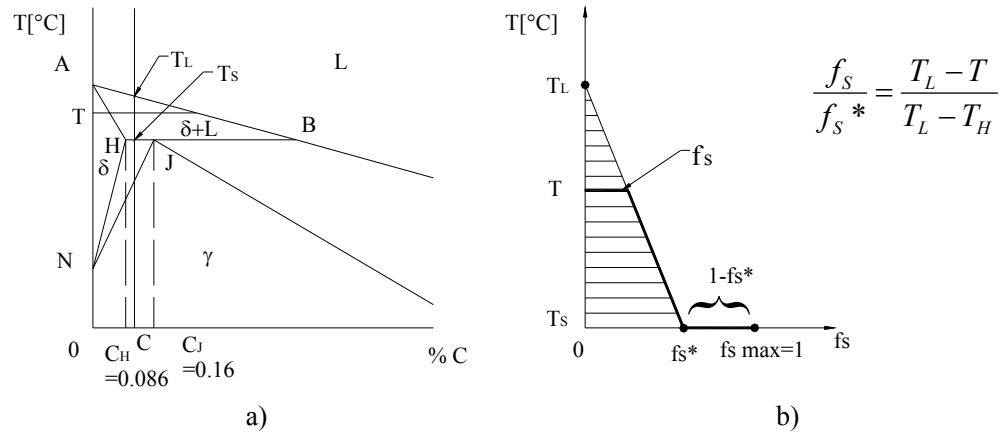a)                                                          b)
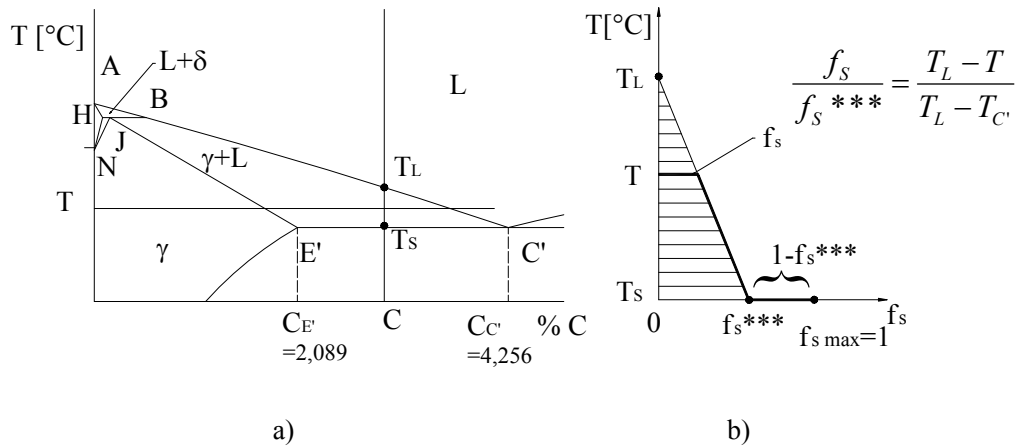
*Fig. 5. Diagram to compute the solidification fraction for Fe – C alloys with carbon*
*content $C_{E'} \leq C \leq C_{C'}$ ( 2,089 ≤ C ≤ 4,256 %C)*
*a) Fe – C diagram,    b) the solidification fraction depending on temperature between $T_L$ and $T_S$*

The solid fraction calculated with this equation has values in the range $0 \div f^{***}$, where $f^{***}$ can be obtained applying the lever law on the level of eutectic horizontal and has the value:

$$f_S^{***} = \frac{C_{C'} - C}{C_{C'} - C_{E'}} \tag{20}$$

In the case of alloys with 2,089 ÷ 4,256 %C (hypoeutectic cast irons) during eutectic transformation, at the eutectic temperature $T_{E'C'}$ the solid fraction grows at constant temperature, from the value $f_S^{**}$ given by eq. (24), to maximum value $f_S = 1$, while release the latent solidification heat. The solid fraction that solidify at the eutectic temperature is $(1 - f^{***})$.

## 4. Conclusions

It can be observed that modelling the solidification fraction variation is much influenced by the equilibrium diagram aspect and by the alloys chemical composition. For this reason there is not an unique model to simulate the alloy solidification including the iron – carbon alloys. Practically for each range of alloys mentioned above (each chemical composition range) must be elaborated a mathematical model and an adequate software to simulate the solidification. In the next steps of this researches it will be create simulation software for steels and cast irons with chemical composition range frequently used casters.

## REFERENCES

**[1]** Crişan A. **: Elaborarea şi turnarea fontelor** -*Cast iron melting and casting* -, Ed. Universitatea Transilvania din Braşov, Braşov, 1996.
**[2]** Soporan V., Vamoş C., Pavai C. **: Modelarea numerică a solidificării** – *Solidification numerical modelling*- Ed. Dacia, Cluj – Napoca, 2003.
**[3]** Sofroni L., Brabie V., Bratu C. **: Bazele teoretice ale turnării** – *Theoretical basis of casting* - Editura didactică şi Pedagogică, Bucureşti, 1980.
**[4]** Soporan V., Constantinescu V. **: Modelarea la nivel macrostructural a solidificării** – *Solidification modelling at macrostructural level* - Ed. Dacia, Cluj – Napoca, 1995.
**[5]** Soporan V., Constantinescu V., Crişan M. **: Solidificarea aliajelor** – *Alloys solidification* - Ed. Transilvania Press, Cluj – Napoca, 1995.

## MODEL MATEMATIC PENTRU VARIATIA FRACTIEI DE SOLID CU TEMPERATURA LA SOLIDIFICAREA ALIAJELOR FIER - CARBON

**Rezumat:** La realizarea softurilor pentru simularea solidificării aliajelor este necesară modelarea matematică a dependenţei fracţiei de solid de temperatură. Ecuaţiile care descriu variaţia fracţiei de solid cu temperatura depind de tipul transformărilor de fază pe care aliajul le suferă în timpul solidificării: transformare eutectică, transformare peritectică, solubilitate variabilă cu temperatura, etc. În lucrare se prezintă relaţiile care descriu variaţia fracţiei de solid în cazul aliajelor fier – carbon, care au fost utilizate de autori pentru realizarea unor softuri destinate simulării solidificării oţelurilor şi fontelor.

# SOLIDIFICATION PATTERN OF IN-MOLD AND LADLE INOCULATED LOW SULFUR HYPOEUTECTIC GRAY CAST IRONS

BY

**M. CHISAMERA[1], S. STAN[1], I. RIPOSAN[1], G. COSTACHE[1], M. BARSTOW[2]**

**Abstract.** *A comparison of in-mold and ladle inoculation treatments was made in low sulfur (0.025%S), low aluminum (0.003%Al), hypoeutectic gray cast irons (CE = 3.5 - 3.6%), typical for electric melted irons using a high steel scrap charge. The present study describes the effect of a Ca,Zr,Al - FeSi alloy at an addition rate of 0...0.25wt.% on thermal analysis parameters and cast iron characteristics (structure and hardness). Eutectic undercooling of the base iron having the above mentioned characteristics is excessively high (39 - 40°C / 102-104°F), generating a relatively high need for inoculation. Lower levels of eutectic undercooling (ΔTm), recalescence (ΔTr) and the undercooling at the end of solidification (ΔT₃) are characteristic for in-mold treatment at lower alloy addition rates, promoting lower tendency for carbides, undercooled graphite, intercellular carbides and inverse chill, respectively. The difference between un-inoculated and inoculated irons is strongly affected by the alloy addition rate, much more for ladle inoculation. Generally, the efficiency of 0.05-0.15wt.% alloy for in-mold inoculation is comparable to or better than 0.15 - 0.25wt.% addition in ladle inoculation procedures. A Ca,Zr,Al - FeSi alloy appears to be effective in low S, low Al, low CE hypo-eutectic gray cast irons, especially for late inoculation.*

**Keywords:** *solidification, in-mold and ladle inoculation, gray cast iron*

## 1. INTRODUCTION

The production of high strength gray cast irons is based on the knowledge that the reduction of carbon and silicon to lower levels corresponds with higher strength development. Increasing tensile strength in gray iron depended on employing the lowest possible silicon content consistent with a gray fracture and machinability of thin sections. This objective was assisted by making additions to the ladle based on various materials (FeSi, CaSi, ZrSi, MgFeSi, Al etc.), to offset the increased risk of carbides and control the graphite size and shape in low carbon equivalent iron.

Inoculation has a vital role to play in the continuing development of cast iron. FeSi containing 75-80% silicon became established as a basis for most common inoculant, although the need to control calcium and aluminum in a ferrosilicon inoculant was not fully understood and was far from satisfactory in the early days of inoculated gray iron production. More complex inoculants were developed and their enhanced performance was based on powerful oxide forming elements (some of which also form sulfides and nitrides) Ca, Sr, Ba, Zr, Ce as individual or associated inoculating elements in FeSi-alloys[1,2].

The problem of fading had been recognized very early on, and it was acknowledged that inoculated iron had be poured in 10 minutes or less, to avoid loss of inoculation effect. The problem of inoculation fade changed with the foundry's adoption of fixed pouring stations, which provided the opportunity to change the inoculant addition

technique. It was soon demonstrated that the most effective solution was the use of late inoculation, where the metal is inoculated in the mold either by the in-mold or an in-stream method. With these techniques there would be no further problem of inoculation fade, using any of the controlled inoculants either as fine particles, lumps, pellets or tablets although poorly nucleated iron from the furnace or the autopour is still an issue.

The chemistry of the base iron and also of the treatment alloys is very important to control the iron structure in more severe eutectic undercooling conditions. A three-stage model for the nucleation of graphite in both un-inoculated and inoculated gray irons has been proposed (Fig. 1): 1) small oxide-based sites (usually less than 2.0μm) are formed in the melt; 2) complex (Mn,X)S compounds (usually less than 5.0μm) nucleate at these microinclusions; 3) graphite nucleates on the sides of the (Mn,X)S compounds which have lower crystallographic misfit with graphite. In inoculated irons, the (Mn,X)S compound is more complex at lower Mn/S ratio and has higher compatibility for graphite nucleation, especially with Ca, Sr as the inoculating elements.
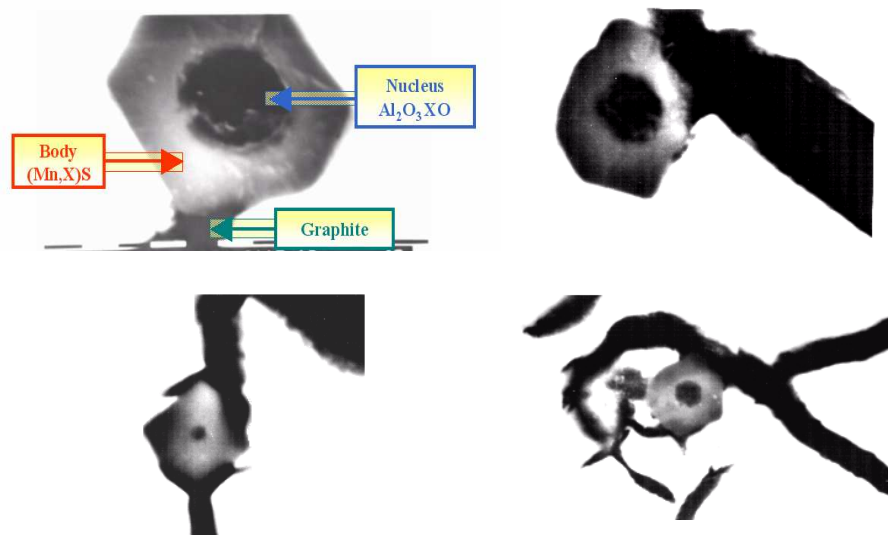


*Fig. 1. Three-stage model for the nucleation of graphite in gray irons.*

It has been found that three groups of elements are important to sustain graphite nucleation in industrial gray cast irons: a) strong deoxidizing elements, such as Al and Zr,  to promote early forming, very small micro-inclusions, which will act as nucleation sites for later formed complex (Mn,X)S compounds; b) Mn and S  to support  MnS type sulfide formation; c) inoculating elements which act in the first stage and/or in the second stage of graphite formation, to improve the effectiveness of (Mn,X)S compounds to nucleate graphite[3-12].

Historically, gray cast irons were melted in a cupola furnace, at more than 0.05%S and more than 0.5%Mn levels, with favorable conditions for formation of MnS-type compounds. In the last two decades, two important events contributed to recognisable changes in gray iron production technology. First of all, small and inefficient cupolas were replaced by a new generation of coreless induction furnaces with medium

frequency (200-1000 Hz) and high specific power supplies (more than 250 Kw/ton). This has revolutionized the iron foundries: high melting speed (usually less than one hour, with high steel charges), so high production rate at lower furnace capacity; no heel required (100% solid charge); larger furnace availability (more than 2 tons, 10 – 20 tons); reasonable stirring ability (high steel scrap charge + carbon raiser - lower cost); higher iron quality for larger scale production. Cupola melting problems (coke availability and price, environmental restrictions, molten iron variability – temperature and analysis) and the competitive performance of the new generation of induction furnaces led to increasing production tonnage of gray iron at low sulfur levels (usually less than 0.05%S) in many parts of the world.

The growing production of ductile iron and compacted graphite iron castings is desirably based on lower sulfur base iron. In many cases, a foundry will produce high and low sulfur base irons in the same shift, for gray iron and ductile/compacted irons, respectively. For these producers, a single low sulfur base iron would be very attractive, using a single inoculant type for all of these irons. The problem is that at low S-levels, gray irons usually solidify with high eutectic undercooling, favorable for carbides and/or undercooled graphite (type-D) (Fig. 2)[7]. Low residual Al level also favors the presence of undercooled graphite (Fig. 3)[8], so the 0.005-0.010%Al range appears to be an optimum level in gray irons, without developing hydrogen pinholes[6,8-9]. It has also been found that preconditioning of the base iron, using Al and Zr additions, is very effective in difficult solidification conditions for gray iron structure formation when levels of sulfur and aluminum are low, as these two elements have a vital role in the first stage of graphite formation [10-12].

Recently, thermal analysis became an important tool to reflect the solidification behavior of cast irons. The cooling curve itself, as well as its derivatives and related temperatures and calculated parameters are patterns that can be used to predict the behavior of irons. The use of thermal analysis can also help assess the inoculation requirements for the melt [13-17].

The current experimental investigation in this paper was designed to mainly evaluate the thermal analysis parameters and structure characteristics of low sulfur (0.025%S), low residual aluminum (0.003%Al) and relatively low carbon equivalent, hypo-eutectic gray irons (3.5-3.6%CE), when subjected to in-mold and ladle inoculation by the same type of inoculant (Zr,Ca,Al -  FeSi) added at various rates (0…0.25wt.%). The inoculant selected is used in both gray and ductile iron production (low Zr contributions are not high enough to interfere with the nodularizing effect of Mg)[18]. Based on the important contribution of Al, Zr and Ca as the active elements from previous investigations[10-12], inoculation technique could also be an important factor in the solidification pattern of low sulfur gray irons.

## 2. EXPERIMENTAL PROCEDURE

A synthetic pig iron was initially produced in an acid lined coreless induction furnace (100Kg, 2400Hz). To ensure a low level of trace elements, a relatively pure charge consisting of clean steel scrap, sand-blasted foundry returns, a low sulfur re-carburizer and ferroalloys was used in the experiment. Typical chemistry of the synthetic pig iron was 3.48%C, 1.72%Si, 0.50%Mn, 0.10%P, 0.025%S at 4.03% carbon equivalent (CE).
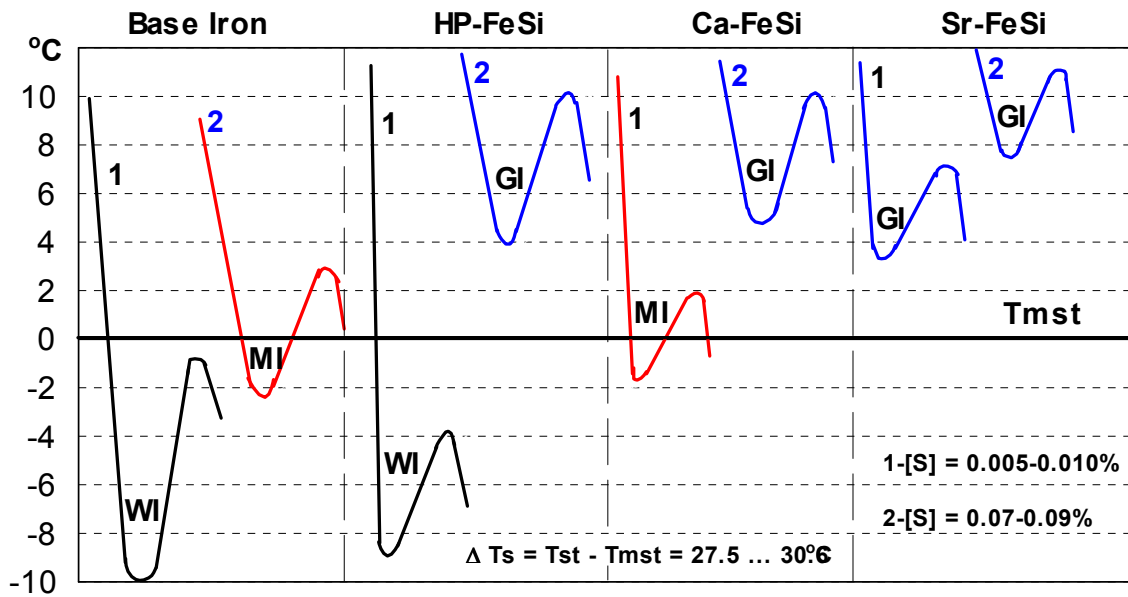
**Fig. 2.** *Relative position of cooling curves at different sulfur levels [0.003%Al].*
*[Wl-White Iron; Ml-Mottled Iron; Gl-Grey Iron]*
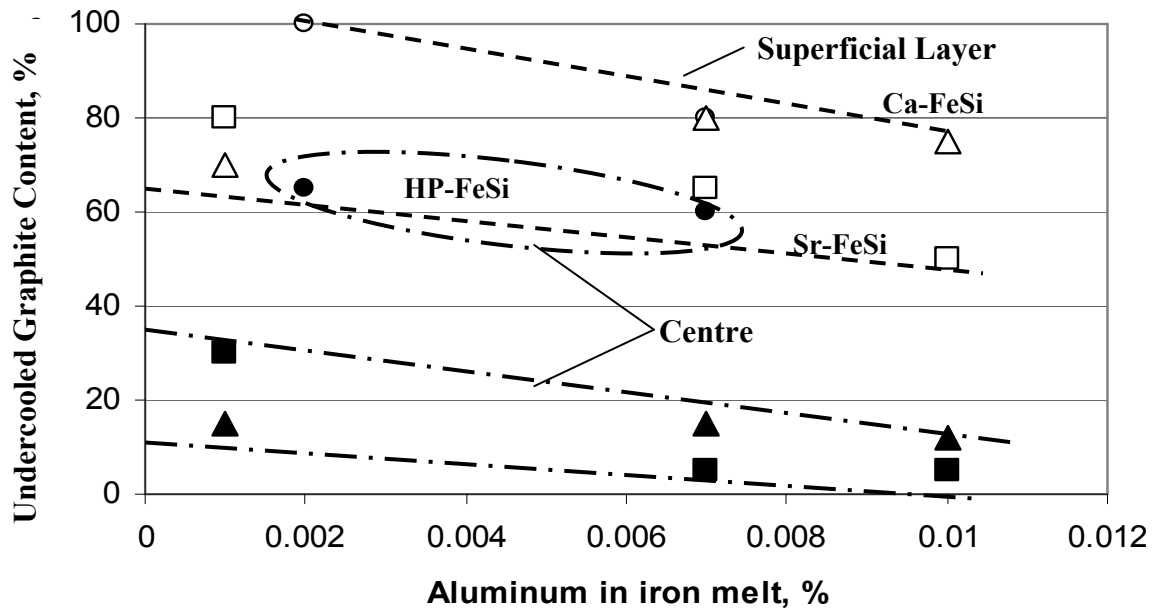


Fig. 3. *Influence of residual Al on the undercooled graphite content [0.08-0.1%S, 15 mm dia.*

Experimental heats were produced in a smaller graphite crucible induction melting (10Kg, 8000Hz), at 94% synthetic pig iron and 6% steel scrap as the metallic charge. The chemistry of the base iron was 3.02%C, 1.65%Si, 0.49%Mn, 0.11%P, 0.025%S, 0.0026%Al, 0.006%Ti, 0.042%Cr, 0.0078%Mo, 0.028%Ni, 0.044%Cu, 0.0016%V, 0.0033%Pb, 0.0037%Sn, at 3.55% carbon equivalent. Un-inoculated and inoculated irons were tested in two experimental programs. Zr,Ca,Al-FeSi alloy (75%Si, 2.2%Ca, 1.5%Zr, 1.2%Al) was used at an addition rate of 0.05…0.25wt.% and in the 0.2-0.7 mm particle size range.

In the first experimental program, the in-mold (M) inoculation method was used (Fig. 4a). Experimental heats were superheated to $1450^{o}C$ ($2642^{o}F$) and maintained at this level for 5 minutes. Thermal analysis was used to evaluate and quantify nucleation characteristics of the different inoculated irons. The thermal analysis was carried out using Quick-Cups with a modulus of approximately 0.75cm (30 mm diameter bar equivalent). In the shell sand cup, Zr,Ca,Al-FeSi alloy was employed at 0.05%, 0.10%, 0.15%, 0.20% and 0.25% addition levels. The cooling curve and its first derivative were considered for un-inoculated and inoculated irons, at different inoculant addition rates.

The base iron was also poured into test casting molds made from green sand. The test castings were all poured at $1430^{o}C$ ($2606.^{o}F$). The specially designed test mold included a central downsprue, which supplied un-inoculated gray iron to a reaction chamber. An American Society for Testing Materials (ASTM A367 specification, $W_{31/2}$ chill wedge, having a 25 mm base with, 45 mm high, 125 mm long) and a round bar specimen (20 mm diameter, 150 mm high) were gated off the inoculation reaction chamber. As molten iron flows into the reaction chamber, it is inoculated and the inoculated iron then flows into a chill wedge and round test bar. The same prescribed amount of the inoculant was added in the reaction chamber as in the shell sand cup tests.

In the second experimental program, successive ladle (L) inoculation was applied (Fig. 4b). Experimental heats were superheated to $1550^{o}C$ ($2822^{o}F$) and tapped at $1471^{o}C$ ($2680^{o}F$). The same prescribed amount of the inoculant was added as in the in-mold/cup tests but in successive steps: 0.05% alloy was added in each step, to the previously treated iron up to a total amount of inoculant of 0.25wt.%. Un-inoculated and ladle inoculated irons were poured into test castings: Quick-cup samples (Thermal Analysis) and test bar molds (chill wedge and round bar specimens), in the same way as in the in-mold/in cups inoculation program.
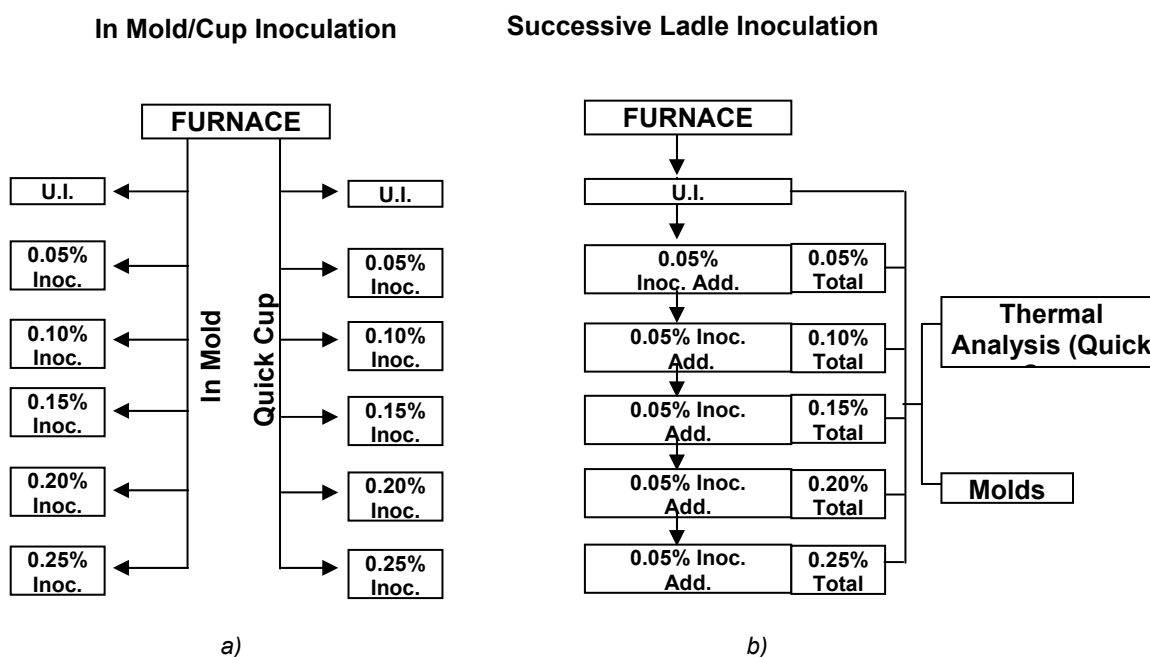


Fig. 4. *Schedule of Experiments [ a) – In-Mold / In Quick-Cup Inoculation; b) – Successive Ladle Inoculation]*

## 3. RESULTS AND DISCUSSION

Figure 5 shows the aspect of a typical cooling curve and its first derivative for a hypoeutectic gray iron (CE < 4.3%) and the significance of the most important events and parameters on these curves. Tst represents the theoretical temperature for carbon to precipitate as graphite, while Tmst is related to the metastable solidification, in which carbon is chemically combined with iron as iron carbide ($Fe_3C$). Tst should be as high as possible and Tmst as low as possible to ensure that the solidification occurs according to the stable system where all the remaining carbon at the eutectic temperature precipitates as graphite.

TAL - temperature of austenitic liquidus, °C;
TSEF - temperature of start of eutectic freezing (eutectic nucleation),°C;
TEU - temperature of eutectic undercooling, °C;
TER - temperature of graphitic recalescence, °C;
TES - temperature of the end of solidification (end of solidus), °C;
TEM - maximum recalescence rate, °C/s;
Tst - graphite eutectic equilibrium temperature, °C;
Tmst - carbide eutectic equilibrium temperature, °C;
ΔTm - maximum degree of undercooling (ΔTm = Tst - TEU), °C;
ΔTr - recalescence degree (ΔTr = TER - TEU), °C;
ΔTs - equilibrium eutectic temperature range (ΔTs = Tst -Tmst), °C
FDES - minimum value of the first derivative of cooling curve on the end of eutectic solidification, °C/s;
**ΔT₁ = TEU – Tmst; ΔT₂ = TER – Tmst; ΔT₃ = TES – Tmst**

Fig. 5. *Typical cooling curve and its first derivative*

There are many elements which individually have favorable or un-favorable influence on the Tst and/or Tmst level. Silicon is the most important influence of these elements in un-alloyed irons especially at very low content of trace element content [Tst = 1153 + 6.7 (%Si), Tmst = 1147 – 12 (%Si)][13,14].

Accordingly the strong role of the chemistry of the experimental irons, is represented by the range of equilibrium eutectic temperature (ΔTs = Tst - Tmst) increasing from $35.6^{o}C$ ($96^{o}F$) (un-inoculated iron) up to $36.2-39.0^{o}C$ ($97.2-102.2^{o}F$) for inoculated irons, depending on the alloy addition rate and the silicon contribution from inoculation, respectively.

Tables 1 and 2 include the most important experimental results, as thermal analysis data, while Figures 6…8 illustrate the effects of the two major influences, i.e. the inoculation technique (in-mold/cup and ladle inoculation) and the inoculant addition rate (0…0.25wt.% alloy), respectively.

In hypo-eutectic irons the austenitic liquidus temperature (TAL) signals the start of solid formation, as pro-eutectic austenite. The TAL temperature can sometimes be reduced by inoculation, while the temperature of the start of eutectic freezing (i.e. the eutectic nucleation temperature-TSEF) should be as low as possible for effective inoculation. This behavior is characteristic for in-mold inoculation (Fig. 6a).

Table 1. Thermal Analysis-Temperature and Time Characteristics

| Inoculation | | Temperatures, °C | | | | | Time, sec | |
|---|---|---|---|---|---|---|---|---|
| Wt.% | Type | TAL | TSEF | TEU | TER | TES | $t_1=t_{(TAL)}-t_{(TEU)}$ | $t_2=t_{(TEU)}-t_{(TES)}$ |
| U.I | M | 1243.2 | 1214 | 1124.7 | 1125.1 | 1100.2 | 106.5 | 39.1 |
| | L | 1238.0 | 1205 | 1122.8 | 1125.2 | 1089.9 | 123.3 | 93.2 |
| 0.05 | M | 1242.8 | 1211 | 1132.5 | 1141.5 | UD | 86.8 | UD |
| | L | 1238.2 | 1215 | 1123.6 | 1127.3 | 1093.9 | 118.3 | 88.4 |
| 0.10 | M | 1242.3 | 1214 | 1133.5 | 1142.3 | 1106.3 | 90.5 | 73.2 |
| | L | 1238.5 | 1210 | 1127.9 | 1134.9 | 1094.4 | 113.4 | 90.1 |
| 0.15 | M | 1240.7 | 1211 | 1135.4 | 1140.6 | 1107.2 | 94.5 | 76.4 |
| | L | 1238.9 | 1207 | 1130.1 | 1137.6 | 1097.4 | 105.3 | 85.6 |
| 0.20 | M | 1241.9 | 1211 | 1135.3 | 1140.1 | 1104.1 | 99.2 | 78.6 |
| | L | 1240.5 | 1211 | 1132.8 | 1139.1 | 1101.2 | 93.0 | 79.2 |
| 0.25 | M | 1239.7 | 1210 | 1136.4 | 1140.2 | 1105.1 | 97.5 | 76.3 |
| | L | 1241.9 | 1210 | 1133.2 | 1138.8 | 1100.8 | 76.4 | 72.0 |

*M-In Mold/Cup Inoculation; L-Ladle Inoculation

Table 2. Thermal Analysis – Representative Parameters

| Inoculation | | Cooling Curve Parameters, °C | | | | | First Derivative Parameters, °C/s | |
|---|---|---|---|---|---|---|---|---|
| Wt.% | Type | $\Delta T_m=T_{st}-TEU$ | $\Delta T_r=TER-TEU$ | $\Delta T_1=TEU-T_{mst}$ | $\Delta T_2=TER-T_{mst}$ | $\Delta T_3=TES-T_{mst}$ | TEM | FDES |
| U.I | M | 38.9 | - | -3.3 | -2.9 | -27.8 | 0.032 | -2.3 |
| | L | 40.8 | 2 | -5.2 | -2.8 | -38.1 | 0.114 | -1.79 |
| 0.05 | M | 31.3 | 9 | 4.9 | 13.9 | UD | UD | UD |
| | L | 40.2 | 4 | -4.0 | -0.3 | -33.7 | 0.157 | -2.12 |
| 0.10 | M | 30.6 | 9 | 6.4 | 15.2 | -20.8 | 0.588 | -3.13 |
| | L | 36.2 | 7 | 0.8 | 7.8 | -32.7 | 0.463 | -2.40 |
| 0.15 | M | 28.9 | 5 | 8.7 | 13.0 | -19.5 | 0.314 | -3.13 |
| | L | 34.2 | 8 | 3.4 | 10.9 | -29.3 | 0.363 | -2.88 |
| 0.20 | M | 29.3 | 5 | 9.1 | 13.9 | -22.1 | 0.254 | -2.77 |
| | L | 31.8 | 6 | 6.6 | 12.9 | -25.0 | 0.336 | -3.22 |
| 0.25 | M | 28.4 | 4 | 10.6 | 14.4 | -20.7 | 0.217 | -3.23 |
| | L | 31.6 | 6 | 7.4 | 13.0 | -25.0 | 0.310 | -3.45 |



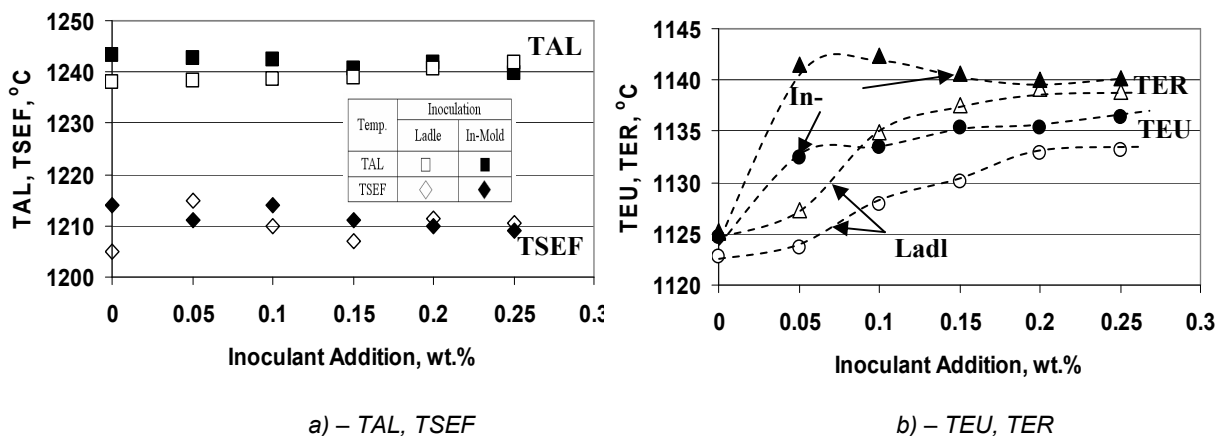*a) – TAL, TSEF*                              *b) – TEU, TER*

Fig 6. *Representative temperatures at the beginning of solidification.*

The most pronounced effect of inoculation is that the temperatures of eutectic undercooling (TEU) and graphite recalescence (TER) are increased (Fig. 6b). When

TEU is reached the combined heat generated from the release of specific heat and latent heat (from the first austenite dendrite solidification and latent heat from the start of eutectic freezing) just balance the heat losses. The eutectic reaction then occurs and the released energy causes the temperature to rise until TER is reached. Un -inoculated irons are characterized by low TEU and TER temperatures. Although inoculation increases both of these temperatures, the amount of the increase is dependent on the inoculant addition rate and inoculation technique. TER level is stabilized less time compared to the TEU level, at increasing inoculant additions, especially for in-mold/cup treatment. Late inoculation appears to be more efficient compared to ladle inoculation, at low inoculant addition rates, such as 0.05-0.10wt.% level. No big difference in efficiency from the inoculation technique was found for more than 0.20wt.% alloy additions.

The sensitivity of irons to form undercooled graphite morphologies during solidification (such as type-D graphite) or even free carbides is mainly illustrated by the eutectic undercooling parameters. Conventionally, undercooling is defined with reference to the graphitic equilibrium eutectic temperature (Tst), as $\Delta Tm = Tst - TEU$. A high value for undercooling means
that it takes a longer time before eutectic freezing starts (Fig. 7a), which increases the risk for macro-shrinkage and suck-in.

On the other hand, if TEU is close to the white eutectic temperature but above it (TEU > Tmst), then the risk of undercooled graphite increases. Free carbides occur typically where TEU < Tmst.

The relationship of the start of the eutectic reaction (TEU) compared to the metastable (white) eutectic temperature (Tmst) is revealed by $\Delta T_1 = TEU - Tmst$. For the end of the eutectic reaction temperature, the parameter $\Delta T_2 = TER - Tmst$ was introduced. The efficiency of inoculation is measured by its ability to decrease the $\Delta Tm$ level and to increase the $\Delta T_1$ and $\Delta T_2$ levels, respectively (Fig. 7 b,c). In all cases, the in-mold / cup inoculation is clearly more effective compared to ladle inoculation, represented by variation of the $\Delta T_1$ and $\Delta T_2$ parameters. In both experimental programs, the un-inoculated irons start and end the eutectic reaction in the white iron field ($\Delta T_1 < 0$, $\Delta T_2 < 0$). Inoculation is known to move the solidification pattern to the gray iron example. Increasing the alloy addition led to an increasing separation of both the TEU and TER events from the metastable (white) eutectic temperature. Thus inoculation acts initially to avoid free carbide formation and, later, to limit the possibility of undercooled graphite formation. This performance is improved by increasing the inoculant addition rate, especially for the in-mold/cup treatment. The difference between un-inoculated and inoculated irons is strongly affected by the alloy addition rate, much more so for ladle inoculation, as the inoculation index ($I_2$) shows (Fig. 7d). The late inoculation technique is consistently at a higher efficiency for the entire range of inoculant additions but especially at the lower levels (less than 0.20wt.%).
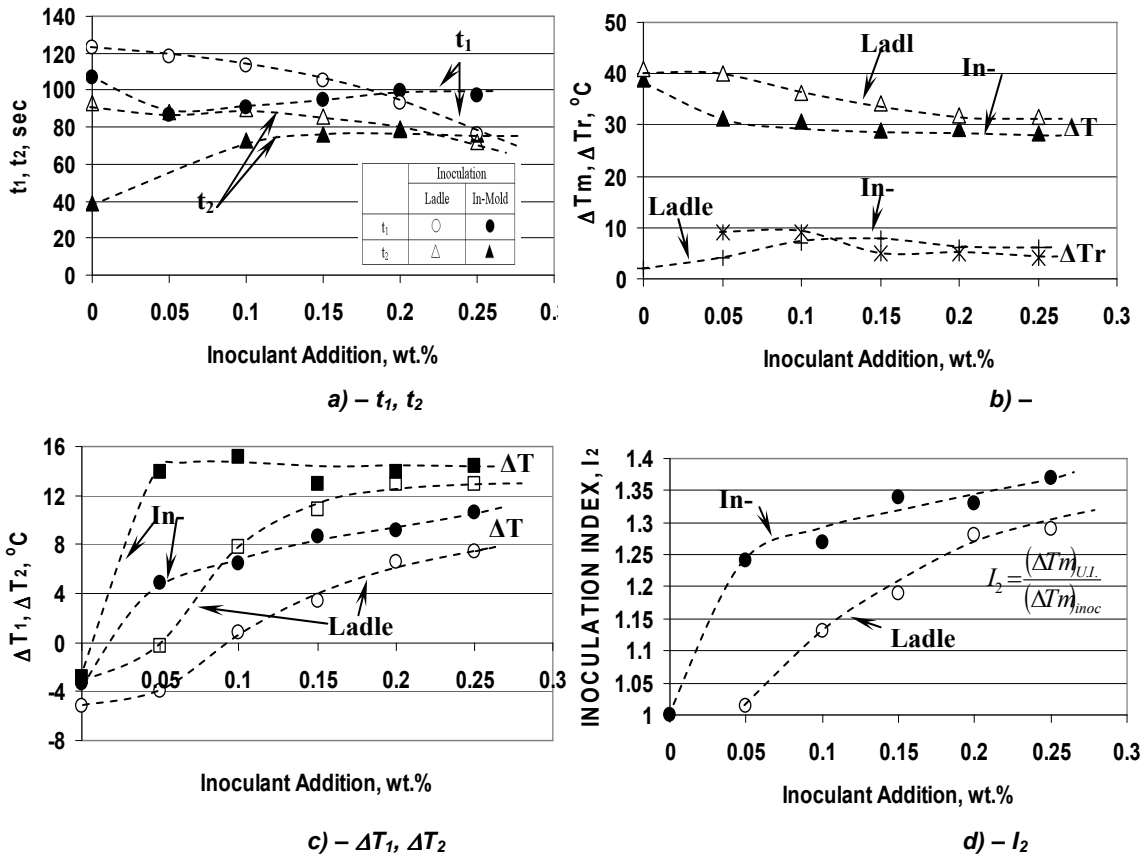
*Fig. 7. Representative parameters of eutectic solidification*

In many cases, graphitic recalescence ($\Delta Tr = TER - TEU$) is also an important parameter to evaluate the behavior of inoculated irons. It is a function of the amount of austenite and graphite that are precipitated during the first part of eutectic freezing. With high recalescence values, there might be a risk of micro-shrinkage and porosity, especially in soft molds such as green sand molds (high volume expansion causing pressure against a thinner metal skin). Figure 7b shows the evolution of the level of recalescence ($\Delta Tr$), as inoculant additions increase. A peculiar difference appears in the behavior of the in-mold/cup and ladle inoculated irons. At no more than 0.1wt.% alloy addition, high recalescence level characterizes the in-mold treated irons especially due to the higher TER temperature. An opposite result was obtained for these two inoculation techniques at more than 0.10wt.% alloy addition rate, when higher recalescence was typical for ladle inoculated irons. Lower differences were obtained between the two techniques for more than 0.20wt.% inoculant.

The end of the eutectic solidification is also very important, especially because the micro-shrinkage occurs at the latter part of solidification, usually at hot spots or parts with a large cooling modulus. White iron solidification as intercellular carbides and / or inverse chill formation is also dependent on the position of the temperature of the end of solidification (TES), compared to the metastable (white) eutectic temperature (Tmst). Figure 8 illustrates the evolution of TES, its position given Tmst ($\Delta T_3 = TES - Tmst$) and of the FDES (the first derivative at solidus), as the inoculant addition rate increases. TES solidus temperature is an important parameter that is sensitive to certain elements. This point can be found at the latest part of the first derivative, as the

lowest of the negative peak. Experimental un-inoculated and inoculated irons have a solidus temperature range (TES) of 1090°C to 1107°C (1994-2024.6°F), but lower than the solidus temperature under metastable conditions (Tmst equal to 1125 to 1128°C / 2057-2062°F). Because this difference ($\Delta T_3$ parameter) is generally more than 20°C (68°F), these irons will be sensitive to chill tendency and micro-shrinkage formation.

A preferred end of solidification means high solidus temperature and low level of the $\Delta T_3$ parameter (usually as low negative value, as TES < Tmst in most cases). A low value of FDES (more negative) is also favorable as it correlates to a high amount of graphite at the end of freezing. Figure 8 shows that the solidification pattern of inoculated irons is more favorable compared to that of un-inoculated irons.



a) - TES

b) - $\Delta T_3$

c) - FDES
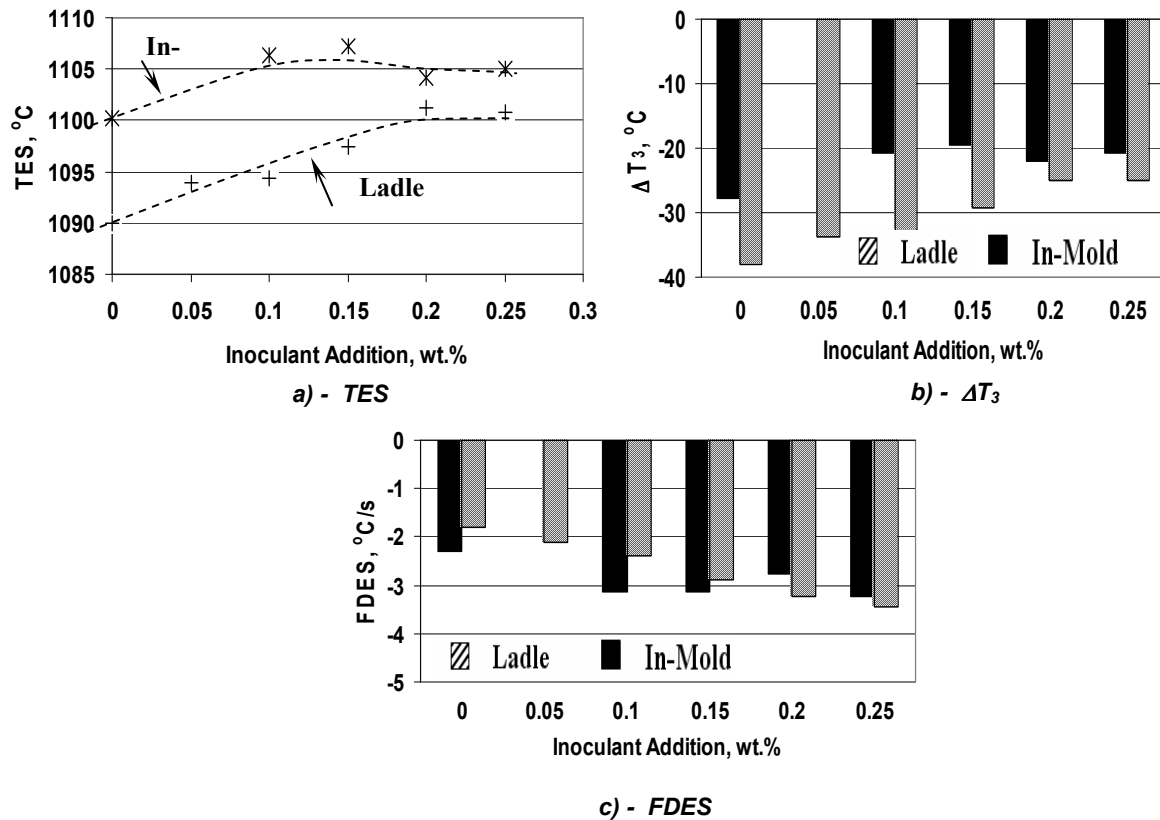
Fig. 8. *Representative parameters at the end of solidification*

Increasing the alloy addition improves the behavior of irons at the end of solidification but in a different manner for in mold/cup and ladle inoculation methods. 0.10-0.20wt.% inoculant stabilizes the parameters representing solidification at a favorable level for in-mold/cup inoculation compared to 0.20-0.25wt.%, for ladle inoculation.

The ASTM $W_{31/2}$ Chill Test Wedge method was used to evaluate chilling tendency. The design of the test specimen promotes an accelerated cooling rate, and favors the formation of chill at the apex of the wedge. The area nearest the apex, which was entirely free of any eutectic cells or gray spots, was designated as clear chill. The chill depth measured from the junction of the gray fracture and showing the first appearance of chilled iron was designated as total chill. At low carbon equivalent level and lower sulfur and residual aluminum, the base iron has a high chill tendency. Despite this situation, the in-mold inoculation by Ca, Zr,Al-FeSi alloy was very effective at very

low addition rates  (Fig. 9), according to its ability to decrease the degree of eutectic undercooling (Fig. 10).

The effects of inoculation were also analyzed by comparing the microstructures of irons treated with different amounts of Ca,Zr,Al-FeSi alloy, with both inoculation techniques, utilizing the 20 mm diameter bars. The graphite morphology was drastically improved. The amount of undercooled graphite decreased with increasing inoculant addition rates, up to

mainly type-A graphite, as Figures 11a and 12 show. The presence of ledeburite and cementite was eliminated for 0.05wt.% and 0.15wt.% addition rates (Fig. 11b).  Again, the in-mold inoculation was more effective in avoiding undercooled graphite morphologies and free carbides, compared to ladle inoculation. A predominantly pearlitic structure (90-100% pearlite) was obtained in all cases: 90-98% pearlite for ladle inoculation compared to 98-100% pearlite for in-mold inoculation.
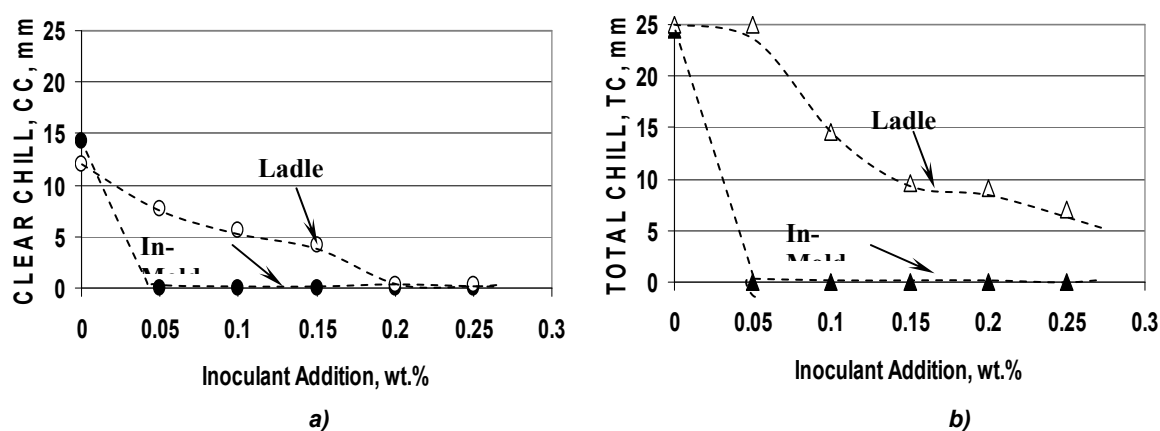


Fig. 9. *Clear chill (a) and total chill (b) of tested irons*
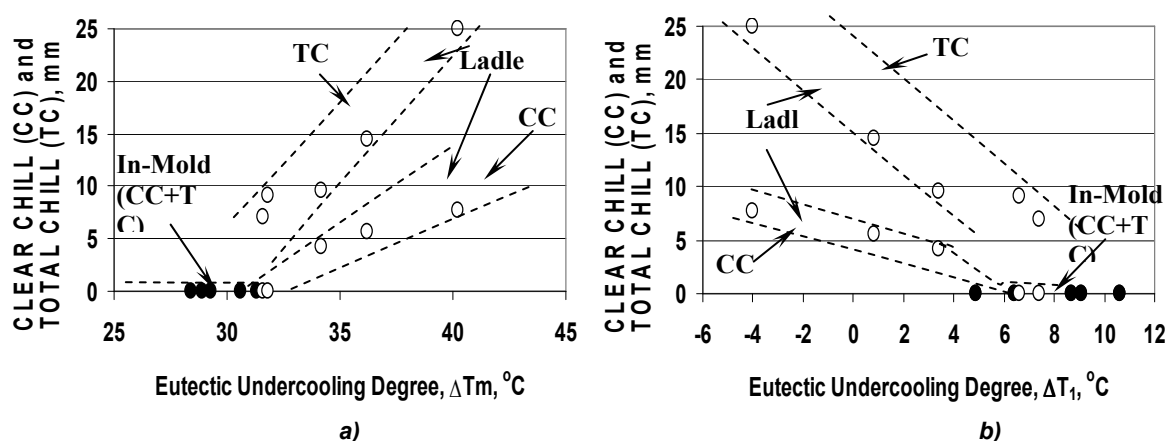


Fig. 10.  *Influence of eutectic undercooling □Tm (a) and □T₁ (b) on the clear chill (CC) and  total chill (TC) of inoculated irons.*

The effect of inoculation with various alloy additions on Brinell hardness was studied using 20 mm diameter bars. Brinell hardness values decreased with inoculant additions, regardless of inoculation technique type. The in-mold inoculation reduced

hardness values more rapidly than did ladle inoculation, according to the variation in amount of free carbides (Fig. 13).



a)                                                    b)
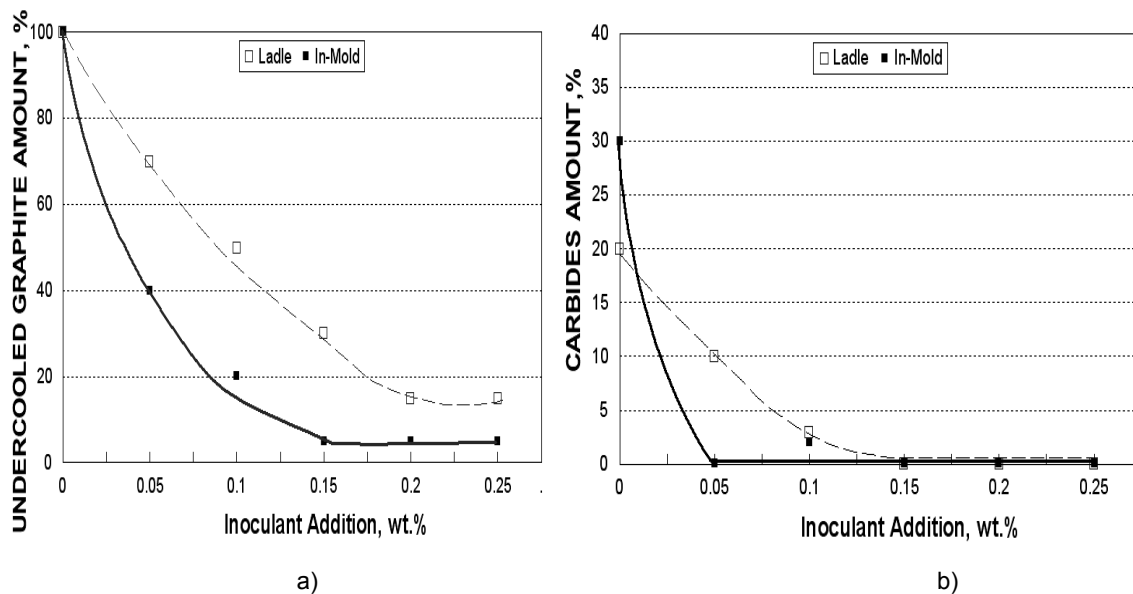
Fig. 11. *Undercooled graphite (a) and free carbides (b) amount of un-inoculated and inoculated irons*
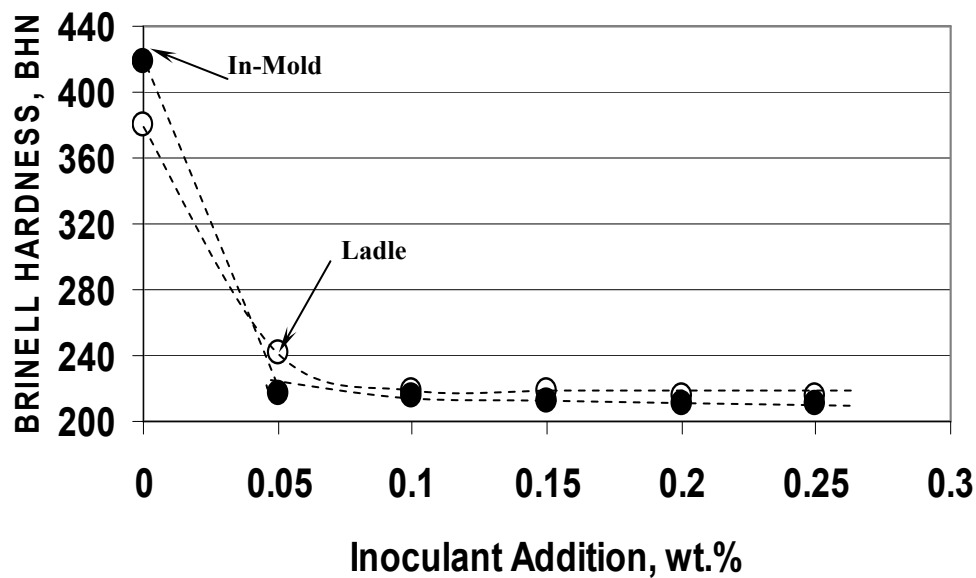


Fig. 13. *Brinell hardness of un-inoculated and inoculated irons (20 mm diameter bars).*
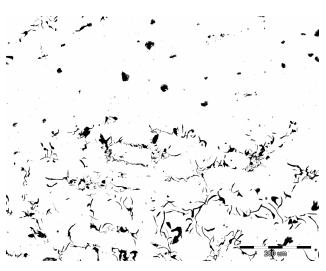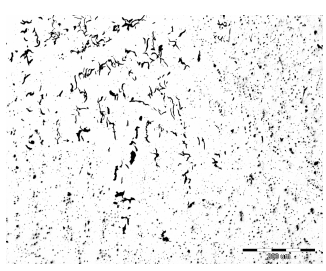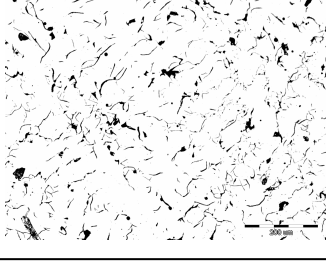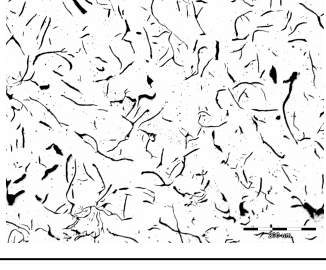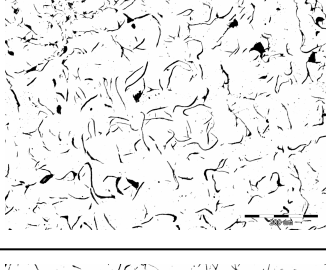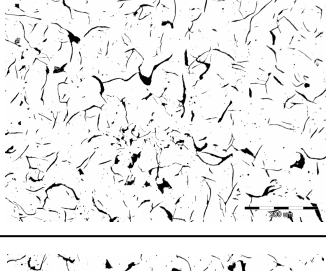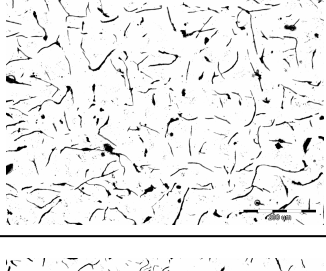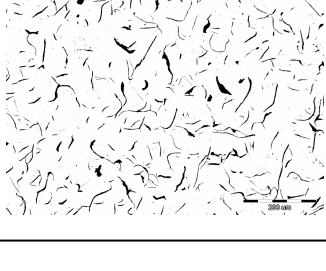
| Inoculant Addition, wt.% | Inoculation Technique | |
|---|---|---|
| | In Ladle | In Mold |
| UI | | |
| 0.05 | | |
| 0.10 | | |
| 0.15 | | |
| 0.20 | | |
| 0.25 | | |

*Fig. 12. Graphite morphology in un-inoculated (UI) and inoculated gray cast irons (0.05…0.25 wt. % alloy).*

# 4. CONCLUSIONS

Generally, the optimal cooling curve varies for different castings (due to their configuration) and various types of mold materials due to mold stability. It was found that the solidification pattern of the low sulfur and low residual aluminum gray irons as tested was influenced not only by the inoculant addition rate (0…0.25wt.%), but also by the inoculation technique (in-mold and ladle):

- Eutectic undercooling of the base iron having 0.025%S, 0.003%Al and 3.5%CE is excessively high (39-40$^{o}$C / 102-104$^{o}$F), demonstrating a relatively high need for inoculation;
- Under these conditions, the in-mold inoculation had a significant effect compared to ladle inoculation, at lower inoculant usage (less than 0.20wt.%);
- Lower levels of eutectic undercooling ($\Delta Tm$), recalescence ($\Delta Tr$) and undercooling at the end of solidification ($\Delta T_3$) are characteristic for in-mold treatment at lower inoculant addition rates, promoting lower tendency for carbides, undercooled graphite, intercellular carbides and inverse chill;
- The difference between un-inoculated and inoculated irons is strongly affected by the alloy addition rate, much more so for ladle inoculation;
- Generally, the efficiency of 0.05-0.15wt.% alloy for in-mold inoculation is comparable to or better than 0.15-0.25wt.% additions in ladle inoculation procedures  (Table 3);
- A Zr,Ca,Al-FeSi alloy appears to be efficient in low S, low Al low CE hypo-eutectic gray cast irons, especially for late inoculation.

Table 3. Representative Parameters of the Solidification of Inoculated Gray Irons
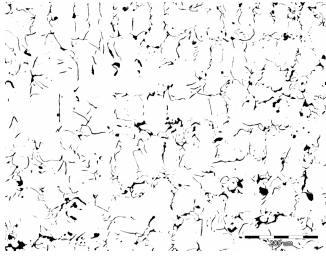
| Representative Parameter | Literature Optimal Value | The Experimental Best Values | | | |
|---|---|---|---|---|---|
| | | In Mold/Cup Inoculation | | Ladle Inoculation | |
| | | Representative Value | Minimum Alloy Addition Rate, (wt.%) | Representative Value | Minimum Alloy Addition Rate, (wt.%) |
| $\Delta Tm=Tst-TEU$, ($^{o}$C) | 20-35 (UI) | 39 | - | 40 | - |
| | < 25 (Inoc.) | 28 | 0.15 | 32 | 0.20 |
| $\Delta T_1=TEU-Tmst$, ($^{o}$C) | 25 | 9 | 0.20 | 7 | 0.25 |
| $\Delta Tr=TER-TEU$, ($^{o}$C) | 2-5 | 4-5 | 0.15 | 5-6 | 0.20 |
| $\Delta T_3=TES-Tmst$, ($^{o}$C) | < 20 | 20 | 0.15 | 25 | 0.20 |
| FDES, ($^{o}$C/s) | < (-3.5) | -3.25 | 0.15 | -3.45 | 0.25 |
| Clear Chill, (mm) | 0 | 0 | 0.05 | 0 | 0.15 |
| Total Chill, (mm) | 0 | 0 | 0.05 | 6 | 0.25 |
| Carbides, (%) | 0 | 0 | 0.05 | 0 | 0.15 |
| D-Graphite, (%) | 0 | 5 | 0.15 | 15 | 0.20 |

[1]*POLITEHNICA University of Bucharest, Romania*
[2]*Consultant Metallurgist, Fremont, California, USA*

**REFERENCES**

1. Loper Jr.,C.R. and Gundlach, R.B., "Inoculation What is it and How Does Inoculation Work", *AFS International Inoculation Conference,* Chicago, (1998).
2. Loper Jr.,C.R., "Inoculation of Cast Iron-Summary of Current Understanding", *AFS Transactions*, Vol. 107, pp.523-528 (1999).
3. Chisamera, M., Riposan, I. and Barstow, M., "The Importance of Sulphur to Control Graphite Nucleation in Cast Iron", *AFS International Inoculation Conference*, Chicago, (1998).
4. Riposan, I., Chisamera, M., Stan, St. and Skaland, T., "Graphite Nucleant (Microinsclusion) Characterization in Ca/Sr Inoculated Irons", *International Journal of Cast Metal Research*, Vol. 16, No.1-3, pp.105-111 (2003).
5. Riposan, I., Chisamera, M., Stan, St., Skaland, T., and Onsoien, M.I., "Analyses of Possible Nucleation Sites in Ca/Sr Over Inoculated Gray Irons", *AFS Transactions*, Vol. 109, pp.1151-1162 (2001).
6. Riposan, I., Chisamera, M., Stan, St. and Skaland, T., "A New Approach to Graphite Nucleation Mechanism in Gray Irons", *Proceedings of the AFS Cast Iron Inoculation Conference*, Sept. 29-30, 2005, Schaumburg, USA, pp.31-41 (2005).
7. Chisamera, M., Riposan, I., Stan, S. and Skaland, T., "Undercooling, Chill Size, Structure Relationship in Ca/Sr Inoculated Grey Irons under Sulphur/Oxygen Influence", *64th World Foundry Congress*, Paris, France, Sept. 11-14, 2000, Paper RO-62.
8. Riposan, I., Chisamera, M., Stan, S. and Skaland, T., "The Key Role of Residual Al in Chill Tendency and Structure Characteristics of Un-Inoculated and Ca/Sr Inoculated Grey Irons", *66th World Foundry Congress*, Istanbul, Turkey, Sept. 2004, pp. 775-790.
9. Chisamera, M., Riposan, I., Stan, S. and Skaland, T., "Investigation of Effect of Residual Aluminum on Solidification Characteristics of Un-Inoculated and Ca/Sr Inoculated Gray Irons", *AFS Transactions*, Vol. 112, pp. 867-877, (2004).
10. Riposan, I., Chisamera, M., Stan, St., Ecob, C. and Wilkinson, D., "Role of Al, Ti, Zr in Grey Iron Preconditioning/Inoculation", *World Foundry Organization (WFO) Technical Forum*, Dusseldorf, Germany, 12-14.06.2007.
11. Riposan, I., Chisamera, M., Stan, S., Toboc, P. and Ecob, C., "High Efficiency Preconditioning of Electrically Melted Grey Cast Irons", *68th World Foundry Congress*, Chennai, India, February 7-10, 2008.
12. Preseed Preconditioner Booklet, ELKEM Foundry Products Division, www.foundry.elkem.com (2007).
13. Sillen, R.V., "Optimizing Inoculation Practice by means of Thermal Analysis", *AFS International Inoculation Conference*, Chicago, (1998).
14. Sillen, R.V., Novacast Technologies, www. novacast.se, (2006).
15. Sparkman, D., "Understanding Thermal Analysis of Iron", *AFS Transactions*, Vol. 102, pp.229 (1994).
16. Sparkman, D. and Bhaskaram, C.A., "Chill Measurement by Thermal Analysis", *AFS Transactions*, Vol. 104, pp.969-976 (1996).
17. Gunay, Y., Decirmenci, S., Metan, I. and Sirin, B., "The Application of Adaptive Thermal Analysis System (ATAS) on Grey and Ductile Iron Production", *66th World Foundry Congress*, 06-09.09.2004, Istanbul, Turkey.
18. ZIRCINOC Inoculant-Product Data Sheet, ELKEM Foundry Products Division, www.foundry.elkem.com (2007).

**SOLIDIFICAREA FONTELOR CENUŞII HIPOEUTECTICE TURNATE CU CONŢINUT SCĂZUT DE SULF MODIFICATE ÎN FORMĂ ŞI ÎN OALĂ**

(Rezumat)

*O comparaţie a tratamentelor de modificare în formă şi în oală a fost realizată pentru fonte cenuşii hipoeutectice turnate (CE=3.5÷3,6%) cu conţinut scăzut de sulf şi aluminiu, tipic pentru fontele elaborate electric utilizând o încărcătură cu conţinut ridicat de deşeuri de oţel. Acest studiu descrie efectul unui aliaj Ca,*

*Zr, Al-FeSi la un adaos de 0...0,25% asupra parametrilor analizei termice şi caracteristicilor fontei turnate (structură şi duritate). Subrăcirea eutectică a fontei considerate ce are caracteristicile menţionate mai sus, este excesiv de mare (39÷40 $^0$C/ 102÷104$^0$F) determinând necesitatea modificării. Nivele mai mici ale subrăcirii eutectice (ΔTm), recalescenţa (ΔTr) şi subrăcirea la sfârşitul solidificării(ΔT$_3$)sunt caracteristice pentru tratamentul în formă la adaosuri de aliere mai mici, determinând o tendinţă mai scăzută pentru formarea carburilor, grafitului subrăcit, carburilor intercelulare şi apariţia răcirii inverse. Diferenţa dintre fontele nemodificate şi cele modificate este puternic afectată de cantitatea de modificator, în mare măsură pentru modificarea în oală. În general, eficienţa unui adaos de 0,05÷0,15 %masice pentru modificarea în formă este comparabilă sau mai bună decât un adaos de 0,15÷0,25 %masice în cazul modificării în oală. Un aliaj Ca, Zr, Al-FeSipare a fi eficient pentru fontele cenuşii turnate hipoeutectice, în special pentru modificarea finală.*

# MAGMASOFT® – COMMITTED TO CASTING EXCELLENCE

### BY

### VIOREL DIORDUC

**Abstract:** *MAGMA – Building Trust in Simulation. Since its founding in 1988, MAGMA GmbH has been the pacesetter in defining a new direction for the foundry industry. Its use of foundry simulation has provided new insights into the casting process. New methods for optimizing castings and foundry processes have come from innovative developments. Today, casting process simulation tools have been successfully merged with metal casting engineering experience. The development of these technologies and their worldwide acceptance closely corresponds to the growth in technical understanding, software products and competent service provided by MAGMA, its subsidiaries and its R&D partners.*

**Keywords:** *casting, simulation, foundry, experiment, verification*

## Castings – a part of life

Castings play an important role in our daily lives. Although often painted or coated or even hidden behind plastic parts, they offer a stable inner structure and serve an important function in all kind of components in day-to-life. In mobile phones, laptops, cameras, kitchen appliances, sewing machines, bicycles, motorcycles and cars they are a necessity just as in ships, trains, airplanes or in civil constructions.

## Casting and design

"Castings should also be designed as such" or "Castings allows complete freedom of design". Both statements are true. If you wish to make use of the advantages to integrate multiple functions into a single component, you have to consider the individualities of castings such as process dependent mechanical properties. That's why the use of simultaneous engineering and CA-Technologies is so important.

## Casting simulation integrates

Casting designers and foundry men need to work closely together. This leads to the realization of castings that are high in value and meet the performance demands. Integrating casting simulation into the design process chain is a prerequisite for successful applications.

Today's casting design is strongly supported by computer aided technologies. The design is done using CAD tools, finite element analysis (FEA) is applied to evaluate the performance of the component and prototypes are manufactured using RP technologies. Topology optimization is used to layout a casting design.

Casting simulation offers comprehensive information for the designer as well as for manufacturing.

## What is Casting Simulation?

In any case, it is not magic and not illusion, although it is still often treated as such. In casting simulation, modern information technology and the 4000 year old tradition and experiences of foundry technology come together. As casting simulation was born at several universities worldwide in the eighties, the mathematicians didn't understand the foundry men, and vice versa. At that time, no one imagined that casting simulation had potential to revolutionize a whole world branch and its technology.

## What is Needed…?

In order to take advantage of all benefits that casting simulation has to offer, a number of conditions must be met. First of all, it is necessary to have knowledge of the casting process and its accompanying problems that can only be gained through experience in the foundry. Without this knowledge, it is difficult to correctly formulate the problems to be simulated or to evaluate and interpret the simulation results. In addition, a binding agreement needs to be reached as to how the information won through simulation will be put into action on the shop floor. Finally, the foundry man needs a trustworthy simulation program, which is continuously tested, maintained and improved.

## Complete Solutions

The effective use of casting simulation can only take place if all of the important building blocks are present. These blocks include: import of CAD data and completion of the geometry using a 3D modeler; accurate models that mathematically describe the complex casting phenomena; a database with thermo-physical data for cast alloy, mold materials, cores, etc.; an interactive, intelligent user interface that can be understood by the foundry man; and interfaces to other CAE tools that allow the integration of simulation in the casting design process.

The successful use of simulation requires more than hardware, software and user. The foundry also has to be convinced that the simulation program will continue to grow and improve in the future. The development potential of the software provider is essential in this respect. The use of the software must be supported through training, good documentation, and use-case examples. Support needs to be competent, effective and available locally. The exchange of experiences and ideas with other users is guaranteed through user meetings and other seminars.

## Easy to Use

"Simulation will only be effective, when the computer feels the heat of the foundry". That means that the simulation program has to speak the language of the foundry man and needs to deliver information that can be directly translated into

action by him. In this respect, "user friendly" means more than a pretty user interface and includes the closest possible integration in the decision making process in engineering, quality assurance or production planning. User friendly also means that the simulation delivers the required results when they are needed. Thus, the time required for geometry preparation, automatic enmeshment, calculation and result evaluation all plan important roles.

## Physics

Casting is the most complex of production processes, and the quality of a casting is determined through complex physical, metallurgical and chemical process as well as through following production steps (e.g. heat treatment or machining). That is why it is not enough to simply simulate "mold filling" or "solidification". Rather, the casting quality has to be simulated. It is not possible to "make a deal" with the physics – 80% accuracy means 0% trust in the answers obtained. When casting properties should be predicted, the influencing parameters used by the foundry man – such as melting practice or metallurgy – have to be considered by the simulation program (see Figure 1).
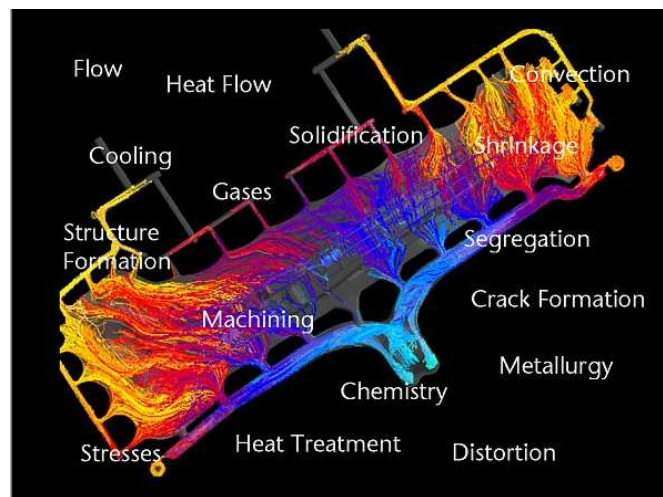


*Figure 1: Physics.*

## Modeling

The term "modeling" means, in general, an idealized reproduction of an object or a process. A good model reproduces the important characteristics of the original, but also makes intelligent simplifications where possible. In the modeling of a complex, technical process like casting it is necessary to identify, quantify and include the characteristic mechanisms and parameters into the model.

## Solution Algorithms

To solve the complex physical problems, it is necessary to divide the casting and mold geometries into small elements – the mesh – over which the equations can be

solved (see Figure 2). Regular (structured) or irregular (unstructured) meshes can be used. Both approaches are, when used correctly, comparable. A quick and automatic generation process is one advantage of structured mesh. Whichever mesh is used, the physical phenomena considered in the models solved on the enmeshment is of the most critical importance.



*Figure 2: Solution Algorithms.*

## Hardware

Although it was often necessary to have expensive workstations to carry out intensive simulations, today many calculations can be completed using laptops. Good PC's are now standard hardware for casting simulation. Nonetheless, computers are never fast enough – more and more physics is considered in the programs, the models become more and more complex, and the answers need to be there earlier and earlier. When simulation programs are parallelized, it is possible to take advantage of the extreme power of parallel computers. These "clusters" cost less than workstations used earlier. With the appropriate software installed on a cluster, "experimentation on the monitor" or automatic optimization becomes reality.

## Geometry

Simulation means checking different variations. Therefore, casting simulation requires the geometry of the gating and risering system and the complete mold in addition to a 3D model of the raw casting. Geometries for filters, riser sleeves, chills in sand castings or the cooling lines in die casting are not normally considered by the casting designer, and need to be added as quickly and easily as possible. For this reason, a simulation tool has construction capabilities that are similar to those of 3D CAD program (see Figure 3).
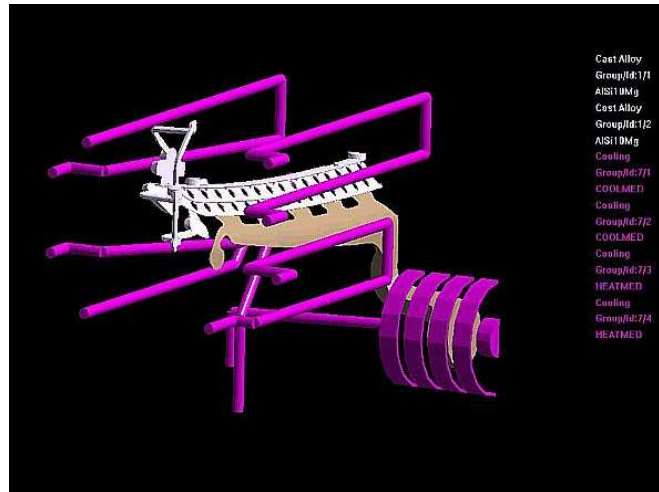
*Figure 3: A complete model for the simulation.*

## Integration

Simulation is more than hardware, software and user. It is only as good as its integration in the foundry. Simulation in an "ivory tower" produces pretty pictures, but not real results. That is why it is so important that all areas of the foundry consider the simulation results and use them in their decision-making processes (see Figure 4). Only in this way can areas such as quality assurance, product development and sales profit from the results. With this integration, simulation also becomes a management tool: communication, decision-making structures, transparency, standardization and employee education are supported. The foundry becomes more competitive.
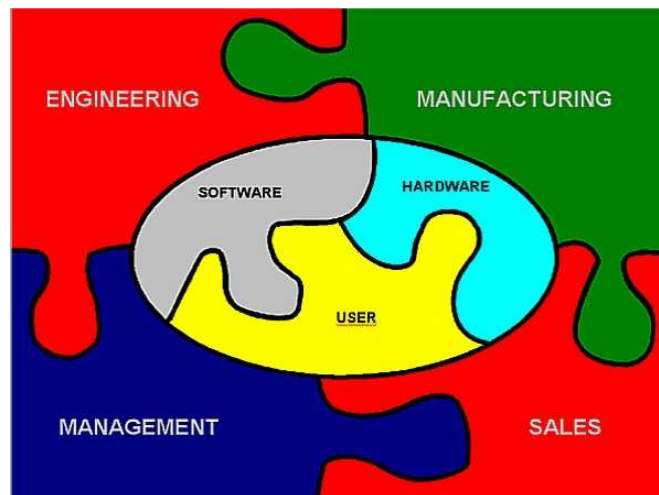


*Figure 4: Integration of casting simulation into the foundry.*

## Communication

In addition to information exchange within the foundry, simulation also supports communication with customers or development partners. This leads to a strengthening of the competence of the foundry. A frictionless exchange of data is

needed: between the foundry and the designer for consideration of simulation results in FE calculations; between the foundry and pattern-toolmaker for the return of changed or distorted geometries; between foundry and customer through simple exchange of experience with "concurrent engineering" tools over the internet.

## Visualization

Simulation produces millions of number. To create information out of this flood of data, the results have to be visualized. Only in this way, can knowledge be created. Modern results visualization delivers more than just pretty pictures – it must be possible to intuitively understand the calculated results. The information needs to be prepared and compressed by the software. Castings are three-dimensional and these dimensions can be made touchable already today using "virtual reality". The animation of the casting process delivers the fourth dimension – time.

## Experiments

No new simulation model without good experiments! This is true not only for the verification of the model. As simulation takes account to an increasing degree the real conditions in the foundry, such as metallurgy and melt practice, experiments become the basis for new model development. Good experiments couple physics with casting properties. Here (see Figure 5), the solidification pattern of cast iron test specimens in a sand mold as a function of different cooling conditions is shown. Only by using such information can new solidification models be developed, which allow the reliable prediction of casting properties.



*Figure 5: Practical experiments to follow the solidification pattern.*

## Verification

How exact is simulation? This question has been answered hundreds of times over the last 25 years. Castings are instrumented with thermocouples, plexiglas models are built, X-ray apparatus is used for real-time investigations (see Figure 6). All of

these investigations have shown that the equations describing the flow, heat transport and stress development are valid for casting processes. The critical point is that the inputs to the simulation reflect the real casting processes. Then, simulation is more accurate than the measurement techniques used for its validation – it delivers results at every location at every time (shown here is the filling of a water model).
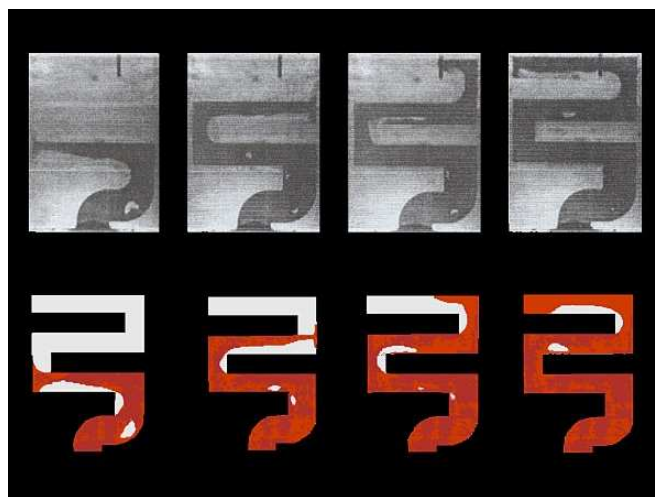


*Figure 6: The verification of simulation using the X-Ray method.*

## Conclusions

Optimizing metal castings requires deep process insight. Simulation is one important tool in this effort. Combined with casting knowledge, MAGMA helps the foundry men to find solutions to today metal casting challenges, from design through production to performance of the component. Metallurgists, process engineers and other experts understand how to convert simulation results into real world casting solutions.

***Where you find castings, you find MAGMA!***

**MAGMASOFT® – PRODUCE EXCELENŢA ÎN TURNARE**

**Rezumat***:* Încă de la înfiinţarea din 1988, *MAGMA GmbH* a fost instituţia care a definit o nouă direcţie pentru industria de turnătorie. Utilizarea la simularea în turnătorie a determinat o nouă înţelegere a procesului de turnare. Metode noi de optimizare a turnării şi proceselor din turnătorie au fost determinate de progresele inovative. Astăzi, mijloacele de simulare a procesului de turnare a fost cuplat cu succes cu experienţa turnării metalelor. Dezvoltarea acestor tehnologii şi acceptarea lor largă corespunde creşterii în înţelegerea tehnică, produselor software şi consultanţei asigurate de MAGMA, filialele ei şi partenerii R&D.

# A CRITICAL ANALYSIS OF INTENSIFYING THE HEAT TRANSFER PROCESSES

BY

## A.A. MINEA, A. DIMA

**ABSTRACT**: *Metals heating in the furnace are conditioned with the determination of metal heating time into a furnace with known basic characteristics. Heating time of the charge is main component of furnace function time and is traced in power consumption of the equipment. The theoretic study of industrial furnaces gas dynamics used at theoretic determination of an optimum circulation of the air in the chamber for decreasing furnace function time. There are also obtained information regarding the dependency between the equipment walls temperature and the circulation speed of the air into work chamber.Protecting the environment became, at this time, a major problem of all the humanity.In the present article, on the basis of the new scientifically ways to board the "TO KNOW HOW" area, we are proposing for analysis another way to board the sustainable development concept.*

**KEYWORDS:** *industrial development, heat transfer, new concept*

## 1. INTRODUCTION

The critical analysis of intensifying techniques of heat transfer was realize by itself identification of the applied methods regardless the process specific.

Bellow there will be presented all the intensification techniques of heat and mass transfer processes such as
- Turbulence promoters
- Oscillations
- The increase of transfer surface
- The increase of turbulence degree of the medium
- By increasing the moving force (potential difference) of transfer process
- Other methods.

### 1.1. The intensification of transfer processes by using turbulence promoters

The turbulence promoters induce a supplementary local turbulence which leads to increasing transfer speed.

*The intensification of energy transfer through surface turbulence promoters.* Heat transfer can be intensified by modifying the surface state pursuant to artificial roughness introduction. These realize a flow modification in limit layer which lead to increasing superficial coefficient of heat transfer but also friction coefficient. There are the following used roughness types: channel, rib, granular.

Ribs like channel type represent profiles mechanically processed in the heat exchange surface wall and are shaped as annular channels thread type with 1 till 6 beginnings,

trapezoidal and triangular types or with other different geometries of the grooves. In figure 1 there are presented some thread type roughness.
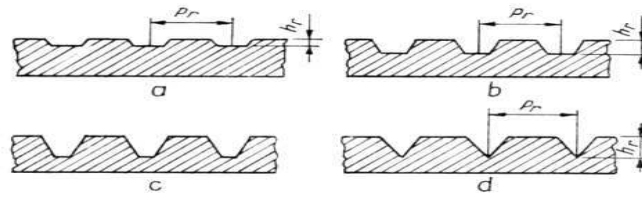


*Figure 1. Thread type roughness:*
*a, c – Trapezoidal thread with a beginning; b – trapezoidal thread with 6 beginnings; d – triangular thread*

Rib type roughness is realized as:
-           Thin metallic bands welded longitudinally or transversal on the exterior of the pipes;
-           Rectangular or triangular ribs transversal, helicoidally and lamellar processed on the exterior surface of spiral tubes;
-           Free or welded wire rings on the exterior or interior surfaces.
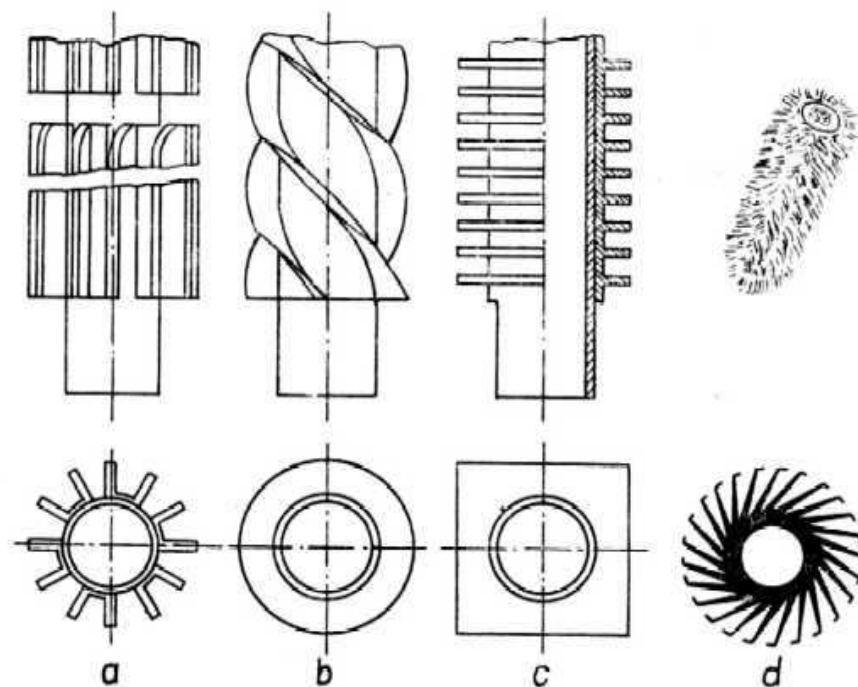


*Figure 2. Tubes with exterior ribs*
*a – longitudinal; b – helicoidally; c – radial; d - lamellar*

In figures 2 and 3 it is presented this roughness type.
Granular roughness is asperities with different shapes and dimensions obtained through metallic surfaces friction with paper and diamond paste.

Some studies regarding the roughness effect of the thread type on the heat transfer in nuclear reactors took to an efficiency criterion: $E_r = \dfrac{\alpha_r}{\alpha}\dfrac{f}{f_r}$; where $\alpha_r$ and $\alpha$ are convective transfer coefficients, in roughness presence and in its absence; f, $f_r$ – friction coefficients for smooth pipe and for roughness pipe.

For the same studies regarding the thread type roughness shows that maximum efficiency is get at the value: $p_r / h_r = 23...28$; where: $p_r$ is channels' step; $h_r$ – roughness height.

This criterion permits the comparison of the different roughness types.

***The intensification of energy transfer through turbulence shifting promoters of the fluid.*** The intensification of heat transfer is made with shifting promoters which create an artificial turbulence within the mass of the fluid.

Figure 3. Exterior roughness

*a – welded wire curl; b – free fibers*
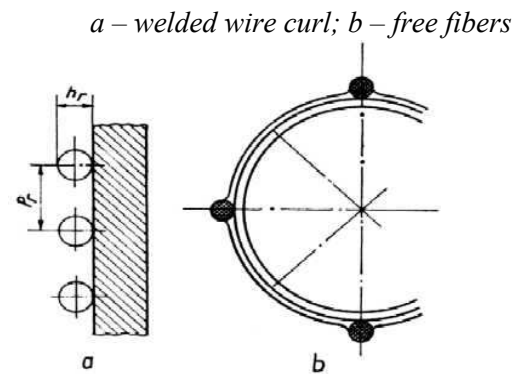


In figure 4 there are presented some promoters types by their montage within the pipes. These are:

- Plane curls;
- Swirling paddles;
- Conical surfaces;
- Twist metallic bands.
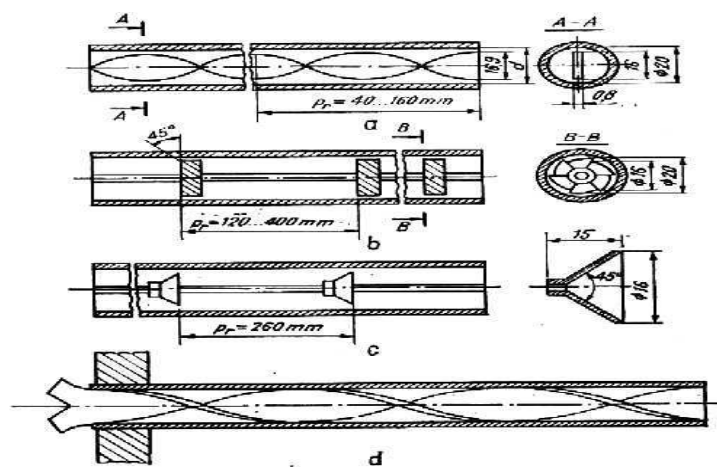


*Figure 4. Turbulence promoters mounted in the pipes*
*a – plane curl; b – Swirling paddles oriented under a 45° angle towards flowing current; c – conical surfaces; d – twist metallic bands.*

In practice the highest efficiency is get by using the devices with swirling paddles at numbers Re < $10^4$.

Also by placing the turbulence promoters on the exterior surface of the interior tube circular space, there are increases of heat flow about 60% in regard to the case without turbulence promoters.

## 1.2. The intensification of transfer processes through oscillations

This consists in superposition of some oscillatory moving over the normal moving of the fluids. They are created by using pulsations, mechanic, sonic and ultrasonic vibrations.

The oscillations applied to fluids are vibrations applied to the apparatus or in contact solid surface with the fluid or the pulsations applied to fluid medium.

*The use of vibrations for energy transfer intensification*

In heat transfer of Monophasic fluids mostly the horizontal cylinders and vertical surfaces were submitted to vibrations. The researches showed that the most convenient vibrations which lead to increasing the heat transfer coefficients are those applied to forced convection. The obtained effects are diverse by varying from transfer coefficient diminishing till its increasing about 300% and the phenomenon depends on the system and the vibration intensity which is defined as the product between amplitude (a) and oscillation frequency (ν). When vibration intensity is very big it also appears cavitations phenomenon. In this case it is produced a significant loss of heat transfer.

*The use of pulsations for energy transfer intensification*

In order to produce pulsations in the fluid there are used pulsation generators which can be flow switcher and piezoelectric transducers. These realize the pulsation of 1 Hz until ultrasounds of $10^6$ Hz.

Numerous researches were made for determining the sound effect on heat transfer from a horizontal cylinder to air.

The sound field was axially or transversal oriented towards horizontal or vertical surfaces. Thus, heat transfer coefficients, at free convection in liquids, can rise from 30% till 450% by the use or sounds and ultrasounds.

This transfer way is much more expensive than the use of forced convection (for example a simple agitator).

*The use of vibrations and pulsations in mass transfer intensification*

The oscillations use leads to mass transfer processes intensification (extraction, dissolution, sublimation) or in the operations with simultaneous heat and mass transfer (evaporation, correction, drying). Also for mass transfer, the intensification is realized both through decreasing transfer resistance as a result of turbulence increase in limit layer and fluid volume, and by increasing contact surface between phases. .

The intensification of mass transfer processes through vibration was realized for film fluid columns, column fillings, columns with continuous phase and a disperse phase bubble type, drops, solid particles and columns with agitation devices.

The vibrations applications to the filling columns determine mass transfer intensification because it realizes a uniform distribution of the liquid in the filling, a uniform cover of contact surface, relatively high flow speeds of the phases, high speed gradients at interface and turbulence in liquid film.

## 2. HEAT TRANSFER INTENSIFICATION BY SURFACES EXTENSION

The extension of heat exchange surface is used as an intensification method of convection processes for the fluids that realize small convection coefficients like gases. According to Newton relation $Q = \alpha S ( t_p - t_f)$, for a given difference between the wall and fluid temperature and a low value of $\alpha$ coefficient, the increase of heat flow Q can be done by increasing surface S.

The extension of heat exchange surface makes with the help of some ribs with different geometric shapes (longitudinal, radial, acicular, etc.) attached to a support surface (basic) made of the same material with support wall or of different materials.

The calculus of the ribs is based on the following simplifier hypotheses:

-     thermal regime is constant in time;
-     thermal conductivity of ribs material $\lambda$ = const.;
-     the rib is cooled by a fluid with uniform temperature $t_f$ = const., convection coefficient is constant on the entire rib surface, $\alpha$ = const.;
-     the temperature of rib's base is uniform, there are no contact heat resistances between rib and support wall;
-     the thickness of the rib is small comparing to its height so that temperature gradients can be neglected;
-     there are no interior heat sources in the rib, $q_v = 0$.

Based on these hypotheses heat transfer through rib will be unidirectional conduction with convection.
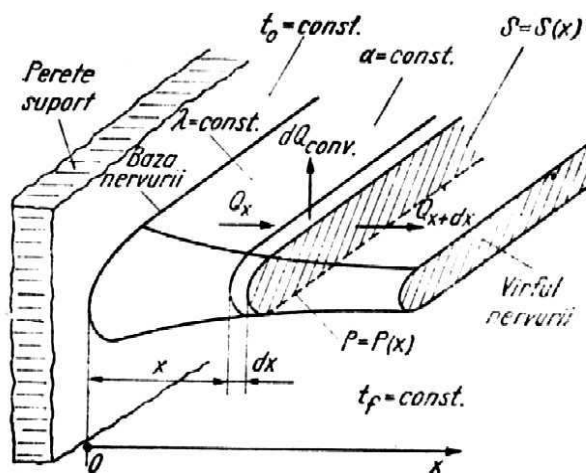


*Figure 5. Longitudinal rib with variable transversal section*

*The variable transversal section rib.* It is considered a rib with variable transversal section $S = S(x)$ and variable perimeter $P = P(x)$, in contact with a fluid with temperature $t_f$ = constant and its convection coefficient $\alpha$ = constant (figure 5.). In a

certain transversal section, including its lateral perimeter, the rib's temperature is the same: $t = t(x) > t_f$.

The temperature of rib's base is $t_0 = $ constant.

For volume element of dx thickness from the rib it can be written the next thermal balance:

$$Q_x = Q_{x+dx} + dQ_{conv},$$  (1)

where: $Q_x$ is heat flux that crosses x plan;

$Q_{x+dx}$ – heat flux that crosses x+dx plan;

$dQ_{conv}$ – heat flux transmitted to the fluid through convection.

It is obtained the differential equation after the balance calculus:

$$\frac{d^2t}{dx^2} + \frac{1}{S}\frac{dS}{dx}\frac{dt}{dx} - \frac{\alpha P}{\lambda S}(t - t_f) = 0.$$  (2)

If we introduce variable exchange $\theta = t - t_f$, where $\theta$ represents temperature excess between wall and fluid in $^0C$, and the report is noted as $m^2 = \alpha P / \lambda S$, ( $m^{-2}$ ); where:

$$m = m(x) = +\sqrt{\frac{\alpha P}{\lambda S}} , (m^{-1}).$$

The differential equation gets the general form

$$\frac{d^2\theta}{dx^2} + \frac{1}{S}\frac{dS}{dx}\frac{d\theta}{dx} - m^2\theta = 0.$$  (3)

*The constant transversal section rib.* For this type belongs the straight rib with constant thickness with rectangular profile. For it, $S = $ const., so that differential equation has the form

$$\frac{d^2\theta}{dx^2} - m^2\theta = 0.$$  (4)

*The optimum profile rib.* Usually, the ribs are made of materials with high thermal conductivities or corrosion resistant, both cases being very expensive. That is why it is searched the accomplishment of some ribs with minimum metal consumption for a certain quantity of heat.

The problem consists in determining the longitudinal profile of the rib so that unitary thermal flow transmitted through conduction remains constant from where it results that $d\theta/dx = C_1 = $ const. So, we have $\theta = C_1 x + C_2$, respectively a linear variation of the difference between lateral surface and fluid temperatures.

The only longitudinal rib that has a linear distribution of temperature difference $\theta$ is concave parabolic rib which fulfills the condition of minimum material consumption.

Technologically the execution of a longitudinal concave rib is difficult. In addition this profile has a low mechanical resistance. Taking into consideration that weight difference between a concave rib and a triangular one is very small, the latest being easy to realize, it can be accepted for practice use a triangular rib as an optimum form. Also from resistance motives the triangular rib is modified as a trapezoidal rib.

## 3. CONCLUSIONS

The determination of research directions realized through analytic analysis of intervention possibilities on heat processes at average temperatures.

The researches will be directed towards theoretical and practical research of electric furnaces and the simulation of industrial heat processes.

The theoretical methods of energetic efficiency are differentiated by heat installation specific. The main purpose is to reduce parking time of the charge in the installation therewith realizing the technologic objectives imposed by the process.

Hereinafter it will be emphasized some theoretical methods for energetic efficiency by presenting the physical-mathematical apparatus specific to chosen installation.

**REFERENCES**

1. M Mulas; S Chibbaro; G Delussu; I Di Piazza; M Talice, **Efficient parallel computations of flows of arbitrary fluids for all regimes of Reynolds, Mach and Grashof numbers ,** International Journal of Numerical Methods for Heat & Fluid Flow, Volume 12, Number 6, 2002,  (pp. 637 - 657)

2. M Piller; E Nobile, **Direct numerical simulation of turbulent heat transfer in a square duct**, , International Journal of Numerical Methods for Heat & Fluid Flow, Volume 12, Number 6, 2002,. (pp. 658 - 686)

3. Assunta Andreozzi; Oronzio Manca; Vincenzo Naso, **Natural convection in vertical channels with an auxiliary plate**, , International Journal of Numerical Methods for Heat & Fluid Flow, Volume 12, Number 6, 2002,  (pp. 716 - 734)

4. K.J. Hsieh; F.S. Lien**,  Conjugate turbulent forced convection in a channel with an array of ribs** ,International Journal of Numerical Methods for Heat & Fluid Flow, Volume 15, Number 5, 2002, (pp. 462 - 482)

5. M Raisee; A Noursadeghi; H Iacovides , **Application of a non-linear k- model in prediction of convective heat transfer through ribbed passages ,** International Journal of Numerical Methods for Heat & Fluid Flow, Volume 14, Number 3, 2002, (pp. 285 - 304)

6. E. N. Pis'mennyi, A. M. Terekh, V. A. Rogachev, V. D. Burlei, A. I. Rudenko,  **Calculation of Convective Heat Transfer of Plane Surfaces with Wire-Net Finning Immersed in a Cross-Flow**, HeatTransRes.no.1-2/2005, pp. 39-46

7.  Kamel Hooman, **Effects of Temperature-Dependent Viscosity on Thermally Developing Forced Convection through a Porous Medium ,** HeatTransRes.no.1-2/2005, pp132-140

8. V. A. Kalitko, A. L. Mosse, **Plasma-Fired Processes of Treatment of Toxic and Radioactive Waste in a Shaft Furnace with a Filter Bed of Combustible Material ,** HeatTransRes.no.5-6/2004, pp.6

9. P. A. Pavlov, **Heat and Mass Transfer under the Conditions of Rapid Heating,** HeatTransRes.no.1-2/2005, pp.5

10. V. T. Borukhov, V. I. Timoshpol'skii, G. M. Zayats, et al., **Structural Properties of Dynamic Systems and Inverse Problems of Mathematical Physics ,** Journal of Engineering Physics and Thermophysics,Volume 78, Number 2, 2005, ISSN: 1062-0125, pp. 201 - 215

11. V. A. Kudinov, V. V. Dikop, S. A. Nazarenko, et al, **On One Method of Solving Nonstationary Heat-Conduction Problems for Multilayer Structures,** Journal of Engineering Physics and Thermophysics,Volume 78, Number 2, 2005, ISSN: 1062-0125, pp. 225 - 230

12. Yu. S. Teplitskii, **On the Cluster Structure of a Circulating Fluidized Bed,** Journal of Engineering Physics and Thermophysics,Volume 78, Number 2, 2005, ISSN: 1062-0125, pp. 316 - 322

# O ANALIZA CRITICA A INTENSIFICARII PROCESELOR DE TRANSFER

**REZUMAT:** *Aceasta lucrare prezinta o analizaa critica a intensificarii proceselor de transfer de caldura., incepand cu cateva metode specifice de marire a turbulentei procesului. In a doua parte este prezentata o metoda de intensificare a convectiei, prin extinderea suprafetelor de schimb de caldura. In prezenta lucrare, pe baza perceptelor noii modalitati stiintifice de abordare a domeniului „TO KNOW HOW”, va propunem spre analiza o alta modalitate de abordare a conceptului de intensificare a proceselor de transfer.*

# A THEORETICAL APPROACH OF THE DENDRITIC MORPHOGENESIS THROUGH THE FRACTAL THEORY

BY

**IRINEL CASIAN-BOTEZ[1], IOAN CARCEA[2], PETRICA NICA[3], MARICEL AGOP[3]**

**Abstract:** Considering that the motion of microphysical object takes place on continuous but non-differentiable curves, i.e. on fractals, some properties of the dendritic 'field' using the scale relativity theory in the topological dimension $D_T = 3$ are analyzed. In the one-dimensional differentiable case, the dendritic morphogenesis process is achieved by cnoidal oscillation modes of the speed field and an Oldfield's relation type is obtained. In the non-differentiable case, the fractal kink spontaneously breaks the vacuum symmetry by tunneling and generates coherent structures. Since all the properties of the speed field are transferred to the thermal one and the fractal potential acts as an energy accumulator, a micro-domain having the same super-cooling degree (virtual crystallization germ) appears. The local coherence of these structures generates a stable crystallization germ and the global one generates the dendrite (as a crystallization grain).

## 1. INTRODUCTION

Dendritic growth is the common mode of solidification encountered when metals and alloys freeze under low thermal gradients. The growth of the dendritic in pure metals depends on the transport of latent heat from the moving crystal-melt interface and influence the weaker effects like the interfacial energy[1].

The first theoretical treatment of the "free" dendrite growth problem was established in[2]. Additional considerations, such as the effect of curvature on the melting point[3], stability[4] and eventually the anisotropy of the surface tension[5] were also considered. Other dendritic theories for constrained growth, such as directional solidification of dilute binary alloys between microscope slides, have been developed in[6-10].

Recently, the 'dendrite problem' was reexamined in a more general context of non-linear self-organizing pattern formation phenomena[6,11] and particularly, in the fractal theory[12]. From this perspective, in the present paper, the dendritic morphogenesis process through the fractal theory (Scale Relativity Theory[13,14]) is analyzed.

## 2. MATHEMATICAL MODEL

The theoretical description of microphysical systems is generally based on Schrödinger's wave mechanics, Heisenberg's matrix mechanics, or on Feynman's path-integral mechanics. Another approach is the hydrodynamic formulation of quantum mechanics. Scale Relativity Theory (SRT)[13,14] is a new approach to understand quantum mechanics, and moreover physical domains involving scale laws,

such as chaotic systems. It is based on a generalization of Einstein's principle of relativity to scale transformations. Namely, one redefines space-time resolutions as characterizing the state of scale of reference systems, in the same way as velocity characterizes their state of motion. Then one requires that the laws of physics apply whatever the state of the reference system, of motion (principle of motion-relativity) and of scale (principle of SRT). The principle of SRT is mathematically achieved by the principle of scale-covariance, requiring that the equations of physics keep their simplest form under transformations of resolution.

A non-differentiable continuum is necessarily fractal and the trajectories in such a space (or space-time) own (at least) the following three properties (for details see Appendix A): i) The test particle can follow an infinity of potential trajectories: this leads one to use a fluid-like description; ii) The geometry of each trajectory is fractal (of dimension 3 – for other details on the fractal dimension see[15,16]). Each elementary displacement is then described in terms of the sum, $d\mathbf{X} = d\mathbf{x} + d\xi$, of a mean classical displacement $d\mathbf{x} = \mathbf{v}dt$ and of a fractal fluctuation $d\xi$, whose behavior satisfies the principle of SRT (in its simplest Galilean version). It is such that $\langle d\xi \rangle = 0$ and $\langle d\xi^3 \rangle = (6D^2/c)dt$ where $D$ defines the fractal/non-fractal transition, *i.e.* the transition from the explicit scale dependence to scale independence and c is the light speed in vacuum.. The existence of this fluctuation implies introducing new third order terms in the differential equation of motion; iii) Time reversibility is broken at the infinitesimal level: this can be described in terms of a two-valuedness of the velocity vector for which we use a complex representation, $V = (v_+ + v_-)/2 - i(v_+ - v_-)/2$. We denoted by $v_+$ the "forward" speed and by $v_-$ the "backward" speed.

These three effects can be combined to construct a complex time-derivative operator (see Appendix A)

$$\frac{\delta}{dt} = \frac{\partial}{\partial t} + V \cdot \nabla + \frac{D^2}{c}\nabla^3 \tag{1}$$

Now, the first Newton's principle in its covariant form $\delta V/dt = 0$, becomes (see Appendix A)

$$\frac{\delta V}{dt} = \frac{\partial V}{\partial t} + V \cdot \nabla V + \frac{D^2}{c}\nabla^3 V = 0 \tag{2}$$

*i.e.* **a Korteweg – de Vries (KdV) type equation in a fractal space-time**. This means that, both of the differential scale and the fractal one, the complex acceleration field, $\delta V/dt$, depends on the local time dependence, $\partial_t V$, on the non-linearity (convective) term, $V \cdot \nabla V$, and on the dispersive one, $\nabla^3 V$. Moreover, the behaviour of a "non-differentiable fluid" is viscoelastic or hysteretic type. A such result is in agreement with the opinion given in[14]: the non-differentiable fluid can be described by Kelvin-Voight or Maxwell rheological model with the aid of a complex quantities e.g. the complex speed field, the complex acceleration field etc.

From Eq.(2) and by the operational relation $V \cdot \nabla V = \nabla(V^2/2) - V \times (\nabla \times V)$ we obtain the equation:

$$\frac{\delta V}{dt} = \frac{\partial V}{\partial t} + \nabla\left(\frac{V^2}{2}\right) - V \times (\nabla \times V) + \frac{D^2}{c}\nabla^3 V = 0 \tag{3}$$

If the motions of the "non-differentiable fluid" are irrotational, *i.e.* $\boldsymbol{\Omega} = \nabla \times V = 0$ we can choose $V$ of the form:

$$V = \nabla\phi \tag{4}$$

with $\phi$ a complex speed potential. Then, equation Eq.(3) becomes:

$$\frac{\delta V}{dt} = \frac{\partial V}{\partial t} + \nabla\left(\frac{V^2}{2}\right) + \frac{D^2}{c}\nabla^3 V = 0 \tag{5}$$

and more, by substituting Eq. (4) in Eq. (5), we have

$$\nabla\left(\frac{\partial\phi}{\partial t} + \frac{1}{2}(\nabla\phi)^2 + \frac{D^2}{c}\nabla^3\phi\right) = 0 \tag{6}$$

This yield:

$$\frac{\partial\phi}{\partial t} + \frac{1}{2}(\nabla\phi)^2 + \frac{D^2}{c}\nabla^3\phi = F(t) \tag{7}$$

with $F(t)$ a function of time only. We realize that Eq. (5) have been reduced to a single scalar relation (7), i.e. a Bernouilli-type equation.

If $\phi$ simultaneously becomes complex speed potential and wave-function, i.e. $\phi = -2iD\ln\psi$, with $D$ the Nottales' coefficient[13,14], the Eq.(7), up to an arbitrary phase factor which may be set to zero by a suitable choice of the phase of $\psi$ i.e. $F(t) \equiv 0$, implies the non-linear Schrödinger type equation:

$$D^2\Delta\psi + iD\partial_t\psi + \left(-2D^2\Delta\ln\psi + \frac{iD^3}{c}\nabla^3\ln\psi\right)\psi = 0 \tag{8}$$

For $2m\hbar = D$ with $\hbar$ the reduced Planck's constant and $m$ the rest mass of a test particle[13,14], the Eq. (8) takes the standard form:

$$\frac{\hbar}{2m}\Delta\psi + i\hbar\partial_t\psi - U\psi = 0$$

where $U$ is the complex potential:

$$U = \frac{\hbar}{m}\Delta\ln\psi - i\frac{\hbar^6}{4m^2c}\nabla^3\ln\psi$$

Let us consider the relation (4) in the form:

$$V = v + iu \tag{9}$$

According to our previous observations (see also the Appendix A), $v$ will correspond to the classical speed given by the differential part of $V$, and $u$ will correspond to the fractal speed given by the non-differential part of $V$. By replacing (9) in Eq.(5) and separating the real part from the imaginary one, we obtain the following system:

$$\frac{\partial v}{\partial t} + v\nabla v - u\nabla u + \frac{D^2}{c}\nabla^3 v = 0$$

$$\frac{\partial u}{\partial t} + v\nabla u + u\nabla v + \frac{D^2}{c}\nabla^3 u = 0$$

(10a, b)

In the differentiable case, i.e. $u = 0$, the system (10a,b) becomes:

$$\frac{\partial v}{\partial t} + v\nabla v + \frac{D^2}{c}\nabla^3 v = 0 \qquad (11)$$

Considering that the dendritic morphogenesis process is one-dimensional[8-12], Eq. (11) takes the standard form of the KdV equation[17]:

$$\frac{\partial v}{\partial t} + v\frac{\partial v}{\partial x} + \frac{D^2}{c}\frac{\partial^3 v}{\partial x^3} = 0 \qquad (12)$$

Using the dimensionless parameters[11,12], $\phi = (v/v_0)$, $\tau = \omega_0 t$, $\xi = k_0 x$ and the normalizing conditions[11,12] $k_0 v_0 = D^2 k_0^3/c = 6\omega_0$, Eq. (12) becomes:

$$\partial_\tau\phi + 6\phi\partial_\xi\phi + \partial_{\xi\xi\xi}\phi = 0 \qquad (13)$$

Through the substitutions $w(\theta) = \phi(\xi,\tau)$, $\theta = \xi\text{-}u\tau$, where $(\omega_0,k_0,v_0)$ are parameters characterizing the critical speed field of the dendrites (for other details see[11,12]), the Eq. (13), by double integration, becomes:

$$\frac{1}{2}w'^2 = F(w) = -(w^3 - \frac{u}{2}w^2 - gw - h) \qquad (14)$$

with $g$, $h$ two integration constants. If $F(w)$ has real roots, they are of the form

$$e_1 = 2a\frac{E(s)}{K(s)}, \quad e_2 = 2a\left[\frac{E(s)}{K(s)} - 1\right], e_3 = 2a\left[\frac{E(s)}{K(s)} - \frac{1}{s^2}\right] \qquad (15a\text{-}c)$$

with

$$a = \frac{e_1 - e_2}{2}, \quad s^2 = \frac{e_1 - e_2}{e_1 - e_3}, \quad K(s) = \int_0^{\pi/2}(1 - s^2\sin^2\varphi)^{-1/2}d\varphi, \qquad (16a\text{-}d)$$

$$E(s) = \int_0^{\pi/2} (1 - s^2 \sin^2 \varphi)^{1/2} d\varphi$$

and $K(s)$, $E(s)$ the complete elliptic integrals[19]. Then, the solution of Eq. (13) has the expression

$$\phi(\xi, \tau) = 2a \left( \frac{E(s)}{K(s)} - 1 \right) + 2a cn^2 \left\{ \sqrt{a} s^{-1} \left[ \xi - 2a \left( \frac{3E(s)}{K(s)} - \frac{1+s^2}{s^2} \right) \tau + \xi_0 \right]; s \right\} \qquad (17)$$

where cn is the Jacobi's elliptic function of s modulus[19] and $\xi_0$ constant of integration. As a result, the dendritic morphogenesis process is achieved by one-dimensional cnoidal oscillation modes of the speed field. This process is characterized through the normalized wavelength,

$$\lambda = \frac{2sK(s)}{\sqrt{a}} \qquad (18)$$

- see Fig.1, and the normalized phase velocity

$$u = 4a \left[ 3 \frac{E(s)}{K(s)} - \frac{1+s^2}{s^2} \right] \qquad (19)$$

- see Fig 2.
-
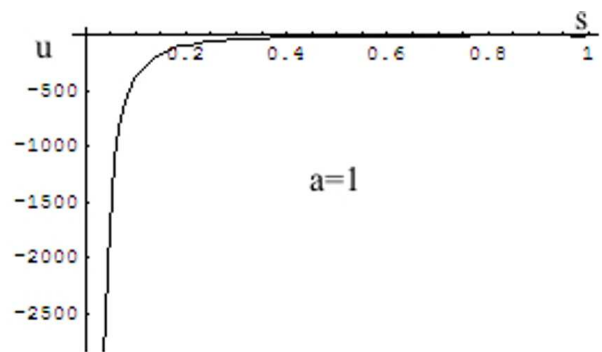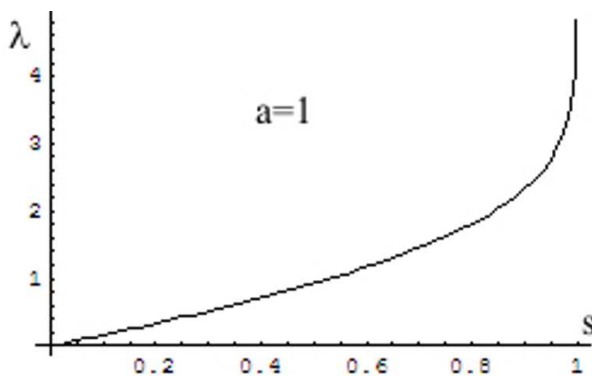


**Fig. 1.** *The dependence of the normalized wave length λ with s.*

**Fig. 2.** *The dependence of the normalized phase speed u with s.*

Then: i) the parameter $\lambda$ from Eq. (18) corresponds through $\lambda \equiv R$ to the normalized dendritic tip radius, and $u$ from Eq. (19) to the normalized dendritic growth

speed. Moreover, by eliminating the parameter $a$ from relations (18) and (19), one obtains

$$uR^2 = A(s), \ A(s) = 16\left[3s^2 E(s)K(s) - (1+s^2)K^2(s)\right] \tag{20}$$

where the quantity $A(s)$ is numerically evaluated. For $s = 0 - 0.7$, $A(s) \approx$ const. – see Fig. 3, and the Eq. (20) takes the usual form (Oldfield's relation type[11]):

$$uR^2 = const. \tag{21}$$
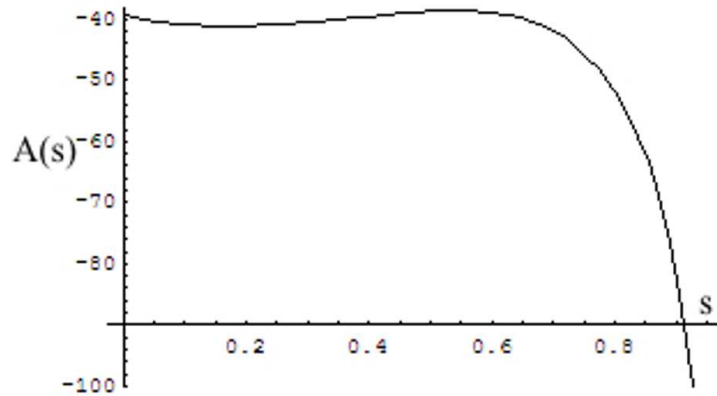


Fig. 3. The dependence $A = A(s)$

ii) through the $D$ coefficient, the parameter $s$ becomes a measure of the supercooling degree (for details see[11,12]). Thus, for an increased supercooling degree, i.e. $s \to 0$, the normalized dendritic growth speed ($u$) is high and the normalized dendritic tip radius ($R$) is small – see Figs 1 and 2. On the contrary, for a decreased supercooling degree, i.e. $s \to 1$, $u$ is small and $R$ is high – see Figs 1 and 2; iii) the one-dimensional cnoidal speed oscillation modes contain as subsequences, for $s = 0$ the one-dimensional speed harmonic waves, for $s \to 0$ the one-dimensional speed waves packet and for $s \to 1$ the one dimensional speed solitons packet. These subsequences describe the dendritic dynamics. For $s = 1$, the solution (17), with the substitutions $\phi_0 = e_3$ and $k^2 = (e_1 - e_3)/2$, becomes the one-dimensional speed soliton

$$\phi(\xi,\tau) = \phi_0 + 2k^2 \sec h^2\left[k\left(\xi - \left(4k^2 + 3\phi_0\right)\tau + \xi_0\right)\right] \tag{22}$$

of amplitude $2k^2$, width $k^{-1}$ and phase velocity $u = 4k^2 + 3\phi_0$. This subsequence describes the dendrite as an quasi-autonomous structure.

In the non-differentiable case the Eq.(14), with the substitutions $w = (u/4)f^2$ and $i\eta = (u/4)^{1/2}\theta$ and with the restriction $h = 0$, becomes a Ginzburg-Landau type equation[17]:

$$\partial_{\eta\eta} f = f^3 - f \tag{23}$$

It results: i) the $\eta$ coordinate has dynamic significations and $f$ variable, probabilistic ones (for details see also [13,14]). The space-time becomes a fractal one (for details see [13,14]) and the fluid acquires fractal properties (fractal fluid by short); ii) according to [18] we can build a field theory with spontaneous symmetry breaking (see appendix B). The fractal kink,

$$f_k(\eta) = f(\eta - \eta_0) = tanh\left[\frac{1}{\sqrt{2}}(\eta - \eta_0)\right] \qquad (24)$$

spontaneously breaks the vacuum symmetry by tunneling and generates coherence structures. This mechanism is similar with the one of superconductivity[20]; iii) through an analogy with the Bohm's potential[21], the fractal potential[22] takes a very simple expression which is directly proportional to the states density of the fractal fluid, *i.e.*

$$Q = -\frac{2mD^2}{f}\frac{d^2f}{d\eta^2} = 2mD^2\left(1 - f^2\right) \qquad (25)$$

When the states density[22], $f^2$, becomes zero, the fractal potential takes a finite value, $Q = 2mD^2$. The fractal fluid is normal and there are no coherent structures in it. When $f^2$ becomes 1, the fractal potential turns to zero - the entire quantity of energy of the fractal fluid is transferred toward its coherent structures. Then the fractal fluid becomes coherent through self-structuring. Therefore, one can assume that the energy from the fractal fluid can be stocked by transforming all the environment's entities into coherence structures and then 'freezing' them. The fractal fluid act as an energy accumulator through the fractal potential; iv) substituting (24) in (25) the fractal potential becomes the fractal soliton (a soliton in a fractal space-time)

## 3. CONCLUSIONS

The main conclusions of the present paper are the following: i) through the scale relativity theory in the topological dimension $D_T = 3$, in the differentiable case the dendritic morphogenesis process is achieved by one-dimensional cnoidal oscillation modes of the speed field; ii) for different supercooling degrees, the one-dimensional cnoidal speed oscillation modes contain the one-dimensional speed harmonic waves, the one-dimensional speed waves packet, the one dimensional speed solitons packet and the one dimensional speed soliton. The first three subsequences describe the dynamics of the dendrite, while the last one describes the dendrite as a quasi-autonomous structure; iii) an Oldfield's relation type is obtained; iv) in the non-differentiable case we can build a field theory with spontaneous symmetry breaking. The fractal kink spontaneously breaks the vacuum symmetry by tunneling and generates coherent structures. Moreover, the fractal fluid acts as an energy accumulator through the fractal potential; v) usually, the speed field is proportional to a square root of a normalized temperature (for details see[9-11]). Then, all the properties of the speed field are transferred to the thermal one. In our opinion, the thermal fractal soliton corresponds to a micro-domain having the same supercooling degree (virtual

crystallization germ). The local coherence of these structures generates a stable crystallization germ and the global one generates the dendrite (as a crystallization grain).

[1]*Electronics and Telecommunication Faculty, "Gh. Asachi" Technical University,*
[2]*Materials Science and Engineering Faculty, Technical "Gh. Asachi" University*
[3]*Physics Department, Technical "Gh. Asachi" University*

## REFERENCES

[1] M.B. Koss, J.C. LaCombe, L.A. Tennenhouse, M.E. Glicksman, E.A. Winsa, **Metallurgical and Materials Transactions A**, Vol. 30A, 3177-3190 (1999);

[2] G.P. Ivantsov, **Dokl. Akad. Nauk** USSR 58, 1113, (1947);

[3] D.E. Temkin, **Dokl. Akad. Nauk** USSR 132, 1307 (1960);

[4] J.S. Langer and H. Müller-Krumbhaar, **Acta Metall**. 26, 1681 (1978);

[5] R. Brower, D. Kessler, J. Koplik and H. Levine, **Phys. Rev. Lett**. 51, 1111 (1983);

[6] A. Karma and W.-J. Rappel, **Phys. Rev. E**. 53, 3017 (1995);

[7] R. Trivedi, J. Cryst. **Growth 49**, 219 (1980);

[8] W. Kurz and D.J. Fisher, **Fundamentals of solidification** (Trans Tech Publications, 1989), 3rd Ed.

[9] E. Ben-Jacob, N. Goldenfeld, J.S. Langer and G. **Schon: Phys.Rev.** A **29** (1984) 330

[10] D. Kessler, J. Koplik and H. Levine: Phys. Rev. A **31**(1985) 1712

[11] M.E. Glicksman and S.P. Marsh: **The dendrite** (in *Handbook of Crystal Growth*, Edited by D.T. Hurle, Elsevier, 1993, vol. 1) 1076-1122

[12] M. Agop, P. Nica and I. Carcea: **Mat Trans JIM 42** (2001) 197-206

[13] L. Nottale, **Fractal Space-Time and Microphysics, Towards a Theory of Scale Relativity** (World Scientific, Singapore, 1992)

[14] L. Nottale, Chaos, **Solitons and Fractals 7**, 877 (1996)

[15] B. Mandelbrot, **The fractal geometry of nature,** Ed. Freeman, San Francisco, 1982

[16] J.F. Gouyet, **Physique et structures fractals**, Ed. Masson, Paris, 1992

[17] E. A.Jackson: **Perspectives in nonlinear dynamics**, ed. Cambridge University Press, Cambridge, 1991.

[18] Chaichian, M., Nelipa, N.F.: **Introduction to gauge field theories**. Springer-Verlag. Berlin, Heidelberg, New York, Tokyo (1984)

[19] Bowman, F., **Introduction to elliptic function with applications**, English University Press, London, 1955.

[20] Poole, C.P., Farach, H.A., Geswich, R.J.: **Superconductivity.** Academic Press. San Diego, New York, Boston, London, Sydney, Tokyo, Toronto (1995)

[21] Bohm, D.: *A* **Suggested Interpretation of the Quantum Theory in Terms of "Hidden"** *Variables. I,* Phys. Rev. **85**, 166-179 (1951)

[22] M. Agop, N. Forna, I. Casian-Botez, C. Bejenariu, **New Theoretical Approach of the Physical Processes in Nanostructures,** *J. CTN, in press, 2008.*

**APPENDIX A**

There are continuous curves which are not fractals but have points where they are not differentiable, in these points we find the left and right derivative. We try now to make a link to these concepts.

Let $P(x^1, x^2)$ be a point of the fractal curve and let us consider a line which starts from this point and let $Q$ be the first intersection of this line with the fractal curve. We denote by $x^1 + dX^1$, $x^2 + dX^2$ the coordinates of $Q$, thus $\boldsymbol{PQ}$ is a vector of components $dX^1$, $dX^2$. We denote by $dX^i_+$ the components of the vector $\boldsymbol{PQ}$ for which $dX^1 > 0$, hence they are at the right of the line (d) and by $dX^i_-$ the case when $dX^1 < 0$, such as is the case for the vector $\boldsymbol{PQ'}$ – see Fig. 4.
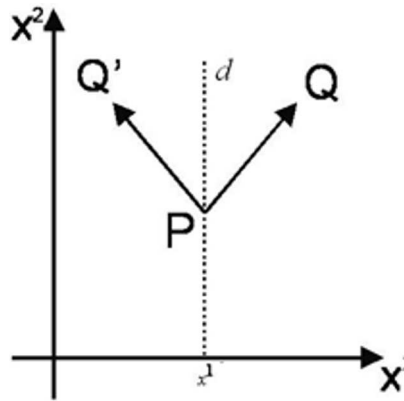


Fig. 4 *The continuous curves which are not fractals but have points where they are not differentiable*

Considering all the lines (segments) which start from $P$, we denote the average of these vectors by $dx^i_\pm$ i.e.

$$\left\langle dX^i_\pm \right\rangle = dx^i_\pm \quad (i = 1,2) \tag{A1}$$

Therefore we can write

$$dX^i_\pm = dx^i_\pm + d\xi^i_\pm \tag{A2}$$

If the considered average value is additive, then it results from Eq.(A2)

$$\left\langle d\xi^i_\pm \right\rangle = 0 \tag{A3}$$

Here $dx^i_\pm$ are the left and right differentials of the classical variables, and $d\xi^i_\pm$ describe the fractal characteristic.

Using Eq.(A2) in the vectorial form, $dX_\pm = dx_\pm + d\boldsymbol{\xi}_\pm$, the speed fields take the form:

$$\frac{dX_\pm}{dt} = \frac{dx_\pm}{dt} + \frac{d\boldsymbol{\xi}_\pm}{dt} \tag{A4}$$

We denoted by $(dx_+/dt) = v_+$ the "forward" speed and by $(dx_-/dt) = v_-$ the "backward" speed.

While the speed - concept is classically a single concept, if space-time is non-differentiable, according to[13,14] , we must introduce two speeds ($v_+$ and $v_-$) instead of one, even when going back to the classical domain. This "two-valueness" of the speed vector is a new, specific consequence of non-differentiability that has no standard counterpart (in the sense of differential physics), since it originates from a breaking of the symmetry ($dt \rightarrow -dt$). Such a symmetry was considered self-evident up to now in physics (since the differential element $dt$ disappears when passing to the limit), and therefore it has not been analyzed on the same footing as the other well-known symmetries. Note that it is actually different from the time reflection symmetry $T$, even though infinitesimal irreversibility implies global irreversibility[13,14] .

At this point we cannot favor $v_+$ rather than $v_-$. The only solution is to consider both the forward ($dt > 0$) and backward ($dt < 0$) processes together. Than, we can use the *complex speed*[13,14]:

$$V = \frac{v_+ + v_-}{2} - i\frac{v_+ - v_-}{2} = \frac{dx_+ + dx_-}{2dt} - i\frac{dx_+ - dx_-}{2dt} \qquad (A5)$$

According to[13,14], if $(v_+ + v_-)/2$ may be considered as differentiable (classical) speed, then the difference $(v_+ - v_-)/2$ is the non-differentiable speed.

Using the notations $dx_\pm = d_\pm x$, Eq.(A5) becomes:

$$V = \left(\frac{d_+ + d_-}{2dt} - i\frac{d_+ - d_-}{2dt}\right)x \qquad (A6)$$

This enables us to define the operator[13,14] :

$$\frac{\delta}{dt} = \frac{d_+ + d_-}{2dt} - i\frac{d_+ - d_-}{2dt} \qquad (A7)$$

Let us now assume that the curve describing the movement (continuous but non-differentiable) is immersed in a 3-dimensional space, and that $X$ of components $X^i$ (i = $\overline{1,3}$) is the position vector of a point on the curve. Let us also consider a function $f(X,t)$ and the following Taylor series expansion up to the third order:

$$df = f(X^i + dX^i, t + dt) - f(X^i, dt) = \left(\frac{\partial}{\partial X^i}dX^i + \frac{\partial}{\partial t}dt\right)f(X^i,t) +$$

$$+ \frac{1}{2}\left(\frac{\partial}{\partial X^i}dX^i + \frac{\partial}{\partial t}dt\right)^2 f(X^i,t) + \frac{1}{3!}\cdot\left(\frac{\partial}{\partial X^i}dX^i + \frac{\partial}{\partial t}dt\right)^3 f(X^i,t) \qquad (A8)$$

If we neglect all the derivatives of second order (this is our assumption), a condition more than sufficient for the deviation from linearity, then Eq.(A8) becomes:

$$df = f(X^i + dX^i, t + dt) - f(X^i, dt) = \left(\frac{\partial}{\partial X^i}dX^i + \frac{\partial}{\partial t}dt\right)f(X^i,t) + \frac{1}{3!}\cdot\left(\frac{\partial}{\partial X^i}dX^i + \frac{\partial}{\partial t}dt\right)^3 f(X^i,t)$$

From here, the forward and backward average values of this relation, using notations $dX_\pm^{\,i} = d_\pm X^i$, take the form:

$$\langle d_\pm f\rangle = \left\langle \frac{\partial f}{\partial t}dt\right\rangle + \langle \nabla f \cdot d_\pm \mathbf{X}\rangle + \frac{1}{6}\left\langle \frac{\partial^3 f}{\partial X^i \partial X^j \partial X^k}d_\pm X^i d_\pm X^j d_\pm X^k\right\rangle + \frac{1}{2}\left\langle \frac{\partial^3 f}{\partial X^i \partial X^j \partial t}d_\pm X^i d_\pm X^j dt\right\rangle +$$
$$+\frac{1}{2}\left\langle \frac{\partial^3 f}{\partial X^i \partial t^2}d_\pm X^i (dt)^2\right\rangle + \frac{1}{6}\left\langle \frac{\partial^3 f}{\partial t^3}(dt)^3\right\rangle \tag{A9}$$

We make the following stipulations: the mean values of the function $f$ and its derivates coincide with themselves, and the differentials $d_\pm X^i$ and $dt$ are independent, therefore the averages of their products coincide with the product of average. Thus Eq.(A9) becomes:

$$d_\pm f = \frac{\partial f}{\partial t}dt + \nabla f \langle d_\pm \mathbf{X}\rangle + \frac{1}{6}\frac{\partial^3 f}{\partial t^3}\langle (dt)^3\rangle + \frac{1}{2}\frac{\partial^3 f}{\partial X^i \partial X^i \partial t}\langle d_\pm X^i d_\pm X^j\rangle \langle dt\rangle +$$
$$+\frac{1}{2}\frac{\partial^3 f}{\partial X^i \partial t^2}\langle d_\pm X^i\rangle \langle (dt)^2\rangle + \frac{1}{6}\frac{\partial^3 f}{\partial X^i \partial X^j \partial X^k}\langle d_\pm X^i d_\pm X^j d_\pm X^k\rangle \tag{A10}$$

so that, further using Eq.(A2) in the form of Eq.(A1),

$$d_\pm f = \frac{\partial f}{\partial t}dt + \nabla f d_\pm \boldsymbol{x} + \frac{1}{6}\frac{\partial^3 f}{\partial t^3}(dt)^3 + \frac{1}{2}\frac{\partial^3 f}{\partial X^i \partial X^j \partial t}\left(d_\pm x^i d_\pm x^j + \langle d\xi_\pm^i d\xi_\pm^l\rangle\right)dt +$$
$$+\frac{1}{2}\frac{\partial^3 f}{\partial X^i \partial t^2}d_\pm x^i (dt)^2 + \frac{1}{6}\frac{\partial^3 f}{\partial X^i \partial X^j \partial X^k}\left(d_\pm x^i d_\pm x^j d_\pm x^k + \langle d\xi_\pm^i d\xi_\pm^l d\xi_\pm^k\rangle\right) \tag{A11}$$

Since $d\xi_\pm^i$ describes the fractal properties of the fractal curve which has the fractal dimension $D_F$ (for details see[15,16]), it is natural to impose $\left(d\xi_\pm^i\right)^{D_F}$ to be proportional to time parameter $dt$, *i.e.*

$$\left(d\xi_\pm^i\right)^{D_F} \sim dt \tag{A12}$$

Even the average value of the fractal coordinate, $d\xi_\pm^i$, is null (see (A3)) for the high order of the fractal coordinate average the situation can be different. For example, let us consider the mean $\langle d\xi_\pm^i d\xi_\pm^j d\xi_\pm^k\rangle$. If $i \neq j \neq k$ this average is zero due the independence of $d\xi^i$ from $d\xi^j$ and $d\xi^k$. Therefore, using Eq.(A12) and an adequate choice of the constant of proportionality, we can write:

$$\langle d\xi_\pm^i d\xi_\pm^j d\xi_\pm^k\rangle = \delta^{ijk}\left(\frac{6D^2}{c}dt\right)^{3/D_F} \tag{A13}$$

with

$$\delta^{ijk} = \begin{cases} 1, & if \quad i = j = k \\ 0, & if \quad i \neq j \neq k \end{cases}$$

$D$ is a constant which defines the fractal/non-fractal transition, i.e. the transition from the explicit scale dependence to scale independence[13,14]. Particularly, in the SRT model, $D$ has the form[13,14]. $D = \lambda \cdot c / 2$, with $\lambda$ a length scale and $c$ the speed of light in the vacuum. This

length scale is to be understood as a structure of scale space not of standard space (for example see the definition of the Compton length[13,14] ).

Through a generalization of Peano type curves which cover a three-dimensional cube[13,14] i.e $D_F$ asymptotically tend to the topological dimension[13,14] $D_T = 3$, the Eq.(A12) becomes:

$$\left\langle d\xi_\pm^i d\xi_\pm^j d\xi_\pm^k \right\rangle = \delta^{ijk}\left(\frac{6D^2}{c}dt\right) \tag{A14}$$

where we considered that:

$$\begin{cases} \left\langle d\xi_+^i d\xi_+^j d\xi_+^k \right\rangle > 0 \text{ and } dt > 0 \\ \left\langle d\xi_-^i d\xi_-^j d\xi_-^k \right\rangle < 0 \text{ and } dt < 0 \end{cases}$$

In such conjecture, two interaction scales (the non-fractal by means of the classical variables $dx_\pm^i$, and the fractal one through the variables $d\xi_\pm^i$) and the transition between them through the proportionality coefficient $D$ are obtained. Then Eq.(A11) may be written under the form:

$$d_\pm f = \frac{\partial f}{\partial t}dt + \nabla f d_\pm \boldsymbol{x} + \frac{1}{6}\frac{\partial^3 f}{\partial t^3}(dt)^3 + \frac{1}{2}\frac{\partial^3 f}{\partial X^i \partial X^j \partial t}d_\pm x^i d_\pm x^j dt + \frac{1}{2}\frac{\partial^3 f}{\partial X^i \partial t^2}d_\pm x^i (dt)^2 +$$
$$+ \frac{1}{6}\frac{\partial^3 f}{\partial X^i \partial X^j \partial X^k}d_\pm x^i d_\pm x^j d_\pm x^k + \frac{\partial^3 f}{\partial X^i \partial X^j \partial X^k}\delta^{ijk}\left(\frac{D^2}{c}dt\right) \tag{A15}$$

If we divide by $dt$ and neglect the terms which contain differential factors (for details on the method see[13,14] , Eq.(15) is reduced to:

$$\frac{d_\pm f}{dt} = \frac{\partial f}{\partial t} + \boldsymbol{v}_\pm \nabla f + \left(\frac{D^2}{c}dt\right)\nabla^3 f \tag{A16}$$

with

$$\nabla^3 f = \frac{\partial^3 f}{\left(\partial X^1\right)^3} + \frac{\partial^3 f}{\left(\partial X^2\right)^3} + \frac{\partial^3 f}{\left(\partial X^3\right)^3}$$

Let us calculate, under the circumstances *(δf/dt)*. Taking into account Eq.(A17), and Eq.(A15), we obtain:

$$\frac{\delta f}{dt} = \frac{1}{2}\left[\frac{d_+ f}{dt} + \frac{d_- f}{dt} - i\left(\frac{d_+ f}{dt} - \frac{d_- f}{dt}\right)\right] = \frac{1}{2}\left(\frac{\partial f}{\partial t} + \boldsymbol{v}_+ \nabla f + \frac{D^2}{c}\nabla^3 f\right) + \frac{1}{2}\left(\frac{\partial f}{\partial t} + \boldsymbol{v}_- \nabla f + \frac{D^2}{c}\nabla^3 f\right) -$$
$$- \frac{i}{2}\left[\left(\frac{\partial f}{\partial t} + \boldsymbol{v}_+ \nabla f + \frac{D^2}{c}\nabla^3 f\right) - \left(\frac{\partial f}{\partial t} + \boldsymbol{v}_- \nabla f + \frac{D^2}{c}\nabla^3 f\right)\right] = \frac{\partial f}{\partial t} + \left(\frac{\boldsymbol{v}_+ + \boldsymbol{v}_-}{2} - i\frac{\boldsymbol{v}_+ - \boldsymbol{v}_-}{2}\right)\nabla f + \frac{D^2}{c}\nabla^3 f \tag{A17}$$

or using Eq.(A6):

$$\frac{\delta f}{dt} = \frac{\partial f}{\partial t} + \boldsymbol{V} \cdot \nabla f + \frac{D^2}{c} \nabla^3 f \qquad (A18)$$

This relation also allows us to give the definition of the non-differentiable operator:

$$\frac{\delta}{dt} = \frac{\partial}{\partial t} + \boldsymbol{V} \cdot \nabla + \frac{D^2}{c} \nabla^3 \qquad (A19)$$

We now apply the principle of scale covariance, and postulate that the passage from classical (differentiable) mechanics to the non-differentiable mechanics which is considered here can be implemented by replacing the standard time derivative $d/dt$ by the complex operator $\delta/dt$ (this results in a generalization of the principle of scale covariance given by Nottale in[13,14]. As a consequence, we are now able to write the equation of geodesics (a generalization of the first Newton's principle) in a non-differentiable space-time under its covariant form:

$$\frac{\delta V}{dt} = \frac{\partial V}{\partial t} + \boldsymbol{V} \cdot \nabla V + \frac{D^2}{c} \nabla^3 V = 0 \qquad (A20)$$

## APPENDIX B

Let us consider the Eq.(23) in the form

$$\partial_{\eta\eta} f = f^3 - f \qquad (B1)$$

*i.e.* a Ginzburg-Landau type equation[17). Equation (B1) is obtained from the variational principle $\delta \int L d\boldsymbol{x} = 0$ applied to the Lagrangean density

$$L = \frac{1}{2} \left( \partial_\eta f \right)^2 - V(f) \qquad (B2)$$

with the potential

$$V(f) = \left( \frac{f^4}{4} \right) - \left( \frac{f^2}{2} \right) \qquad (B3)$$

and $d\boldsymbol{x}$ the elementary volume.

Equation (B3) have the solutions $f_1 = 0$, $f_{2,3} = \pm 1$. By calculating the second derivative with respect to $f$ of the potential entering (B3) and substituting the extreme values into the result of this differentiation, we find $V_{ff}(0) = -1$, $V_{ff}(\pm 1) = 2 > 0$ *i.e.* the solution $f = \pm 1$ is associated with the minimum energy. The physical states associated with the minimum of energy defines the vacuum states. Hence, the model under consideration has double degenerated vacuum states (for details see[18)).

From (B2) it result both energy,

$$\varepsilon(f) = \int_{-\infty}^{\infty} d\eta \left[ \frac{1}{2} \left( \partial_\eta f \right)^2 + V(f) \right] \tag{B4}$$

and the energy relative to the vacuum:

$$\varepsilon(f) - \varepsilon(f_v) = \int_{-\infty}^{\infty} d\eta \left[ \frac{1}{2} \left( \partial_\eta f \right)^2 + \frac{1}{4} \left( f^2 - 1 \right)^2 \right] \tag{B5}$$

Because all terms in (B5) are positive and in view of the infinite limits of integration, the finiteness of the energy implies that at $\eta \to \pm \infty$

$$\partial_\eta f = 0, \ \left( f^2 - 1 \right)^2 / 4 = 0 \tag{B6}$$

From this, it follows that for $\eta \to \pm \infty$ the function $f(\eta)$ tends to its vacuum values $f_v \to \pm 1$.

To find the explicit form of the solution of (B1), we multiply it by $\partial_\eta f$ and integrate over η. It results:

$$\frac{1}{2} \left( \partial_\eta f \right)^2 = -\frac{f^2}{2} + \frac{f^4}{4} + \frac{1}{2} f_0 \tag{B7}$$

where $f_0$ is an integration constant. From this we have

$$\eta - \eta_0 = \int_0^f \frac{df}{\sqrt{\dfrac{f^4}{2} - f^2 + f_0}} \tag{B8}$$

where $\eta_0$ is another constant of integration. For an arbitrary, $f_0$, to this general solution corresponds an infinite value of the energy $\varepsilon(f)$. To obtain the solution with finite energy, we make use of the boundary conditions $f_v = \pm 1$. From (B7) it results that $f_0 = 1/2$. Replacing this value of $f_0$ into (B8), the solution $f_k(\eta)$ of the field equation (B7) with a finite energy is:

$$f_k(\eta) = f(\eta - \eta_0) = tanh \left[ \frac{1}{\sqrt{2}} (\eta - \eta_0) \right] \tag{B9}$$

This is called the fractal kink solution (a kink solution in a fractal space-time).

Combining (B5) with the expression $f_v = 1$ and the expression for $f_k$, we obtain the energy of the fractal kink relative to the vacuum:

$$\varepsilon(f_k) - \varepsilon(f_v) = \frac{2\sqrt{3}}{3} \tag{B10}$$

Therefore the fractal kink solution was obtained by a spontaneous symmetry breaking.

A topological method[18] can be applied because the admissible number of fractal kinks is determined by the topological properties of the symmetry group of equation (B1). In this context, the following problems must be solved: i) the number of admissible fractal kink solutions determined by the topological properties of equation (B1); ii) the topological charge. The fractal kink solution can be considered as mapping of a spatial zero-sphere $S^0$, taken at infinity onto the vacuum manifold model of (B1). The homotopy group for this model is $\Pi_0(Z_0) = Z_2$, *i.e.* the model gives rise to two solutions: a constant solution $f_v$ and the fractal kink solution.

The associated topological charge is:

$$Q = \frac{1}{2} \int_{-\infty}^{\infty} j(\eta)d\eta = \frac{1}{2} \int_{-\infty}^{\infty} \frac{df}{d\eta}d\eta = \frac{1}{2}\left[f(+\infty) - f(-\infty)\right] \qquad (B11)$$

The vacuum solution (absence of spatial gradients) and the fractal kink solution can be characterized by attributing the $Q = 0$ and $Q = 1$, respectively (the result it obtained by an adequate normalization of $f$).

## O TEORIE A MORFOGENEZEI DENDRITICE BAZATĂ PE TOERIA FRACTALILOR

**Rezumat:** Considerind ca miscarea particolelor are loc pe curbe continue, dar nediferentiabile, adică pe curbe fractalice, sunt analizate anumite propietăţi ale cimpului "dendritic" folosind reoria relativităţii de scară în spaţiul topologic de dimensiune 3. În cazul diferenţiabil monodimensional, morfogeneza dendritică se realizează prin moduri cnoidale de oscilaţie ale câmpului de viteze, conform relaţiei lui Oldfield. În cazul nediferentiabil, nodurile fractalice rup in mod spontan simetria vidului prin tunelare şi generează structuri coerente. Deoarece toate proprietăţile cîmpului de viteze pot fi transferate cîmpului de temperaturi, iar potenţialul fractalic acţionează ca un acumulator de energie, apar micro-domenii cu acelaşi grad de suprarăcire (germeni virtuali de cristalizare). Coerenta locală a acestor structuri generează un germene stabil de cristalizare, iar germenele global genereaza dendritele (ca un grăunte de cristalizare).

# CONTROLLING THE VARIABLES INVOLVED IN THERMAL TREATMENT BY SIMULATION ON PHYSICAL MODEL

BY

**B. FLOREA\*, C. BĂLESCU\*,V. MIREA\*, GH. FLOREA\*\***

**Abstract**. *To achieving the physical-chemical modifications in right way of the material subuded to the heating processing is important to assure some value of the installation's  variables (temperature, pressure,level, flowmeter, chemical composition of the atmospher, etc.).It is important  to keep the constant values of those variables  in timp and in whole space of work and from this reason the paper*

**Keywords**: *modelling, simulation, thermal treatment*

## 1. The necessity to control the variables involved in thermal treatment process

The paper is proposing to present a new method to control the variables involved in thermal treatment process using simulation on the physical model with the scope to reduce the specific combustible consumption to the blast furnace which have gas support as combustible.

The efficiency  of using the energy represent  an economical necessity  by reducing the spending with combustible from the whole cost of production because this is as soon as most expensive on the world market.

Because the natural energetic resources  exploited with the present technologies are decreasing year by year it is important to improve the installations with combustible support.

The reduction of the energetic consumption in concordance with quality increasing of the products, depends by controlling the variables involved in the processes.

For a correct achieving of the physico-chemical modification of the material subdued to the heating  is necessary to be assuring some values of the installation variables (temperature, pressure, flowmeter, etc.).

Keeping the constant values of those variables must be made in time and work space.

At the modern industrial thermal installations result that the quality terms required to control the variables  in special the higher  precision induce to the most types of thermal installations the automatization of the controlling process and if the whole parameters can't be controlled need to be controlled at least the temperature of the process.

## 2. Researches viewing the simulation on the physical model of the thermal treatment process

To describe the behavior of the bigger industrial processes where must be adopted a solution of controlling and command it is used two methods:

-mathematical modelling;

-using a physical model.

Many times to achieve a mathematical model basis on a series of mathematical relations which describe the physico-chemical processes leads to obtain a few enough complicated relation.

Using the research  for choosing the solution of the variable's  controlling involved in thermal treatment process basis on the physical model need to be achieved at a small level the industrial installation and using a few fluids with same properties as the industrial process.

At the simulation on the physical model it has been used the installation achieved with equipment made by Festo company, installation which exists in „The Science and Material Engineering" Faculty from Bucharest.

The simulation installation is made from a few modulus which allow to test different types of process from metallurgical industry with the purpose to find an optimal  solution for those.

Because it has a modular features , these individual modulus can be combined to simulate the most complex processes like flowing and temperature processes or temperature and pressure processes.

At this installation  achieving we followed this features:

-it is important to have a modular behavior to can be extended step by step;

- to be orientated through industrial processes to be used also the industrial equipments;

-easy way to transport this;

- because at the simulation it is used water it is safety in exploatation;

- it allows to be used new technologies to be tested and implemented in industrial field.

The principal equipments of this installation are:

- two tanks;
- a centrifugal pomp;
- two electrovalves;
- for manual valves;
- a heating unit;
- plastic pipes;
- pression sensor;
- temperature's sensor;
- flowmeter sensor;
- industrial controller;
- electrical components;
- mechanical components

To lead the processes, the installation allows to lead them from a controlling console and also can communicate by RS232 or Profibus with a personal computer to monitorezing them.

This facility to monitorize the processes allows to user to make tests and to see the process behavior as in industrial environment.

## 3. The simulation results on the physical model

Analysing the simulation equipment we can see the clasical controlling of the thermal treatment process parameters.

From modular features reason of the installation by the manual valves we can establish some ways to optimal tuning controller for process parameters.

From practice is known that teh important thing in thermal treatment is to adapt the combustible flowing controller in function of the temperature from aggregate's inside.

For monitorizing the process we achieved with aid of the Intouch support a softwrae called PCS( process controlling system).

In figure 1 is presented the general draft of the simulation installation.

By clicking over the *process controlling* button it is launched the diagram form figure 2 which allow to establish the parameters of the controller to optimizing the combustible flowing in concordance with reference value.
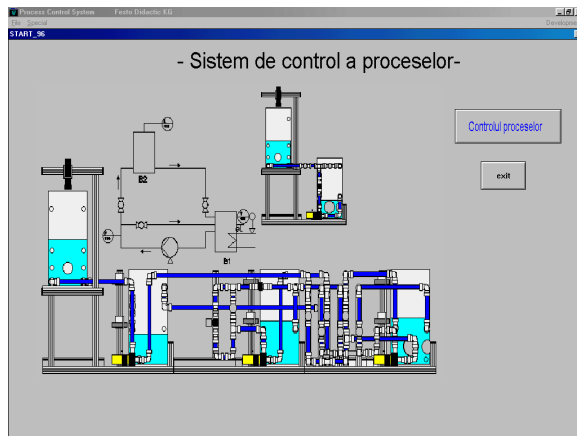


Figure 1. The general draft of the simulation installation
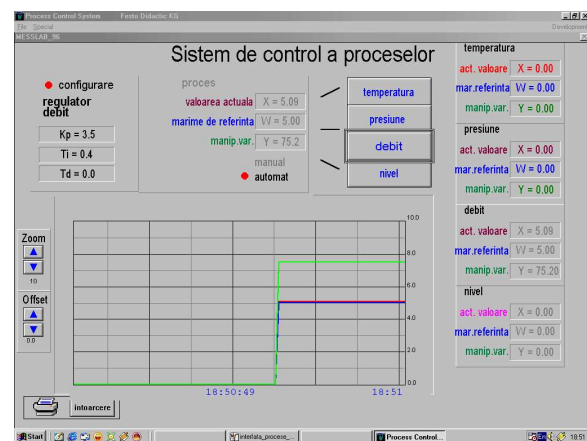


Figure 2. The simulation result of the flowing combustible controlling

## 3. Conclusions

The simulation on the physical model allows the variables' controlling and optimizing involved in thermal treatment process.

In same time this installation together with the monitorizing software achieve an educational package for „The Science and Material Engineering" faculty students.

## REFERENCES

1. Florea B. **Instalatie de laboarator si soft pentru simularea controlului si conducerii echipamentelor metalurgice**, Teza doctorat, 2007
2. Semenescu A., Bălescu C., Oprescu I., Mirea V., Semenescu C.V., Florea B., **Control of Technological Processes for Materials Processing**, Ed. Printech, Bucureşti, 2006
3. Florea B., Florea Gh., Chiriac Al., Croitoru Gh., **Modelling and optimisation of engineering systems**, Proceeding of the 45th International Seminar on Modelling and Optimisation of Composites, Odessa, April 28-29, 2006
4. Florea B., Volintiru P., Stănescu, Al., Vasilescu P., **Program de simulare a conducerii proceselor metalurgice**, Conferinţa ştiinţifică UgalMat 2005 ,,Tehnologii şi materiale avansate'', 20-22 octombrie, 2005

## CONTROLUL VARIABILELOR CE INFLUENTEAZA PROCESUL DE TRATAMENT TERMIC PRIN SIMULARE PE MODEL FIZIC

**Rezumat**.Pentru realizarea corectă a modificărilor fizico-chimice ale materialelor supuse încălzirii, este necesar să fie asigurate anumite valori ale variabilelor instalaţiei (temperatură, presiune, compoziţie chimică a atmosferei etc.).Menţinerea valorilor constante ale acestor variabile trebuie să aibă loc atât în timp, cât şi în totalitatea spaţiului de lucru si din acest punct de vedere lucrarea prezinta o metoda de reglare utilizand simulari pe un  model  fizic .

# EXPERIMENTAL MODEL FOR FLOWING ANALYSIS OF MODELING AT CASTING ALLOYS

BY

**CONSTANTIN BRATU, IOAN MARGINEAN, SORIN ADRIAN COCOLAS**

**Abstract**: Experimental model conceived for analysis of modeling process for flowing alloys followed putting in evidence correlation between the defining parameters of flowing equation, correlation experimental model and process parameters, have at base the sensitive element of temperature witch indicate the evolution of alloy level on flowing direction i.

**Keywords**: Experimental model; Flowing; Casting; Simulation;

## 1. MATHEMATICAL BASIS FOR FLOWING PROCESS AND GEOMETRY OF EXPERIMENTAL MODEL

### 1.1. Mathematical equation of process

Regarding simulation on computer of flowing process in cavity of the experimental model (EM) has been utilized:

- Mathematical equation of correlation between flowing section at critical level and the time parameter;
- For generalization of casting varied alloys procedure (ferrous, non-ferrous, light or heavy) it had in sight correlation time-alloy characteristics;
- Mathematical relation used.

Analysis of flowing process was made in an interval tagged by two limits (laminar flowing and maximum filling time of form).

For establish the quantifiable parameters of flowing process we used mathematical equation with this form:

$$Vm1_i := \mu_i \cdot \sqrt{2 \cdot g \cdot H}$$

$$Vm2_{i,j} := \mu_i \cdot \sqrt{2 \cdot g \cdot (H - h_j)}$$

$$VcrFc_i := \left(\frac{h_i}{\delta}\right)^{0.290 \ln\left(\frac{\sqrt{2 \cdot g \cdot h_i}}{100}\right)}$$

$$Sa_{lim} := \frac{Vp}{\tau lim \cdot V_{lim}}$$

$$Sp_{lim} := \frac{2 \cdot Sa_{lim}}{1.5}$$

$$Vl := \frac{Vp}{S \cdot \tau lim}$$

$Vm1_i$ – medium speed of filling at ½ from height of EM, mm/s;

$Vm2_{i,j}$ - medium speed of filling at ½ from height of EM, mm/s;

$Vl$ - speed limit of filling the piece, mm/s;

$Vp$ – piece volume , $mm^3$;

S – section of metal feeder, mm$^2$;

$\tau$ lim – limit time, s;

$V_{lim}$ - speed limit of flowing, mm/s;

$Sa_{lim}$ – limit section of metal feeder, mm$^2$;

$Sp_{lim}$ – limit section of trumpet, mm$^2$;

$VcrFc_i$ – critical speed for ferrous alloy, mm/s;

$\delta$ – wall thickness, mm;

g – gravitational acceleration, mm/s$^2$;

$\mu_i$ – coefficient of loosing speed;

H – piece height, mm;

$h_j$ –index variation for calculus of medium speed;

$h_i$ – height variation at differed value for H.

## 1.2. Geometry of experimental model

For program testing of working and realization of the mathematical model regarding flowing testing was projected the experimental geometrical model.

Location of experimental model in casting piece it used the trace the elimination of perturbation in experimental process, particularly characteristics sightings for alloys flowing at casting and of solidification and contraction process.

Experimental model position in casting form, what constitute the experimental model it is presented in figure 1.2.1



*Figure 1.2.1. – Experimental model geometry for used for testing*

Alloy flowing for filling the piece (EM), simulated on computer in program „matlab" in plan (2D) it is represented for various moments of filling in figure 1.2.3.
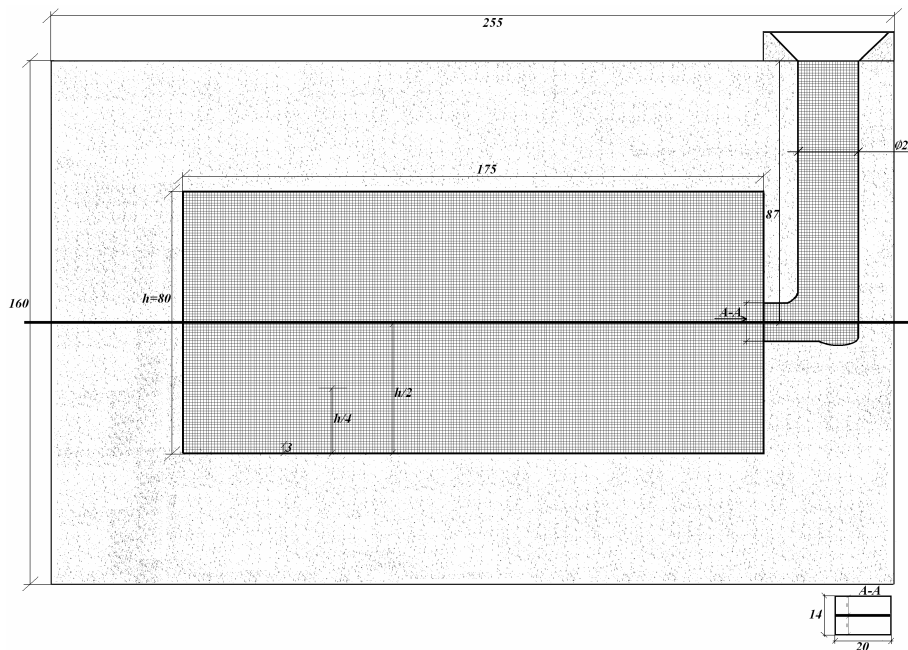
*Figure 1.2.2. Experimental model position in form for testing and measurement points of casing parameters.*
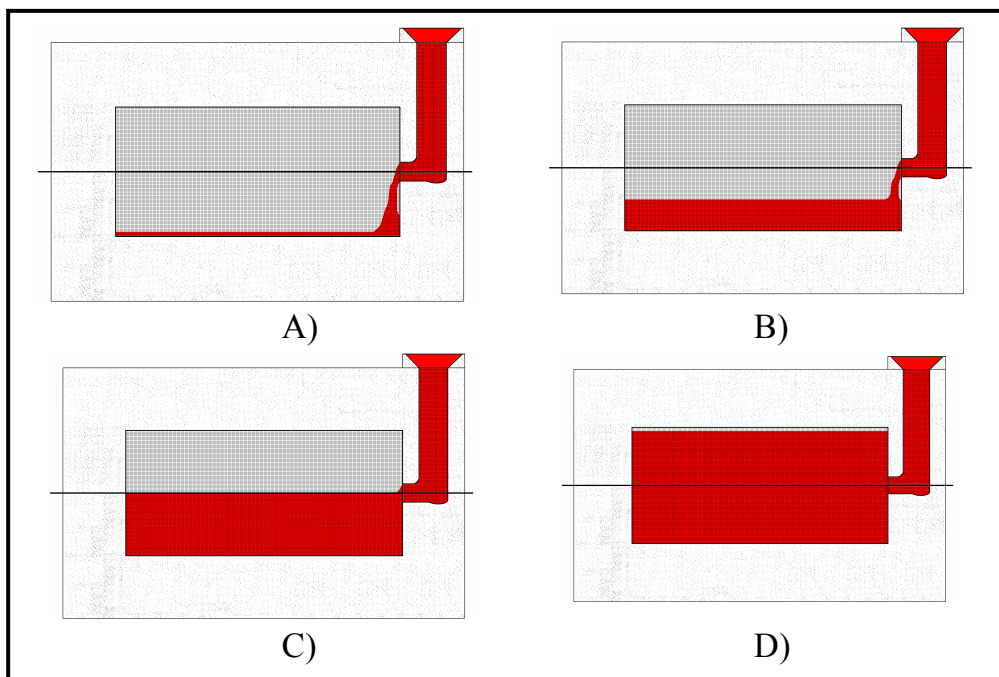


*Figure 1.2.3. 2D image for evolution of alloy filling process of the experimental model particularly for a ferrous alloy:*
*a) initial moment ($\tau \sim 1 \cdot 10^{-1}$s); b) at filling moment for ¼ from h ($\tau \sim 1$s);*
*c) at filling moment for ½ from h ($\tau \sim 2$s); d) nearly the end of filling process ($\tau \sim 4$s).*

## 2. DATES PROCESSING IN PROGRAM "MATCAD" OF THE EQUATION WHO DEFINE THE PROCESS

Utilizing the experimental model previously used and using the „matcad" software for various conditions from preliminary experimental program in order to determine the optimal casting technology and trace the flowing process of alloy was possible graphical visualization of variation domain, the basic parameters needed for alloy flowing characterization.

Image of this result it is presented in figures  2.1.÷2.11.
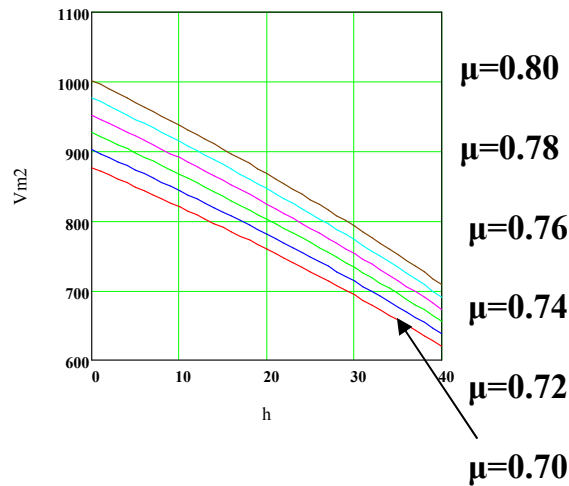


*Figure 2.1. Filling variation of on piece height  "h" for various values of the coefficient of loosing speed  μ.*

$$H := 80 \qquad j := 1..41 \qquad g := 9807$$

$$Vm1_i := \mu_i \cdot \sqrt{2 \cdot g \cdot H} \qquad Vm2_{i,j} := \mu_i \cdot \sqrt{2 \cdot g \cdot (H - h_j)} \qquad VcrFc_i := \left(\frac{h_i}{\delta}\right)^{0.290 \ln\left(\frac{\sqrt{2 \cdot g \cdot h_i}}{100}\right)}$$
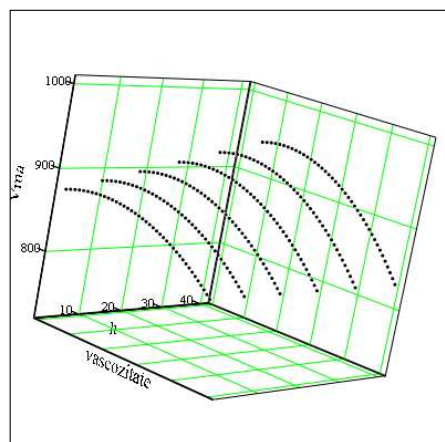


| $VcrFc_i =$ |
|---|
| 0.614 |
| 1 |
| 1.55 |
| 1.752 |
| 1.957 |
| 2.137 |
| 2.667 |
| 2.763 |

*Figure 2.2. Distribution of speed field at second level of filling*
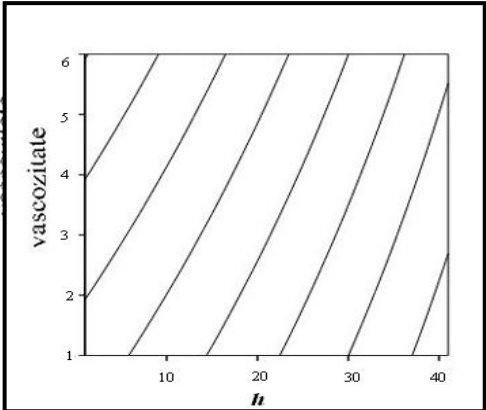
*Figure 2.3. Alloy viscosity variation on height of piece function of speed field.*
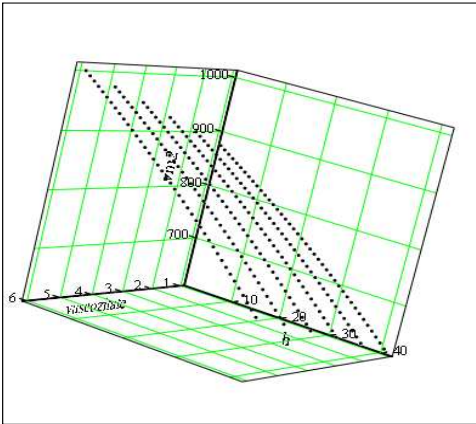


*Figure 2.4. Medium speed distribution at filling the form with alloy.*
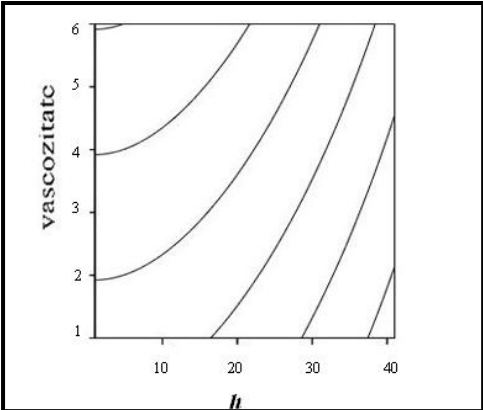


*Figure 2.5. Alloy viscosity variation on piece height  function by medium speed.*
.
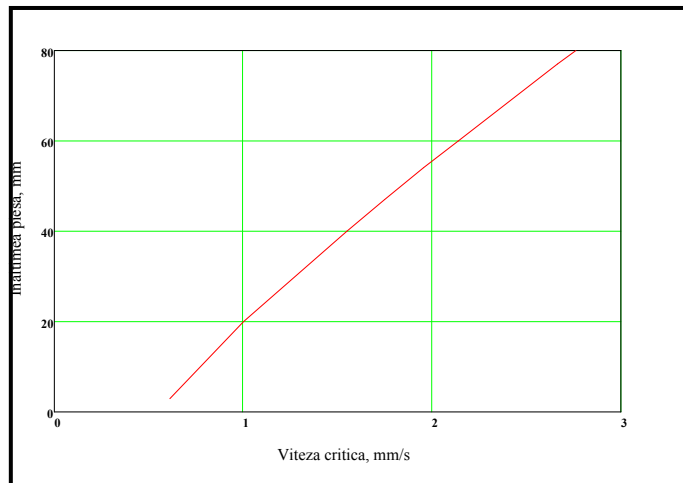
*Figure 2.9. Critical speed variation on piece height specifically for  not-appearing
casting defects (ferrous alloy).*

Both EM as the utilized program allow choosing optimal solution for
parameters what characterize flowing what makes possible projecting of EM meant for
using at mathematical modelling of process with take place at casting piece.

Speed limit calculus and filling time variation can be presented in this way:

$L := 175 \quad \delta := 20 \quad \tau lim := 5 \quad i := 1 .. 8$

$S := 14 \cdot 20 \quad Vl = 200 \quad h := 80$

$lim := 1 .. 6$

$Vp := L \cdot l \cdot h = 2.8 \times 10^5 \qquad Sp_{lim} := \dfrac{2 \cdot Sa_{lim}}{1.5}$

$Vl := \dfrac{Vp}{S \cdot \tau lim} \qquad\qquad Sa_{lim} := \dfrac{Vp}{\tau lim \cdot V_{lim}}$

| $Sa_{lim} =$ | $Sp_{lim} =$ | $V_{lim} :=$ |
|---|---|---|
| 560 | 746.667 | 100 |
| 280 | 373.333 | 200 |
| 186.667 | 248.889 | 300 |
| 140 | 186.667 | 400 |
| 112 | 149.333 | 500 |
| 93.333 | 124.444 | 600 |
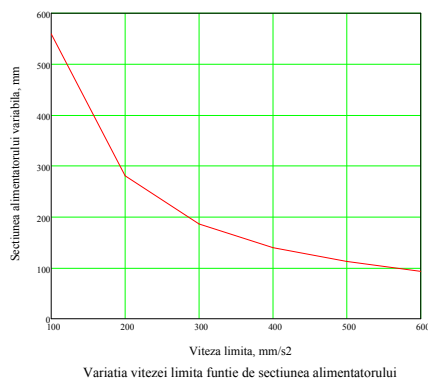


*Figure 2.10. Speed limit distribution
function alimentary section.*
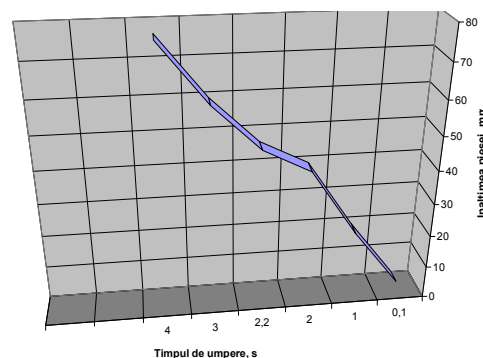


*Figure 2.11. Filling time variation
function by piece height.*

## 3. CONCLUSION

From information in this paper there are following conclusion:
- for actual technical condition (from hardware and software point of view) it is possible designing of casting piece such in order to assure a computer simulated flowing  close to the real alloy flowing at casting in piece.

One of big problems witch confront the designers at making the casting technology it is the problems of thermical nodes and the possibility of elimination from the interior of casting piece. The simulation program accomplish offers possibility of conduct the flowing and solidification process in order to eliminate completely the thermical nodes from casted piece.

Phenomena witch appear in this condition became very hard to be simulated owning to factors witch influence the alloy flowing process and make the mathematical model witch describe these process to be complicated and with high errors.

Commercial programs existing now on world plan tackle the alloy modeling flow, thermical transfer, with phase transformation with elimination of latent heat of solidification, but no less the phenomena bound by alloy contraction in solidification period and development of shrinkage hole at piece solidification.

It can be say that the utilized program  both and EM allow choosing optimal solution for parameters witch can characterize flowing, what can make possible designing of a EM for mathematical modeling of process witch take place at casting ferrous and non ferrous alloy, with applying at determination of an casting technology with reduce consumption of materials and energy.

Establishing the optimal dimension for alimentary section and flowing control in horn gate and form cavity allow maximum utilization of liquid alloy, favoring growing the characteristic factor dressing, reducing the material consumption of materials and energy, as well and the diminution of specific manual labor through shorting the fabrication cycle.

### REFERENCES

1. Sofroni, L., Brabie, V., Bratu, C., **Bazele teoretice ale turnarii**, Editura Didactica si Pedagogica, Bucuresti, 1980.
2. Bratu, C., Sofroni, L., Nica, Gh., **Termofizica solidificarii pieselor turnate**, Editura Performantica, Iasi, 1997
3. Moldovan, P., Panait, N., Margineanu, St., **Bazele tratarii topiturilor metalice neferoase**, Editura Intact, Bucuresti, 1998.
4. Vasile Soporan, Călin Vamoş, Carol Pavel , **Modelarea numerică a solidificării**, Editura Dacia , 2003
5. Carcea, I., **Bazele elaborarii metalelor, aliajelor si superaliajelor neferoase**, Editura Cermi, Iasi, 1998.
6. Mihai Ştefan, Dumitru Mihai, ş.a. **Metode numerice şi implementarea lor pe calculator**, Editura Tehnopress, Iaşi, 2004, ISBN 979-702-087-1
7. Adenis, D.J.P., Coats, K.H., Ragone, D.V., **An analysis of the Direct-Chill-Casting Process by Numerical Methods**, J. Inst. Metals, 91, 1961-63.

8.  Chen, C.W., Chon, H.Y., Li, C.R., Shei, C.T., Hwang, W.S., **Comparation of different computational fluid dynamics technique on their applications to the modeling of mold filling in casting**, Trans. Japan Foundrymen's soc., Vol. 12, 1993.
9.  CeEx 260/2006 CeEx 260/2006 – **Modelarea matematică a proceselor care au loc la turnarea pieselor metalice în vederea reducerii consumurilor materiale şi de energie**.

**MODEL EXPERIMENTAL PENTRU ANALIZA MODELARII CURGERII LA TURNAREA ALIAJELOR**

**Rezumat:** Aranjamentul experimental conceput in vederea analizarii procesului de modelare la curgere a aliajelor a urmarit punerea in evidenta a corelatiei dintre parametrii ce definesc ecuatiile de curgere, corelatia aranjament experimental  parametrii de process, are la baza elemental sensibil de temperatura care indica evolutia nivelului de aliaj pe traseul curgerii.

# IMPROVEMENT ON CAST-IRONS CORROSION PROPERTIES FOR DECORATIONS THROUGH METALLIC COATINGS USING THE VIBRATING ELECTRODE METHOD WITH Ti ELECTRODE

BY

**CARMEN NEJNERU, MANUELA PERJU, TUDOR RAILEANU,
ANDREI SANDU, MARIA LUNGU**

**Abstract:** *The paper presents a study on corrosion of phosphorus cast irons used for art objects in exterior decorations. The study continues with the proposal of an increase solution of corrosion resistance by using metallic coatings with the help of vibrating electrode.*

**KEYWORDS:** *vibrating electrode, scanning electron microscopy (SEM), EDX analysis, corrosion*

## 1. INTRODUCTION

Cast-iron used for decorations is a cast-iron with phosphorus eutectic that has good fluidity properties. The ornaments applied on old buildings covers, gates of fences must have a good corrosion resistance and must correspond esthetically.



*Fig.1. Pieces of mould cast-iron used for exterior ornaments*

One of the used methods, to fulfill this purpose, is titan coating. It can be done through many methods like galvanic coating (nickel plating), oxy-acetylene flame welding coating, spraying thermal coating etc.

At this paper, titan coating method has tested with vibrating electrode.

The Ti and Ti alloys have a very good corrosion resistance.

Thus, these materials resist in subacid non-oxidizing mediums or concentrated and powerful oxidizing at temperature ranges between 500 and 700°C.

Titanium's use is essential in some chemical technologies where medium's aggressively is very powerful. It is used in manufacturing chlorine, acetaldehyde, phtalic anhydride, nitric acid, terephthalic acid, in manufacturing salt desalinization installations, nitriding or pickling bathes, etc.

Titanium's oxidation resistance con be increased by beryllium alloying (max.6%).

## 2. THEORETICAL CONSIDERATIONS

### 2.1. Estimation of instantaneous corrosion current intensity and corrosion rate

Necessary main size for corrosion speed calculus when immersing an alloy in corrosive medium is the density of instantaneous corrosion current. For its estimation uses *polarization resistance method*.

This method serves for determining corrosion current at metals and alloys corrosion potential by using, for this purpose, *linear polarization curve* achieved for relative small over tensions. Corrosion current determined in this way represents corrosion current that appears at metal/corrosive medium interface when metal is immersed in solution and cannot be directly measured through electrochemical methods. This represents, in fact, *an instantaneous corrosion current*.

The method bases on the evaluation of polarization resistance, $R_p$, which is defined as tangent slope at potential-current density curve [E = f(j)] in equilibrium point (E = $E_0$ or $\eta$ = 0), meaning free corrosion potential:

$$R_p = \left[ \frac{\Delta E}{\Delta j} \right]_{E=E_0} \qquad (1)$$

Corrosion speed calculated with relation (2):

$$v_p = 3{,}27 \cdot \overline{\left( \frac{A}{z} \right)} \cdot \frac{J_{cor}}{\rho} \qquad \text{[mm/year]} \quad (2)$$

where **A** – represents atomic mass of alloy chemical element that suffers electrochemical corrosion, **z** – is electric charge of the metallic ion in solution, $\rho$ - alloy density and **J** – density of instantaneous corrosion current.

## 2.2. Analysis of corrosion process based on cyclic polarization curves

Another characterization method of corrosion processes is cyclic potentiometry. In this method, polarization curves trace gradually, first for ascending and then descending values of work electrode potential by recording circuit current. There are much more ways to represent data according to the goal and process that must emphasized. Often used are representations $J = f(E)$ or $I = f(E)$ and semi logarithmic representation: $E = f(\log J)$ Sometimes, these curves are improperly named "hysterezis curves". From the analysis of cyclic polarization curves we can achieve information referring to the type of the electrochemical process, that takes place at electrode/medium interface (such as generalized corrosion, located corrosion, passivation, species reductions or oxidations from solution). The evaluation of characteristic potentials (corrosion potential, penetration potential and re-passivation potential, transpassivation potential, protection potential) and check of some secondary electrochemical processes that take place at electrode's surface or in electrolyte (oxidations, reductions of catalyzed processes etc.).

## 3. MATERIALS AND METHODS

It has used for studies phosphorus cast-iron whose composition determined through emission spectrometry was – using a Foundry-Master emission spectrometer (WAS AG - Worldwide Analytical System AG):

*Table 1 - Chemical composition*

| Chemical composition, % | | | | | | | | |
|---|---|---|---|---|---|---|---|---|
| Material | Fe | C | Si | Mn | P | S | Cr | Ni | Cu |
| Phosphorus cast-iron | 91.8 | 4.50 | 1.54 | 1.03 | 0.620 | 0.140 | 0.0969 | 0.0572 | 0.148 |



a)             b)
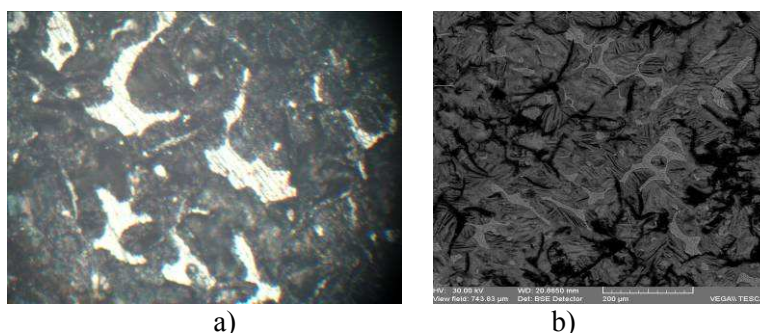
*Fig.2. Phosphorus cast-iron – a) optical microscopy, scale X400, b) photos of the basic material made with scanning electron, scale X200*

This was sparking coated so that:
- sample 1: Titan – a layer
- sample 2: Titan – two layer
- sample 3 was not covered (blank sample)

The samples covered with vibrating electrode were made photos of surface microstructure by using scanning electron microscope according to the figures:
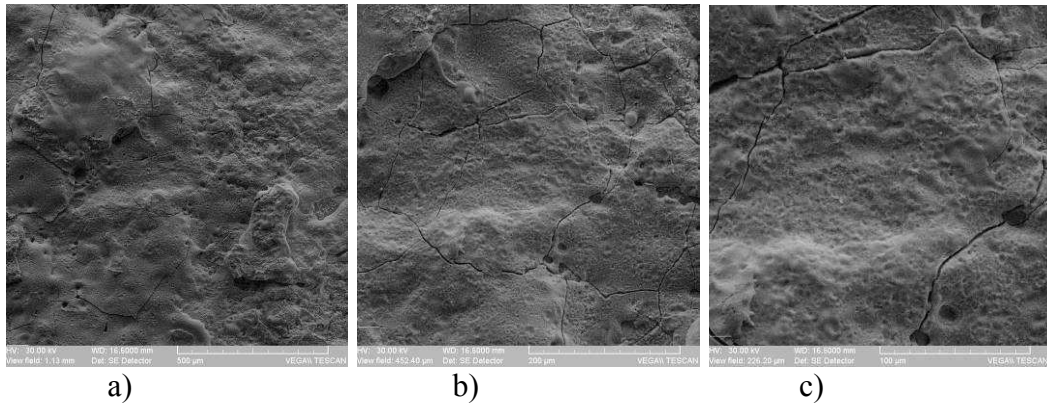
*Fig.3. Photos made with scanning electron for Ti coatings – one layer on phosphorus cast-iron support; a) scale X200; b) scale X500; c) scale X1000*
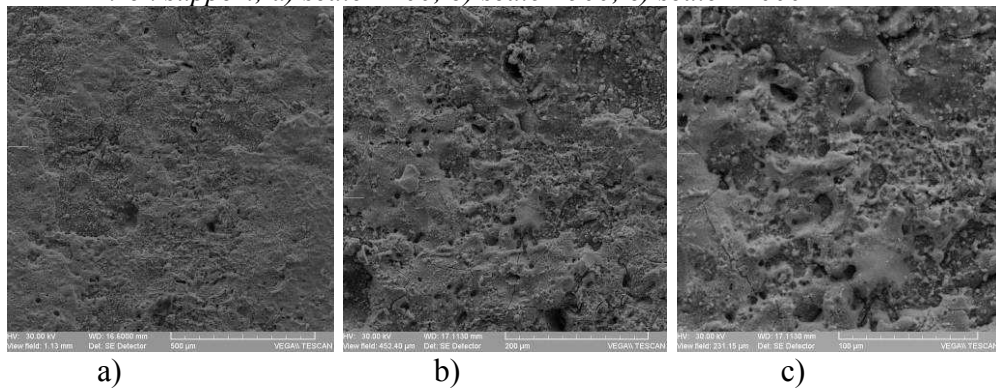


*Fig.4. Photos made with scanning electron for Ti coatings – two layers on phosphorus cast-iron support; a) scale X200; b) scale X500;c) scale X1000*
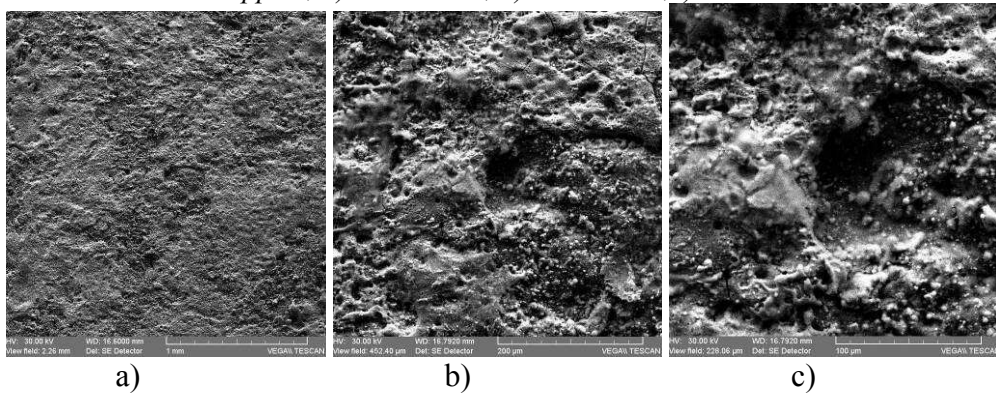


*Fig.5. Photos made with scanning electron for Ti coatings – one layer on phosphorus cast-iron support – corrosion in seawater; a) scale X100; b) scale X500; c) scale X1000*
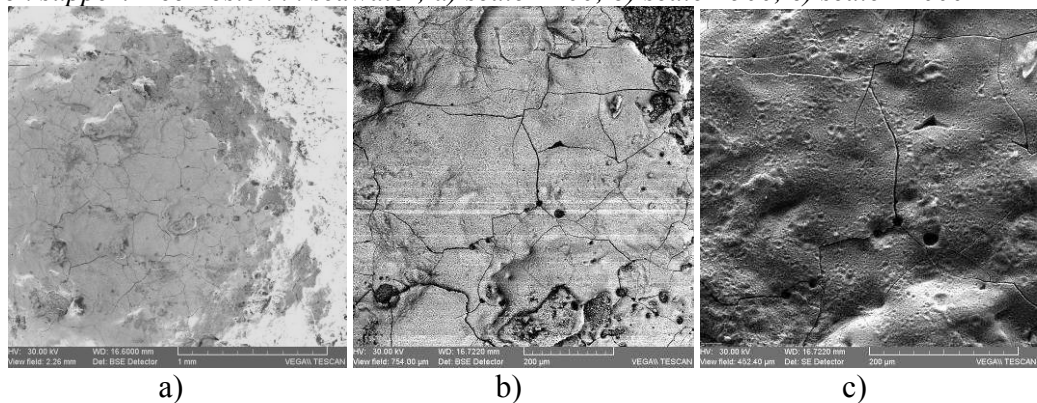


*Fig.6. Photos made with scanning electron for Ti coatings – two layers on phosphorus cast-iron support - corrosion in seawater ; a) scale X100; b) scale X300;c) scale X500*

Electrochemical corrosion studies have been made in sea water from Romanian beach, at Constanta, and had the composition expressed in g $L^{-1}$**:** $Cl^-$ - 8.26: $HCO_3^-$ – 0,183; $CO_3^{2-}$ – 0.022; $SO_4^{2-}$ – 1.137; $Na^+$ - 4.47; $K^+$ - 0.158; $Ca^{2+}$ - 0,203; $Mg^{2+}$ - 0,557.  To this composition corresponds a salinity of 15.0 g $L^{-1}$.

Corrosion behavior realized through rapid electrochemical tests namely dynamic potentiometer. Measurement of open circuit potential and potential-dynamic polarizations realized with VoltaLab 21 potentiometer (Radiometer, Copenhaga). Data acquisition and processing made with VoltaMaster 4 software. A cell with three electrodes equipped with an agitation system used. Electrodes, made cylindrical, were mounted into a Teflon support that permits their connection to spinning electrode of the electrochemical system.
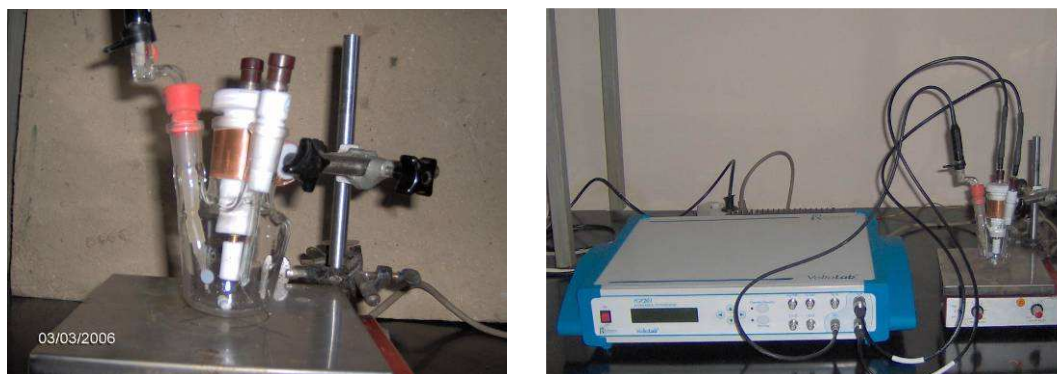


*Fig.7. Apparatus for corrosion determination*

It used as auxiliary electrode, a platinum electrode and as reference a saturated calomel electrode. The measurements made at $25^oC$, and the electrolyte was naturally aerated.

Linear polarization curves were recorded at a scanning speed of the electrolyte potential of 1 mV/s, into a potential range of $\pm$ 150 mV around opened circuit potential. Cyclic polarization curves were recorded with a speed of 10 mV/s in potential range (-700 …+1500 mV).

Corrosion potential at zero corrosion currents $E_0 \equiv E$ (I=0), Tafel slopes ($b_a$ and $b_c$, polarization resistance ($R_p$), density of corrosion current ($J_{cor}$) and corresponding corrosion speed ($v_{cor}$) were evaluated by using the facilities offered by VoltaMaster4 software.

*Table 2 – Parameters of corrosion process for phosphorus cast-iron in seawater (unsettled)*

| Det | Linear polarization | | | | | | Cyclic polarization | | |
|---|---|---|---|---|---|---|---|---|---|
| | $E_0$ (mV) | $b_a$ (mV) | $b_c$ (mV) | $R_p$ (Ohm. $cm^2$) | $J_{cor}$ (mA/$cm^2$) | $v_{cor}$ ($\mu$m/an) | $E_{cor}$ (mV) | $E_{tr}$ (mV) | $J_{1500}$ (mA/ $cm^2$) |
| 1 | -760 | 49 | -536 | 1100 | 0.0209 | 245 | -694 | -673 | 298 |
| 2 | -757 | 56 | -607 | 1060 | 0.0233 | 273 | -737 | -671 | 295 |
| 3 | -762 | 48 | -365 | 1480 | 0.0144 | 168 | -740 | -668 | 286 |
| Average | -760 | 51 | -503 | 1210 | 0.0195 | 229 | -724 | -671 | 293 |

The analysis of polarization and data from table 2 allow us to emphasize the following:

- Smaller value of cathode constant spells a high value of polarization resistance and a smaller instantaneous corrosion current.
- Due to high values of Tafel cathode slope (due probably to diffusion processes) transpassivation potential is situated in negative values range and, in this case, being bigger (near towards positive value) than corrosion potential.
- Instantaneous corrosion current has relative small values although thermodynamic corrosion tendency is high (corrosion potential has high negative values).
- Under the action of an exterior electric field (applied overpotential) corrosion speed increases $10^3 - 10^4$ times towards instantaneous corrosion speed: density of corrosion speed being directly proportional with the potential applied to the electrode.

Density current values corresponding to the overpotential of 1500 mV (ESC), $J_{1500}$, drew out from cyclic polarization curves in order to analyze overpotential influence on corrosion speed. These values are presented in the last column of table 1. It easily notices that corrosion current density under an exterior electric field touches high values, of the order of hundreds $mA/cm^2$, while instantaneous current densities were of the order of tens of microamper/$cm^2$.

The parameters of corrosion process in seawater of cast-iron samples sparking coated estimated through the same procedures.

*Table 3 – Parameters of corrosion process in seawater for Ti coated samples, one and two layers*

| Sample | Linear polarization | | | | | | Cyclic polarization | | |
|---|---|---|---|---|---|---|---|---|---|
| | $E_0$ (mV) | $b_a$ (mV) | $b_c$ (mV) | $R_p$ (Ohm.cm$^2$) | $J_{cor}$ (mA/cm$^2$) | $v_{cor}$ ($\mu$m/an) | $E_{cor}$ (mV) | $E_{tr}$ (mV) | $J_{1500}$ (mA/cm$^2$) |
| 1 (one layer) | -653 | 58 | -320 | 715 | 0.0298 | 349 | -652 | -649 | 189 |
| 2 (two layers) | -679 | 68 | -462 | 655 | 0.0376 | 439 | -667 | -623 | 184 |
| Blank sample | -760 | 51 | -503 | 1210 | 0.0195 | 229 | -724 | -671 | 293 |

It seems that thermodynamically through coating with different metallic layers from materials more noble than cast-iron with high amount of phosphorus it would take place a reduction of corrosion tendency; potential values for coated samples where corrosion current intensity is zero, $E_0$, are smaller than the values of the materials that are not coated. This is only a false impression because simultaneous with reduction of corrosion potential takes also place a decrease of polarization resistance. This brings on the increase of instantaneous corrosion current and tie to this it increases corrosion speed. Through sparking with metals more noble than cast-iron it does not achieve a corrosion resistance increase but, on the contrary, their decrease. This behavior explains if we admit that through this procedure basic material coating is not total so that between uncoated parts and coated material there are micoholes that accelerate corrosion processes.
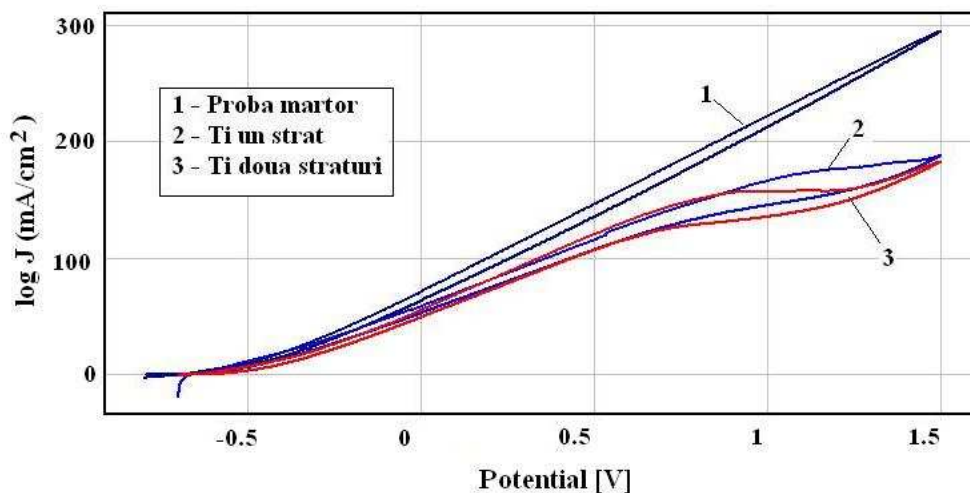
*Fig.8. Cyclic polarization curves for Ti coated samples through vibrating electrode and blank sample*
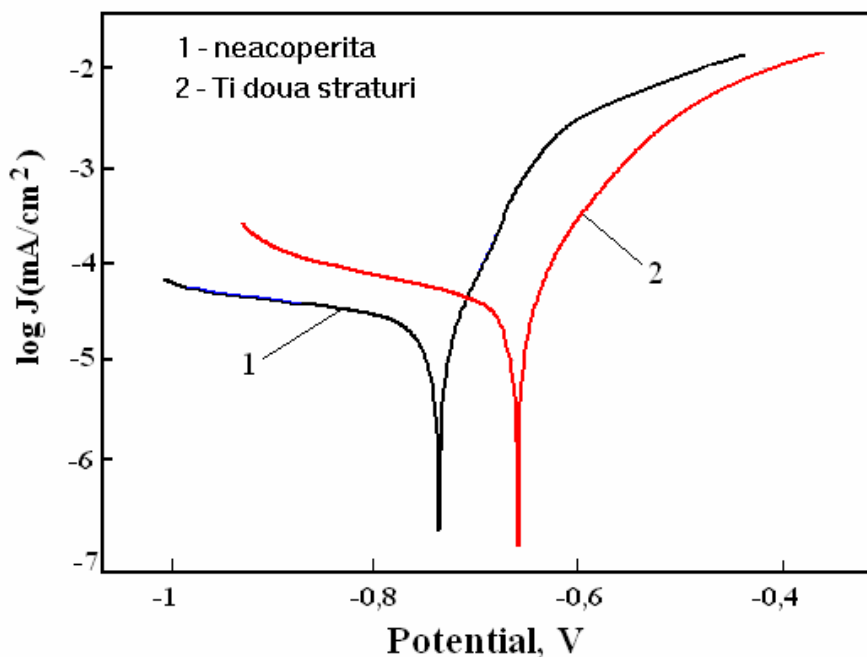


*Fig.9. Comparison between linear polarization curves for sparking coating samples*

Data analysis from this table emphasizes the following:

- As for blank sample, corrosion tendency of sparking samples, in seawater is very high; corrosion potential being situated in negative electrode potential range -730 … +630 mV;
- Polarization resistance for coated samples is smaller than blank sample, while instantaneous corrosion current and corrosion speed are bigger;
- Transpassivation potentials are very close to corresponding corrosion potential for all samples but like uncoated cast-iron, these are shifted towards positive values but with much smaller values;

When metal is positively polarized by applying a potential different of corrosion potential (equilibrium potential) there can take place into system oxidation reactions on metal surface. In this case, tense corrosion or simulated corrosion takes place and corrosion current values are much bigger than instantaneous corrosion current (situation corresponds to the immersed alloy in corrosion medium). From cyclic polarization curves, presented in figure 5 – in coordinates J = f (E), we can notice that dependency between potential applied to the electrode and corrosion speed is practically linear and cathode branch is inferior to anodic curve and very close to it, in the same time. Such a behavior is characteristic to generalized corrosion thus, being excluded any kind of localized corrosion.

Speed of stimulated corrosion is much higher than instantaneous corrosion speed. For comparison between different samples, in last column of table 2, current densities are presented, densities that correspond to some overpotentials of 1500 mV. Just sample 3 presents a more intense corrosion while the other three samples present a less intense corrosion.

## 4. CONCLUSIONS

1) It notices in Ti coating with vibrating electrode method an improvement of corrosion resistance for multiple layers when deposition degree increases and when microcrevasse (cracks) are coated too. These appear in primary coating (of the first layer) and form electric cells that improve corrosion. The method assures along the improvement of corrosion resistance, in case of acid rains, and esthetic quality increase of the decorative object.

2) Corrosion gets away harder in materials coated with Ti with vibrating electrode method due to all surface corrosion instead of pitting type corrosion. Coated materials corrode with a higher difficulty than uncoated material, this can be observed in table 2 meaning that polarization resistance is smaller in coatings instead of blank sample and corrosion speed in coating is bigger than in blank samples.

**REFERENCES**

1. J.O'M. Bockris, A.K.N. Reddz, „**Modern Electrochimistry**". Vol. 2. New York, Plenum Press, 1970;
2. E. Gileadi,"**Electrode Kinetics for Chemists**, Chimical Engineers and Material Scientists,VCH, 1993;
3. D. A Jones.,"**Principles and Prevention of Corrosion**", New York , Macmillan, (1992).
4. M. Stern, A.L Geary., *J.* **Electrochem. Soc**., 104**,** 56 (1957).
5. M. Stern, A.L Geary., J. **Electrochem. Soc**., 105, 638 (1958).
6. R.G. Kelly, J.R. Scully, D.W. Shoesmith, R.G. Buchheit, „**Electrochemical Techniques in Corrosion Science and Engineering**", Marcel Dekker Inc., New York, 2003.
7. Philippe Marcus ed., „**Corrosion Mechanisms in theory and practice**", Marcel Dekker Inc., New York, 2002.

**ÎMBUNĂTĂȚIREA PROPRIETĂȚILOR DE COROZIUNE ALE FONTELOR TURNATE PENTRU DECORAȚIUNI PRIN ACOPERIRE URILIZÂND METODA ELECTRODULUI VIBRATOR CU ELECTROD DE Ti**

**Rezumat.** Lucrarea prezintă un studiu al coroziunii fontelor cu fosfor pentru decorațiuni.

# LAMELLAR GRAPHITE CAST IRON VIBRATED DURING SOLIDIFYING

BY

**GELU BARBU, VASILE COJOCARU FILIPIUC, SERGIU STANCIU**

**Abstract:** In this paper I have studied the influence of vibrations over tensile breaking strength and over the structure and repartition of chemical elements of foliated cast iron.

**Keywords:** *casting, vibration, mechanic properties*

## 1. VIBRATIONS

Vibration is the motion of the particles of an elastic body or medium in alternately opposite directions from the position of equilibrium, periodically in time.

When the vibrations are beying applied, a series of physical processes appear, like the action of count forces, the mass macroscopic transfer, cavitation phenomenons, the amplification of the overcooling degree and the changing of the conditions of solid-fluid equilibrium. Thus, shearing forces appear, which act on the growing dendrits, at the solid-fluid severance limit. The macroscopical mass transfer depends on the correlation between the amplitude and the frequency of the movement, the crystalls which belong to the moving fluid will come into collision with the branch of the dendrits in the braxket, resullting a breaking effort $\tau_r$, given by the relation:

$$\tau_r = \frac{1}{2}\rho_c W^2$$

In which $\rho_c$ is the density of the crystals and W – the speed of the fluid.

The displacement of the alloy acomplishes in flowing regime given by the Reynolds criterion, in the expression interviening the amplitude and the casting frequency. When the relative speed between the fluid and the crystals is bigger than a critical speed, the cavitation phenomenon appears.

After the destruction of the cavitation bubble, the gases from the interior of it commpresses itself almoust adiabatic. The performing implosion is attended by an important rising of the local pressure, which may have as an impact the crashing of the crystals current growing.

But the possibility that at high amplitudes of the vibrating movements also exists, and also, to appear voids in the casted material and splashes at the exterior surface.

The mechanic-physical treatments, applied to the alloys in liquid state intensifies the vibration in the limitation layers, which conduces towards collateral currents, changes the hydrodynamical situation at the limit between the solidified layer and the walls of the shape, so it changes the conditions of the heat convector transfer

and the macroscopical mass transfer; thus, the speed grows and the solidification time reduces.

The vibrations influence the superficial tension between the phasels (solid-liquid) in the purpose to reduce it, to conduce to the shrinking of the minimum radius of the nucleuses on which these do not remelt but they follow a development process.

The propitious effect on the appearance on the solid phase owes to the conglomerate processes of the subcritical germs and the activation of the heterogeneous surfaces.

Among the technological effects of the application of the vibrations at solidification: the homogenization and the finishing of the solidification structure, the amplification of the compaction of the casted material, the degasing of the alloy, the shrinking of the segregations, the expulsion of unmetallic inclusions and the increase of the capacity of yielding alloy.

It is known that through vibration, while solidification of the metallic material structure it finishes, by finishing obtaining and emending some mechanic-physic properties.

## 2. EXPERIMENTATIONS

I have analysed the influence of vibrations over the structures obtained by solidification of foliated grey cast iron.

The 1 figure shows the plant sketch
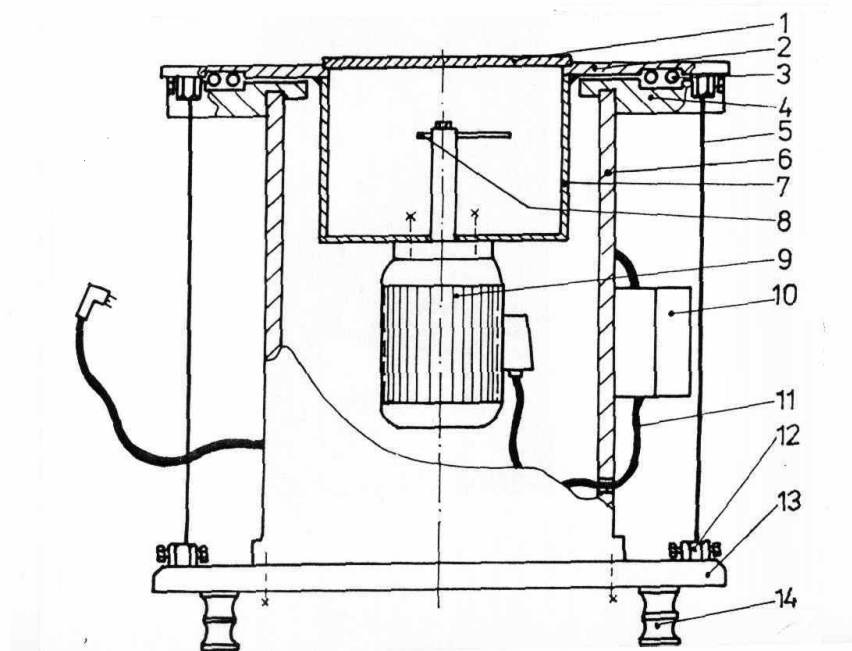


*Fig. 1. The sketch of the circular-horizontal vibrating plant: 1 – protecting cover; 2 – vibrating plate; 3 – balls; 4 – guide; 5 – cables; 6 – vibrating body; 7 – eccentric case; 8 – eccentric; 9 – engine; 10 - contact; 11 – power cable; 12 – cables screw fastening; 13 – base plate; 14 – support devices.*

Other vibrating plants have, like working principle, a vibrating plate which is supported by elastic metallic columns those ones involving moulds with limited weights (that's because there are loss in energy for columns movement and there is knee danger etc).

Our plant elimines the main disadvantage, presented previously, by the placing of the vibrating plate on a rigid support through the agency of some metallic balls.

The vibrating source is assured by an eccentric (metallic) trained by an electric engine, being likely to regulate the frequency and the amplitude.

As I have previously presented, this device produces mechanic vibrations by means of an eccentric operated by an electric engine. The vibrations are transmitted by means of the case, rigidly fixed to the motor with the help of four screws, to vibration table.

On the inferior side of vibrating mass there is a ring shaped channel whose surface comes in contact with the bearing balls situated in another channel with the same shape found in the guidance and support body of the device. These balls have the role to support the vibration table and to allow the performance of horizontal oscillating movements. In order to eliminate the possibility that the vibration table overcome the working position at high amplitudes, the latter is anchored to the ground plate of device by means of four suspending wires.

The elaboration aggregate is a black lead furnace with a medium frequency (8.000 Hz) and with a capacity of approximate 30 kg of metal.

I have elaborated a foliated grey cast iron with the following chemical composition: 3,8% C; 2,9% Si; 0,6% Mn; 0,15% P; 0,04% S.

The load required to elaborate the iron consisted of high purity iron with the following chemical composition: 3, 6…4,2% C; 1,75% Si; 0,75% Mg; 0,03% P; 0,02% S. After weighing, the load was introduced in the furnace and melted. 25 kg of high purity iron have been introduced, a quantity limited by the capacity of the pot.

In order to obtain the desired chemical composition, it was necessary to correct the percentage of Si in order to achieve the concentration of 2, 9% Si in comparison with the concentration of 1, 75% Si of the metallic load.

Thus, a ferrosilicon hardening alloy – FeSi75 - was used whose chemical composition is the following: 70…79% Si; 0, 70% Mn; 0, 4 % Cr; 0, 05% P; 0, 04% S; 0, 1% C; 2, 5 % Al. This hardening alloy was introduced in a metallic bath the moment when the iron was overheated at a temperature of $1450^oC$.

The iron cast was performed in special shapes for samples.

The two mould parts were achieved from core mixture, obtained after the following recipe: sodium silicate dry sand in a proportion of 6%.

One of the mould parts was used to cast on the vibrating device and the other one was used to cast the gravitationally and statically solidificated sample probes.

The cast was performed with a hand pot handled by one person.

The evacuation of the iron from the furnace was performed when the iron achieved the level of $1420^oC$.

The probe for static solidification was cast the first.

| Type of iron obtained | Tensile breaking strength value [N/mm] | | Type of solidification |
|---|---|---|---|
| | 1 | 2 | |
| Foliated cast iron | 156-1 | 146-1 | Vibrated |
| | 136-1 | 129-1 | Non-vibrated |

The samples were processed in order to be submitted to the probe of tensile breaking strength.

The results obtained were the following:
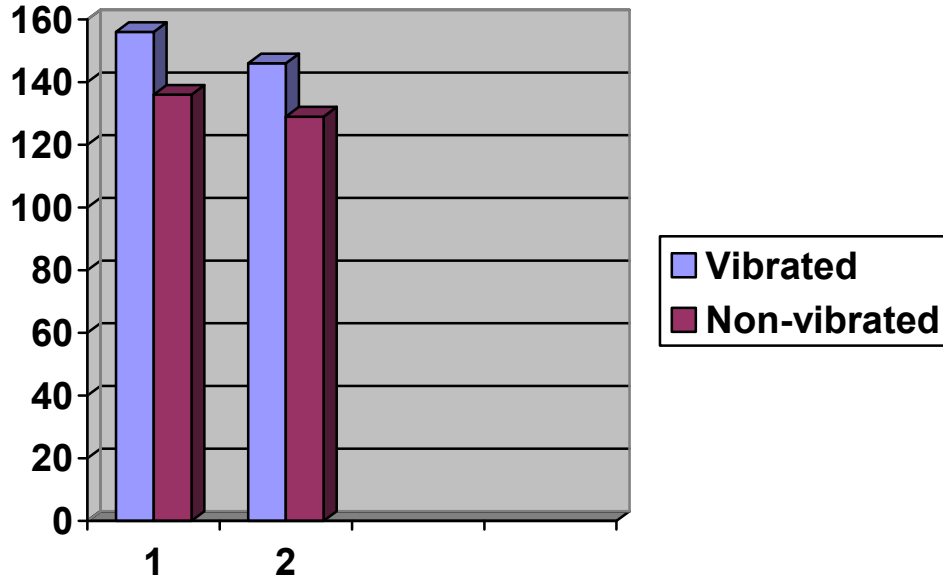


*Figure 2 Comparative graphic of the results obtained during tension.*

As it can be observed, the cast iron under the influence of vibrations present a stronger resistance to traction. Another conclusion can also be interpreted according to the form and the distribution of metallic grounds in breaking.

Figure 3 presents the microstructures of samples in breaking at a power of 100 x.
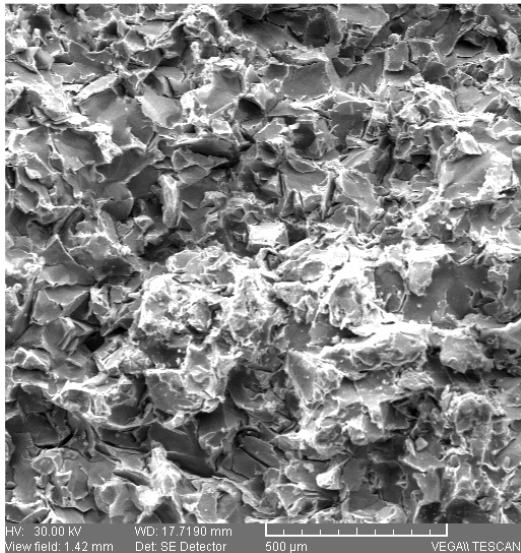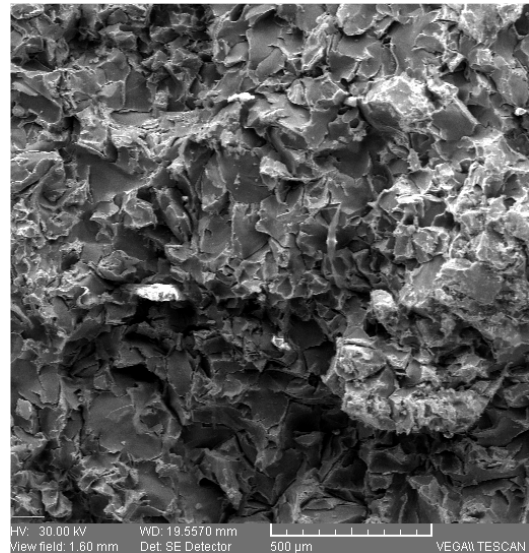


*a. vibrating foliated cast iron*                     *b. non-vibrating foliated cast iron.*
*Figure 3 Microstructure in breaking of cast iron at a microscope power of 100 x.*

Figure 4 presents the microstructures of the same iron, but at a microscope size of 300 x.
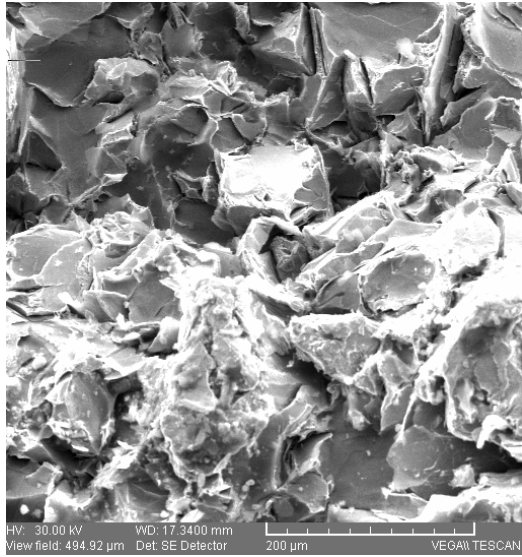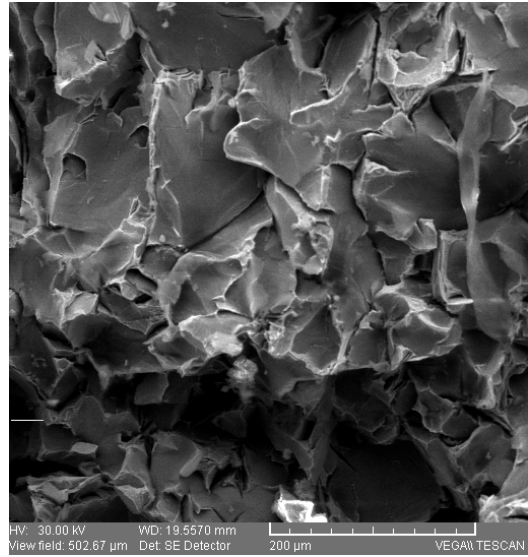


a. vibrating foliated cast iron                    b. non-vibrating foliated cast iron
*Figure 4 Microstructure in breaking of cast iron at a microscope power of 300 x.*

Figure 5 presents the same iron, but at a microscope power of 1000 x.
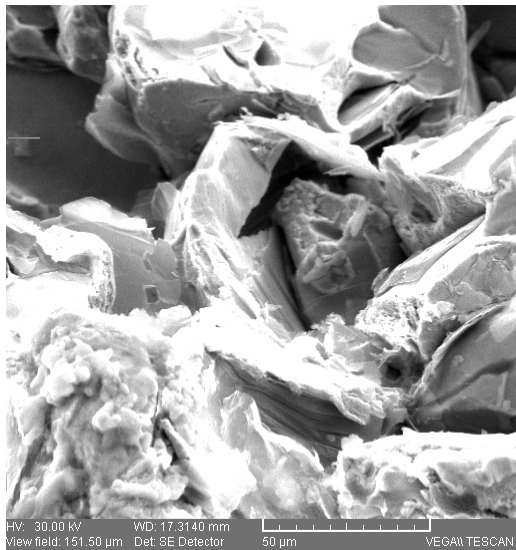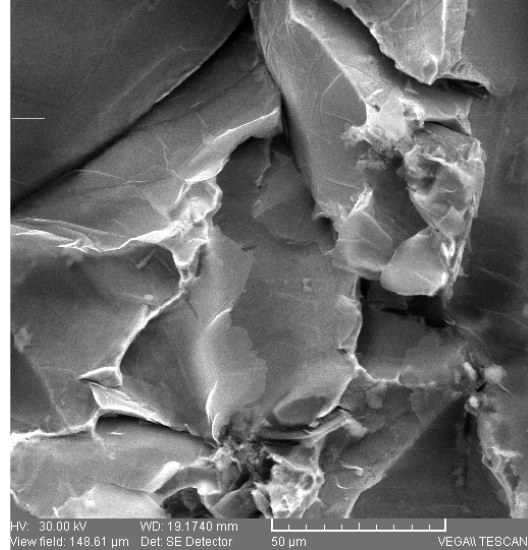


a. vibrating foliated cast iron                    b. non-vibrating foliated cast iron
*Figure 5 Microstructure in breaking of cast iron at a microscope power of 1000 x.*

Comparing these microstructures we can observe the following:

● in the case of vibrating iron a higher finesse of grains can be observed in comparison with non-vibrating iron;

● at the same time, the distribution of black lead is much more uniform in the case of cast iron under vibrations in comparison with those gravitationally cast;

● in the case of vibrating nodular cast iron, it can be observed that the iron nodules have small dimensions;

● the form of black lead nodules is much more spheroid in the case of cast iron under vibrations;

● the orientation of crystal breaking plans is much more homogenous in the case of vibrating iron that the nodular and foliated ones, fact that explains the stronger strength to tensile breaking registered through the great number of breaking plans met in the case of vibrating iron (the plans are oriented in a larger proportion on the same direction);

● it can also be observed the fact that the size of breaking plans is different in the case of the two irons: in the case of vibrating iron the number of planes is higher fact that explains once again the difference of tensile breaking strength between the two types of iron: vibrating and non-vibrating.

## 3. CONCLUSIONS

The irons solidified under the influence of vibrations have mechanical properties highly superior to gravitationally cast iron due to their homogenous structure and uniform distribution of black lead in the metallic matrix.

The size of the grains differ in the case of both types of iron, being more refined and more uniformly dispersed in the case of vibrating iron (b, c, d).

In the case of vibrating foliated iron cast we can observe that the foliated black lead are very well shaped being more compact than those of non-vibrating iron (a, b).

We can also observe that in the case of vibrating foliated iron cast the black lead foils are less branched than those of non-vibrating cast iron.

**REFERENCES**

1. Barbu, G., - **Solidificarea aliajelor sub influenta vibratiilor**, Ed. Vasiliana'98, Iasi 2003;
2. Barbu G., Cojocaru V., Carcea I. - **Instalatie de turnare cu vibrare**, **brevet inventie** Romania, nr. 108.934 Bl / 1994;
3. Darie S. - **Vibratoare electrice**, **Editura tehnica**, Bucuresti, 1987;
4. Stefanescu FL.- **Procese fizice care au loc la vibrarea aliajelor turnate. Efecte tehnologice. Principii de proiectare a instalatiilor de turnare**, Metalurgia, nr.9, 1987;

**VIBRATII APLICATE LA SOLIDIFICAREA FONTELOR CU GRAFIT LAMELAR**

**Rezumat:** In aceasta lucrare s-a studiat influenta vibratiilor asupra rezistentei la rupere prin tractiune si asupra structurii si repartitiei elementelor chimice dintr-o fonta cu grafit lamelar.

# NEW EUROPEAN REQUIREMENTS ON RISK AT WORK PREVENTION IN SMALL AND MEDIUM SIZED ENTERPRISES

BY

**MIHAI – OCTAVIAN VÎNTURACHE**

**Abstract.** *Occupational Health and Safety (OHS) represents today one of the most advanced field of the social policy of the European Union, due to the priority allowed to the risk at work prevention in all Member States. A safe and healthy working environment is an essential element of the quality of work. The European Commission enlarged the aim of its activities in favor of information, guidance and promotion of a healthy working environment, by paying particular attention to small and medium sized enterprises (SMEs). The lack of effective measures to ensure OHS can result in absenteeism, in the wake of workplace accidents and occupational illnesses, and can lead to permanent occupational disability. The new Strategy on health and safety at work for 2007-2012 proposes to step up the EU ambition and to aim for a 25 % reduction in the total incidence rate of accidents at work by 2012 in EU-27, by improving health and safety protection for workers. The Member States must ensure that EU legislation takes full effect, in particular by the enforcement of the EU directives. There is a need to focused to the particular circumstances and needs of SMEs, specially as regards risk assessment and the involvement and training of workers.*

**Keywords.** *Health and safety at work, accident at work, prevention, small and medium sized enterprises*

## 1. The workplace accidents

Decent work sums up the aspirations of people in their working lives. It involves opportunities for work that is productive and delivers a fair income, security in the workplace and social protection for families, better prospects for personal development and social integration, freedom for people to express their concerns, organize and participate in the decisions that affect their lives and equality of opportunity and treatment for all women and men.

The survey „*Safety in numbers*" 2003, of the International Labour Organization shows that in entire world every year occurred about

- 250 millions work accidents,
- 160 millions occupational diseases,
- 2 millions fatal work accidents.

This means about 8 work accidents every second and 4 fatal work accidents every minute!

The statistics published by Romanian Labour Inspection and Public Health Institute contains some important data about workplace accidents:

- in 2004 occurred 5694 work accidents (430 fatalities) and 770 new occupational diseases;

- in 2005 occurred 4878 work accidents (475 fatalities);
- in 2006 occurred 5764 work accidents (353 fatalities).
  This situation are reflected in the Figure 1.
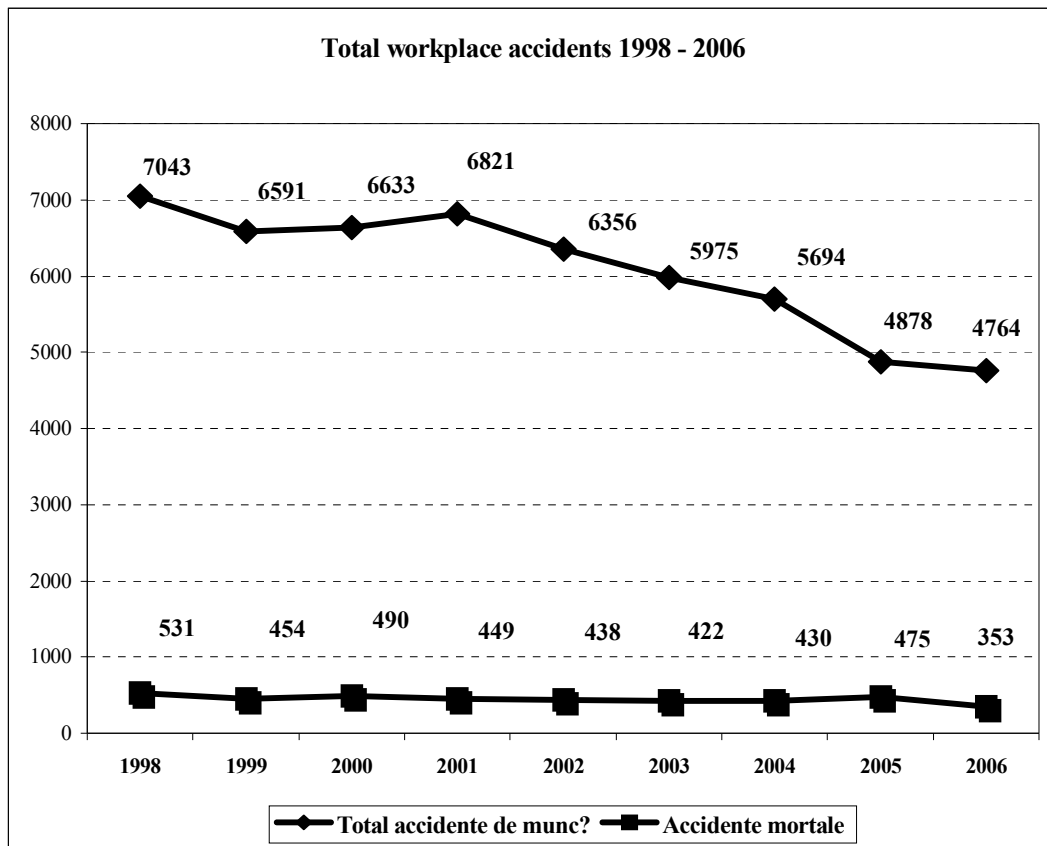


Figure 1

The small and medium sized enterprises (SMEs) are recognized as the engines of local economy and the major source of present and future employment in all countries.

Unfortunately, an important number of the workplace accidents occurs in SMEs, because of their precariousness and workplaces instability, and this affect all the Member States from European Union.

In Romania, 2230 work accidents occurred in SMEs, from the total numbers of work accidents registered in 2006 which is 5764. Those accidents occurred as follows:

- 180 (53 fatalities) in SMEs under 9 workers;
- 598 (81 fatalities) in SMEs with 10 to 49 workers;
- 1425 (100 fatalities) in SMEs with 50 to 299 workers.

Figure 2 shows the evolution of accident's number in SMEs in the last years.

For this reason the European Commission has widen the scope of its activities in favor of information, guidance and promotion of a healthy working environment, by paying particular attention to SMEs.
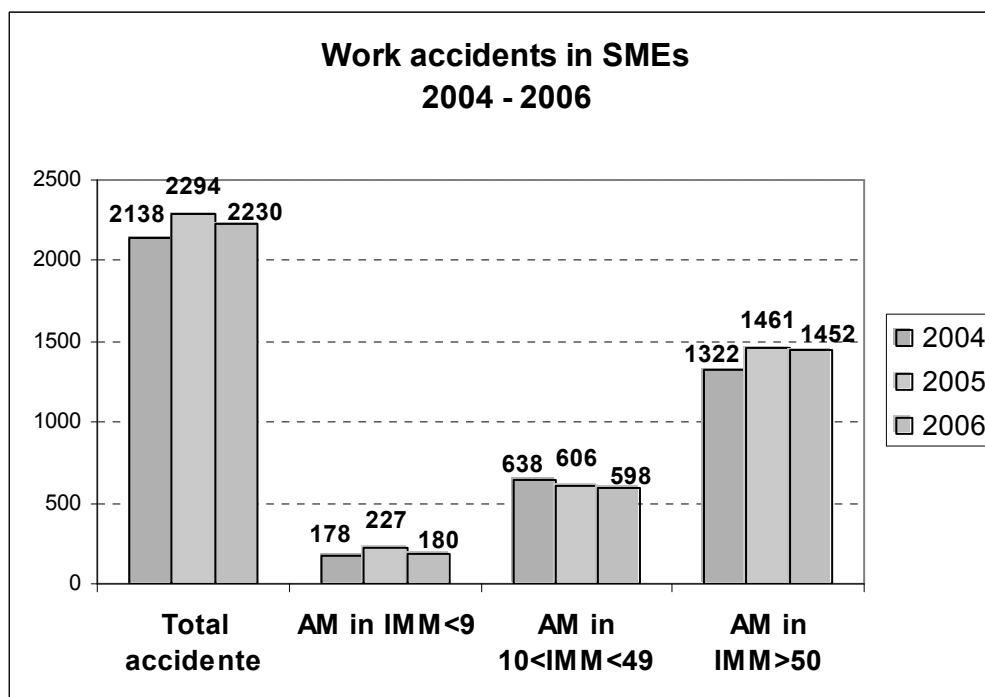
Figure 2

Higher business competitiveness must represent a strong commitment for the top management. This goal needs a full compliance with the whole market rules, including health and safety at work legislation.

The company competitiveness and the implementation degree of the health and safety at work measures, in the framework of a workplaces "welfare" action program, are related. For this reason and taking into account the important number, the causes and circumstances of the workplace accidents, the concern for its diminution must be considered an important issue of the company top management.

## 2. EU policy regarding health and safety at work

Occupational Health and Safety represents today one of the most advanced field of the social policy of the European Union, due to the priority allowed to the risk at work prevention in all Member States.

About 150 million working days are lost each year due to work-related accidents. This is a huge cost for businesses and a huge cost in terms of human suffering for the victims and their families, and also an important cost for the society as a whole, as illustrated in Figure 3.

Workplace accidents can mean pain and disability and can affect the worker's life, both in and out of work. Disruptions to production and bad publicity following an accident are just some of the costs for businesses and organizations. Demands on public services, such as healthcare and social security, also increase. Estimated Member State costs due to work accidents vary from 1–3 % of gross national product.

**Work accidents induce costs on many parties (Krüger, 1997)**
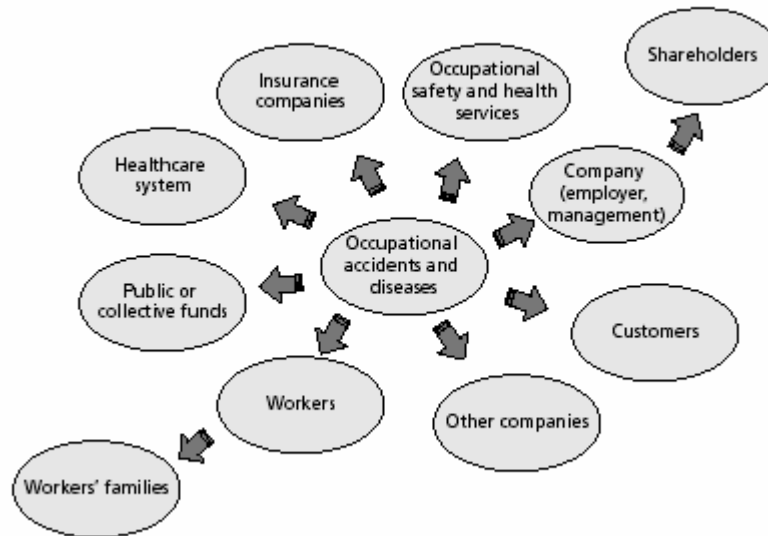


Figure 3

The objective that the EU set at the European Council in Lisbon (March 2000) and in Nice (December 2000) is to create more jobs and of better quality. A safe and healthy working environment is an essential element of the quality of work.

The European Commission is concerned about the costs of „non-social policy" for Europe and they have prioritized the need to develop knowledge of the economic and social costs arising from occupational accidents and illnesses.

In March 2002, the European Commission adopted a Communication on the Community strategy on health and safety at work for 2002-2006, which was meant to be an instrument for adapting to changes in society and work. The analysis behind that strategy was generally right, but it was still sorely lacking in practical measures and a timetable.

On 21 February 2007, the European Commission published a Communication, setting out its proposals for a new European occupational safety and health Strategy to run from 2007-2012. The new strategy is called „*Improving quality and productivity at work: Community strategy 2007-2012 on health and safety at work"*. This Strategy succeeds the former strategy „*Adapting to change in work and society: a new Community strategy on health and safety at work 2002-2006."* It will set the agenda for the next five years in terms of OHS policy development in Europe.

The new Community strategy should make it possible to pursue a much more active policy so as to give impetus to individual Member States' national prevention strategies and set minimum criteria for the key components of national preventive systems.

The Community strategy 2002-2006 has seen a significant fall in the rate of accidents at work. The new strategy for 2007-2012 proposes to step up the UE ambition and **to aim for a 25 % reduction in the total incidence rate of accidents at work by 2012 in EU-27** by improving health ând safety protection for workers and as one major contribution to the success of the Growth and Jobs Strategy.

In spite of the progress achieved, the latest results of the fourth European survey of working conditions show that many workers in Europe continue to perceive that their jobs pose a threat to their health or safety:

-   almost 28% of workers in Europe say that they suffer from non-accidental health problems which are or may be caused or exacerbated by their current or previous job;
-   35% of workers on average feel that their job puts their health at risk.

A number of challenges in the field of health and safety, which were identified during the previous reporting period, are continuing to grow in importance. These include:

-   demographic change and the ageing of the working population;
-   new employment trends, including the increase in self-employment, outsourcing and increased employment in SMEs;
-   new and larger flows of migrants towards Europe.

Certain types of occupational illnesses becoming more common (musculo-skeletal disorders, infections and illnesses associated with psychological stress). The nature of occupational hazards is changing in tandem with the acceleration of innovation, the emergence of new risk factors (violence at work, including sexual and psychological harassment, and addictions) and the transformation of work patterns (working life is becoming more fragmented).

An ongoing, sustainable and uniform reduction in accidents at work and occupational illnesses continues to be the prime objective of the Community strategy for the period 2007- 2012. In the Commission's view, the overall objective during this period should be to reduce by 25% the total incidence rate of accidents at work per 100 000 workers in the EU 27.

In order to achieve this ambitious goal, the following main instruments are proposed:

-   guarantee the proper implementation of EU legislation;
-   support SMEs in the implementation of the legislation in force;
-   adapt the legal framework to changes in the workplace and simplify it, particularly concerning SMEs;
-   promote the development and implementation of national strategies;
-   encourage changes in the behavior of workers and encourage their employers to adopt health-focused approaches;
-   finalize the methods for identifying and evaluating new potential risks;
-   improve the tracking of progress;
-   promote health and safety at international level.

After evaluating the situation at European level, the Commission will investigate whether a recommendation needs to be made which invites the Member States to take steps to facilitate access to good quality prevention services, where the requisite expertise is not available within the company; this is of particular relevance to SMEs.

## REFERENCES

\*\*\*        *Green Paper - Modernizing labour law to meet the challenges of the 21st century*,
            Commission of the European Communities, COM(2006) 708 final, Brussels, 2006
\*\*\*        *Improving quality and productivity at work: Community strategy 2007-2012 on health
            and safety at work*, Commission Of The European Communities, COM(2007) 62,
            final, Brussels, 2007
\*\*\*        *Inventory of socioeconomic costs of work accidents*, European Agency for Safety and
            Health at Work, Luxembourg: Office for Official Publications of the European
            Communities, 2002

## NOILE CERINŢE EUROPENE DE PREVENIRE A RISCURILOR DE MUNCĂ ÎN INTREPRINDERILE MICI ŞI MIJLOCII

**Rezumat.** *Securitatea şi sănătatea în muncă (SSM) reprezintă în prezent unul din domeniile cele mai importante ale politicii sociale a Uniunii Europene datorită priorităţii acordate prevenirii riscurilor în muncă, în toate Statele Membre. Un mediu de muncă sigur şi sănătos este un element esenţial pentru calitatea muncii. Comisia Europeană a extins sfera activităţii sale în favoarea informării, stabilirii de linii directoare şi promovării unui mediu de muncă sigur şi sănătos, acordând o atenţie specială întreprinderilor mici şi mijlocii (IMM). Lipsa măsurilor efective pentru asigurarea SSM poate conduce la absenteism, ca urmare a accidentelor de muncă şi îmbolnăvirilor profesionale şi de asemenea la incapacitate profesională. Noua strategie referitoare la SSM pentru perioada 2007-2012 propune reducerea cu 25% a numărului total de accidente până în 2012 în UE-27, prin îmbunătăţirea condiţiilor de securitate şi sănătate în muncă. Statele Membre trebuie să se asigure că legislaţia UE are deplin efect, în special prin aplicarea directivelor europene. Se impune acordarea unei atenţii speciale circumstanţelor şi necesităţilor particulare ale IMM-urilor, în special cu privire la evaluarea riscurilor, implicarea şi instruirea lucrătorilor.*

# NODULAR GRAPHITE CAST IRON VIBRATED DURING SOLIDIFYING

BY

**GELU BARBU, VASILE COJOCARU FILIPIUC, SERGIU STANCIU**

**Abstract :** *This paper is the result of a series of researches regarding the influence of vibrations on nodular cast iron. Determinations of mechanic properties, structure and segregations have been established by comparing the cast in static and dynamic conditions.*

**Keywords:** *vibration, mechanic properties, casting*

## 1. INTRODUCTION

From the existing researches it has been determined that the realization of cast pieces under the influence of vibrations presents a series of advantages in comparison with static cast.

First of all, the structure of pieces cast in dynamic conditions is more homogenous from a chemical point of view and present a higher degree if finesse due to the increase of cooling speed but also due to the fragmentation of dendrites in course of solidification.

We also obtain an increase of the compaction of the cast pieces as a result of the fact that the liquid alloy penetrates better the existent capillaries in the moment of the solidification, as a consequence of the decrease of the superficial tension of the liquid alloy. The increase of the compaction is due to the fragmentation of biphasic zone.

The degasification of alloys is also a favourable consequence of vibrations. Under the action of vibrations it takes place an increasing of the superficial tension and of the viscosity together with an increase (through attachment) of the bubbles volume, fact that means that favourable creation conditions are forming and also of ascension of gas separators.

Due to the fact that mechanical oscillations reduce the temperature differences on the section of cast pieces, we will obtain cast pieces with smaller thermal voltages.

The elimination of non-metallic inclusions is accelerated in the case of using the vibrations when casting because of the fact that it produces a series of effects as: increasing the possibility of collision and coalescence of inclusions, increasing their elimination speed; uniform repartition of the particles left in al the mass of the ally; reducing the dimensions of the particles left by means of a general finishing of the structure of the cast alloy.

Due to the effects of vibrations those of reducing the viscosity and the artificial tension, and also through the dynamic effects that they generate it produces an increase of fluidity, in spite of the fact that during vibrations the transfer of heat is intensified.

The domains in which it applies the cast under the influence of vibrations are diverse: dental alloys, continuous casting, mixture mould casting, metallic mould casting, etc.

Because of the reduces possibilities of control of the way in which the solidification of alloys is realized, the mechanism for influencing the vibrations over the characteristics of cast pieces is not yet elucidated because there are many theories that explain the phenomenon that take place.

The main research directions in this field are related to obtaining the effects desired and optimally establishing the vibration process parameters: frequency, amplitude, vibration time, vibration manner.

## 2. EXPERIMENTATIONS

I have elaborated a nodular cast iron with the following chemical composition: 3, 8% C; 2, 9% Si; 0, 6% Mn; 0, 15% P; 0, 04% S.

The load required in order to elaborate the iron consisted of high purity iron with the following chemical composition: 3, 6… 4, 2% C; 1, 75% Si; 0, 75% Mg; 0, 03% P; 0, 02 % S. 25 kg of high purity iron have been introduced, a quantity limited by the capacity of the pot.

A quantity of 1, 5% of modifier was placed in the cast pot. When evacuated in the pot with liquid metal at a temperature of $1450^{o}$C, the latter registered a reaction with the modifier producing a burning reaction of Mg vapours from the modifier.

After the completion of evacuation and modification reaction, the modifier had a nodular effect for a period of only 15 minutes. That is why immediately after cleaning the cinders from the surface of the metallic bath and of the casting pot, the material is cast in the two moulds, the first for gravitational solidification and the second fixed on the operating vibrating table.

The samples were processed in order to determine the tensile breaking strength. In order to obtain the desired chemical composition, it was necessary to correct the percentage of Si in order to achieve the concentration of 2, 9% Si in comparison with the concentration of 1, 75% Si of the metallic load.

Thus, a ferrosilicon hardening alloy – FeSi75 - was used whose chemical composition is the following: 70…79% Si; 0, 70% Mn; 0, 4 % Cr; 0, 05% P; 0, 04% S; 0, 1% C; 2, 5 % Al. This hardening alloy was introduced in a metallic bath the moment when the iron was overheated at a temperature of $1450^{o}$C.

| Type of iron obtained | Tensile breaking strength value [N/mm] | | Type of solidification |
|---|---|---|---|
| | 1 | 2 | |
| Foliated cast iron | 582 | 595 | Vibrate |
| | 538 | 551 | Non-vibrated |

In order to obtain the nodular cast iron, the modification was performed in the casting pot. It was used a NODULUN 10 – 4 modifier, a ferroalloy with a content of Mg and Mischmetall (rare soils), with the following chemical composition: 10% Mg;

1, 5% Mischmetall (FeSiCaMgCe); 42% Si; 1, 5% Al. The casting of the two types of iron was performed in special forms for samples.

The results obtained were the following:
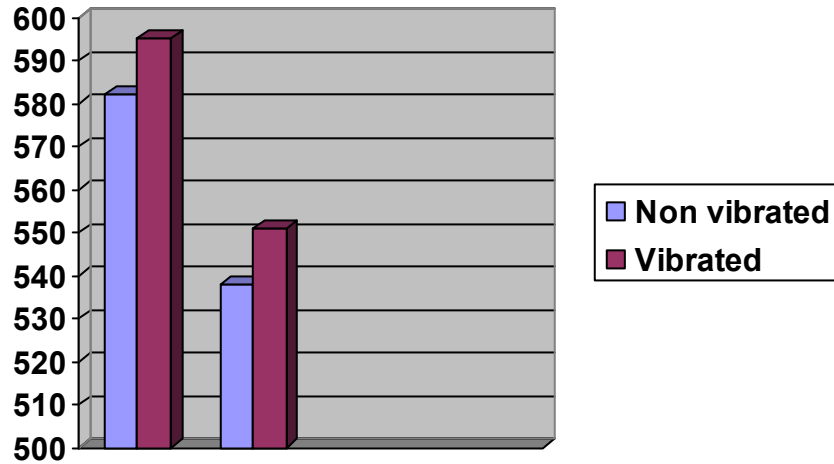


*Figure 1 Comparative graphic of the results obtained during tension.*

As it can be observed, the cast iron under the influence of vibrations present a stronger resistance to traction, both in the case of nodular cast iron and in the case of foliated cast iron.

Another conclusion can also be interpreted according to the form and the distribution of metallic grounds in breaking. Figure 2 presents the microstructures of samples in breaking at a power of 100 x.
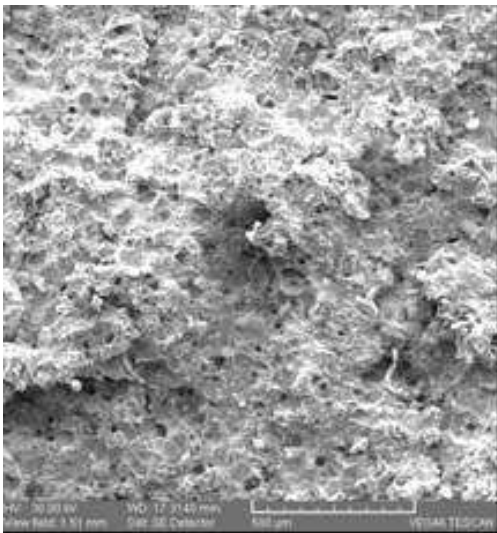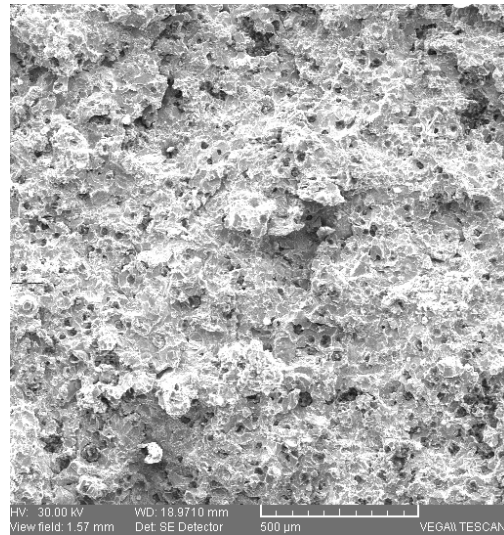


*a) vibrating nodular cast iron;*          *b) non-vibrating nodular cast iron.*
*Figure 2 Microstructure in breaking of cast iron at a microscope power of 300 x.*

Figure 3 presents the microstructures of the same iron, but at a microscope size of 300 x.
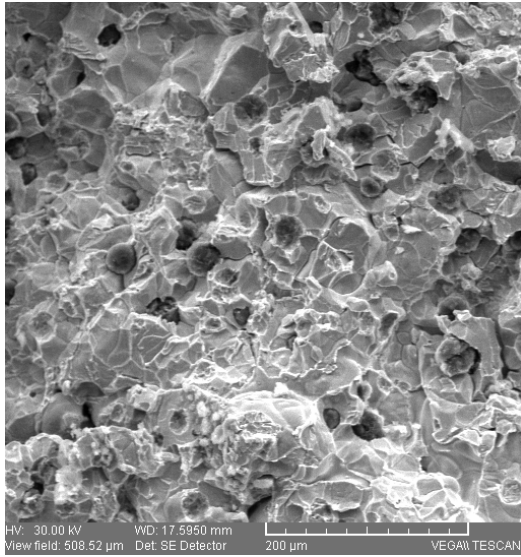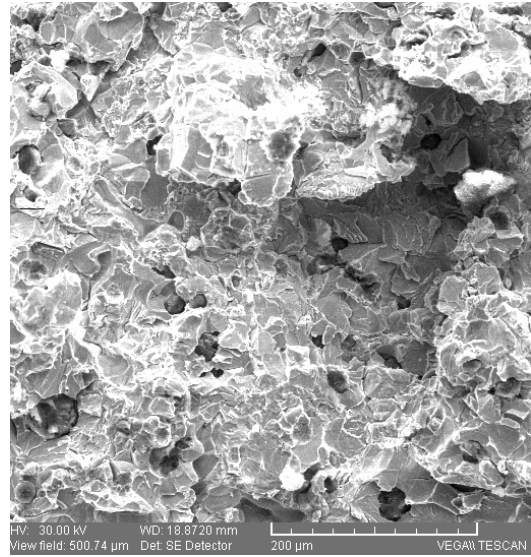


a.vibrating nodular cast iron                    b. non-vibrating foliated cast iron
*Figure 3 Microstructure in breaking of cast iron at a microscope power of 300 x.*

Figure 4 presents the same iron, but at a microscope power of 1000 x.



a. vibrating nodular cast iron                    b. non-vibrating nodular cast iron
*Figure 4 Microstructure in breaking of cast iron at a microscope power of 1000 x.*

Comparing these microstructures we can observe the following:

● in the case of vibrating iron a higher finesse of grains can be observed in comparison with non-vibrating iron;

● at the same time, the distribution of black lead is much more uniform in the case of cast iron under vibrations in comparison with those gravitationally cast;

● in the case of vibrating nodular cast iron, it can be observed that the iron nodules have small dimensions;

● the form of black lead nodules is much more spheroid in the case of cast iron under vibrations;

● the orientation of crystal breaking plans is much more homogenous in the case of vibrating iron that the nodular and foliated ones, fact that explains the stronger strength to tensile breaking registered through the great number of breaking plans met in the case of vibrating iron (the plans are oriented in a larger proportion on the same direction);

● it can also be observed the fact that the size of breaking plans is different in the case of the two irons: in the case of vibrating iron the number of planes is higher fact that explains once again the difference of tensile breaking strength between the two types of iron: vibrating and non-vibrating.

## 3. CONCLUSIONS

In conclusion, the irons solidified under the influence of vibrations have mechanical properties highly superior to gravitationally cast iron due to their homogenous structure and uniform distribution of black lead in the metallic matrix.
- In the case of vibrating foliated iron cast we can observe that the foliated black lead are very well shaped being more compact than those of non-vibrating iron (a).
- We can also observe that in the case of vibrating foliated iron cast the black lead foils are less branched than those of non-vibrating cast iron (a, b)
- The size of the grains differ in the case of both types of iron, being more refined and more uniformly dispersed in the case of vibrating iron.

**REFERENCES**

1 . Barbu, G., - **Solidificarea aliajelor sub influenta vibratiilor**, Ed. Vasiliana'98, lasi 2003;
2. Barbu, G. - **Contributii la imbunatatirea structurii aliajelor metalice prin turnare sub influenta vibrarii**, **Teza de doctorat**, Universitatea Tehnica "Gh. Asachi", lasi, iulie 1998;
3. Barbu Gelu, Cojocaru V., Carcea I. - **Instalatie de turnare cu vibrare**, **brevet inventie** Romania, nr. 108.934 Bl / 1994;
4. Stefanescu FL., Bratu C., - **Cercetari privind influenta vibrarii asupra compactitatii aliajelor turnate**, **Metalurgia, nr.5**, 1985.

**VIBRATII APLICATE LA SOLIDIFICAREA FONTELOR CU GRAFIT NODULAR**

**Rezumat**: Acesta lucrare este rezultatul cercetarilor privind influenţa vibratiilor asupra fontelor cu grafit nodular. Determinarea proprietatilor mecanice şi structurii s-a efectuat atat pe probe turnate static cat si dinamic.

# NUMERICAL SIMULATIONS OF HOLLOW LIQUID XE JET FORMATION FOR LASER-PLASMA GENERATION

BY

## PETRU-EDWARD NICA[1*], MARICEL AGOP[1], IOAN CARCEA[2]

**Abstract** *The formation mechanism of capillary hollow liquid Xe jet in vacuum is investigated. Such jets are used as non-contaminating targets for soft X-ray and extreme-ultraviolet sources by means of laser produced plasmas. The strong evaporation explains jet freezing and the gradual increase of inner gas pressure. By using hydrodynamic arguments, the time dependencies of the jet parameters are numerically computed for a hollow jet having a thin wall. The pressure of the inner gas steeply increases to a maximum value, from where the condensation on the inner jet wall occurs. The physical processes which are involved in jet generation are discussed.*

**Keywords:** *numerical simulation, laser-plasma generation*

## I. INTRODUCTION

At present, intense efforts are made to optimize an extreme ultraviolet (EUV) radiation source for the next generation of lithography technologies. Laser produced plasmas are attractive due to their small size, high brightness and high spatial stability. However, the conventional targets have limited operating time and produce debris[1] which may destroy or coat the EUV collecting optics that are positioned close to the plasma. The amount of produced debris can be limited by replacing conventional solid targets with gas[2], gas-cluster[3], liquid-jet[4,5], or liquid-droplet[5] targets. Such regenerative targets provide fresh material for operation without interruption and allow the use of high repetition-rate lasers, thereby having potential for high average power. Furthermore, noble gases like xenon eliminate the coating problem, being considered as non-contaminating target materials[1].

Recently, the hollow Xe targets[5,6], *e.g.* liquid Xe hollow jet, are considered to improve the conversion efficiency of the laser energy into EUV radiation by increasing the plasma life-time and reconverting plasma expansion energy. However, a stable laser–plasma generation requires a spatially stable liquid jet because the operating point should be far from the nozzle[5,7,8] It is the main motivation for studying the jet stability.

In the present paper, the obtaining mechanism of liquid Xe hollow jet is analyzed. Taking into account the jet vaporization, cooling and freezing, its radius dependencies on time, on nozzle temperature and jet velocity are numerically computed.

## II. THEORETICAL MODEL

When the liquefied inert gas jet is injected into vacuum, the strong evaporation will quickly cool the jet, leading to rapid freezing. Moreover, for a hollow jet, two different evaporation rates, from the inner and the outer walls, give a pressure difference which gradually increases

---
* Email: pnica@ch.tuiasi.ro

the tube radius and can lead to the jet destabilization. The inward and outward molecular fluxes, $\phi_{in}$, $\phi_{out}$, are given by[9)]

$$\phi_{in} = \frac{\alpha}{4} \sqrt{\frac{8}{\pi k_B T \cdot m}} [p_v(T) - p_{in}], \quad \phi_{out} = \frac{\alpha}{4} \sqrt{\frac{8}{\pi k_B T \cdot m}} [p_v(T) - p_{vac}], \quad (1a,b)$$

where $\alpha$ is the sticking coefficient, $T$ the temperature, $k_B$ the Boltzmann constant, $m$ the atomic mass, $p_v(T)$ the saturated vapor pressure, and ($p_{vac}$, $p_{in}$) are the vacuum chamber and the inner pressure, respectively.

Having a thin wall of the hollow jet, the thermal field is uniform across the jet section. Thus, by extending the results from Ref. [8], the jet temperature as function of time can be expressed in the form

$$\frac{dT}{dt} = \begin{cases} -\dfrac{2L_v m[\phi_{out} r_{out} + \phi_{in} r_{in}]}{\rho_l(T) C_{P(l)}(T)[r_{out}^2 - r_{in}^2]}, & (t < t_{fi} \text{ i.e. } T > T_f) \\ 0, & (t_{fi} < t < t_{sol} \text{ i.e. } T = T_f) \\ -\dfrac{2(L_v + L_f) m[\phi_{out} r_{out}(t_{fi}) + \phi_{in} r_{in}(t_{fi})]}{\rho_s(T) C_{P(s)}(T)[r_{out}^2(t_{fi}) - r_{in}^2(t_{fi})]}, & (t > t_{fi} + t_{sol}, \text{ i.e. } T < T_f) \end{cases}, \quad (2a\text{-}c)$$

where $t$ is the time, $L_v$, $L_f$ the specific latent heat of vaporization and fusion, $C_P$, $\rho$ the specific heat and density. The subscripts ($l$, $s$) refer to the liquid and the solid state. The inner and outer hollow jet radii, $r_{in,out}$ (see Fig. 1) were considered constant below the freezing point temperature ($T_f$=161.36K), i.e. by the time of freezing initiation ($t_{fi}$). It should be noted that all quantities except $m$ from the right side of Eqs. (2a,b) are time-dependent, even indirectly by means of temperature dependence on time. After the solidification starts, the liquid-solid transition occurs in a time given by

$$t_{sol} = \frac{\rho_l(T_f)[r_{out}^2(t_{fi}) - r_{in}^2(t_{fi})]L_f}{2m \cdot r_{out}(t_{fi})\phi_{out}(T_f)[L_v + L_f]} + \frac{r_{in}(t_{fi})}{r_{out}(t_{fi}) \cdot \phi_{out}} \int_{t_{fi}}^{t_{fi}+t_{sol}} \phi_{in} dt. \quad (3)$$

In Eq. (3) the outward flux is taken constant due to the constant jet temperature ($T = T_f$) during the solidification process and the inward flux is time-dependent through the time dependence of the inner pressure – see Eq. (1a). However, the contribution of the second term from the right side of Eq. (3) can be neglected because the inner gas pressure increases rapidly towards the saturation curve, leading to the decreasing of inward molecular flux. This will be shown below.
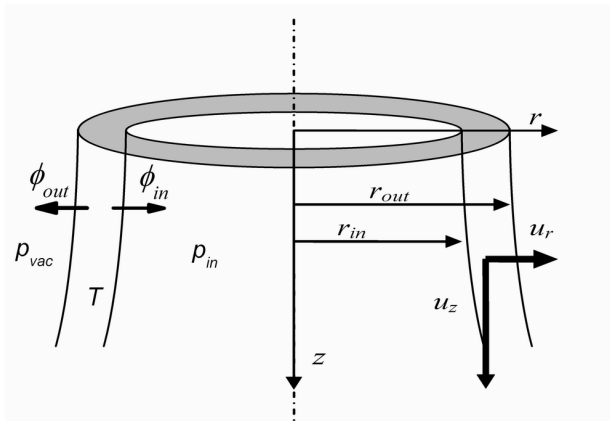


Figure 1: *The geometry of the hollow liquid Xe jet*

By considering the inner gas as ideal, the inner pressure dependence on time is given by

$$\frac{dp_{in}}{dt} = k_B T \frac{2\phi_{in}}{r_{in}} + \frac{p_{in}}{T}\frac{dT}{dt} - \frac{2p_{in}}{r_{in}}\frac{dr_{in}}{dt},$$ (4)

where the first term is due to the evaporated molecules from the inner wall, the second term is due to the inner gas cooling, and the third term is due to inner jet radius dependence on time. The inner gas temperature is approximated as being identical with the jet temperature. Furthermore, we approximate that all the inner gas parameters are constant inside a given cross-section of the jet, and vary only along the $z$-axis with time.

The time dependence of the jet radius is given by two factors: the mass loss due to the evaporation and the pressure difference between the inner and outer gas. For the practical case of interest when the initial Xe jet temperature is $T_0$=190K, the relative mass loss due to the evaporation up to freezing initiation, *i.e.* $dM/M = (c_{P(l)}(T)/L_v)dT$,[8] can be estimated using the thermophysical constants from Ref. [10] to be 10.04%. Consequently, this aspect will be neglected in the followings and only the liquid hydrodynamics will be considered. For a laminar incompressible viscous flow of the jet, it is described by the well-known Navier-Stokes and the continuity equations,

$$\frac{\partial \boldsymbol{u}}{\partial t} + (\boldsymbol{u}\cdot\nabla)\boldsymbol{u} = -\frac{\nabla p}{\rho} + \frac{\eta}{\rho}\Delta\boldsymbol{u},$$
$$\nabla\cdot\boldsymbol{u} = 0$$ (5a,b)

where $\boldsymbol{u}$ is the velocity. Assuming a constant axial velocity ($u_z$ - see Fig. 1) and using cylindrical coordinates for describing the liquid jet, the above equations become

$$\frac{\partial u_r}{\partial t} - \frac{u_r^2}{r} = -\frac{1}{\rho}\frac{\partial p}{\partial r} - \frac{\eta}{\rho}\frac{\partial^2 u_r}{\partial z^2},$$
$$\frac{\partial u_r}{\partial r} = -\frac{u_r}{r}$$ (6a,b)

$u_r$ being the fluid radial velocity and $\eta$ the viscosity.

Since the jet dynamics in radial direction is a free boundary problem, additional difficulties arise in solving the system of Eqs. (6a,b) coupled with Eqs. (2a-c) and Eq. (4).[11] Therefore, let us consider Eq. (6b) in the form

$$u_r = \frac{u_{r,in}r_{in}}{r},$$ (7)

where $u_{r,in}$ is the inner wall radial velocity. By averaging on the wall thickness, it results

$$\bar{u}_r = u_{r,in}\frac{r_{in}}{r_{out}-r_{in}}\ln\left(\frac{r_{out}}{r_{in}}\right).$$ (8)

Then, Eq. (6a) can be approximated as

$$\frac{d}{dt}\left(u_{r,in}\frac{r_{in}}{r_{out}-r_{in}}\ln\left(\frac{r_{out}}{r_{in}}\right)\right) = \frac{2(r_{in}p_{in,wall}-r_{out}p_{out,wall})}{\rho_l(T)(r_{in}^2-r_{out}^2)} - \frac{\eta(T)}{\rho_l(T)}\frac{1}{u_z^2}\frac{d^2}{dt^2}\left(u_{r,in}\frac{r_{in}}{r_{out}-r_{in}}\ln\left(\frac{r_{out}}{r_{in}}\right)\right),$$ (9)

where the $z$ – coordinate dependence was regarded as time-dependence (the constant axial velocity is assumed), and

$$u_{r,in} = dr_{in}/dt , \ r_{in} = r_{in}(t) , \ r_{out}(t) = \sqrt{r_{in}^2(t) + d_0^2 + 2r_{in}(0)d_0} \qquad (10a\text{-}c)$$

with $r_{in}(0)$ and $d_0$ the inner radius and respectively the hollow jet wall thickness at the initial time. The total pressures on the inner and outer wall, ($p_{in,\ wall}$ , $p_{out,\ wall}$) are given by three contributions: i) the ambiental hydrostatic pressure ($p_{in}$, $p_{vac}$); ii) the pressure due to the superficial tension ($-\sigma_l(T)/r_{in}$, $\sigma_l(T)/r_{out}$), where $\sigma_l$ is the superficial tension coefficient; iii) the vaporization induced inner and the outer pressures ($p_{in,vi}$, $p_{out,vi}$) which are expressed using Eq. (1a,b) by [9]

$$p_{in,vi} = m \cdot \phi_{in} v_{th} = \frac{2\alpha}{\pi}(p_v(T) - p_{in}), \quad p_{out,vi} = m \cdot \phi_{out} v_{th} = \frac{2\alpha}{\pi}(p_v(T) - p_{vac}), \quad (11a,b)$$

$v_{th}$ being the thermal velocity. Consequently, it results:

$$p_{in,wall} = \frac{2\alpha}{\pi}(p_v(T) - p_{in}) + p_{in} - \frac{\sigma_l(T)}{r_{in}}, \quad p_{out,wall} = \frac{2\alpha}{\pi}(p_v(T) - p_{vac}) + p_{vac} + \frac{\sigma_l(T)}{r_{out}} . \ (12a,b)$$

The one-dimensional problem expressed by the system of Eqs. (2a-c), (4) and (9) with the expressions given by Eqs. (1a,b), (3), (10a-c) and (12a,b) was numerically solved. The unknown functions are: $T=T(t)$, $p_{in}=p_{in}(t)$, $r_{in}=r_{in}(t)$. Thermophysical properties of Xe and their temperature dependencies are taken from Ref. [10]. For the vacuum pressure, $p_{vac}$=98 Pa is assumed, and the same value is taken for the inner gas initial pressure. The analyzed geometry corresponds to an annular nozzle having $r_{in}(0)$=70 μm and $r_{out}(0)$=75μm. For the sake of simplicity, we considered the ($\alpha$) coefficient in our calculations as being 1. However, the molecular dynamic simulations (for example see the computations from Ref. [12] for Ar) show that it depends on the particle impact energy as well as on the surface temperature.[13] Typically, $\alpha$ is ranged between 0 and 1, and for a successfully understanding of the evaporation and condensation processes, an expression for the energy flux is also required.[13]

### III. NUMERICAL RESULTS

The results of the numerical calculations for a hollow jet with axial velocity $u_z$=0.5 m/s are plotted in Fig. 2 and Fig. 3 for the cases of two initial temperatures, $T_0$=190K and $T_0$=170K. Figs. 2a)-c) shows time dependencies of the jet temperature, inner gas pressure, inward and outward molecular fluxes. In Fig. 3 the inner gas state is plotted by using the equilibrium diagram of Xe.

The following regions can be distinguished for $T_0$=190K (see dashed marks in Fig. 2 and their correspondent in Fig. 3):

i) A-B region: the inward and outward fluxes decrease as the jet temperature decreases. Meantime, the inner gas pressure also increases because of the inward evaporation, which furthermore rapidly decreases of the inward molecular flux. At B-point the inner pressure reaches its maximum value, the inward flux becomes zero, and the inner gas state reaches the saturation curve as shown in Fig. 3. By comparison, for $T_0$=170 K, the solidification is earlier initiated and the saturation curve is not reached (see dotted curves in Figs. 2a)-c));

ii) B-C region: the outward evaporation keeps cooling the jet, but the inner gas is oversaturated and is condensing, *i.e.* a negative inward molecular flux;

iii) C-D region: at the C-point the liquid jet starts freezing. After $t_{fi}$ = 2.02 μs, the fusion temperature, $T_f$=161.36 K is reached. Consequently, the temperature and outward flux become constant for $t_{sol}$ = 6.7 μs. The inner flux rapidly tends to zero (see Fig. 2a) and the inner gas

state goes toward the liquid-gas saturation curve at constant temperature, $T_f$ (see Fig. 3). This allows us to neglect the second term in the right-side of Eq. (3);
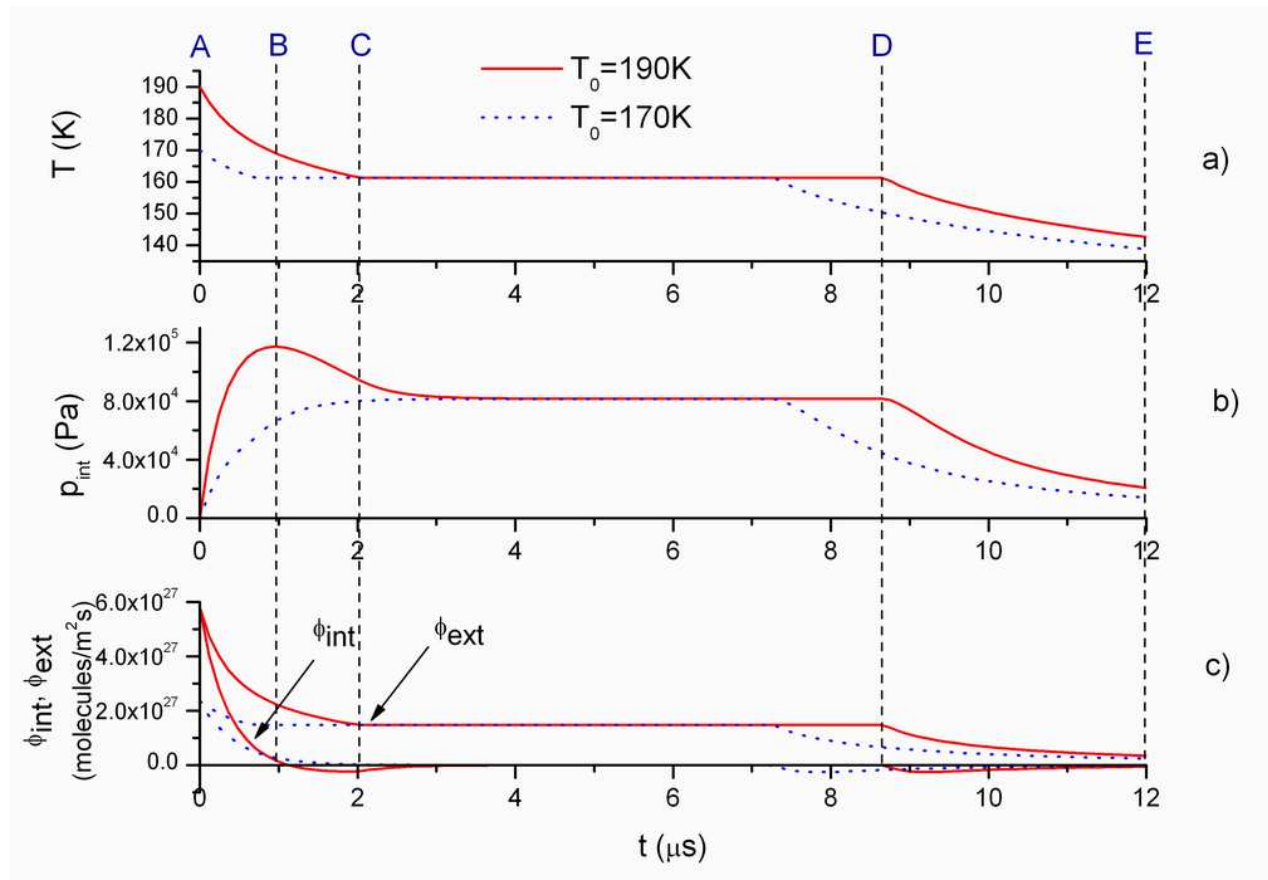


Figure 2a)-c): *The time dependencies of the jet temperature (a), the inner gas pressure (b), the inward and outward molecular fluxes (c), for the jet initial temperatures $T_0=190K$ (continuous line) and $T_0=170K$ (dotted line), and the initial axial jet velocity, $u_z=0.5$ m/s*

iv) D-E region: the jet cooling continues due to the outward evaporation and a low negative inward flux determines inner condensation, since the inner gas is in an oversaturated state.

In Fig. 4 the inner radius time-dependencies for $T_0=190K$ and various velocities are plotted up to the freezing point. The time domain is taken below $t_{fi} = 2.02$ μs since the freezing initiation time was found to vary with less than 1% in respect with the axial velocity.

The following results: i) the increase of the jet inner radius *vs.* time becomes more significant with the increasing the jet velocity; ii) as a test for the result accuracy, the arbitrary increasing of the viscosity coefficient by $10^5$ times gives a constant radius; iii) neglecting the second term in the right-side of Eq. (9), the curve corresponding to a non-viscous fluid are overlapping with the curve corresponding to $u_z=10$ m/s and viscous state. This suggests that at such velocity the role played by viscosity becomes negligible. It should be noted that the present analysis is limited to the laminar flow. Thus, assuming the tube thickness as the characteristic length, the corresponding Reynolds numbers at the nozzle exit are found to be less than 2500.

Figure 3: *Inner gas evolution on the phase diagram for the initial jet temperature $T_0=190K$ (continuous line) and $T_0=170K$ (dashed line)*



\

Figure 4: *Inner jet radius dependence with time for $T_0=190K$ and various axial velocities*

## IV. CONCLUSIONS

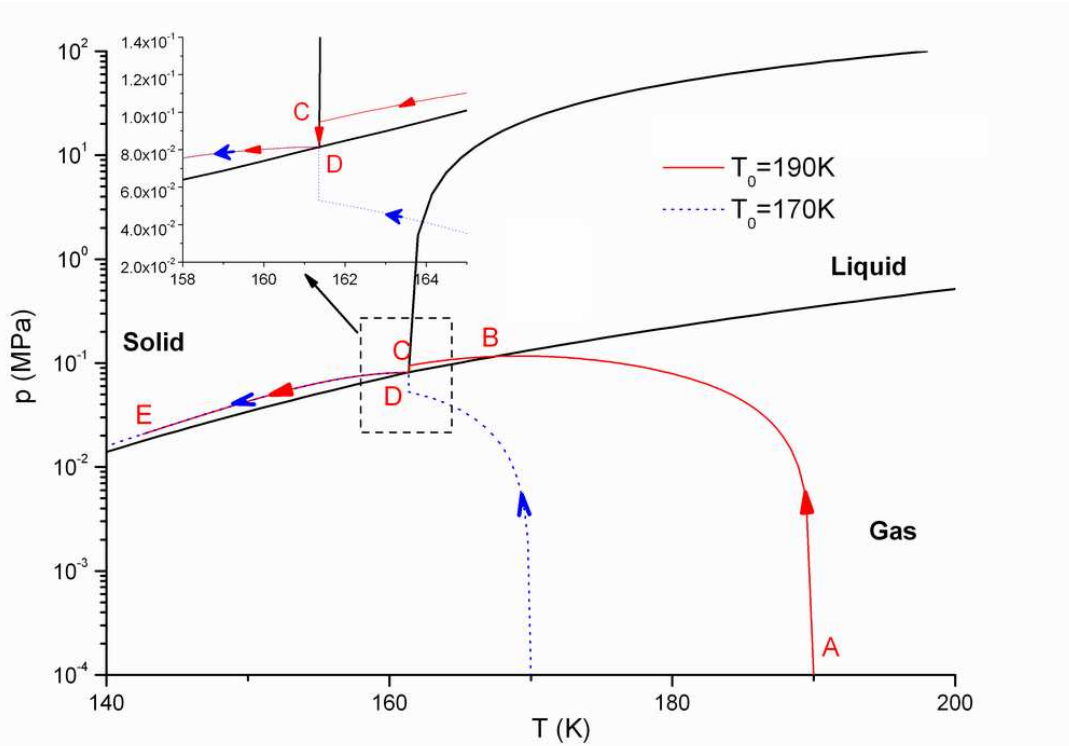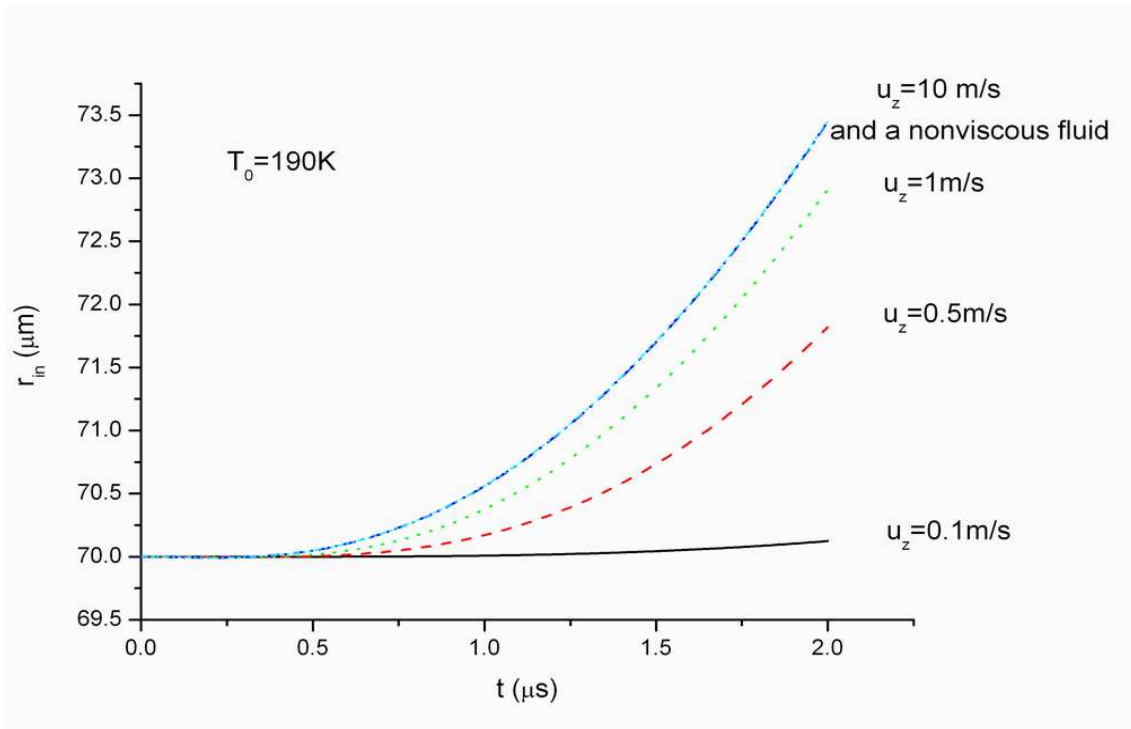The main conclusions of the present paper are as follows:

i) The mechanism of obtaining a hollow Xe liquid jet was analyzed. For wall thicknesses of tens of micrometers, the thick wall model was used for the mathematical treatment;

ii) Having a thin jet wall, the temperature across the jet section is considered uniform. The pressure difference between the inner and outer region gradually increases the jet radius. Using hydrodynamic arguments, the time dependence of radius is established;

iii) The pressure of the inner gas steeply increases to a maximum value, from where the condensation on the inner jet wall occurs.

*[1]Department of Physics,*
*[2]Faculty of Materials Science and Engineering*
*Technical "Gh. Asachi" University, Iasi,*

## REFERENCES

1. Turcu, J.C.E., Dance, J.B., 1999. X-Rays from Laser Plasma, John Wiley & Sons, Chichester.
2. Kubiak, G. D., Bernardez, L., Krenz, K., 1998. High-power extreme ultraviolet sources based on gas jets. In  Emerging Lithographic Technologies II, Ed. Vladimirsky, Y., Proc. SPIE 3331, 81-89.
3. Fiedorowicz, H., Bartnik A., 1996. Demonstration of soft X-ray lasing with Neon-like Argon and Nickel-like Xenon ions using a laser-irradiated gas puff target. Phys. Rev. Lett. 76, 415-418.
4. Berglund, M., Rymell, L., Hertz, H.M., 1998. Cryogenic liquid-jet target for debris-free laser-plasma soft x-ray generation.  Rev. Sci. Instrum. 69, 2361-2364.
5. Inoue, T., Nica, P.E., Kaku, K., Shimoura, A., Amano, S., Miyamoto, S., Mochizuki, T., 2006. Studies on cryogenic Xe capillary jet targets for laser-produced plasma EUV-light source. Proc. SPIE, 6151, 132-133.
6. Miyamoto, S., Amano, S., Inoue, T. , Nica, P.E., Shimoura, A., Kaku, K. Sekioka, T., Mochizuki, T., 2006.  EUV Source developments on laser-produced plasmas using cryogenic Xe and lithium new Scheme target. Proc. SPIE, 6151, 134-135.
7. Hansson, B.A.M., Rymell, L., Berglund, M., Hemberg, O., Janin, E., Thoresen, J., Mosesson, S., Wallin, J., Hertz, H. M., 2002. Status of the liquid-xenon-jet laser-plasma source for EUV lithography. Proc. SPIE 4688, 102-109.
8. Hansson, B.A.M., Berlung, M., Hemberg, O., Hertz, H.M., 2004. Stabilization of liquefied-inert-gas jets for laser-plasma generation. J. Appl. Phys. 95, 4432-4437 .
9. Ho, T. C., 2002. Fluid Handbook, Chapter 8, Edited by J.M. Saleh, McGraw-Hill, New York.
10. Rabinovic, V.A., Vaserman, A.A., Nedostup, V.I., Veksler, L.S., 1987. Thermophysical Properties of Neon, Argon, Krypton, and Xenon, National Standard Data Service of the USSR. a series of property tables, Hemisphere Springer-Verlag, Berlin, and data supplied by NIST (http://webbook.nist.gov/chemistry/fluid).
11. Acheson, D.J., 1990. Elementary Fluid Dynamics, Oxford University Press.
12. Yasuoka, K., Matsumoto, M., Kataoka, M., 1994. Evaporation and condensation at a liquid surface. I. Argon. J. Chem. Phys. 101, 7904-7911.
13. Bond, M., Struchtrup, H., 1994. Mean evaporation and condensation coefficients based on energy dependent condensation probability. Phys. Rev. E 70, 061605.

# SIMULĂRI NUMERICE ALE FORMĂRII UNUI JET TUBULAR DE XENON PENTRU GENERAREA PLASMELOR LASER

## (Rezumat)

*Se analizează mecanismul formării în vid a unui tub capilar de Xenon lichid. Astfel de jeturi sunt folosite ca ţinte necontaminante pentru sursele de radiaţii X-moi şi extrem ultraviolet prin intermediul plasmelor produse cu ajutorul laserului. Evaporarea puternică explică îngheţarea jetului şi creşterea graduală a presiunii gazului interior. Folosind argumente hidrodinamice, se calculează numeric parametrii unui jet având o grosime subţire a peretelui. Presiunea gazului interior creşte brusc la o valoare maximă, iar apoi se realizează condensarea pe pereţii interiori. Se discută procesele fîzice implicate în generarea jetului.*

# SOFTWARE APPLICATIONS FOR DESIGN OF THE FOUNDRIES TECHNOLOGICAL PROCESSES

BY

**Ion CHIRA**

**Abstract.** *The present work stands for a brief synthesis of the last ten years accomplishments in the field of softs dedicated to foundry technologies. this view of the main applications that inforced themselves in the technological practice from abroad and, partially from romania, should frame the computer work informatic future tendencies, technological designing in the cad/cae-cam/cim systems, the general levels and standards against which we must lead the structure of the metallurgic national department, organization of the foundries and their management, towards maximum efficiency and optimal interconnection to the european circuit.*

**Keywords:** expert systems, technological softs, computer technological operations leading

## I. OPPORTUNITIES OF COMPUTER FOUNDRY TECHNOLOGIES DESIGNING

Nowadays, the pouring technology design is still based on old empyrical methods, such as the one mentioned by Chvorinov (1940), a method that is based on the solidification time assessment according to the M mode.

The first computer numerical simulations of the solidification process were made by Eyres and other America researchers who, starting from 1946, applied the finished differences method to a simple piece solidification study.

In 1970, Pehlke and his contributors made a significant double study for the poured pieces solidification process. In this regard, they checked, by experiments and calculations, very simple pieces poured in classic forms and compared the different variants of the finished differences method.

In 1985, Ohnaka sets the direct finished differences method; Patankar approached the volume elements method, and Hang set the border elements method.

The solidification proces modeling through numerical methods have been the object of five international conferences „*Shaping of casting, welding and advances solidification processes*".

Nowadays, a lot of metallurgical and technology designing enterprises from the metallurgical industry launched some programmes for the shaping of solidification, flowing and mixture filling in the pouring forms such as SOLSTAR, MAGMA SOFT, PROCAST.

With *CAD/CAM* programmes one can achieve the pouring technology optimization of a certain benchmark; the operation becomes efficient either in extremely valuable unique piece production (turbines, rolling mill cylinders, hydraulic bodies for nuclear power stations, big MU carousels) or in mass production, when assimilating a specialized manufacturing: auto, farming machines, textile equipments, aeronautic industry, birotics and computers.

## II. THE POURING  TECHNOLOGY COMPUTER WORK

The computer assisted designing starts from the classic technology; the first stage consists of computer work for the technological process, namely and afterwards, the optimization of the technological stages (pouring, filling the pouring form cavity with melting charge, cooling, solidification, temperature gradient in piece and form wall thickness etc.) on the basis of specific,dedicated applications.

For example, let's take into consideration the case of high pressure pouring process (TPI), a domain with a high degree of mechanization-automatization-robot using, namely formulating the subject as a *the designing of a TPI technological cell.*

The computer work strategy of this hypothetical technologic process „The TPI technologic functional cell", imposes a series of stages and levels of conception - development:

- expert system  (SE) base setting and conceiving stage, at modulus architecture level;

- global architecture generation of the dosing and pouring process and of communication between submodulus;

- commands instrumentation and transmission to the conducted object (melting charge processing in the refining precincts, one pouring dosing and the compression room supply with the respectiv melting charge dose, mould oiling and locking, remaking the cycle);

- synthesis of the whole technological process mathematic model, as general supervising source of the designed expert  system. An expert system, meant for industrial development applications contains the following basic components (see Fig. 1). The cognitive system, whose task is to organize, memorise, update and offer, in the benefit of the rezolutive system –cognition pieces of the usage specific field;

- *The self-organizing, self-adaptating and self-control system* supervises the other components functionning, establishes the dynamic connection between them, meanwhile assuring their structural adaptation to the functional requirements and specific contextual situations of the particular problems to be solved.

For an industrial process, such as the *High pressure pouring integrated technologic cell (TPI)*– the computer conducting scheme is principially presented in Figure 2. The thermic-technologic *refining,dosing and pouring* operations, in the presented scheme can be detailed, and  the principle component elements can be particularized. The standard configuration architecture of the expert system and the soft correspondances designing with real technical-technologic elements consist of (see Fig. 3):

1. *Automatics elements:* Identification of process behaviour models; Automatic leading of the technological process, with informatic captators and interfaces;

2. *Supervising:* Process documents emission; Cartographic vectoring, as a complex computer graphic representation.
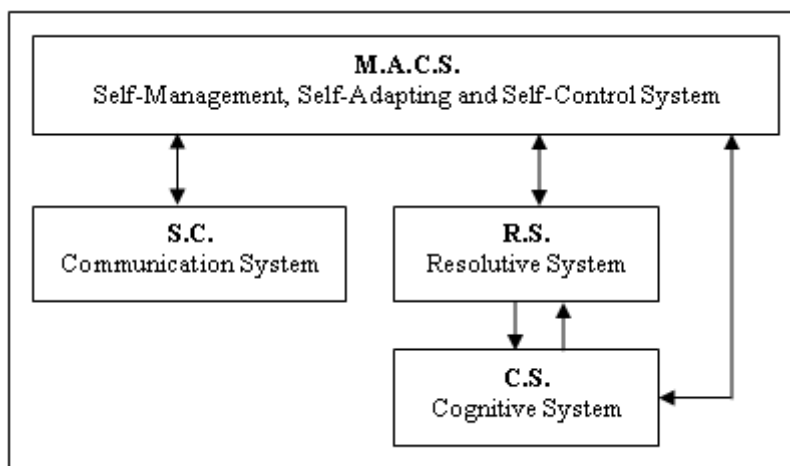
Fig. 1 Basic modulus in an expert system architecture

One can notice that the computer leading strategy of such a thermical-metallurgic process, under performance conditions (taking into consideration a large number of variable parameters), is a very difficult objective to touch, which requires optimal solving solutions and represents a situation that imposes a new approach and interdisciplinary treatement. In Figure 4, we presented the scheme of a technic data flow proposal within a foundry, that is in the course of assimilating the technology designing on the computer, through shaping and simulation of melting charge pouring-flowing, solidification-cooling in a form, or the difficult issue of pouring network heasing and optimising.

Similarly, in Figure 5, we indicate a logical succession for the poured pieces solidification shaping and simulation, and in Figure 6, we introduced the solidification model setting stages.



Fig. 2 Principially schemed and simplified representation for computer leading of an industrial technologic process

Fig. 3 The architecture of the piloting expert system of the TIP pouring step, in the integrated technological cell.

## III.    PRINCIPLES IN TECHNOLOGIC SOFTWARE ELEMENTS DESIGNING

### 3.1 The metallic melting charge flow during the pouring process.

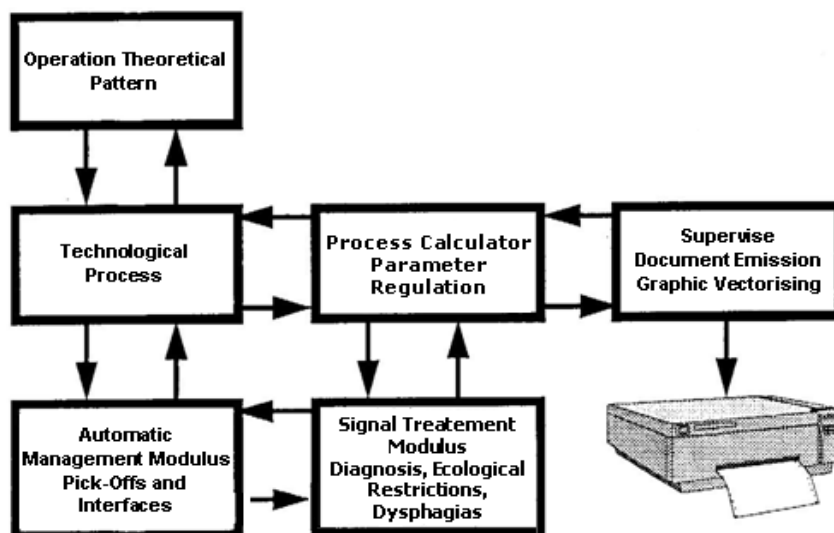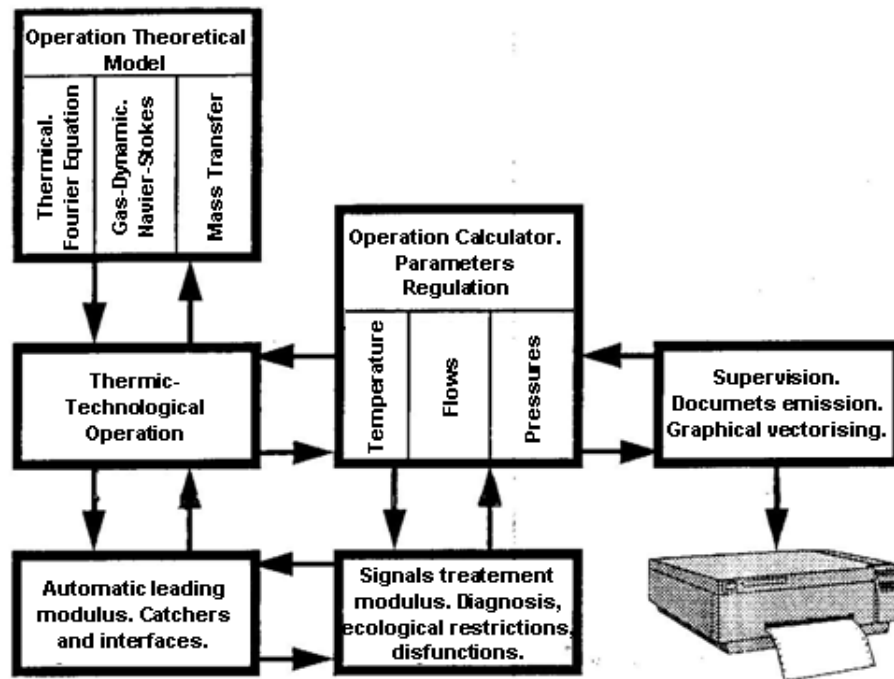The numeric simulation of the pouring processes, therefore the hydraulic elements and metallic melting charges flow are recent history due to the *NAVIER-STOKES* flowing situation and the nonliniar thermic transfer equations complexity in a tridimensional system. Solving these equations using numerical methods, the finished differences and finished elements methods were possible together with hardware and operating system development.

The programmes meant to solve the fluids flowing and mixtures solidifications problems appeared only in the 1980s due to the complex problems generated when solving fluid's free surface behaviour. At the present time, much significance has been given to the programmes that start from the finished differences method because of the rapidity with which they solve the flowing problems and, so, due to their efficiency in industrial applications where the response time is essential.

The mixture's flow under gravitational, viscid and pressure gradient's forces is decribed by the speed and pressure field whose evolution is given in the Navier-Stokes equation, the continuity equation and the free surface conditions.

### 3.2 Solidification of metallic melting charges during cooling in the pouring form

The thermical transfer during the flowing and solidification processes is ruled by the *FOURIER EQUATION* – thermic conductibility. This equation is accompanied

by the initial and limit conditions, *Cauchy Type* (when we consider the external environment temperature and the global coefficient of heat exchange between environment and the analysed system, as programme input data; this case appears when the heat exchange conditions are given to the system's external part, through thermic convection), *Dirichlet* (when we consider as input data the temperature of the ingot surface or of the poured piece ) and *Neumann* (when we consider as input data the thermic flow on the border segment considered, as in the case of radiations or external heat source). The specific equations that we mentioned apply to the participant domains.

To solve the physical shaping we must use different techniques and methods; the special literature shows numerous case studies in this field. For example, with the *SOLA - VOF = Solution Algotithm - Volume of Fluid method*, based on an explicit finished differences scheme, applied on a crossing 3D graphic grating, we can solve  a series of problems with regard to steel ingots pouring.

## IV.  DEDICATED TECHNOLOGICAL  SOFTS

### 4.1.  The MAGMA soft Programme

*Modular structure. Brief descriprion of capabilities.*

*The programme package dedicated to <MAGMA soft> piece pouring* is one mainly meant to simulate the flowing and heat transfer phenomena; the package was developed for *UNIX* operating system computers**,** with *X-Windows*  graphic interface.

*MAGMA soft* is a modular package, that contains: Project management; Preprocessor, which includes geometry defining; Optional transfer from CAD packages and network generating with finished elements; Main processor for process description and numeric calculations; Postprocessor for results visualising and assesment; Thermophysical data collection and manipulation. All modulus are written in standard **C** or *FORTRAN 77***.**

*Main moduluss for fluid dynamics calculation and heat transfer phenomena:*

a.  *MAGMA/fill* – a modulus to simulate the pouring form filling and fluid flowing process – metallic mixtures. While filling the form, we analyse the melting charge flowing phenomena.

b.  *MAGMA/solid* – solidification modulus with the following features;

c.  *MAGMA/batch* **–** pouring modulus in permanent metallic forms;

d.  *POSTPROCESSOR MODULUS* for results visualizing and validation**.**

*Material thermophysical features database****:***

When needed, the modular architecture allows an up-grade, by adding other modulus such as:

• *MAGMA/hpdc* (low pressure injection pouring = TJP) or *MAGMA/lpdc* (for depression pouring procedings – such as the aspertion pouring);

• *MAGMA/iron* (microshaping for cast iron pouring).

### 4.2  The SOLSTAR Programme

Thus, the *SOLSTAR* programme belonging to *Fonseco*, the *Multimillion 3* version, can calculate and share a piece in 64 milions of volume elements, compared to the *Multimillion 2* variant, which can get 3 milions volume elements at maximum.

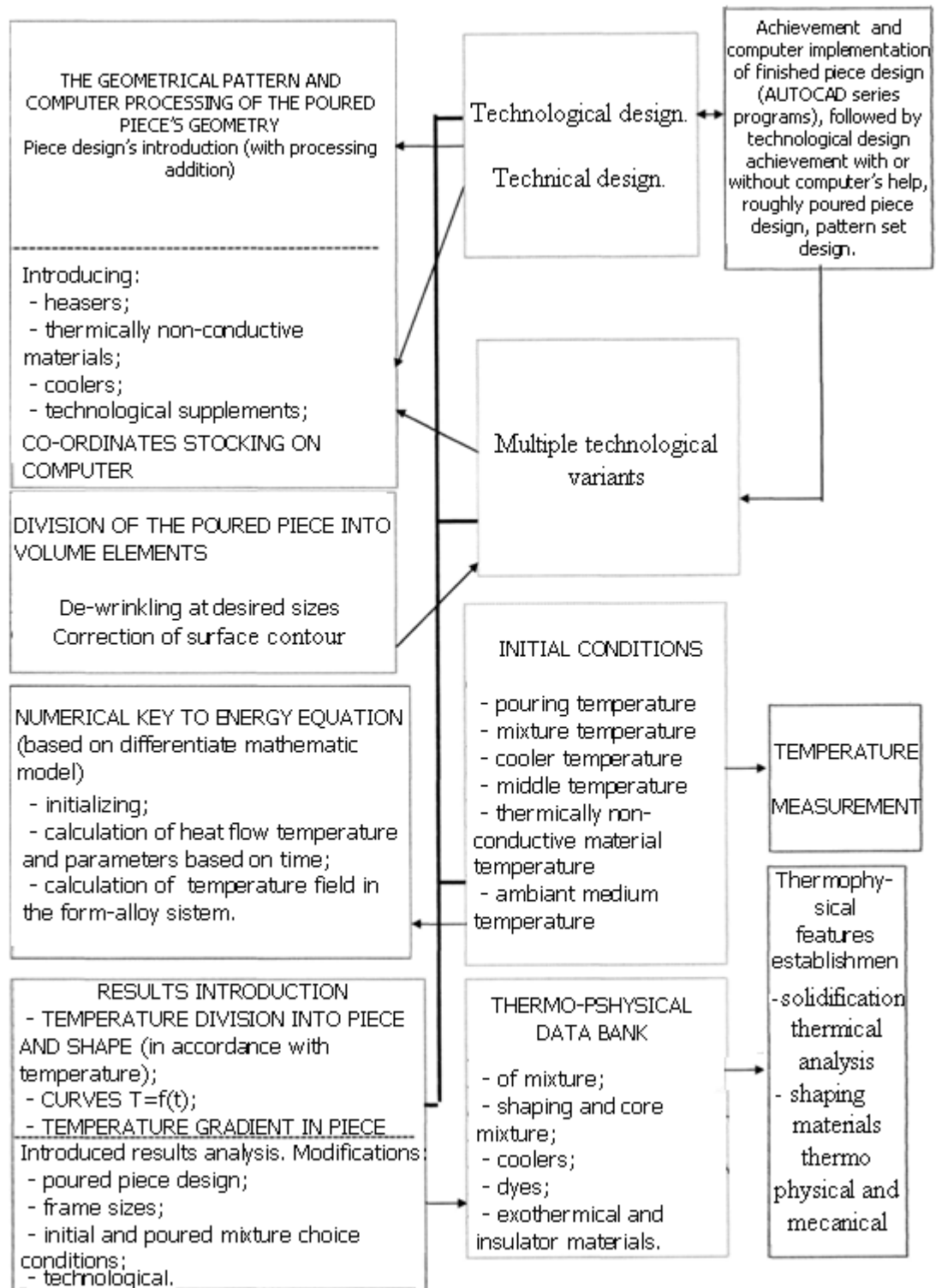Fig. 4 Techic data flow wihtin a foundry.

**4.3 The MAVIS Programme**

The *MAVIS & DIANA* programme, that belongs to the *Alphacast sofware* firm, in cooperation with University of Wales Swansea (Marea Britanie), analyzes different mixtures solidification, poured as mixture or permanent mould, either by classic or pressure pouring. The programme analyzes the heat transfer through the finished

differences method and can determine the size and location of micro and microblister's appearance. With 25 installed programme packages, in Europe, the *MAVIS & DIANA* solidification simulation programmes have a very attractive cost – efficiency ballance.
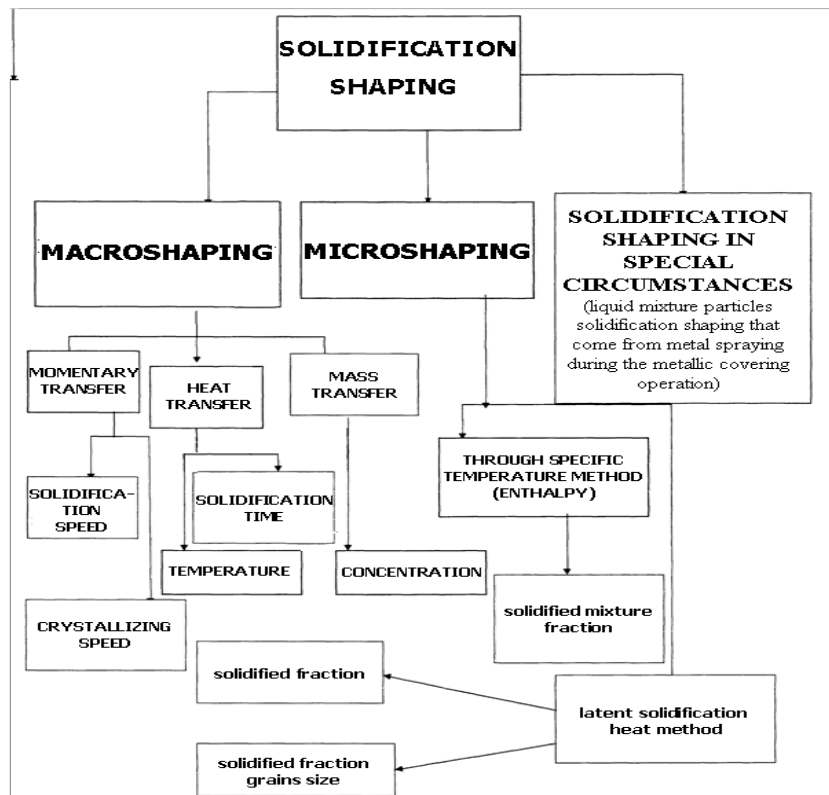


Fig. 5  Representation of the solidification shaping and simulation processes sequences.

### 4.4 The NOVOCAST Programme

The NOVOCAST programme (Sweden), introduced at the GIFA 1989 Congress, simulates the tridimensional mixtures' solidification (3D), involving an interface to take over the pieces drawings, directly poured from AUTOCAD. The programme analyzes the heat transfer through the finished differences method and can set the izosolidus curves, the temperature field within the mixture-form system, the diphasic zone, solidified mixture fraction, the microporosity zones location and size.

### 4.5  The SIMULOR Programme

The SIMULOR programme, created by Silicon grahics, can simulate the mixtures flowing and solidification and starts from the finished volume method. The 2.0 version enjoys a new man-computer interface, much easier to exploit, including a calculation and graphic accelerator, being able to shape solidification and flowing for high complexity pieces.

### 4.6  The PROCAST Programme

The PROCAST Programme, which belongs to the UES (The United States) and 3-MOS (Swiss) firms, is a solidification shaping programme, that analyzes the tridimensional heat transfer (3D) using the finished element mathematic method. The programme can determine the microstructures that appear after solidification and can be

easily adapted to a precision or continuous foundry, being able to determine the necessary conditions for a conducted solidification process.
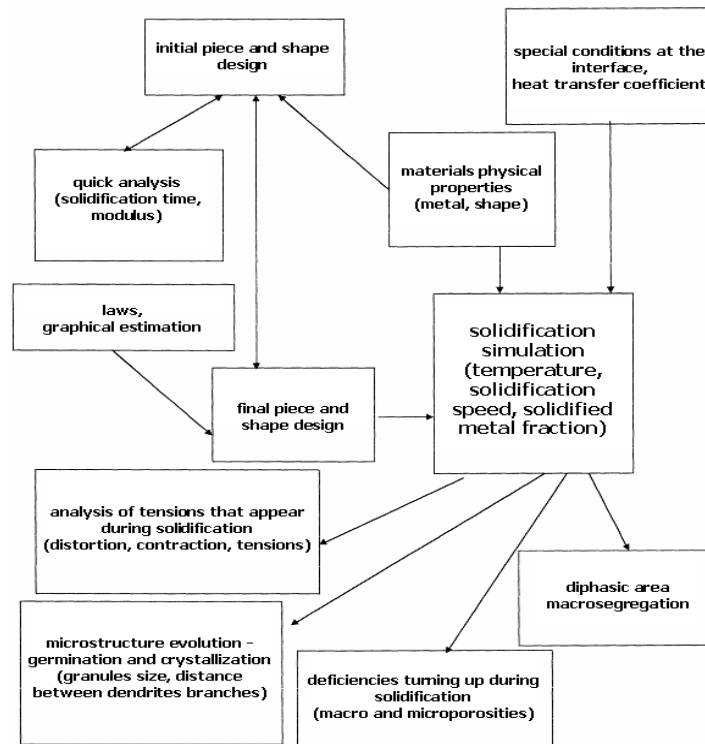


Fig. 6 Representation of a solidification shaping system.

**REFERENCES**

1.   Bratu Ctin. and Popa I. – Solidification coefficient assessment through numerical shaping. In: Foundries Magazine, No. 1, 2000, p. 37 - 39, CZU 621.74 (051), ISSN 1224 - 21 – 44.
2.   Bratu C. – Heat transfer simulation through the finite element method during the solidification operation of the poured pieces. In: Car Bulding, (44), nr. 11-12, 1992, p. 48-52.
3.   Chira I. - Relansin Contract No. 720/2000: Functional pattern achievement of a technological cell (inclusively soft and hard) for under pressure pouring.
4.   Chira I. – Typification of poured pieces' fabrication. In: „Metallurgy", 50, No. 5, 1998, p. 32-39, ISSN 0461–9579.

                                        *Department of Cast Metals*
                                         *Materials Science and Engineering Faculty*
                                         *„Politehnica" University of Bucharest*

**APLICATII SOFTWARE PENTRU PROIECTAREA PROCESELOR TEHNOLOGICE DIN TURNATORII**

**Rezumat.** Lucrarea se doreste a fi o sumara sinteza a realizarilor ultimilor zece ani in domeniul softurilor dedicate tehnologiilor de turnare. Aceasta trecere in revista ar trebui sa contureze tendintele viitoare de informatizare computerizata, proiectrea tehnologica in sistemele CAD/CAE-CAM/CIM, nivelele si standardele generale spre care trebuie sa se fixeze structurarea departamentului national metalurgic, organizarea turnatoriilor si manageriatul acestora, spre o eficienta maxima si interconectarea optima la circuitul european.

# STEPS AND CARRY ON STAGES USING METODOLOGY OF THE COMPUTER IN THE FIELD OF THE CASTINGS

BY

**Ion CHIRA**

**Abstract.** *In the progressed society, the globalization of the information spread brings about a multimodal system, which comprises the entire industrial activity, including the economic agents of foundries type.the computer represents the basis component of an information management system; the metallurgy engineers must become efficient users of the computerized information system and re-learn the designing and leading the technological processes with these inscribed applications. this paper presents the elementary concepts that must be kept in mind when implementing the computerized techniques in the metallurgy field and especially at economic agents of foundries type.*

## I. OPPORTUNITIES IN COMPUTER'S USAGE

### 1.1 The informational system

Computers are everywhere, likely connected to each other and thus, forming computer networks. All this because we more and more realize that the PC facilitates our work. But one must emphasize that a computer is, in fact, a „machine" that processes a series of *data* that we supply to it. Data are the key element in this entire chain. In fact, practice introduces, among other things, two concepts connected to it, namely the *informational* and informatics systems.

### 1.2 The informatic system

The set of elements involved in this entire process of data processing and transmission electronically form an **informatic system**. Within an informatic system, there can be: computers, data transmission systems, other hardware components, a software, processed data, the staff that exploits the calculation technique, theories that support the processing algorithms, etc.

The informatic system cover the most various fields; according to expertise, they are:

- Specialized systems, designed to solve a certain type of issue from a certain field;
- General usage systems, which help solving a large range of problems from several fields;
- Local systems, programmes necessary to process data when data are on one calculation system;

• Network systems, the system works within a computer network, in which case, data and programmes can be distributed to several workstations that are part of that network.

Depending on data localization and the processing place, there are different informatic systems:

1. With centralized data, data are on one calculation system only;

2. With distributed data, data are distributed on several computers within the network;

3. With centralized processing, data processing is being done on one workstation only, regardless of the number of stations that host data to process;

4. With distributed processing, several computers process data come from one or more computers of the network.

After the hierarchical level of informatical systems in the society's organizatorical structure, there are:

• Informatic systems for activities management within economic units;

• Organisation system with group structure;

• Territorial informatic systems;

• Branch, subbrench and national economic systems;

• General use systems.

## II. DATA BASES MANAGEMENT SYSTEMS (SGBD)

An „application" (an achievable programme) is a programme system designed to perform a well determined set of operații on data bases; the application consists of:

1. the very programmes (main programme, coordinator, menu programmes, screens, interrogations, indexes, actualisations, reports);

2. data bases.

*Application's* performance takes place at two levels:

• *Interpretative* – when a programme called „interpreter" takes each enunciation of application, translates it into an internal code and performs error analysis, executes it, then passes to the next enunciation;

• *Compilative* – when the whole application is being translated by the compilator programme into an intermediate code, memorised on the disk, called object code, submitted to suplementary processing by the connection editor in order to get the final achievable form of the application. The performing is done under the operation system's control.

*Achievement of a data base* implies: analysis of the system for which data bases are being built; designing the base structure; loading data into database; data base exploitment maintenance.

*Effective achievement of an application* implies: assign task, task analysis, application design; application coding, modulus testing, implementation of application, application maintenance.

1. *Assign task.* Task is assigned by the application beneficiary, in accordance with the activities that are about to be modeled.

2. *Task analysis.* This operation implies identification of data types, connections between them, necessary operations for their management. Task analysis ends with the

assignment of four „data multitudes", whose rigour and exactitude influence the veracity of application's results: description of input data; description of data stored in the database; list of performed processings on data; description of reports data.

3. *Application design.* At this stage, we achieve data and programmes structure design. Designing programme structure implies detailing the modulus necessary to application achievement: modulus for folders creation, data implementation, processing and result abstraction, error correction etc. These modulus are controled and coordinated by the main programme, that has the following structure: main programme; global picture declaration; global variables initialization; environment state saving (general inițialization).

4. *Application coding.* If at the precedent level called „initial designing of application" the detailing level has a „pseudocode" type, at this stage application is written in a specialized language, respecting the rule imposed by that one.

5. *Modulus testing.* At this stage, modulus are being checked, possible errors are detected and corrected, extreme cases analysis is being performed, tests are being designed.

6. *Application's implementation.* We build the final form of application by gradual integration of tested functional modulus.

7. *Application maintenance.* We must remove the errors pointed out by the user during the warranty period, modernise and upgrade the application.

   *Database users can be:*

• *Non specialist users* (conversational) that are offered a form of communication with database, close to current speech;

• *Specialist users* who know the structure of database;

• *Database administrator* is a special user, who defines database exploitation's objectives, shares users access rights, elaborates database design conception, is in charge of all the activities and operations refering to database, helps defining users' demands etc.

   *Databases languages.* Within „Databases Management Systems" (SGBD), data declaration and and manipulation functions are being done with different languages:

a. *Data defining languages (LDD).* LDD functions are: performs entities and their attributes definition by names, memorising form, length, specifies the connections between data and access strategies to them, assigns confidential different criteria, defines used data automatic validation criteria.

b. *Languages for data manipulation (LMD).* Operations performed on databases require a specialized language, where commands are expressed in sentences that describe actions upon the base. A command has the following structure: - *operation,* that can be an arithmetical or logical calculation, editation, extraction, opening-closing, manipulation (introduction, add, delete etc.); – *selection criteria* (for, while, where etc.); – *access mode* (secvential, indexed etc.); – *edit form;*

c. *Data control languages (LCD).* A database control implies: assuring data confidentiality and integrity; data saving in case of damage; getting performance; solving competition problems;

d. *Universal languages.* An universal language is rarely used to manage a database.
   *The interface between user and SGBD* is achieved in two ways:

- Using a calling mechanism inserted in the application programme. This mechanism can be a CALL or another key word. A system that allows this type of mechanism is called a *SGBD wih a host language;*

- Using a special command, used independently. În this case, the managing syistem is called *autonomous SGBD*. Still, there is a special interface, which is capable to interprete the commands of the sollicitation language.

## III. USINGE THE COMPUTER FOR DESIGN AND RESEARCH-DEVELOPMENT TYPICAL USAGE DOMAINS

Within the general context of optimizing the functioning of the industrial systems, the computer is used to: 1. – the so called designing; 2. –achievement of some data bases; 3. – shaping the technological processe; 4. – leading the processes towards working places; 5. – achievement of Expert Systems = SE.

The first stage of the fabrication – conception/designing, must anticipate the technic-technological evoluţion frame and be at a time level with *< + 2-4 units >*, in an execution report.

Accordingly, the usage of computer and some programmes is implemented and < *authenticated* > during the designing process; implicitely, designing was the first <step> even in the case of number command units, and the peforming processor was subsequently implemented.

At international level, there have already been established a series of principles of the fundamental discipline, the theoretical base, including already known terms elements.

Our country confrunts itself with the same dilemma as in other domains (longlasting development –ecology, globalization, natural resources limitation, energetical alternatives etc.): < *taking the same stepsi, including the failures already known* > or < *selection of the essential points and framing at optimal levels only* >; chosing the variant is conditionned by the difference of the total costs. In this regard, we may think about the < *mechanization-automatization* > stages or integration by < *robotization* >.

We must give a series of explanations as far as terminology is concerned.

The designing working technique, in connection to computer's usage, through the appliance of some apprpopriate programmes and equipments, is defined as *CAD = Computer Aided Design*. The concatenation of the designing programmes with data processing systems, in the engineering science, is generically called *CAE = Computer Aided Engineering*. The integration of an enterprise into a complex and complete system of data monitoring, processing and administration is called *CIM = Computer Integrated Manufacturing*.

The *CAD* applications, with the designing assistance programmes systems are the most famous and are mainly made up of the scheme domains from Figure 1, as it follows:

1. a communication domain organizes data input and output to and from the designing department;

2. a method domain contains the working modulus corresponding to shaping, informing and calculation;

3. a data administration and management field, namely an integrating system of the data bank organizes all the data transfers and stockings between the method algorithms and communication domain on the one hand, and the data banks networks or specialized or standard individual folders, on the other hand;

4. the designing data base containts all the stocked geometrical and nongeometrical data, which are necessary both to the designing methods and to the communication between the projecting operator and the CAD system.

A fundamental characteristic of the CAD systems is made up of the *RID concept = Geometrical Objects Internal Representation.* This system is built on *a real object*; through the abstract process, one can get a *mental virtual object*, from which one can get an informational object, through formalization and multiple filtrations in fundamental specific languages. By a series of transformations and transposings based on the binary code, one can constitute an *internal model* in the computer's memory = *RIM* (see. Fig. 2).

In Figure 3, we give the very simple scheme of the tridimensional representation means essence of *objects − technical bench-marks* and of biunivocal transformations from an informational model (with discrete sizes, quantizable in volumes, surfaces, contours and/or points) to an *internal model of the computer, RIM type*.

An object representation can be achieved through a volume, surface or line model (the so called *the edges models or the wire models*).

The volume model (spatial) can be recomposed in a way oriented towards *bodies* or *surfaces*. For calculations and analytical integrations one needs the internal generation of a *tridimensional body*, therefore, the construction of a spatial model oriented towards bodies. Having a surface model, one is able to sufficiently describe volumes for constant thickness pieces only (e.g. tin pieces) or for rotation symmetry pieces.

Plane and rotation symetru pieces can be clearly described only by the bidimensional representations = < *D Models*>, surfaces or lines. These models are appropriate not only for the internal representation of *views* and *sections*; for the normal-classic drawings execution, this patterns is sufficient (v. fig. 4).

From < *2D Views* >, hand designed, scanned and introduced into the computer, through reconstruction automatic techniques − < *3D Models* > are automatically generated.

*The macros technique* is based on the usage of the already existant geometrical models, namely stocked for simple pieces, classic sets, fundamental structures; from case to case, these *patterns = standard solutions* are submitted to adaptations, adjusting, redimensioning. It is very productive to import from the data bases *stocked-archived representations = finished* elements, pieces and standardized-tipified solutions by usual devices and cars organs.
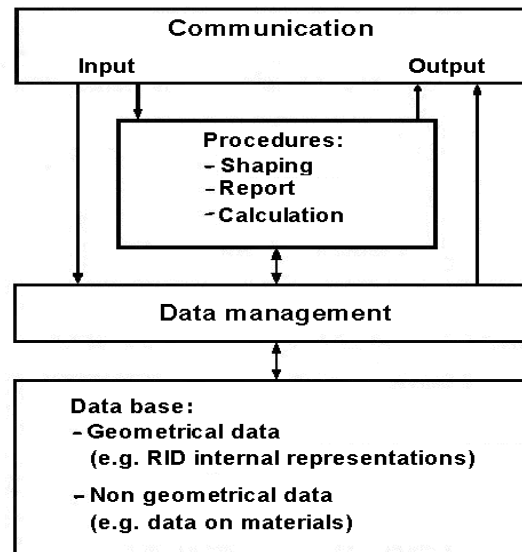
Fig. 1 General structure of the CAD programme systems.
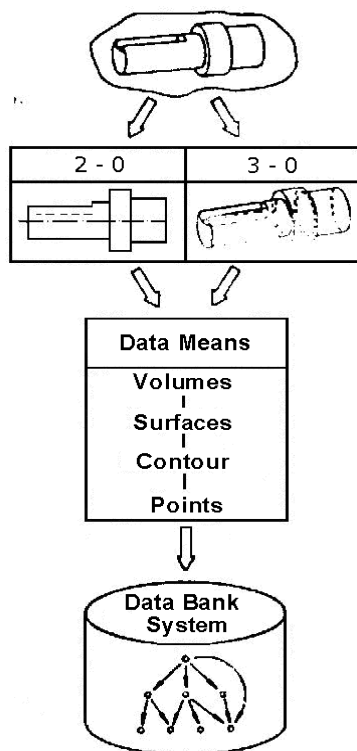


Fig.2. Abstractization models of technic objects.



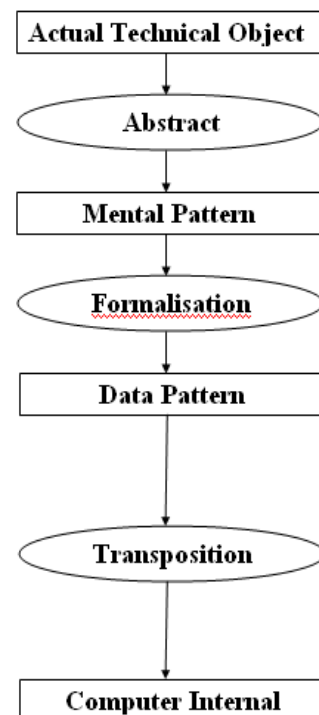Fig.3. RIM principle general scheme of geometrical objects internal representation performing, in the computer's memory.

În the CAD field, a package of programmes can contain a large series of individual programmes and programme systems:

1. *Configuration programmes*, that can integrally perform a geometrical representation, calculation and preprocessing of the designing data, in an interractive

form; in a special way, there must be possible a shaping of the tridimensional geometry of the computer's internal model, on the basis of which rapid, accurate and exact regrant of classic projections of the usual technicalal drawing should be possible.

2. *Programmes specialized in data organization* (the fundamental principles of solving  standardized pieces, materials, cost data, rate-setting times values, data connected to specific consummation); such data banks systems are easy to use with searching dialogue interractive facility programmes;
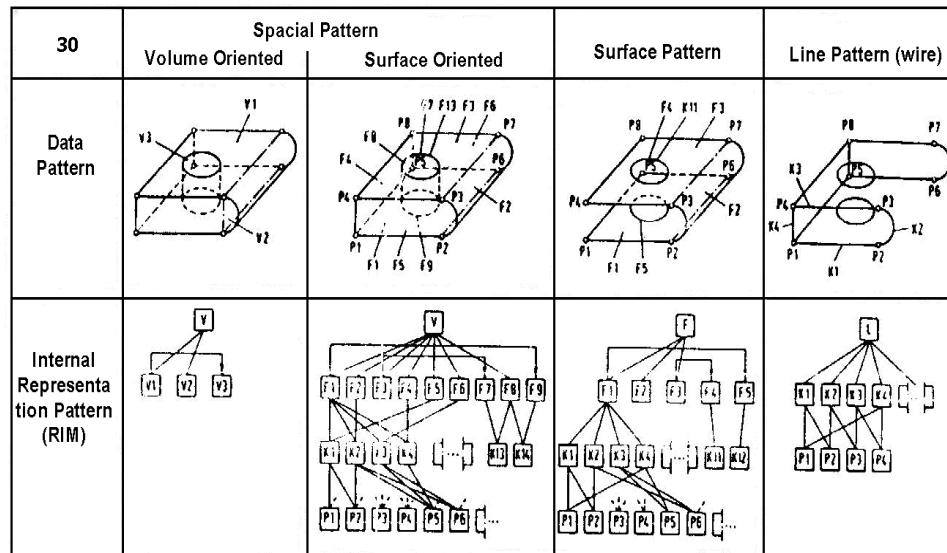


Fig. 4 Types of models for  3D objects, within the informaţional field.

3. *Specialized-dedicated calculation programmes* (resistance, thermic, checking, interpretation, optimization, simulation, graphic representation or those to prove dependance of  a certain size on a certain parameter, such as time, temperature, etc.);

4. *Drawing performing programmes* (generally, the systems for the bidimensional representations are sufficient);

5. *Synthesis programmes* (performing the documentation for the tipodimensional series designs, modular or adaptation constructions; these systems are mainly based on the combination of some modulus or blocks as banchmarks or sets, achieved under variation or modification of some parameters from the initial base).

Alongside with the pure drawing representations, the concatenation of the calculation stages with the geometrical effects communication is very importanţ to designs  and designer's conception activity optimization; in this regard we must mention only the *Finished Element Method = FEM,* a subject we'll talk about later.

## IV. CONDUCTING THE TECHNOLOGICAL PROCESSES

At the level achieved by the most competent units of scientific and technological research, without needing the respective scientists' psysical participation to the problems effective solution, expert cognition availability stands for the central objective of the artificial intelligence applications, known in the world computer's field as *Expert Systems = SEs.*

In principle, SE have been developped under the following form:
- *specialized SEs*, that deal with a specific issue;

- *domain independent SEs*.

If the SE still does not give the right solution, the user fournishes it and the SE will emit, after a series of integration and selfreprogramming sessions, correct *reasonings (judgements)*. Using the *process computers* facilitates control, fixing and leading actions. The leading *activity*, conceived as the *optimal leading*, can be achieved by: 1. – mycrocomputer automatic system solution; 2. – like a SE.

The fundamental criteria that lie at the basis of SE development are: *Necessity* (satisfy industrial or technological requirement); *Capacity* (development according to industrial capacity to cover with resources requirements determined on the basis of the necessity criterium); *Flexibility* (elimination of factors that prevent industry from quick adaptation to requirements and resources unpredictable modifications, determining the transition parameters from one state to another); *Maintenance* (the necessity to maintain the industrial production level correlative to scientific and technicalal development). In the SE case, we get an upper stage of computer leading, with the microcomputer.

## REFERENCES

1.  Chira I. et. al., **Methodological and bibliographical rule for yearly projects in the „Shaping Theory",** Litografia I.P.B.Publishing House Bucharest, 1989.
2.  Chira I., **Reporting and documentation in metallurgical research**, Litografia I.P.B.Publishing House Bucharest, 1989.
3.  Chira I., Paper review: **Hütte – Engineer's Guide. Basis**. Translation from German, following the 29th edition. Tehnica Publishing House Bucharest,. In: Foundries Magazine, No. 1, 1998, p. 32-33, ISSN 1224-21–44.
4.  Chira I., Relansin Contract No. 720/2000: Functional pattern achievement of a technological cell (inclusively soft and hard) for under pressure pouring.

*Received May 19, 2008*                          *∗Department of Cast Metals*
                                                 *Materials Science and Engineering Faculty*
                                                 *„Politehnica" University of Bucharest*

## ETAPELE SI METODOLOGIA DE UTILIZARE A CALCULATORULUI IN DOMENIUL PIESELOR TURNATE

**Rezumat.** In societatea informatizata, globalizarea circulatiei informatiilor realizeaza un sistem multinodal care cuprinde intreaga activitate industriala, inclusiv agentii economici de tipul turnatoriilor. Calculatorul este componenta de baza a unui sistem de gestionare a informatiei; inginerii metalurgi trebuie sa devina utilizatori eficienti ai sistemului informatic computerizat si sa reinvete proiectarea si conducerea proceselor tehnologice cu aceste aplicatii dedicate.Lucrarea prezinta notiunile elementare care trebuie avute in vedere la implementarea tehnicii computerizate in domeniul metalurgic si in special la agentii economici de tipul turnatoriilor.

# SUPERFICIAL LAYERS WITH SPECIAL PROPIERTIES DEPOSED ON STEELS BY ELECTRIC DISCHARGE IN IMPULSE

BY

## ADRIAN ALEXANDRU*, MARIUS HUTANU*

**Abstract:** *This paper work presents the experimental results on the proprieties of superficial layers deposed on steels by electrical discharge in impulse.*

**Keywords**: *electric impulse, electric spark, layers, properties*

## 1. Introduction

The surface engineering, as interdisciplinar technical science is a relative new concept which appeared in high developed countries as a result of the processing of the metallic materials with distinct propierties and as a result of spectacular development of the thermic treatments.

According by David Melford, "Surface Engineering" consists in essence in designing of surface and sublayer between, as a sistem, for conffering performances neither one not having selected separately.

So, the surface engineering is not a simple superficial treatment technology, but is about designing of the system basic material – superficial layer thus it too responsible at it role at rational use of materials and at accesible cost prieces.

In figure 1 are presented the characteristic areas, the proprieties and some of the criterions in consideration at designing of a system basic materials – superficial layer.
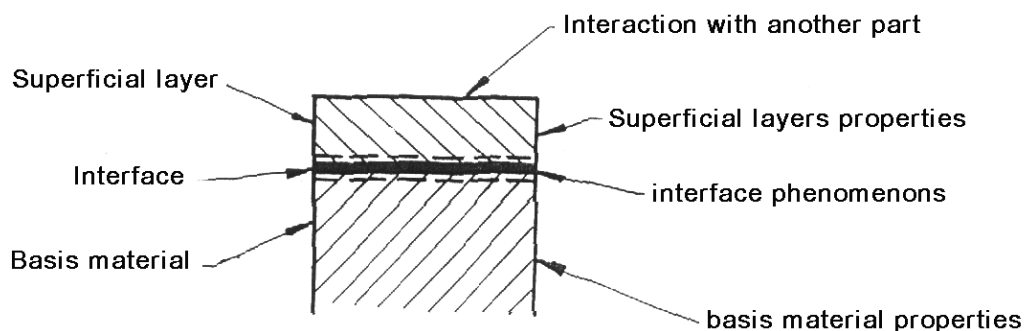


*Figure 1. Characteristically areas and properties*

The obtaining of the thin layers by electric spark presents some advantages as: high adherence of the layers, permits deposition of all materials which have electrical

conductivity, but there are some disadvantages as: residual stress in layer and large roughness.

The deposition and alloying by electric spark (DAES) uses inverse polarity  (the part = cathode, the electrode = anode). In this case the deposition takes place in air or another gas, the electrode making a vibrating movement with or without a rotation.
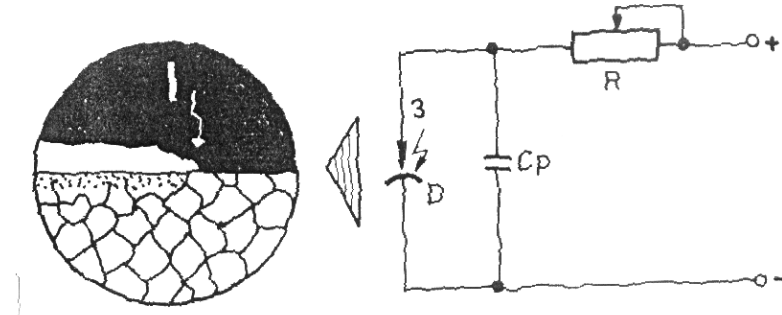


*Figure 2. Superficial hardening by electric spark. a – the process; b – the device*

The deposition process begins when the electrode is near the part at a critical distance ($\cong 10$ μm) when takes place the electrical discharge in impulse (the spark) which ends at the contact of the electrodes.

Because of high energy, on the surface of electrodes appears craters of electric erosion by melting and vaporisation. The obtained material, under the influence of hidrodynamic pressure and hidrodynamic force from the chanel of discharge is deposed on the part in small quantity $(2–3)·10^{-6}$g.

The discharge energy takes values between 8 … 18 Joule at 15 … 220 V, and the intensity of medium current  may be 0,2 … 80 A.

Decreasing the energy of discharge has as result smaller thickness of deposed layers, smaller roughness and the deposed layer is more dense with more clean surface.

The process takes place with a electrode which vibrates at a 50 … 400 Hz frequency. The vapour presente from interelectrodic space is very big ($10^8$ Pa).

The characteristic feature of this process is the polar transfer of the material from electrode or from interelectrode space is limitated by the parameters of work system (the discharge energy) and by the nature of the material from part and electrode.

## 2. Research and results

The research work consist in deposition of wolfram on a unalloyed steel OLC55 – STAS 880-88 (C%% SREN) normalised ($850^0$C/air) and quenched at $840^0$C/oil tempered at $600^0$C/air with work surface grinded at Ra = 5 … 10μm.

The chemical composition of the steel is: 0,57%C; 0,74% Mn; 0,23% Si; 0,022% P; 0,025% S; 0,24% Cr.

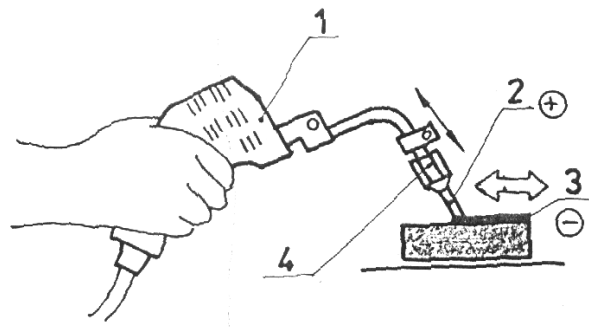The device deposition of thin layers is presented in figure 3.

Figure 3. The device for deposition of thin layers; 1 – vibrator; 2 – electrode; 3 – deposed layer on the part; 4 – device for fixing the electrode

Work parameters at the deposition of the thin layers using on original device for electrical discharge in impulse MAX 101 where:
- the angle of electrode $70^0$
- the energy of discharge in impulse 0,3 J
- tension: 220 V
- current intensity: 1,2 A
- frequency of vibration of electrode: 100 Hz
- productivity: 2 $cm^2$/min
- thickness of deposed layers 0,022 … 0,03 mm
- thickness of the electrodes: 2,2 mm

The sample where in slide shape with dimensions:53x10x1 mm for determination of weight and arrow in time of deposition and cylindrical shape ($\phi$ 8x60 mm) for determination of microhardness, abrasive wear resistance and structure.

On the slide samples where made roughness measurements and carrying of surface on thin layers deposed with W electrode.

By successive deposition on slide samples of more layers of W with different specific time results that the weight of samples increase till third deposition ($M_1$, $M_2$, $M_3$), after that, at fourth deposition, the weight of the samples decrease ($M_4$) as is presented in table 1 and figure 5. the bending arrow of slide sample increases after all four depositions ($a_a$, $a_2$, $a_3$) and decreases after a determination by vibrating electrode without electrical discharge in impulse (table 2; figure 4).

*Table 1*

| Proba | St.in | Mo | M1 | M2 | M3 | M4 | ΔM1 | ΔM2 | ΔM3 | M4Δ | ΣΔMi |
|-------|-------|-----|-----|-----|-----|-----|------|------|------|------|------|
| OLC55 | N | 4,1541 | 4,2804 | 4,2841 | 4,2848 | 4,2775 | 0,1252 | 0,0037 | 0,0007 | -0,0073 | 0,1223 |
|       | C | 4,3218 | 4,3319 | 4,3401 | 4,3409 | 4,3381 | 0,0101 | 0,0082 | 0,0008 | -0,0028 | 0,0163 |
| 42MoCr11 | N | 4,2080 | 4,3405 | 4,3430 | 4,3439 | 4,3405 | 0,1325 | 0,0025 | 0,0009 | -0,0034 | 0,1325 |
|       | C | 4,3511 | 4,3654 | 4,3718 | 4,3791 | 4,3702 | 0,0143 | 0,0064 | 0,0073 | -0089 | 0,0189 |

*Table 2*

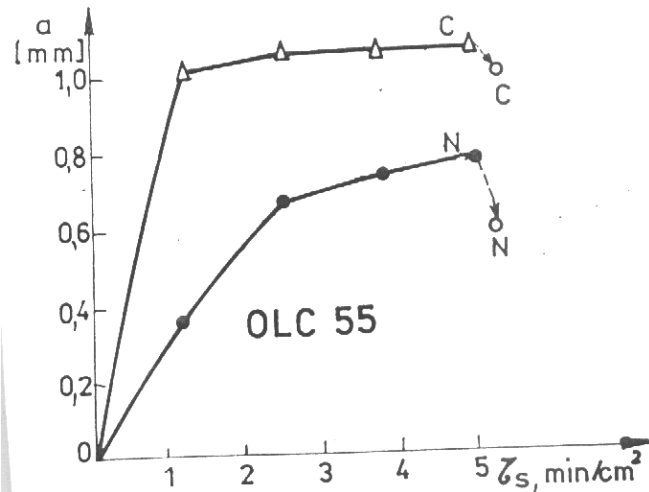| Proba | St.in | $a_o$ | $a_1$ | $a_2$ | $a_3$ | $a_4$ | $a_5$ | $\Delta a_1$ | $\Delta a_2$ | $\Delta a_3$ | $\Delta a_4$ | $\Delta a_5$ |
|-------|-------|-----|------|------|------|------|------|------|------|------|------|------|
| OLC55 | N | 0 | 0,35 | 0,66 | 0,71 | 0,76 | 0,59 | 0,35 | 0,31 | 0,05 | 0,05 | -0,17 |
|       | C | 0 | 1,01 | 1,24 | 1,25 | 1,28 | 1,08 | 1,01 | 0,23 | 0,01 | 0,03 | -0,2 |
| 42MoCr11 | N | 0 | 0,43 | 0,57 | 0,67 | 0,71 | 0,47 | 0,43 | 0,14 | 0,10 | 0,04 | -0,24 |
|       | C | 0 | 0,20 | 0,40 | 0,52 | 0,68 | 0,24 | 0,2 | 0,2 | 0,12 | 0,16 | -0,44 |

*Figure 4. The variation of bending arrow in specific time of deposition on OLC 55 steel*
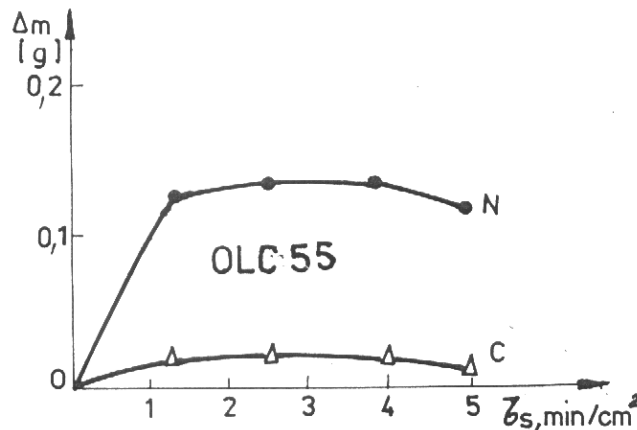


*Figure 5. The variation of weight in specific time of deposition on OLC 55 steel*

From table 1 results that the bigger weight ($\Delta M_1$) is obtained at the deposition of the first layers, at other layers deposed, the weight is smaller and after the fourth deposition the weight decreases.

So, for deposed layers with a certain weight, one or two depositions are necessary. By increasing of the specific deposition time, or of the number of depositions without the layer deposed before is pulverisated and the weight and the final thickness of layer decrease.

The bending arrow (a) is maximum at the first deposition ($a_1$) and increases at the second deposition ($a_2$)then at the next depositions the increase is smaller.

By detension with vibrating electrode without electric spark, the bending arrow decrease.

The deposed weight on steel with the initial state normalised and detensionated is aprox. 10 time bigger at the first deposition ($\tau_s = 1,25$ min/cm$^2$) in comparison with weight deposed on the some steel hardened and detensionated; at the second and third depositions ($\tau_s = 2,5; 3,75$ min/cm$^2$) the deposed weight is small and the difference between the normalised state and the hardened state are of 2 … 3 time biggers at each deposition.

Taking together the weight contribution and the bending arrow obtained after each deposition, results that at the second, third and fourth depositions, however that the

weight contribution is not significant, or even negative, the arrow increase, so appears internal stress.

The final circles from figure 6 are the smaller values of the arrow after detension by vibrating with the electrode without electric spark.

Results that at the deposition and alloying by electric spark (DAES) in terms of this research, the specific time of deposition must be under 2 min./cm$^2$ for obtaining of a weight contribution (thickness of deposed layer) and minimal stress. At the finish of the deposition if is maked a detensionation by vibrating electrode, the stretched stress from layer decreases, removing the danger of fissure of the deposed layer.

From the analysis of the data of Table 3 results:

- the microhardness of the deposited layer does not depend on the initial status of the steel OLC 55;
- the microhardness of the sublayer has a greater value for the improved steel OLC 55 (c) than in a normalised status;
- the deposition of W through electric spark on the normalised steel OLC 55 produces a microalloy of the sublayer, implicitly a substantial growth of the microhardness, while the deposition in the some hardened steel produces a recovery of the sublayer roughness and portance of the surface resulted after the deposition of W with average values: they can be improved only through subsequent remaking (treatments into electrolitic plasma, extra-finishing etc.);

The microstructural analysis of the layer of W deposited on the steel OLC 55 into the 2 sets of thermal treatment (normalization and improvement) effectuated on an optic microscope (Neophot 21) at 100:1 parts into evidence a white, dense layer of big thickness deposited on the hardened steel and a white and less dense and thick layer deposited on the normalized steel. Figure 6, a.b.
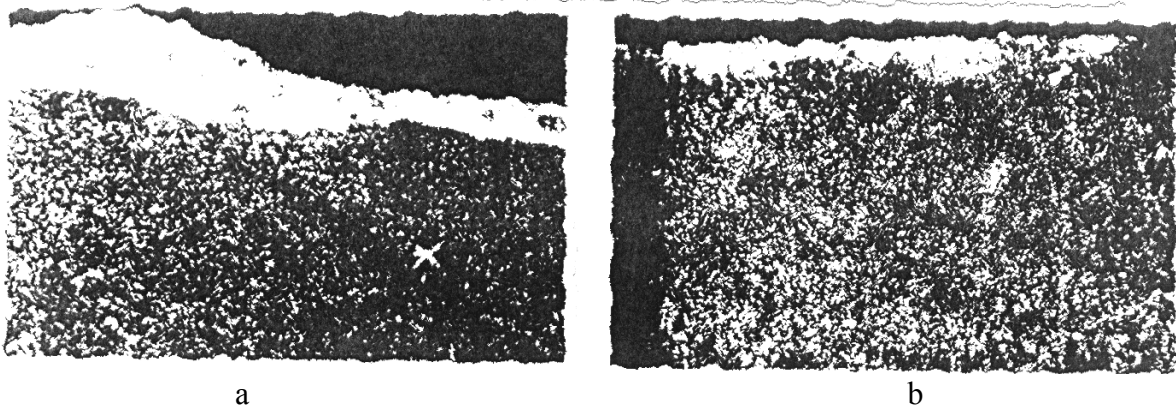


a                                    b

*Figure 6. Steel OLC 55 a white layer deposited with W. a) improved status; b) nominalized status;*

## 3. Conclusions

The thin layer of W deposited on the supports of non-alloyed steel assures the resistance to corrosion to a great hardness, the resistance to wearing on and to the refraction of the pieces. The deposition of these layers of W on steel supports through electric discharge in impulse (the electric spark is an efficient method of obtaining pieces with special properties on the surface.

# REFERENCES

1. Alexandru A., **Contribuţii privind alierea şi depunerea superficială prin scânteie electrică şi influenţa tratamentelor termice asupra caracteristicilor straturilor obţinute ale materialelor metalice**, Teză de doctorat, Iaşi, 2002.
2. Abramciuc A., **Application electrospark alloying in production of electric contact,** In Bul. I.P. Iaşi, 2000.
3. Alexandru A., et al., **Films metallic materials and biomaterials,** In Bul. I.P.Iaşi, Tom XLV, fasc. 1-2, 1999.

## STRATURI SUPERFICIALE CU PROPRIETĂŢI SPECIALE DEPUSE PE OŢELURI PRIN DESCĂRCARE ELECTRICĂ

**Rezumat**: Lucrarea prezintă rezultatele experimentale asupra proprietăţilor straturilor superficale depuse pe oţeluri prin descărcare electrică în impuls.

# THERMAL TREATMENT OF CLEARING SLUDGE IN MICROWAVE FIELD

BY

## EMIL RITI-MIHOC, VIOREL DAN, NARCIS RITI-MIHOC

**ABSTRACT.** *This paper approaches a few aspects regarding the possibilities of clearing sludge dewatering and drying in microwaves field. From a technical and economical point of view the microwave technique represents one of the most interesting heating methods.*

## 1. INTRODUCTION

Clearing sludge is the inevitable waste result of sewage treatment. Its quantity, composition and properties depend on the conditioned water, the chosen water purifying method and the initial purpose of the sewage purification.

As the quantities of such sludge are continuously growing it is extremely necessary to significantly diminish their volume by reducing their water contents. Such a drying degree (a minimum of 90% SS) is obtained by sludge treatment as to the flow chart shown in Figure 1. By such a treatment, besides the minimization of the remaining sludge volume, it also undergoes a purification process and it may lead to the reduction of noxious substances as a result of organic compounds oriented destruction and heavy metals immobilization.

Drying represents the process during which the inner water vaporization and adsorption are achieved, in connection with the sludge particles (~30 %) which cannot be achieved by mechanical dewatering. All the heat necessary for the endothermic reaction must be brought into this process from the outside. The heat transfer over the sludge can be achieved by means of:
-    convection – when the heat is transferred by direct contact from the heating medium to the sludge to be dried;
-    contact, when the heating medium (steam, thermal oil, hot water) does not come into contact with the sludge, but it is directed through a close system.
-    molecular friction, due to extremely fast alignment and realignment of dipole molecules caused by the action of microwaves energy, directly transmitted to the material.

While as for the sludge drying by convection and by contact a diversified range of equipment and fittings is available, the drying procedure with microwaves has not yet been performed at an industrial level. Nevertheless, the researches carried out all over the world were successful.
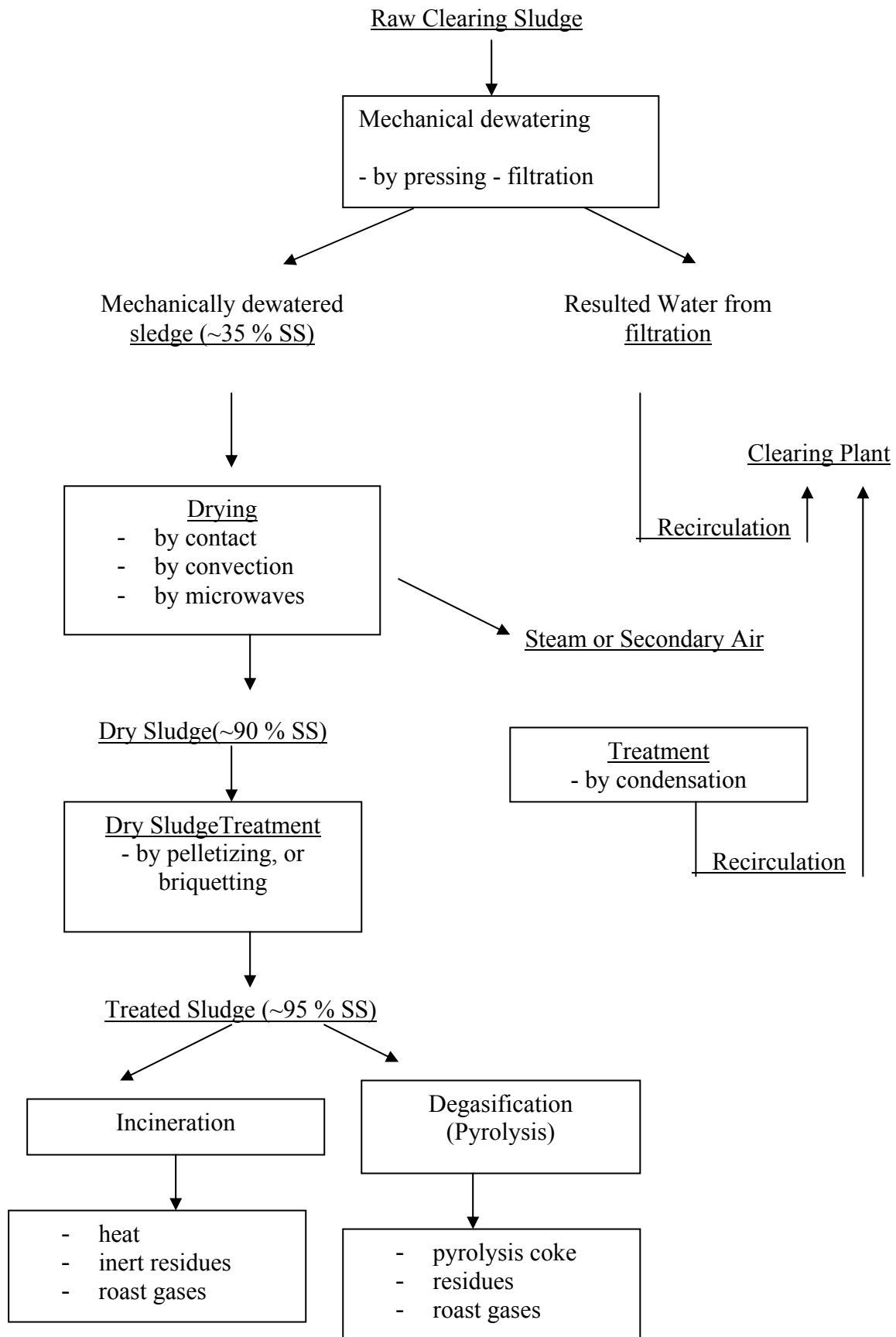
*Figure 1 – Flow chart of clearing sludge treatment*

Such concerns arose in Romania too at the Technical University of Cluj-Napoca where people have performed researches concerning the dewatering and the drying of the clearing sludge in a microwave field in the laboratory fittings – designed and conceived at a frequency of 2,450 MHz and at a power of 5.5 kW

## 2. ISSUES CONCERNING THE TREATMENT OF CLEARING SLUDGE IN A MICROWAVE FIELD
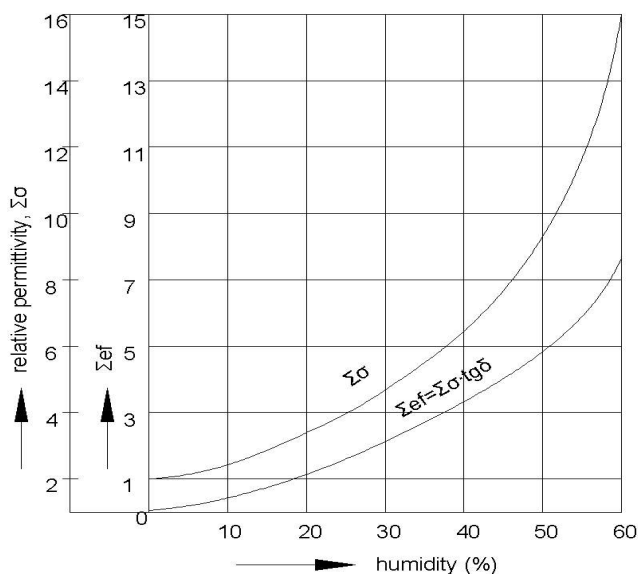


FIGURE 2. – VARIATION OF THE RELATIVE PERMITTIVITY AND EFFECTIVE LOSS COEFFICIENT ACCORDING TO THE DEGREE OF MOISTURE OF THE SLUDGE.

The researches performed aimed at:
- studying the heating power from the point of view of the dielectric properties of sludge;
- establishing the sludge drying dynamics in a microwave field
- elaborating a flow chart of thermal treatment in a microwave field of the clearing sludge.

As far as the heating power of sludge in microwave field is concerned, the most important evaluation parameter is considered to be the effective loss coefficient namely the multiplication $\varepsilon_{ef} = \varepsilon_r \cdot tg\delta$ between the relative permittivity $\varepsilon_r$ and the dielectric phase angle tangent $tg\delta$. The experiments performed underlined the influence of the sludge's degree of moisture on the relative permittivity and the effective loss coefficient. The results obtained are shown in Figure 2.

We have noted that the higher values of sludge moisture the higher relative permittivity and the higher the effective dielectric loss coefficient. Knowing the value of the dielectric loss coefficient allows us to establish the intensity of the electrical field (E) for a frequency (f) considered as constant and which is necessary to provide the optimum field intensity in the sludge (expressed in the relation $W_0 = 0.556 \cdot 10^{-10} \cdot f \cdot E^2 \cdot \varepsilon_r \cdot tg\delta$, in W/m³).

In order to determine the sludge drying in microwave field we have aimed at determining the drying time considering the different degrees of moisture of the clearing sludge

The experiment data obtained are shown in Figure 3.

It can be seen an extremely favorable behavior of clearing sludge in microwave field as dewatering is achieved after a relatively short period reaching moisture values under 0.5 %.

Based on the researches performed on the peculiarities of the heating process in microwave field of clearing sludge, a chart flow of their treatment has been established according to Figure 4.
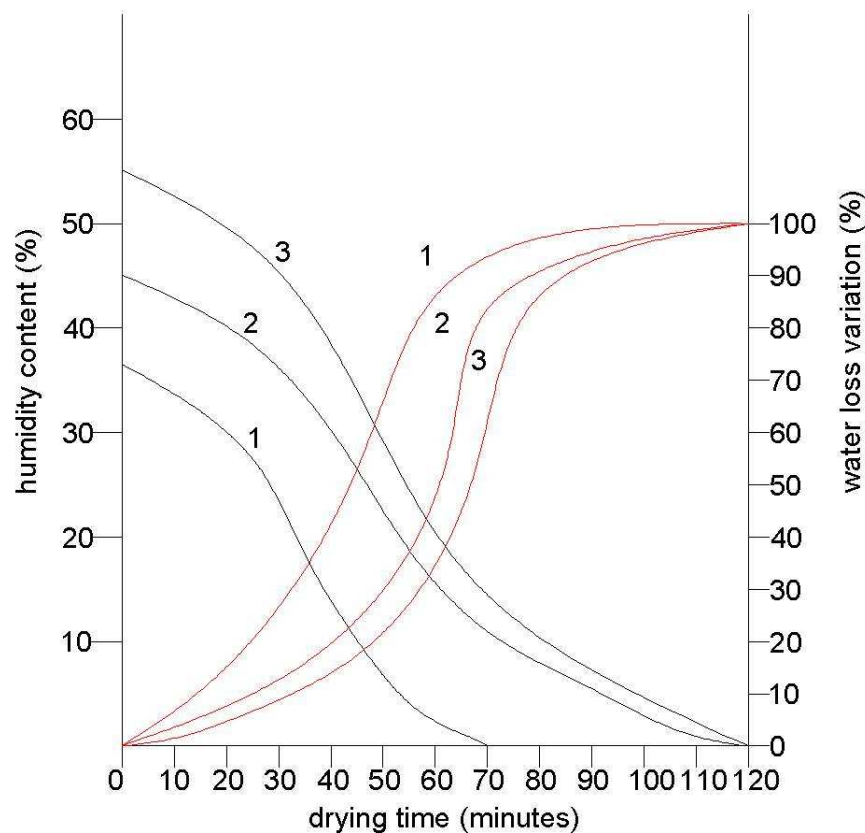


Figure 3. Variation of the moisture contents according to the drying time of sludge in microwave field (1 – sludge sample with an initial moisture of 36 %; 2 – sludge sample with an initial moisture of 44%; 3 – sludge sample with an initial moisture of 57%).

The mechanically dewatered sludge is transported at a constant volume by means of a vane-type pump in the resonance cavity of the microwave plant. The microwave energy in the resonance cavity acts directly on the quantity of sludge in the whole volume. From the drying oven dry sludge is transported in the dry sludge treatment plant, and the dust particles mixed with the water vapors are directed to the dust removal plant.

## 3. CONCLUSIONS

The heating technique using microwaves represents an alternative to the classical heating systems of clearing sludge.

Unlike these, when using microwave energy, heating is produced in the whole material, in all of its sections at the same time no heating medium existent.

Microwave drying represents a self-adjustable process, that is: as the water contents of the sludge diminish the microwave effect diminishes as well.

The drying technique of clearing sludge by means of microwave energy has especially favorable implications on energy consumption, process productivity and makes dewatering possible even at smaller values of moisture.
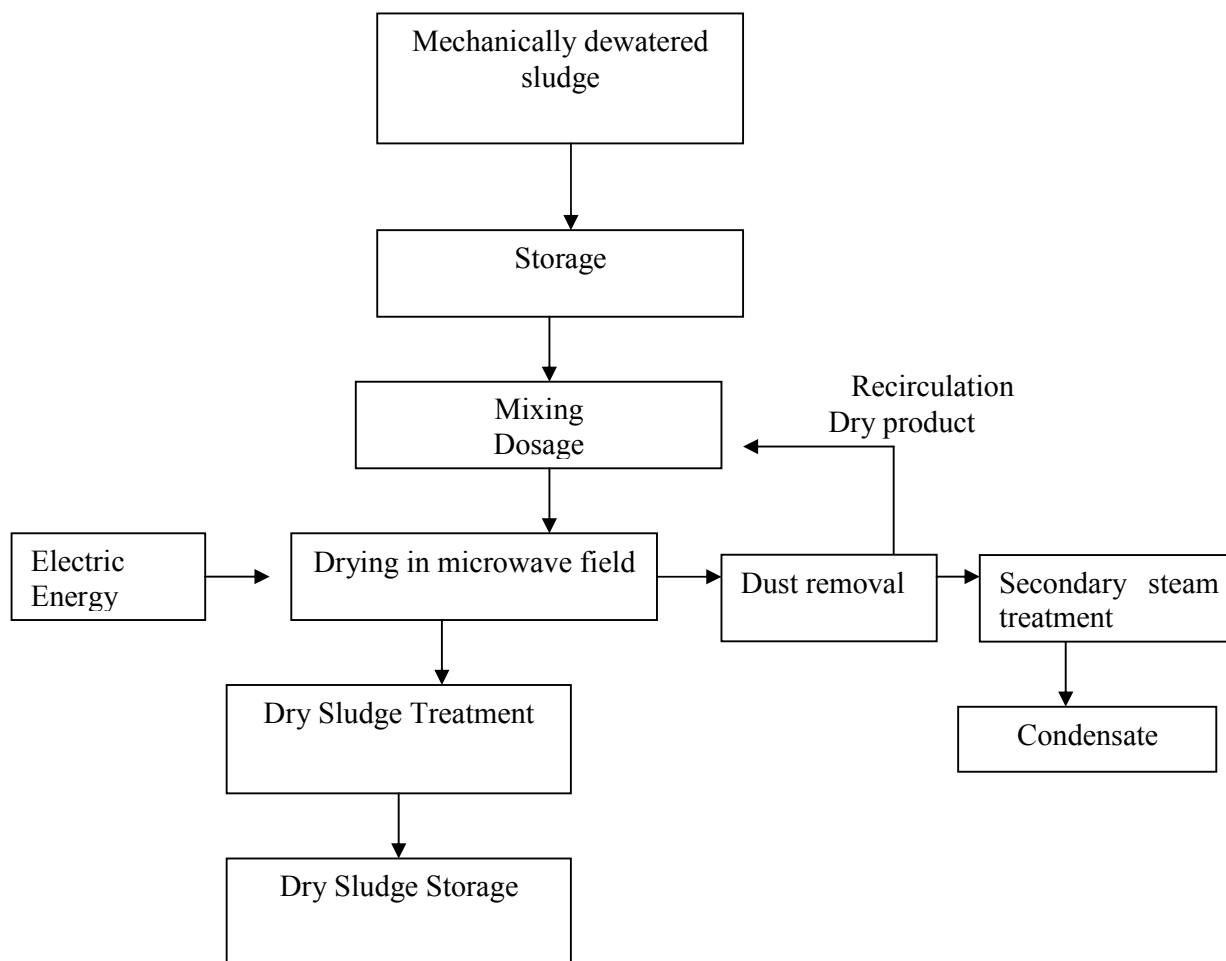


Figure 4. The flow chart of thermal treatment in microwave field of clearing sludge

**REFERENCES**

1. Dan V., ***Using microwave energy in the heating and drying processes of the moulds and the molded cores***, UT Pres Publishing House, Cluj-Napoca, 2001
2. Dima M., ***Urban sewage treatment*** , Junimea Publishing House, Iaşi, 1998
3. Fireteanu V., ***Material processing, electromagnetism***, Politehnica Publishing House, Bucharest, 1995

## TRATAMENT TERMIC DE CURĂŢARE A NĂMOLURILOR ÎN CÂMP DE MICROUNDE

**Rezumat.** *Această lucrare prezintă câteva aspecte privind posibilităţile de curăţare a nămolurilorprin filtrare şi uscare în cuptoare cu microunde. Dintr-un punct de vedere economic şi tehnic microundele tehnice reprezintă una dintre cele mai interesante metode de încălzire.*

# EXPERIMENTAL CHECK OF A MATHEMATICAL MODEL OF SOLIDIFICATION

### BY

### R. CHELARIU, C. ROMAN, I. CARCEA, D. MIHAI

**Abstract.** *The paper shows the experimental results concerning the thermal phenomenon developed during solidification process of non-ferrous alloy. Using a data acquisition system, the evolution of temperature in certain point of castings was recorded. These data were compared with similar data obtained through numerical simulation.*

**Keywords:** *cooling curve, solidification, model, modelling*

## 1. INTRODUCTION

The mathematical modeling of an industrial process is defined by the equation system that describes as correctly as possible the interdependence between its variables. The predictive model consists in an equation system that expresses the link between the dependant parameters and the independent ones so that the response of the process to the variation of the independent parameters may be forecast. To solve this problem, it is necessary that the number of equations of the model should be equal to the number of the dependant parameters.

## 2. MATERIALS AND METHODS

The measurement system and the data procurement system specially conceived for the control of the solidification of the aluminum alloy parts was made in collaboration with SC INFOSTAR SRL Pascani and SC REZISTOTERM SRL Iasi. The measurement and data acquisition module has a capacity of temperature simultaneous registration made of 24 points. The thermocouples of the Fe-constantan system with the wire width of 0.5 mm and the shaft of 4.5 mm have free hot spot. This advantage is so important that it was accepted to cut at every experiment the end of the thermocouple on the length comprised in the part.

At experiments, we used nine thermocouples located in the cavity of the mould according to Figure 1.

Two variants of the casting technology were used.

***First Variant***

The part is obtained in the vertical position with the area with the wall width of 70 mm to the top, according to Figure 1. In this variant, the thermocouples were introduced at various depths onto the right wall of the part as follows:

a) At the section with the 70-mm width:
- The first thermocouple, located at 23.75 mm onto the end wall was introduced at the depth of 17.5 mm;
- The second thermocouple, located on the geometrical axis, was introduced at the depth of 35 mm;
- The third thermocouple, located at 71.25 mm onto the end wall, was introduced at the depth of 52.5 mm;

b) At the section with the 50-mm width:
- The fourth thermocouple, located at 23.75 mm onto the end wall was introduced at the depth of 12.5 mm;
- The fifth thermocouple, located on the geometrical axis, was introduced at the depth of 25 mm;
- The sixth thermocouple, located at 71.25 mm onto the end wall, was introduced at the depth of 37.5 mm;

c) At the section with the 30-mm width:
- The seventh thermocouple, located at 23.75 mm onto the end wall was introduced at the depth of 7.5 mm;
- The eighth thermocouple, located on the geometrical axis, was introduced at the depth of 15 mm;
- The ninth thermocouple, located at 71.25 mm onto the end wall, was introduced at the depth of 22.5 mm;
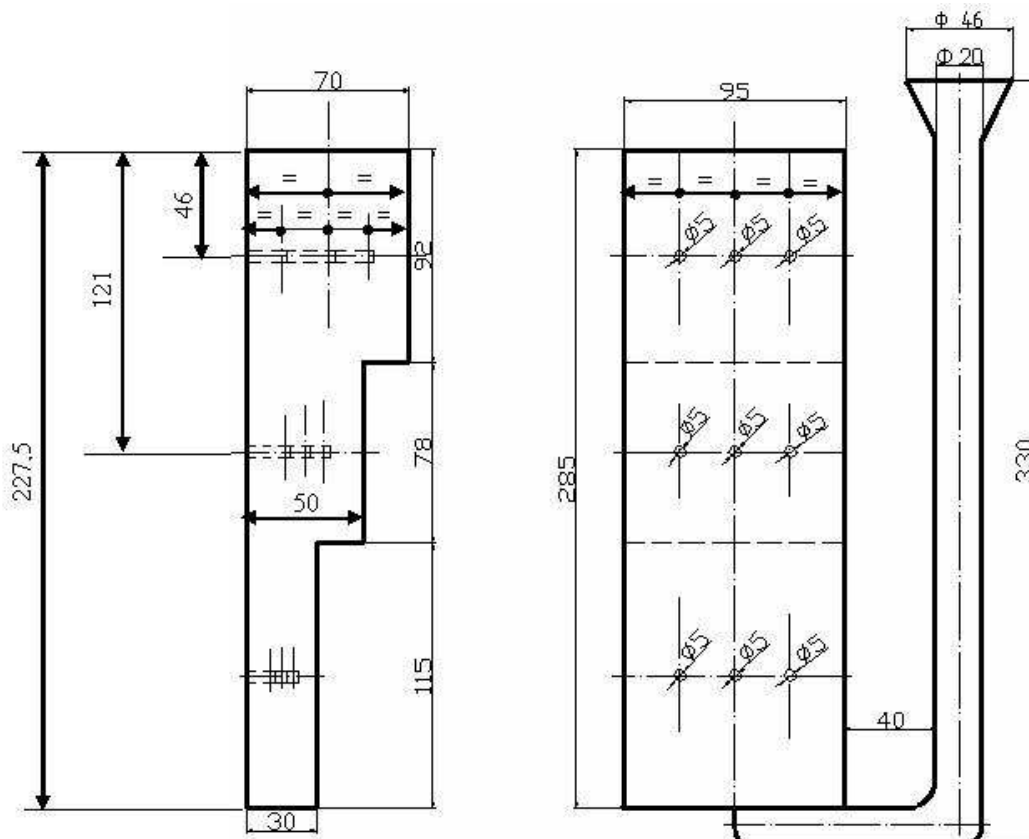


Figure 1. How the thermocouples are located in the analyzed part

*Second Variant*

In this case, the same SDVs, models, apparatuses, devices and work procedures were used like in the 1$^{st}$ variant, the only difference being that the model was overthrown. The obtained part will have the area with the large section at the bottom and the area with the small section at the top.

## 3. RESULTS AND DISCUSSIONS

### 3.1 Analysis of solidification in real conditions of the experimental model

The solidification was analyzed using the experimental cooling curves at the aforesaid points and viewing the shrike holes existing in the volume of the part by sectioning it in the areas of interest.

We made a comparative analysis of the cooling curves in various points for the same casting variant, and the ones corresponding to the same positions but for different casting variants. In the figures below there are presented the curves for the experimental variant 1.
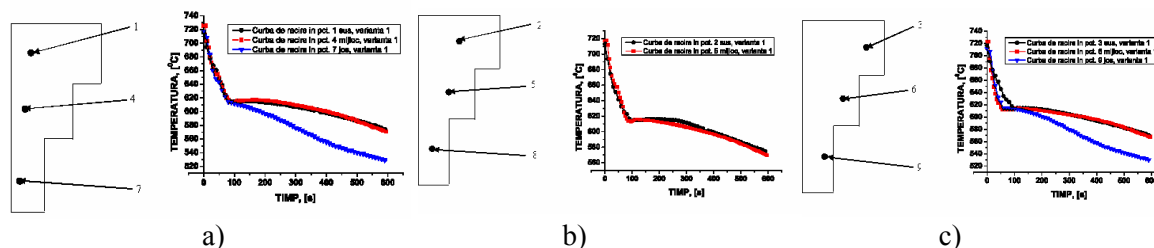


a)                         b)                         c)

Figure 2. Cooling curves for the 1$^{st}$ casting variant: a) section at the distance of 23.5 mm
b) section at the distance of 47.5 mm, c) section at the distance of 71 mm.



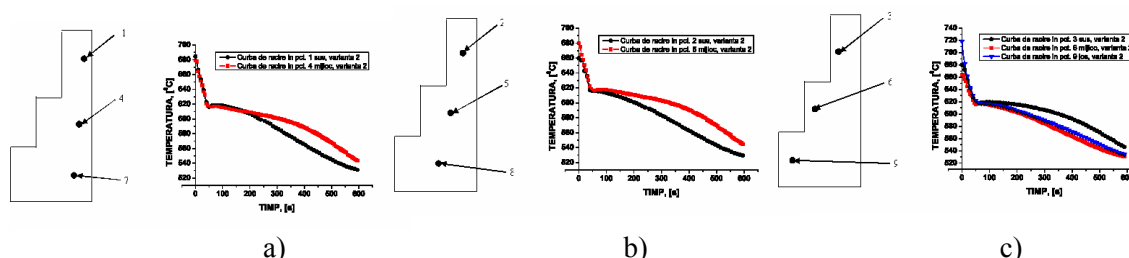a)                         b)                         c)

Figure 3. Cooling curves for the 2$^{nd}$ casting variant: a) section at the distance of 23.5 mm
b) section at the distance of 47.5 mm, c) section at the distance of 71 mm.

Keeping the markings of Figure 2 and Figure 3, the curves for the same point at different casting variants are presented below.

Analyzing the images above, we may draw the following conclusions:
- Although the part has three different wall widths, only for the part with the lowest width we can see a considerable difference of the cooling speed, especially after solidification;
- The area of the level corresponding to the solidification is decreasing as the wall width decreases, so that the area with the lowest width is solidified the first, isolating the areas with a larger width; this led to the occurrence of

shrike holes in the areas with larger width in the absence of feeders or coolers, as we may see in Figure 5;



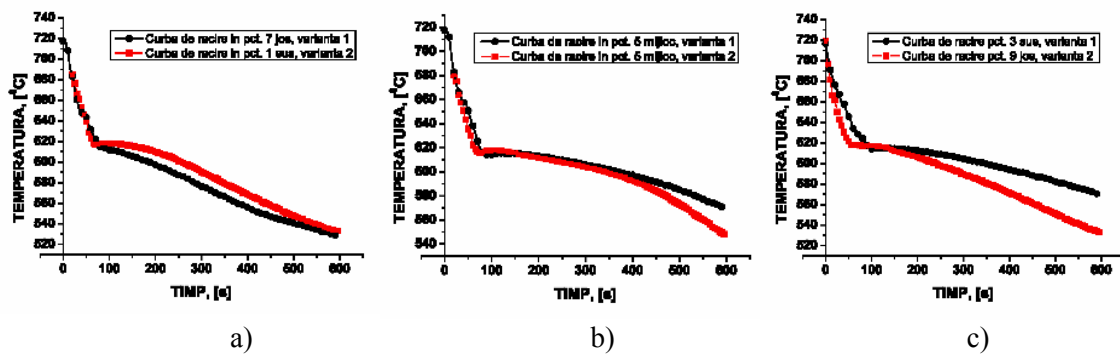a)                                    b)                                    c)

Figure 4. Cooling curves corresponding to identical positions and different casting variants

- The change in the position of the part did not generate significant changes in the solidification process, except that the area with the lowest width solidified the first; although the presence of the macrocavities was not eliminated, nevertheless their volume and position changed (Figure 6).



a)

b)

Figure 5. The position of shrike holes for the two casting variants: a) variant 1: b) variant 2

### 3.2. Correlation and complementarity of the calculation methods and experimental methods

Within the correlation and complementarity study, we considered the following aspects:
- To check the used mathematical model;
- To study the convergence of the adopted calculation method;
- To appreciate the model by the possibilities it offers when factors that influence solidification are studied
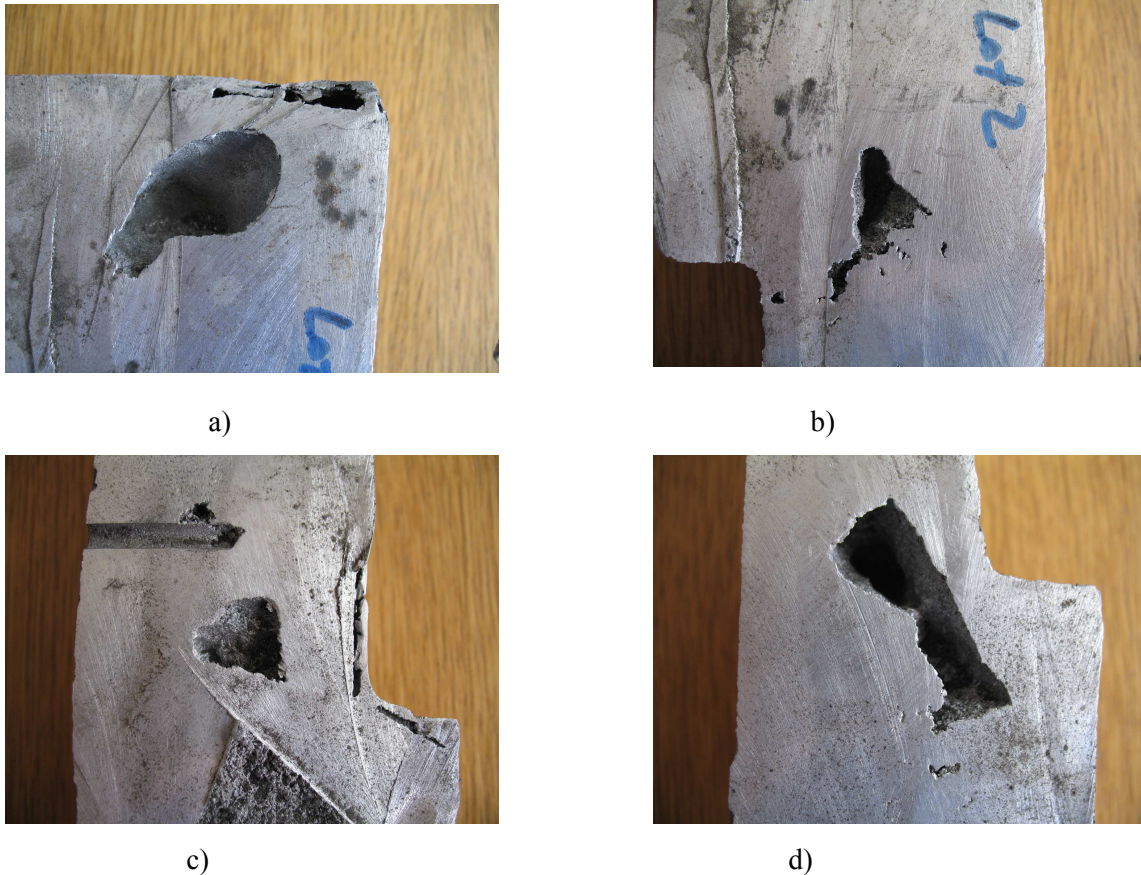
<div align="center">a)</div>



<div align="center">b)</div>



<div align="center">c)</div>



<div align="center">d)</div>

Figure 6. Position and sizes of shrike holes: a), b) variant 1; c), d) variant 2.

*Checking the used physical mathematical model*

The checking of the model is made under quantitative and qualitative aspect. The influence study was made on the aluminum alloy ATSi3Cu4-mark "Setting Plate" that had certain imposed characteristics.

The solidification interval brings to the cooling curve a pseudolevel specific to the loss of the latent solidification heat. From a quantitative point of view, the analysis of the model specific to the solidification process is much more difficult.

From the analyses made, we saw that for the alloy ATSi3Cu4 a good overlapping regarding the solidification times for the calculation method; in the initial phase, the solidification time was 665 seconds compared to 600 seconds that was achieved experimentally.

This difference was decreased by a new appreciation over the thermophysical characteristics of the alloy and of the mixture being formed.

The precision of the results of the model cannot be appreciated singularly, the results being influenced by the parameters of the calculation method and by the values of the thermophysical characteristics. From the analysis of the curves presented in the figure 2 and figure 3 we see a tight closeness between $T_{max}$ and $T_{min}$, which determined a good uniformity of temperatures and the lack of strong temperature gradients, even if the solidification interval is large.

The difference between the experimental curves and the ones resulting from the simulation of solidification on the computer is acceptable, for the case in which we do not know exactly the values of the thermophysical characteristics of the mixture and even of the cast alloy.

### 3.3. Comparative analysis of the cooling curves determined experimentally with the ones obtained by modeling – simulation

In the following figures, there are presented the experimental cooling curves and those obtained by modeling – simulation for the points 3, 5, 9, 1$^{st}$ casting variant.



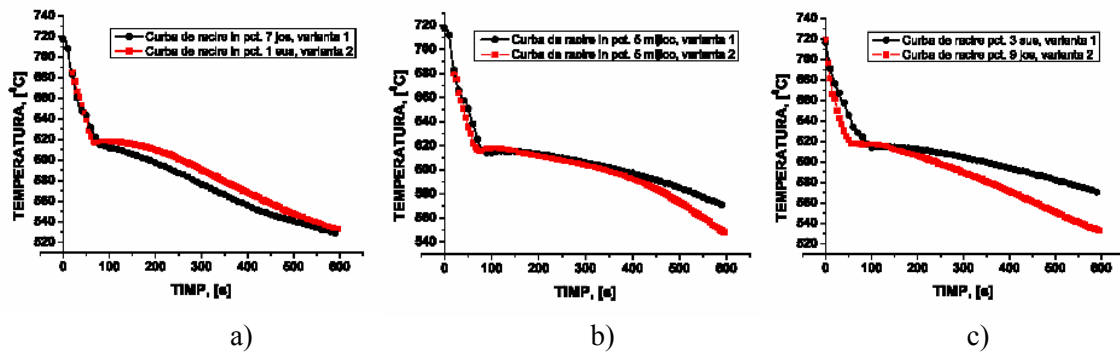|        a)        |        b)        |        c)        |

Figure 7. Experimental and simulated cooling curves corresponding to identical positions for variant 1: a) point 3, b) point 5, c) point 9.

In the following figures we present the experimental cooling curves and those obtained by modeling and simulation in the points 1 … 6, 9 corresponding to the 2$^{nd}$ casting variant.



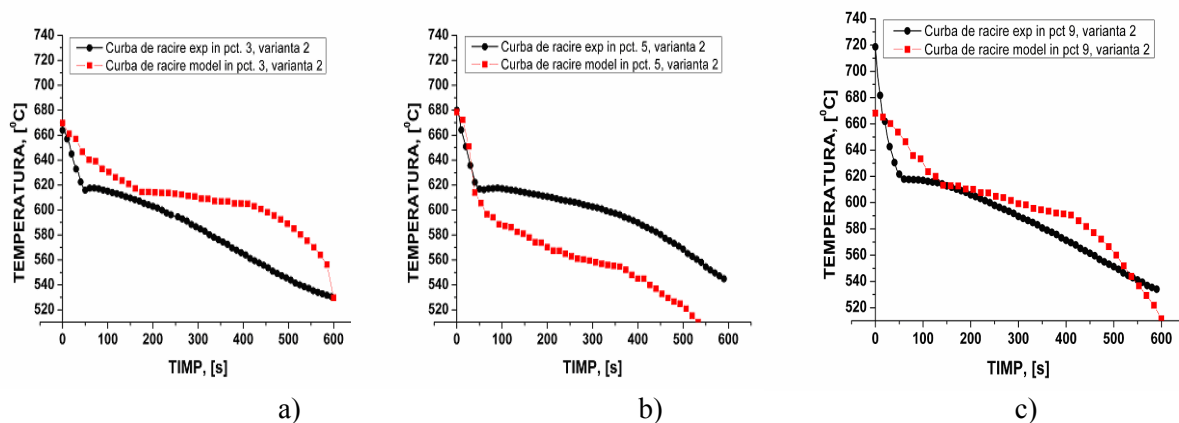|        a)        |        b)        |        c)        |

Figure 8. Experimental and simulated cooling curves corresponding to identical positions for variant 2: a) point 3, b) point 5, c) point 9.

We can see that for some points the correspondence of the curves is sufficiently good, yet for those of the areas with lower wall widths the differences are quite big.

## 4. CONCLUSIONS

The correlation and the correction of the program was made by comparing the cooling curves in certain points of the part, obtained by two methods: a)

experimentally, using a model with measurement and data acquisition system, b) by simulation, using the program that implements numerically the mathematical model of solidification.

Considering correct the mathematical model, the correction of the program was made by reconsidering the thermophysical constants of materials and of the limit conditions in the areas of interest. By these changes, we improved substantially the correlation between the experimental model and the one implemented in the program, yet it is necessary to continue the reevaluation of the achieved program, so that it achieves the purpose for which it was made, that is: to obtain parts cast out of non-ferrous alloys with minimal consumption of power and materials.

**REFERENCES**

1. Soporan V., Vamoş C., Pavai C. **: Modelarea numerică a solidificării** – *Solidification numerical modelling*- Ed. Dacia, Cluj – Napoca, 2003.
2. Soporan V., Constantinescu V. **: Modelarea la nivel macrostructural a solidificării** – *Solidification modelling at macrostructural level* - Ed. Dacia, Cluj – Napoca, 1995.
3. Soporan V., Constantinescu V., Crişan M. **: Solidificarea aliajelor** – *Alloys solidification* - Ed. Transilvania Press, Cluj – Napoca, 1995.
4. Sofroni L., Brabie V., Bratu C. **: Bazele teoretice ale turnării** – *Theoretical basis of casting* - Editura didactică şi Pedagogică, Bucureşti, 1980.

**VERIFICAREA EXPERIMENTALĂ A UNUI MODEL MATEMATIC AL SOLIDIFICĂRII**

**Rezumat.** Lucrarea prezintă rezultatele experimentale privind fenomenul termic ce are loc în timpul procesului de solidificare a unui aliaj neferos. Utilizând un sistem de achiziţie de date, modificarea temperaturii în anumite puncte ale piesei turnate a fost înregistrată. Aceste date au fost comparate cu date similare obţinute prin simulare numerică.